

Yearbook

2010

**Research Institute for
Technical Physics and
Materials Science**

Hungarian Academy of Sciences

<http://www.mfa.kfki.hu/>



**Research Institute for Technical Physics and
Materials Science
Hungarian Academy of Sciences**

Director: Prof. István Bársony
Address: Konkoly-Thege Miklós út 29-33,
H-1121 Budapest, Hungary
Postal: P.O.Box 49, H-1525 Budapest, Hungary
Phone: +36-1-392 2225
Fax: +36-1-392 2226
E-mail: info@mfa.kfki.hu
URL: <http://www.mfa.kfki.hu/>

MTA MFA Yearbook 2010

Editors: Miklós Menyhárd, Csaba S. Daróczi, and Zsolt Zolnai
Published by: MTA MFA, Budapest, Hungary, 2011

CONTENTS

| | |
|--|----|
| Contents..... | 3 |
| Director's Foreword..... | 5 |
| General Information..... | 8 |
| Organisation..... | 8 |
| External Advisory Board..... | 9 |
| Key Financial Figures..... | 10 |
| Publications and Citations of MFA..... | 11 |
| Honoured and Elected..... | 12 |
| Highlights..... | 14 |
| Graphene nanoarchitectures with zigzag edges on SiO ₂ | 14 |
| Synthesized view of nucleation and growth of elemental and //..... | 16 |
| Nano hydroxyapatite and polymer based bio-compatible nanocomposites..... | 20 |
| Notable Events..... | 24 |
| High School Relations..... | 27 |
| Scientific Reports..... | 30 |
| Nanostructure Department..... | 31 |
| Colour changes on cooling of Lepidoptera scales containing photonic//..... | 32 |
| Bioinspired photonic nanoarchitectures from graphitic thin films..... | 34 |
| Silver color production by a novel biologic nanoarchitecture..... | 36 |
| Charge spreading in graphene..... | 38 |
| Comparison of the chemical sensing properties of individual carbon //..... | 40 |
| Graphene nanopatterning with EBL and carbothermal etching..... | 42 |
| Photonics Department..... | 44 |
| NANOMAGDYE: Magnetic nanoparticles combined with //..... | 46 |
| Nondestructive characterization of cast iron by Magnetic Adaptive //..... | 48 |
| Makyoh topography..... | 50 |
| Study of nanocrystalline diamond films fabricated by Microwave //..... | 51 |
| Fabrication and Investigation of Diffractive Optical Elements //..... | 53 |
| Optical critical dimension measurement of photonic structures..... | 54 |
| Development of models and instruments to monitor protein adsorption..... | 55 |
| Accredited Ellipsometry Laboratory in frame of a European //..... | 56 |
| Synchrotron ellipsometry at high photon energies..... | 57 |
| Flagellin Based Protein Layers for Label-free Biosensing//..... | 58 |
| Grating Coupled Optical Waveguide Interferometer for Label-free //..... | 59 |
| Fluid Handling in OWLS Experiments – Injections of Serum Samples..... | 60 |
| Development of integrated process monitoring metrology for the //..... | 61 |
| Development of metrology tools based on electrical and optical //..... | 62 |
| Nanopatterning of macroscopic surfaces by tunable ion-swelling..... | 63 |
| Relationship between structural changes, hydrogen content and //..... | 64 |
| Microtechnology Department..... | 66 |
| Sensitivity tuning of a three-axial force sensor..... | 71 |
| Thermal behaviour of 3-dimensional single crystalline force sensor..... | 74 |
| Separation of biological samples in microscale..... | 77 |
| Sample transport in polymer based microfluidic system..... | 78 |
| Chemically Modified Solid-State Nanopores for Sensing..... | 80 |
| Investigation of silicon-based superhydrophobic surfaces..... | 82 |
| Integration of buried channels in cerebral silicon microprobes..... | 84 |



| | |
|---|-----|
| Microtechnology Department (cont.) | |
| Development of THz detectors | 85 |
| Deposition of Al doped ZnO layers by Atomic Layer Deposition | 87 |
| Growth of CIGS layers by post-selenization of metal precursors | 88 |
| Wafer bonding for microelectronics | 89 |
| MBE related research and development in MFA | 91 |
| LPE growth and optical investigation of InGaAsP/InP double // | 93 |
| Reactive deposition epitaxy growth and electronic properties of // | 95 |
| Reorganization of silica nanoparticles under ion irradiation | 97 |
| Thin Film Physics Department..... | 99 |
| Composition dependence of film structure and morphology in // | 100 |
| Spinodal Decomposition as Phase Separation Mechanism in Thin //..... | 102 |
| Pressure-dependent stability of cubic and wurzite phases within //..... | 104 |
| Determination of grain boundary plane in the TEM exemplified in Si | 105 |
| Progress in producing large grained, low stress multi-crystalline //..... | 107 |
| Microstructure of diamond films grown on nitride HEMT devices | 109 |
| Nitride nanowires grown by MOCVD for solar cells | 111 |
| Aluminium Oxide Films Deposited by Plasma-Enhanced Atomic | 113 |
| Silica/nontronite intergrowth in chloropal | 114 |
| Structure and thermal stability of sputtered Sc _{1-x} Al _x N..... | 115 |
| Experimental determination of the electron elastic backscattering //..... | 116 |
| Growing embedded layer with sharp interfaces by means of ion // | 117 |
| MD-based simulation of ion-erosion and nanotopography on Si | 118 |
| Trial and error method for determination of ion beam induced // | 119 |
| NTPCRASH..... | 120 |
| Nanostructured thin layers for dissolvent vapour sensors | 121 |
| Ceramics and Nanocomposites Department | 122 |
| Silicon nitride-based nanocomposites | 123 |
| Multilayer graphene nanosheets by exfoliation of graphite in // | 124 |
| Nanostructured oxide dispersed strengthened steels | 125 |
| Tungsten Oxide Functional Ceramics | 125 |
| Nanoparticulate Langmuir-Blodgett films | 126 |
| Improvements in FIB TEM Lamella Preparation | 127 |
| Bending modulus measurement of vertical ZnO nanowires | 128 |
| Patterned grown ZnO nanorod arrays for 3D photonic devices | 129 |
| Substrate effect on the growth of vertical nanowires | 130 |
| Highly ordered vertical ZnO nanorods by nanosphere lithography | 131 |
| Organic-inorganic heterostructures for third generation // | 132 |
| Synthesis of horizontal ZnO nanowires for integrated sensor | 133 |
| Complex Systems Department..... | 134 |
| Efficiency of punishments in spatial public goods games | 136 |
| Activities..... | 138 |
| MFA Seminar Talks..... | 139 |
| Research and Development Partners..... | 141 |
| Visitors | 142 |
| Photovoltaic and Ellipsometric services | 143 |
| MFA Publications in 2010 | 147 |

DIRECTOR'S FOREWORD



2010 brought about an „earthquake” in Hungary’s debt-prone economy. After a landslide election victory the new government inherited a severe economic crisis, which had to be countered with immediate central measures, also affecting innovation financing and the continuation of domestic R&D projects. The adverse impact of the (hopefully temporarily) suspended payments and discontinued calls has been very serious, especially on international collaborations co-financed by the EU and the Hungarian innovation agency. We were even ourselves astonished in such circumstances to register a still formidable performance of MFA in financial terms, albeit registering a setback of almost 1 million € in last year’s budget.

The most important organisational change in the life of our institute was that the President of the Hungarian Academy of Sciences appointed the six members of the External Advisory Board (EAB) of MFA, who were nominated by the supervising Department of Physical and Technical Sciences and the MFA management. The head of the EAB is Prof. János Kertész, and the foreign members represent fundamental science (Prof. Lars Hultman from Uni. Linköping, Sweden) and targeted research (Prof. Lothar Frey from Fraunhofer IISB, Erlangen, Germany). Their mandate is to provide the director with independent advice for eventual necessary modifications and adjustments in scientific terms. The President of the Academy also expects them to provide an overall assessment of the activities and progress of the research based upon their regular judgements every three years.

Regarding the scientific-technical achievements, the past year was definitely a success for MFA, as confirmed by the EAB. Besides scientometry, the visibility of MFA activities was enhanced by better PR policy, by our contributions to education support and popularisation of science, research and nanotechnology in particular. Thanks to the consistent policy of the MFA management to invest heavily from own resources in the continuous improvement of the research infrastructure, we were able to acquire more support from European framework projects, and expand our R&D cooperation with domestic and foreign industrial partners, which enabled us to survive in the harsh economic environment. In this regard the institute profited from being leader of the National Technology Platform for Integrated Micro/nanosystems (www.imntp.hu), the Hungarian partner of the European Technology Platforms for Nanoelectronics ENIAC and Photovoltaics. The initial financing for setting up the IMNTP bureau ended in March, but MFA tries to find other ways to continue operation of this office (headed by Dr. Krisztina Szakolczai).

The year 2010 could be justly called the “year of graphene”, not only because of the Nobel Prize in Physics to Geim and Novoselov, but also for the success of MFA researchers particularly in this field. The internationally pioneering contributions of



the group headed by Prof. László P. Biró brought several acknowledgements. Péter Nemes Incze (Ph.D. student) obtained last year (as the third MFA member) the prestigious distinction of Junior Prima Prize in physics. MFA was one of the two research institutes of the HAS obtaining the support of the Research Council for Fundamental Science and Technology of the Korean Republic (KRISS). The new Joint Korean-Hungarian Laboratory for Nanosciences was opened at MFA by the presidents of KRISS and HAS on 27 October 2010 and will be operated for three years financed by the Korean partner. The head of the laboratory, L.P. Biró, obtained on 10 December 2010 the Charles Simonyi Research Grant for his spearhead research on carbon and biological nanostructures.

Péter B. Barna, professor emeritus of our institute, was honoured for his life-achievement in thin film science by the 2010 Prize of the International Vacuum Union. On 25 August he held a well received plenary lecture at the 18th International Vacuum Congress in Peking where the IUVSTA Prize was handed over to him.

A further appreciation of MFA was this year is the election of István Bársony, the Director of the institute by the General Assembly of the Hungarian Academy of Sciences to corresponding member of the HAS. On 9 December he delivered his inaugurate lecture entitled: "Interfaces – interactions – integration".

Miklós Menyhárd, scientific advisor and head of the Scientific Council of MFA was decorated by the Knight Cross of the Order of Merit of the Hungarian Republic on 23 October for his scientific and organisational achievements.

Péter Arató, scientific advisor of MFA, became Doctor Honoris Causa of the University of Miskolc for his decade-long support of education and research at the University.

The representatives of MFA, the Pázmány Péter Catholic University and their 2008 spin-off company TactoLogic were awarded the Millenium Prize of the Hungarian Patent Office on 22 April 2010 for the "efficient enhancement and protection of their intellectual property".

A record number of six Ph.D. degrees were obtained in 2010 by young MFA researchers: Anita Pongrácz (BME), Enikő Horváth (BME), Krisztián Kertész (BME), Fanny Misják (ELTE), Csaba Major (SZTE) and Krisztina Szakolczai (PE). Their scientific contribution is paramount for ensuring a continuous adaptation of the research programme and level of research at MFA to international trends and standards!

Five postdoctoral colleagues received in 2010 the prestigious János Bolyai Research Fellowship of HAS: Krisztián Kertész, Norbert Nagy, Attila Szolnoki, János Volk and Zsolt Zolnai.

Important manifestations of the growing influence of our institute in the scientific life of Hungary are the assignments in research funds and associations as well as the election of MFA members to representative bodies. Three of our colleagues, Gábor Battistig, János Lábár and Béla Pécz were elected as doctoral representatives in the General Assembly of HAS. Béla Pécz became the President of the Hungarian Microscopic Society for the coming four years. László P. Biró was elected as member of the Collegium for Technology and Natural Sciences of the Hungarian Research Fund OTKA for three years.

A pioneering but meanwhile traditional activity of our institute is the organisation of the yearly Summer Camp for junior high school students under the motto “Let’s learn from each other”. From 21-25 June 2010 we again hosted 23 children (15-17 year old) from the schools of the whole Carpathian Basin at our laboratories, thanks to the enthusiastic guidance and support from our whole staff. Some of the best reports written by the children after one week of research at MFA were last year even published in the popular periodical “Élet és Tudomány”. The institute’s Open Day (12 November) and the lecture of I. Bársony and J. Volk “From microelectronics to nanosensorics” held for youngsters in the frame of the action “Students at the Academy” (November 11.) were well visited and received. Over ten young university students (BSc and MSc) were awarded some prize at their universities competitions for their scientific projects carried out at MFA and were invited to the national competition in several categories. All these activities and efforts serve the popularisation of scientific studies and the motivation of young students to select the unfortunately still understated career as researcher later on – and our consequent efforts seem to bear fruits!

Lack of resources did not block our striving for improvement of research conditions. Although only a few smaller instruments could be purchased the preparation and tender for more substantial investments were completed in 2010. The official inauguration of the reconstructed technology complex by the President of HAS in the presence of the press took place in March. We also rebuilt two laboratories and two offices for the Nanostructures Department, and two offices for the administration. The Quality Assurance System was continued, and four laboratories of MFA (Ellipsometry, Nanolab, Microtechnology and Spectroscopy) were rated Strategic Infrastructure by the national authority. The Spectroscopic Ellipsometry obtained as Test Laboratory accreditation in 2010.

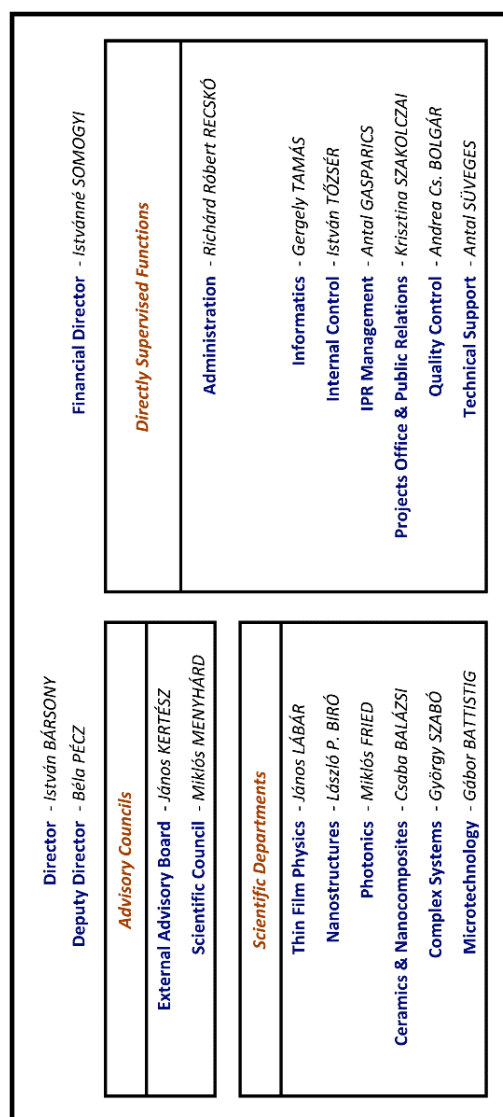
Despite the above financial difficulties, MFA is well on track – as was noted by the External Advisory Board. The coming year will be even more critical to manage, to maintain and even widen the international collaboration will require more concentrated efforts. Nevertheless we hope that the opportunity of an MFA staff-expansion by 20 coworkers, which we obtained by initiating a multidisciplinary collaboration in the new HAS Q2 research complex at the Lágymányos university campus with the partner institutions in chemistry and biology under one roof, will widen our horizon and increase the attractivity of this exciting and exploding materials research field of nano-bio integration.

Budapest, 15 February 2011

István Bársony

GENERAL INFORMATION

Organisation



External Advisory Board

János KERTÉSZ

ordinary member of the HAS
(president)

BME TTK Fizikai Intézet, Elméleti Fizika
Tanszék

1111 Budapest, Budafoki út 6-8.,
Hungary

kerteszk@planck.phy.bme.hu

Árpád CSURGAY

ordinary member of the HAS

PPKE Információs Technológia Kar

1083 Budapest, Práter u. 50/A, Hungary

University of Notre Dame, Center for
Nano Sci. & Technology, France

acsurgay@itk.ppke.hu

acsurgay@nd.edu

Lothar FREY

Univ. Prof.

FhG IISB, Erlangen

91058 Erlangen, Schottkystrasse 10.,
Germany

lothar.frey@iisb.fraunhofer.de

József GYULAI

ordinary member of the HAS

MTA MFA

1121 Budapest, Konkoly-Thege M. út 29-
33., Hungary

gyulai@mfa.kfki.hu

Lars HULTMAN

Univ. Prof.

Thin Film Physics Division, Linköping
University, Sweden, **IFM** Linköping
University, S-581 38 Linköping, Sweden

larhu@ifm.liu.se

Gábor SZABÓ

corresponding member of the
HAS

SZTE TTK Optikai és Kvantumelektro-
nikai Tanszék

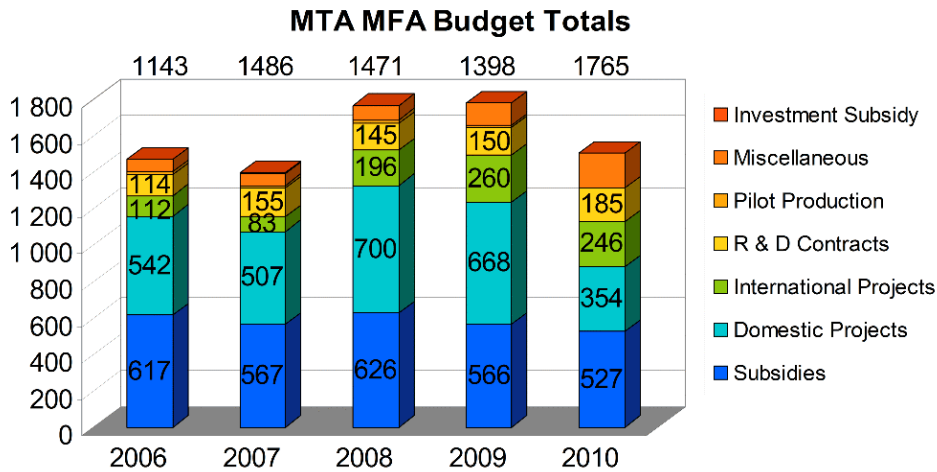
6720 Szeged, Dóm tér 9.

gszabo@physx.u-szeged.hu

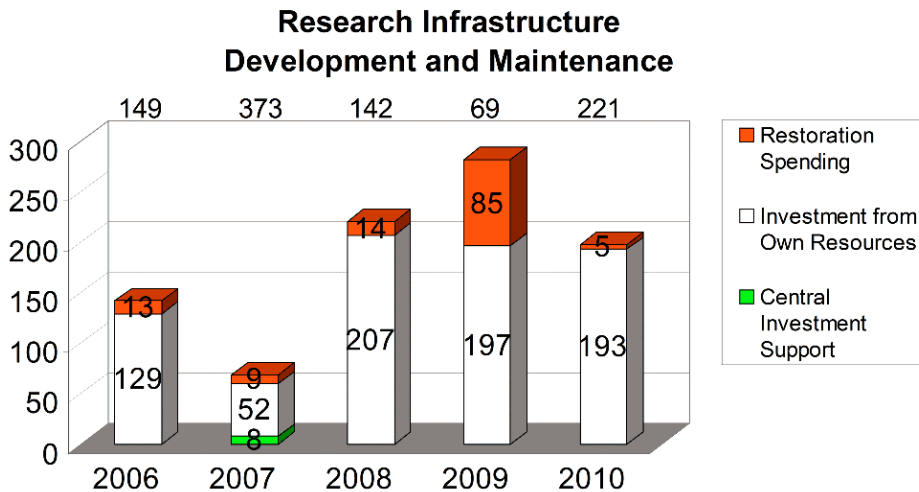


Key Financial Figures

The total budget of MFA in 2009 reached a similar level of about € 6.5 million as in the previous year with significantly improving indices. Beside the decreasing subsidies in 2009 the higher level of the budget of the Institute was mainly facilitated by the increasing success in the participation in international projects.

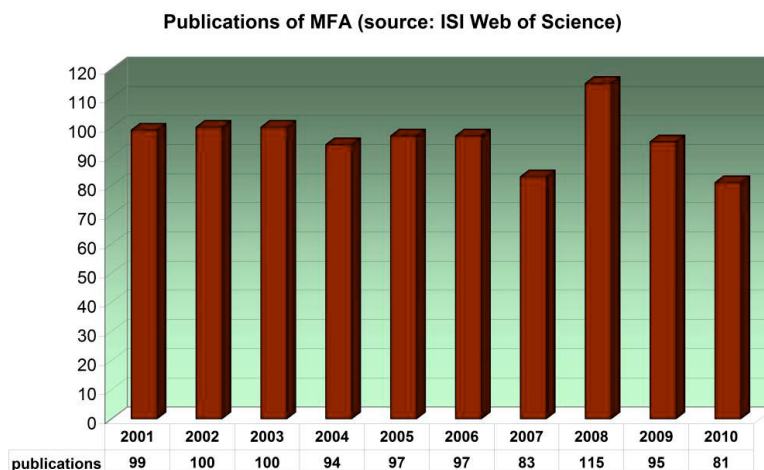


Despite the marginal central investment support, in the last period the research infrastructure of the Institute developed substantially, and in 2009 a significant restoration and extension of the clean room area has been also processed.



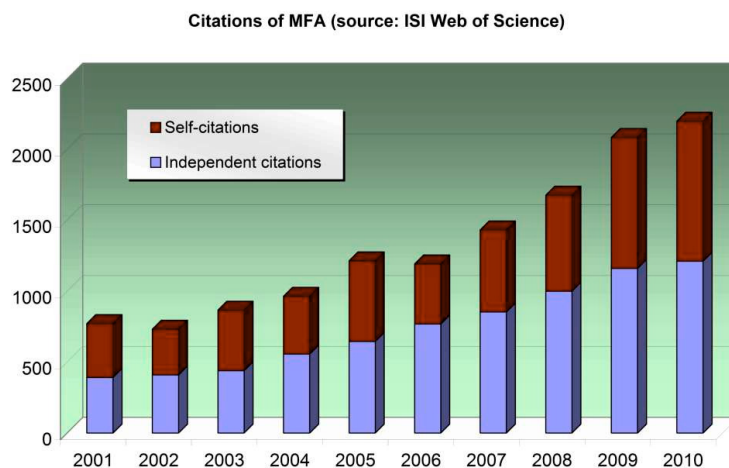
Publications & Citations of MFA

According to the independent database of *Thomson Reuters*, the institute has kept an average publication activity of nearly 100 scientific papers per year during the past decade.



The complete 2010 publication list of MFA – with considerably more titles than listed by ISI Web of Science – is included at the end of this yearbook.

A good measure of the recognition of MFA's scientific activity is the h-index value of 49, and the steady growth of the number of independent citations.



Honoured and Elected



On 22 April 2010 the representatives of the Pázmány Péter Catholic University, and MFA, Tamás Roska and István Bársony, as well as Attila Kis, the acting manager of their 2008 founded spin-off company, TactoLogic Ltd. were awarded by President Miklós Bendzsel with the **Millenium Prize of the Hungarian Patent Office** for the “efficient enhancement and protection of their intellectual property”.



The director of MFA, **István Bársony** was elected by the Assembly of Academicians of HAS corresponding member of the Hungarian Academy of Sciences in May 2010. He held his inauguration lecture entitled “Interactions, interfaces, integration” on 9 December 2010.



On 25 August 2010 **Péter B. Barna**, professor emeritus of our institute, was honoured for his life-achievement in thin film science by the 2010 Prize of the International Vacuum Union.





On 23 October 2010 **Miklós Menyhárd**, the head of the Scientific Council of MFA was decorated by the Knight Cross of the Order of Merit of the Hungarian Republic.



On 24 November **Péter Nemes-Ince** received Junior Prima prize in science, acknowledging his original method to process graphene layers placed onto SiO_2 surface with nm accuracy.



On 10 December 2010 Prof. **László Péter Biró** of MFA received the Charles Simonyi Research Grant for his spearhead research on carbon and biological nanostructures from Minister Miklós Réthelyi, President of HAS József Pálinkás and Lajos Keszthelyi, Chairman of the Curatorial Board.

HIGHLIGHTS

Graphene nanoarchitectures with zigzag edges on SiO₂

OTKA-NKTH grants 67793, 67851 and 67842)

P. Nemes-Incze, G. Magda, K. Kamarás, and L. P. Biró

Graphene has many advantageous properties, but its lack of an electronic band gap makes this two dimensional material impractical for being used in digital nanoelectronics, for example field effect transistors for digital applications. This problem can be circumvented by opening up a confinement induced gap, through the patterning of graphene into ribbons having widths of a few nanometres. The electronic properties of such ribbons depend on their size and the crystallographic orientation of the ribbon edges. Therefore, etching processes that are able to differentiate between the zigzag and armchair type edge terminations of graphene are highly sought after. Our group has shown for the first time that such a controllable, anisotropic, dry etching reaction is possible and we use it to obtain graphene ribbons with zigzag edges [98].

Using the carbothermal reaction of the graphene layer with the SiO₂ substrate itself we can etch hexagonal etch pits into graphene layers, with the pit edges having zigzag edge terminations (as revealed by STM investigation). During carbothermal etching the carbon of the graphene layer edges reduces the SiO₂ substrate material into SiO itself being oxidized at 700 °C in an argon atmosphere.

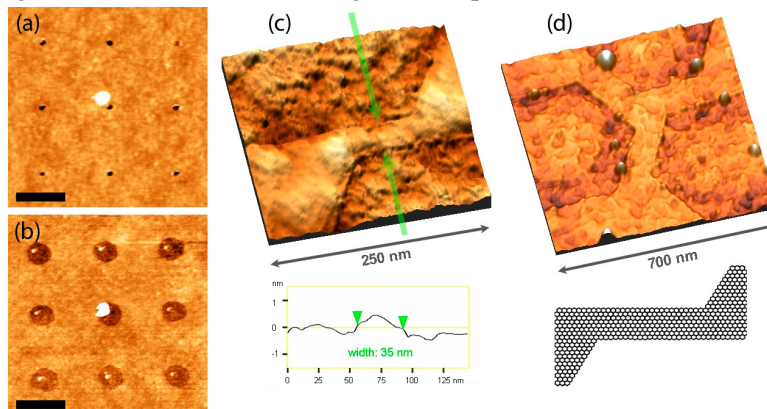


Figure 1. (a) The result of AFM indentation: a 3×3 matrix of holes in graphene. (b) AFM micrograph of the hexagonal holes grown from the defects induced by indentation. Scale bars 500 nm. (c) The image shows a 3D AFM image of a graphene nanoribbon of about 35 nm. The AFM height profile has been acquired at the place shown by green arrows. The inset in the right lower corner shows a scheme of the corresponding atomic structure. (d) The image shows a junction of 3 nanoribbons, with the ribbons having widths of: 93, 100, 101 nm (starting from the upper left ribbon, going clockwise).

We have also demonstrated that the starting positions for the carbon removal reaction can be tailored at will with precision. The starting point of the carbothermal reaction can be controlled by introducing defects into the graphene layer at pre-planned locations. This can be easily achieved, by piercing the surface of the graphene layers using an AFM tip (see Fig. 1a and 1b). Our etching technique is a straightforward and powerful tool to tailor graphene layers in a crystallographically oriented manner by using the hexagonal holes as building blocks for more complex graphene structures, such as graphene nanoribbons (Fig. 1c and 1d).

In collaboration with researchers from the Max Planck Institute for Solid State Physics in Stuttgart, we have been able to measure the Raman spectra of the graphene nanoholes with zigzag edges (Fig. 2), comparing these spectra with data obtained on circular etch holes. The circular holes contain both armchair and zigzag edge terminations, therefore, the difference in the Raman spectra (Fig. 2) is the first experimental confirmation of the theoretical predictions on the absence of the double resonance scattering mechanism responsible for the so called D peak (1350 cm^{-1}) in the Raman spectra of zig-zag edges [71].

The process described here shows great promise in the fabrication of graphene devices having zigzag edges, helping to unlock the experimental aspect of a field of graphene research which up to now has only been the subject of theoretical study.

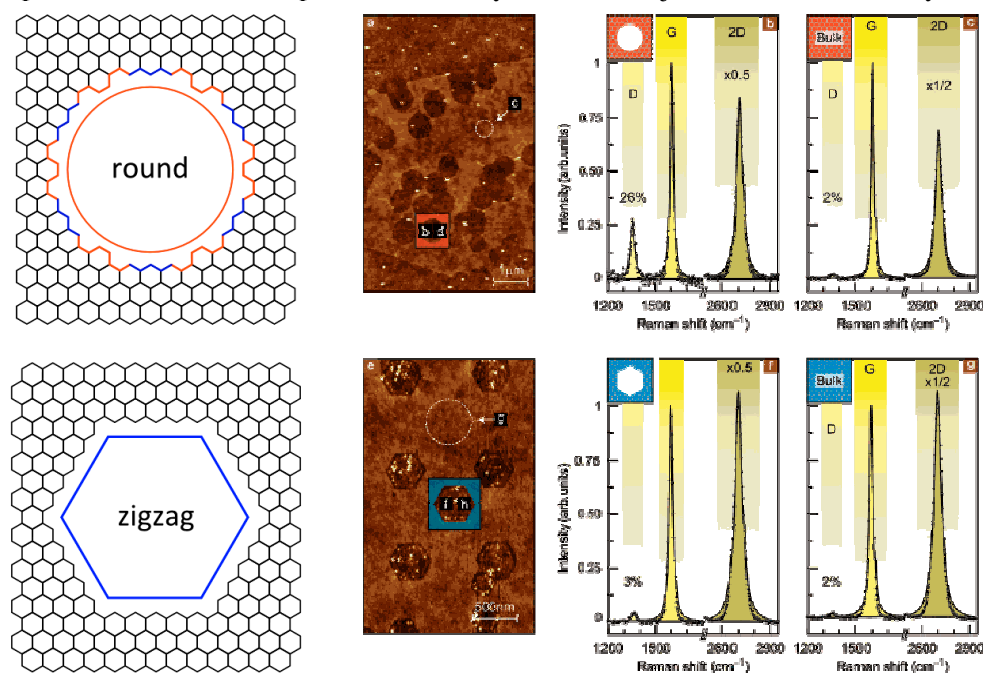


Figure 2. Scheme of circular and zigzag edged holes in graphene. Raman spectra of a graphene sample having round holes (upper panel) and hexagonal holes (lower panel). AFM images of the positions where the Raman spectra on the right-hand side were obtained (a, e). The Raman spectrum of a round hole has a strong D peak (b), whereas the D peak for a hexagonal hole (f) is minimal and only slightly higher than the surrounding bulk value (c and g).

Synthesized view of nucleation and growth of elemental and multi-component polycrystalline thin films

(Extended abstract of the plenary lecture presented at the 18th International Vacuum Congress of IUVESTA, (Beijing, August 23-27, 2010) in the occasion of receiving the Scientific Prize of IUVESTA)

P. B. Barna

Aspects and domains of research, development and production/application of thin films can be arranged in a so called “process chain” according to their causal dependence. This process chain holds for every material system and production technology. It clearly demonstrates that the study and understanding of the mechanisms of structure evolution and their controllability by the process parameters must be a key issue of our activity. Leaving this out of consideration, e.g. investigating only the correlation between deposition parameters and properties, the achieved results can not be well founded.

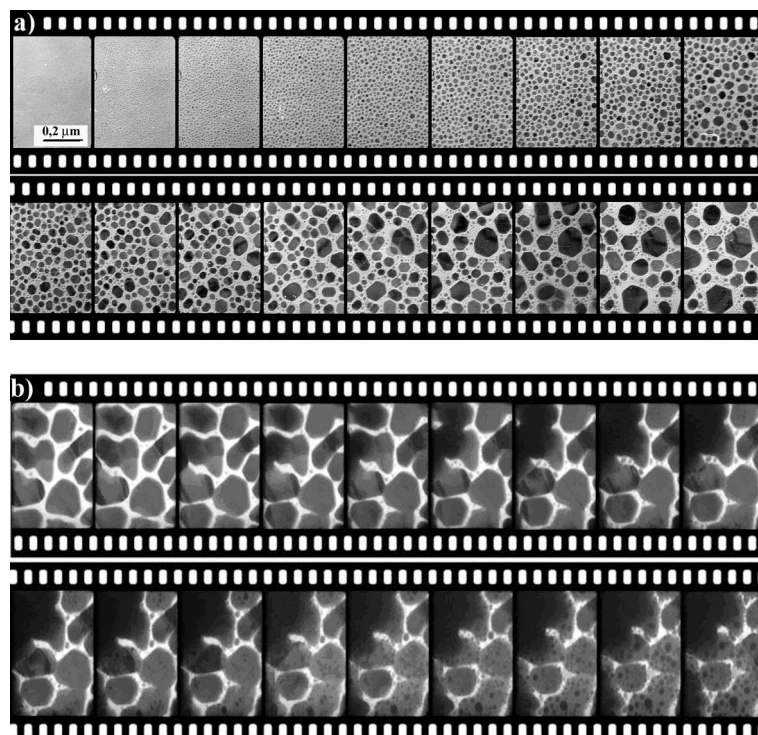


Figure 1 Growth of In films deposited on a-C substrate at 60 °C. In situ transmission electron-microscope experiments a) nucleation, growth and coalescence of crystals; b) operation of co-deposited C as grain refiner additive : segregated C develops a 2D layer on the surfaces, limits their growth and coalescence, while the encapsulation of In crystals by the 2D carbon layer leads to repeated nucleation

Concept of the synthesized view of the structure evolution is based on the following conclusions: the building of the structure by atom-by-atom addition is a self organizing process which is discussed in frames of fundamental phenomena (nucleation, crystal growth and grain growth) as revealed by the early in situ transmission electron-microscopic experiments (Fig. 1). These fundamental phenomena are related to thermally activated atomic processes, like surface and bulk diffusion, atomic interactions on and with the surface. The growth of thin films can be described as a series of fundamental phenomena called the pathway of structure evolution. The pathway includes also the competitive processes (crystal and grain growth) of randomly oriented crystals nucleated on the substrate.

For contamination free, elemental thin films a *temperature structure zone model* (TSZM) can be derived from constructing the pathway of structure evolution in the characteristic temperature range (Fig. 2). This model describes the interdependent development of grain size and shape, orientation of crystals (texture) and surface morphology as the function of temperature and thickness.

Functional thin films are multi-component systems and both the atomic processes and the fundamental phenomena are more complex and have to be determined for each material system. Key issues are the understanding of the nucleation and separation of phases and their interdependent, competitive growth as well.

In a two component system a stable single phase evolves if the condensing vapour beam corresponds to a stoichiometric composition (a stoichiometric compound forms and grows) or the first nucleating phase can dissolve all co-deposited species (a solid solution forms). In these two cases the TSZM of an elemental film (Fig. 2) is valid. If the composition of the condensing vapour beam differs from these, *excess species* appear either in the bulk (leading to supersaturation) or as adatoms on the surface of the growing phase. These excess species are acting as sources of a second phase.

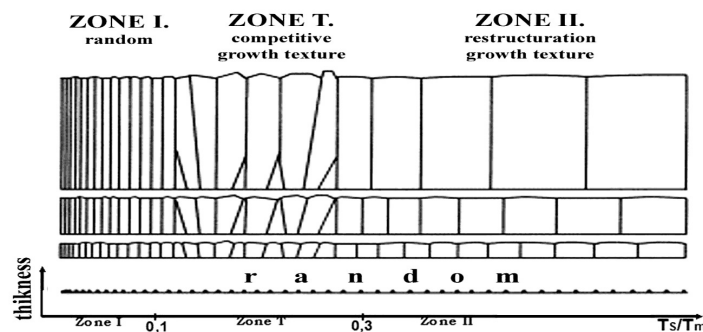


Figure 2 Derived temperature structure zone model of elemental polycrystalline films grown on amorphous substrate.

The structure evolution of the film can be described as the growth of a single supersaturated solid solution phase in the first case, which can later undergo phase

separation. While, in the second case surface excess species are involved in interplaying competitive growth of the first and second phases (Fig.3). Excess species are built into the bulk of the growing film when surface processes are hindered e.g. by fast deposition rate. In this case phase separation will be initiated when thermal activation/time for bulk diffusion will have effect. Nucleation of the new phases occurs when the activation is sufficient for that. No activation for nucleation is a precondition for phase separation when spinodal decomposition is possible. In this case a special nanocomposite can form corresponding to the morphology of epitaxially interrelated domains of different composition but having no phase boundaries between them (left side of Fig.3).

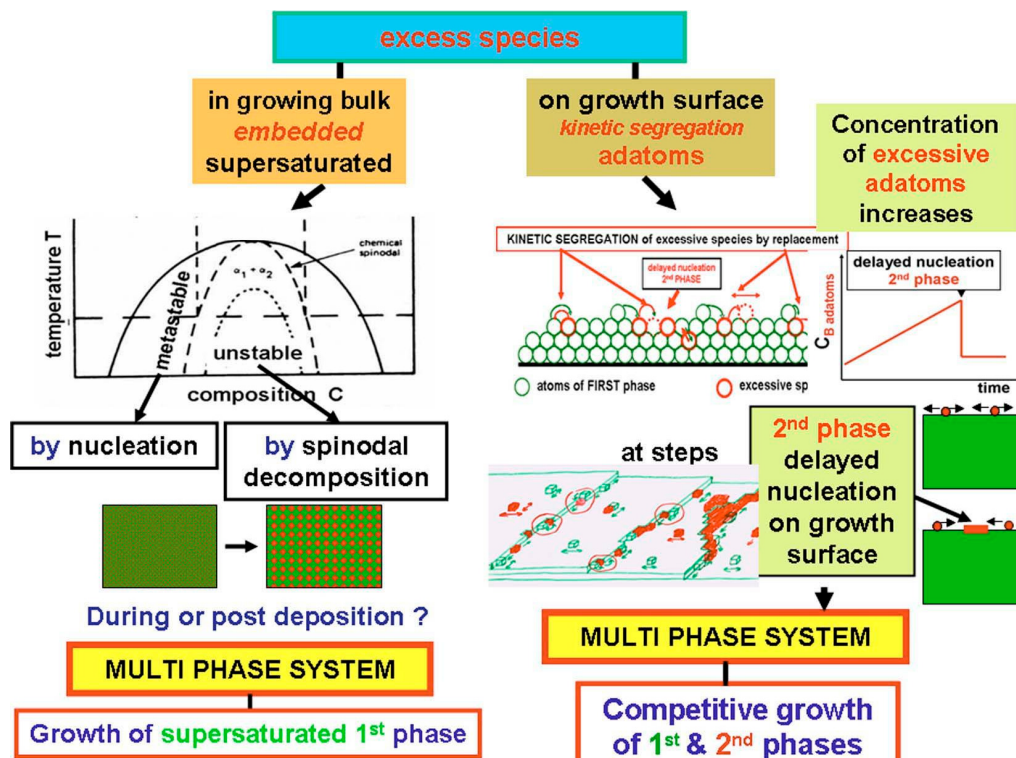


Figure 3 Possible pathways for the formation of 2nd phase.

The direct causal relations characterizing the preparation/structure evolution of thin films are compiled in Fig. 4. An important part of Fig. 4 is the illustration of the *self organizing nature of structure evolution*. It intends to show that the pathway of the atomic processes and fundamental phenomena at any stage of structure evolution are controlled by the actual structure of the growing surface, developed by the preceding atomic processes/fundamental phenomena.

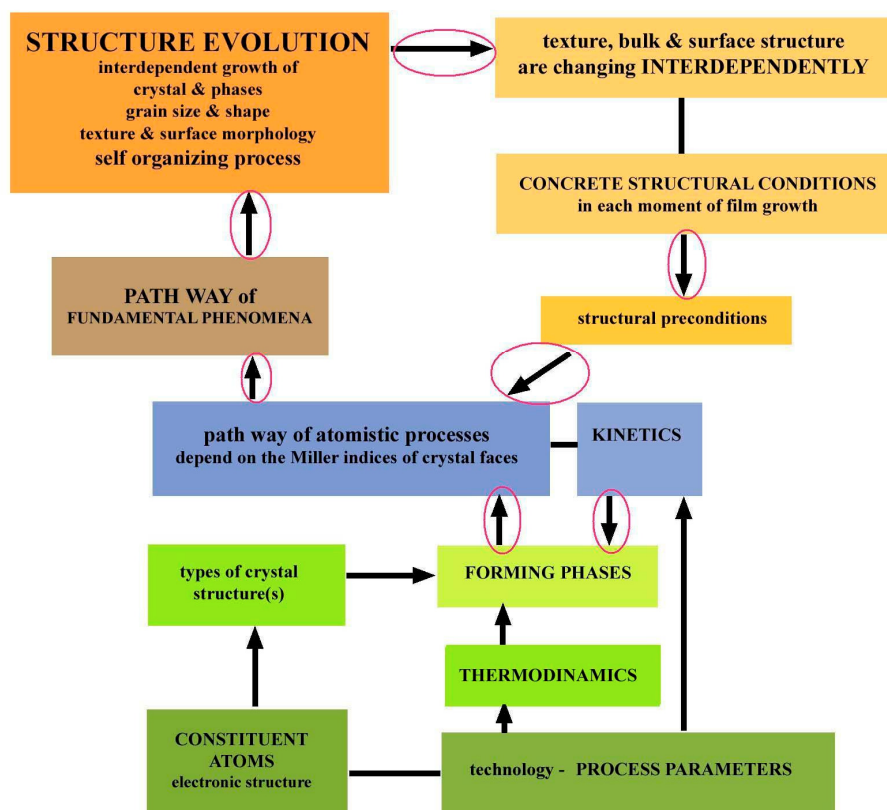


Figure 4 The direct causal relations of process parameters, atomic processes and fundamental growth phenomena illustrating also the way of self organizing nature of structure evolution marked by encircled arrows.

Based on this model it is proposed the study of some hot topics both theoretically and experimentally (simulation and well controlled laboratory experiments applying the most advanced, sophisticated analytical methods) like:

- The surface processes&chemistry at atomic level and their dependence on the process parameters (*MC and MD simulation, complex analysis at atomic level applying advanced analytical techniques*).
- Dependence on the pathway of surface atomic processes and fundamental phenomena on the surface structure, e.g. role of GB-s.
- The structure evolution in its entirety (in situ STM and TEM experiments).

The author has benefited from decades of close collaboration with late J.F. Pócza, A. Barna and G. Radnóczy (MFA, Budapest), as well as continuous discussions with M. Adamik, A. Kovács and F. Misják (MFA, Budapest), late R. Manaila and A. Dévényi (Inst. of Materials, Bucharest), H. Bangert and C. Eisenmenger-Sittner (Technical University, Vienna), J.E. Greene and I. Petrov (University of Illinois) and L. Hultman (Linköping University)

Nano hydroxyapatite and polymer based bio-compatible nanocomposites

(Supported by OTKA BIOCER, TÉT HU-Korea)

C. Balázsi, G. Gergely, M. Tóth, I. Kulcsár, F. Wéber, I. E. Lukács, L. Illés, A. L. Tóth

Nanomaterials used in biomedical applications include nanoparticles for molecules delivery, nanofibres for tissue scaffolds, surface modifications of implantable materials or nanodevices, such as biosensors. The combination of these elements within tissue engineering is an excellent example of the great potential of nanotechnology applied to regenerative medicine. One of this nanomaterials widely used in tissue engineering is hydroxyapatite (HA).

Hydroxyapatite, $\text{Ca}_{10}(\text{PO}_4)_6(\text{OH})_2$ is chemically similar to the mineral component of bones and teeth. HA is part of materials that are classified as bioactive, meaning that it will support bone in growth and osteointegration when used in orthopaedic, dental and maxillofacial applications. Coatings of HA are often applied to metallic implants, especially stainless steels and titanium alloys to improve the bioactivity of surfaces. HA can be produced from biogenic materials like coral, seashell, eggshell (Fig. 1), body fluids and synthetic methods. Various techniques were developed for synthesis of HA, based on solid state reactions, chemical precipitation reactions, hydrothermal reactions, sol-gel methods and mechano-chemical methods using the combination of different calcium and phosphorus starting materials.



Figure 1 Macroscopic view of eggshell.

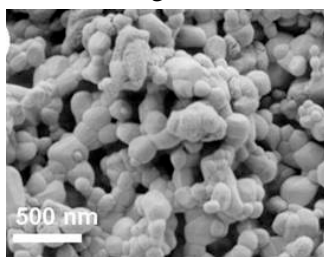


Figure 2 SEM image of HA produced from eggshell.

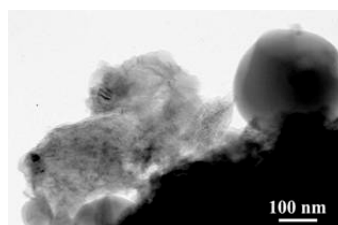


Figure 3 TEM image of HA produced from eggshell.

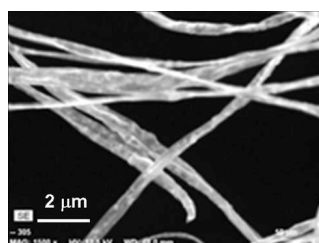


Figure 4 SEM image of acetone – propanol HA fiber.

Hydroxyapatite may be employed in forms such as powders (Figs. 2, 3), porous blocks or beads to fill bone defects or voids. Elaboration processes of the HA have been optimized, nanostructural HA has been achieved by mechanochemistry method. New products, potential tissue engineering scaffolds have been realized by electrospinning (Fig. 4). Our laboratory started to study various kind of HA-polymer hybrid composites with the new equipment purchased by Ceramics and Nanocomposites Department.

Electrospinning gave a three dimensional arrangement of polymer micron and nanofibers. HA nanoparticles were dispersed in a polymer matrix (Fig. 4). This structure has high porosity and large specific surface, consequently provides good conditions for cell attachment, proliferation and spreading. Structural investigations show that the distribution of the HA was homogenous and the average fiber diameter was very uniform: 300-400nm. The EDS spectrum showed the presence of calcium, phosphorus, and oxygen (Figs. 5-7).

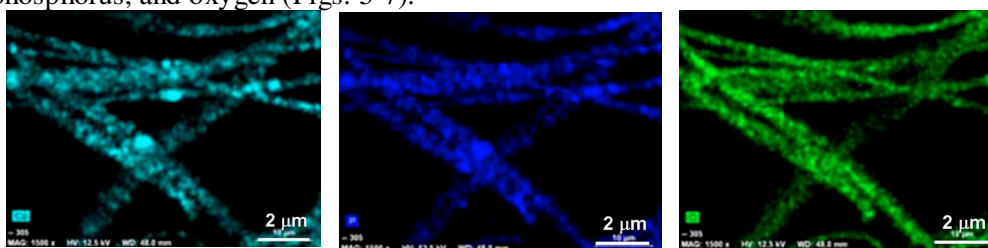


Figure 5 Ca distribution.. Figure 6 P distribution. Figure 7 O distribution..

In co-operation with Department of Materials Science and Engineering, State University of New York at Stony Brook (USA), we developed artificial bone tissue scaffolds based on natural hybrids of cellulose acetate (CA) and nano-hydroxyapatite (nHA) in a bio-mimicking 3D matrix architecture using a single step nano-manufacturing technique. These scaffolds have been used for in-vitro bone regeneration studies for up to 14 days (Fig. 8).

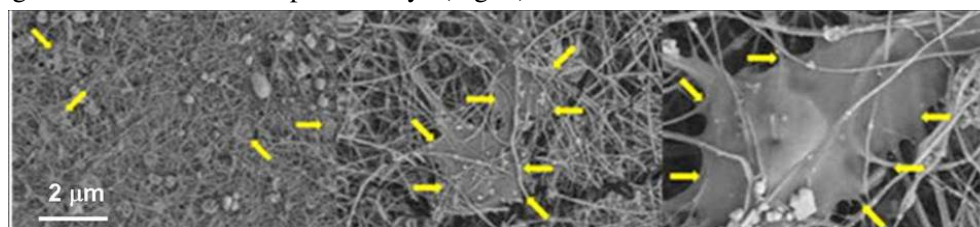


Figure 8 SEM images at different magnification showing the cell morphologies on scaffolds cultured for up to 14 days. Cell attachments are shown by yellow marks.

Osteoblasts grown on these scaffolds were found to interact strongly with the HA nanoclusters that were uniformly distributed on the CA fibers, promoting cell elongation, growth and phenotype retention. Hexagonal apatite crystals were shown to crystallize on the nHA seeds. The natural, open, hybrid, 3D nanoscaffolds thus appear to be most promising bone repair agents.

In co-operation with Hallym University and Gangneung-Wonju National University (Korea) we studied the bone regeneration of nano-hydroxyapatite (nHA) derived from eggshell with or without silk fibroin scaffold and compared to the unfilled control in the animal model (Fig. 9). nHA graft showed much more bone regeneration than unfilled control in both μ -CT (micro computer tomography) analysis and histomorphometric analysis (Fig. 10). All measured variables of the μ -CT analysis showed that grafted groups (nHA and nHA+silk) were significantly higher than the unfilled control groups in both 4 and 8 weeks after operation ($p < 0.05$, statistically

significant value). In histomorphometric analysis, there was no significant difference between groups at 4 weeks after operation. However, nHA group ($40.16 \pm 8.27 \%$) was shown significantly higher bone regeneration compared to the unfilled control ($25.66 \pm 10.98 \%$) or the nHA+silk group ($16.62 \pm 3.05 \%$) ($p < 0.05$). nHA from eggshell showed much more bone formation compared to unfilled control group in both μ -CT analysis and histomorphometric analysis. Considering that the eggshell is easily available and cheap, nHA from the eggshell can be good calcium source in tissue engineering (Fig. 11).

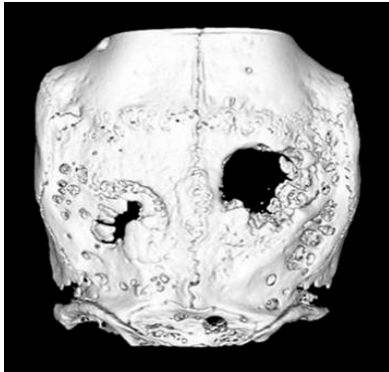


Figure 9 μ -CT of rabbit calvaria showing bone regeneration (the hole is filled with new bone in the left side) in only 8 weeks. Unfilled control on the right.

In co-operation with Department of Human Physiology and Clinical Experimental Research, Semmelweis University (Hungary) we tested the biological properties of nano-hydroxyapatite (nHA)-zirconia (ZrO_2) and carbon nanotube (CNT) composites produced by spark plasma sintering (SPS). Biological compatibility of the constructs was tested by seeding human bone marrow derived mesenchymal stem cells onto autoclave-sterilized composites and kept under standard cell culture conditions. Cell survival and proliferation was monitored for 18 days with confocal microscopy. All of the observed constructs provided suitable surface for cell culture, however, in case when CNTs were present in the mixture accelerated proliferation was observed in cases of low confluency. In vivo

experiments in that rats were used, μ -CT results show that nano-hydroxyapatite powders are acting as excellent bone fillers (Fig. 12).

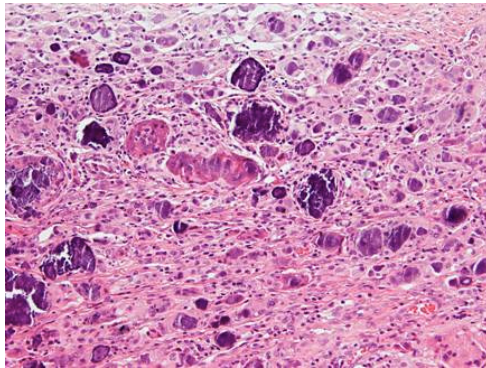


Figure 10 Histological findings at 4 weeks In nano-hydroxyapatite (nHA) groups, nHA particles were agglomerated and formed calcification nodule between loose connective tissue.

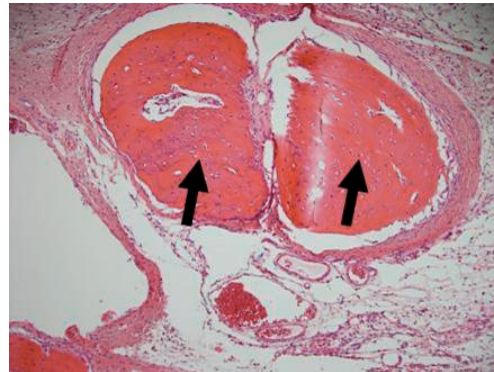


Figure 11 Histological findings at 8 weeks. A well organized lamella new bony islands (marked) were formed in nano-hydroxyapatite (nHA) group.

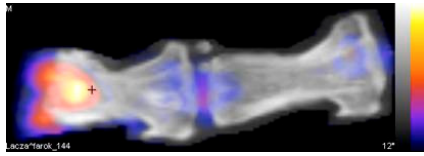


Figure 12 μ -CT of nHA incorporated in rats (red area).

In co-operation with Budapest Technical University, we studied the bone (femur) resistance to applied mechanical loads. Introduction and comparison of material models was also performed. We divided the bone to epiphysis region and corticalis region, and adopted to them the material models of

cortical bone, and spongy bone. Our results in Finite Element Analysis (FEA) show that there can be big differences between bone answers to loads according to different material models. Large forces effects the bone in vertical direction, but the vertical displacement was not so significant comparing to the horizontal values, even the horizontal forces were 15% of the vertical force. As resulted, there will be no higher stress values in the implant then the limit value, though the radius of the implant has a pronounced effect on the evolving stresses (Figs. 13 and 14).

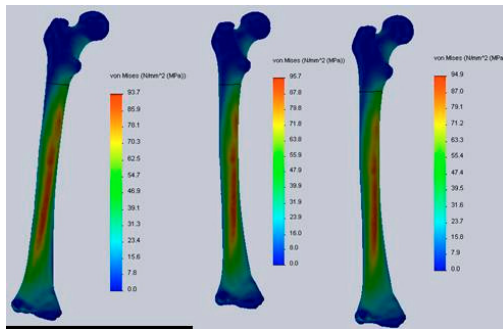


Figure 13 Stress field in different material models of bone.

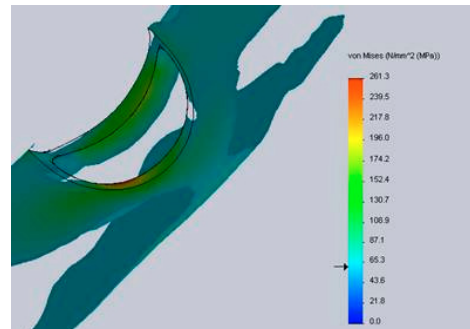
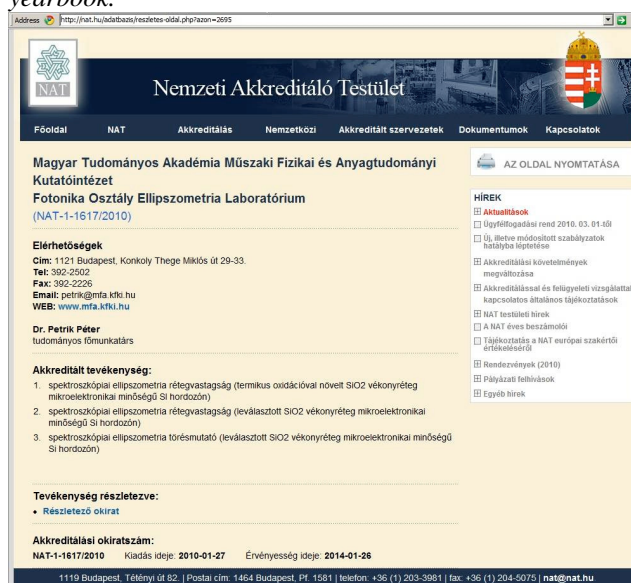


Figure 14 Results showing 65 MPa or higher stresses near implant.

As resulted, the bone regeneration process should allow applying loads to the bones to assure building up a strong bone tissue. In the beginning of the regeneration process the implant should take a larger load from the missing bone tissue, but by time it would be better if the new bone is getting more and more load to prevent osteoporosis. The ideal material of the implant is similar to the bone tissue, helps the bone tissue to regenerate and after regeneration it disintegrates.

NOTABLE EVENTS

According to the below registration displayed on the official [website](http://www.nat.hu) of the Hungarian National Office of Accreditation (NAT), **our ellipsometry laboratory** (of the Photonics Department) **became an accredited Test Laboratory**. Using specially developed optical models, the Laboratory offers services for partners in research and industry to determine thin layer thickness with sub-monolayer resolution, as well as to assess composition and surface quality of various materials. The offered services are described in the leaflet attached to this yearbook.



The screenshot shows the official website of the Hungarian National Office of Accreditation (NAT). The page is titled "Nemzeti Akkreditáló Testület" and features a navigation menu with options like "Főoldal", "NAT", "Akkreditálás", "Nemzetközi", "Akkreditált szervezetek", "Dokumentumok", and "Kapcsolatok". The main content area is for the "Magyar Tudományos Akadémia Műszaki Fizikai és Anyagtudományi Kutatóintézet" (Research Institute for Technical Physics and Materials Science) and its "Fotonika Osztály Ellipszometria Laboratórium" (Photonics Department Ellipsometry Laboratory), with accreditation number NAT-1-1617/2010.

Elérhetőségek
 Cím: 1121 Budapest, Konkoly Thege Miklós út 29-33.
 Tel: 392-2502
 Fax: 392-2226
 Email: petrk@mta.kti.hu
 WEB: www.mta.kti.hu

Dr. Petrik Péter
 tudományos főmunkatárs

Akkreditált tevékenység:

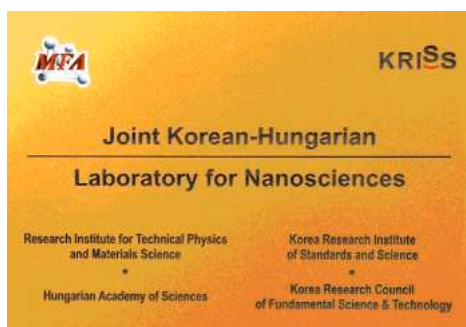
1. spektroszkópiai ellipszometria rétegvastagság (termikus oxidációval növelt SiO₂ vékonyréteg mikroelektronikai minőségű Si hordozón)
2. spektroszkópiai ellipszometria rétegvastagság (leválasztott SiO₂ vékonyréteg mikroelektronikai minőségű Si hordozón)
3. spektroszkópiai ellipszometria torésmutató (leválasztott SiO₂ vékonyréteg mikroelektronikai minőségű Si hordozón)

Tevékenység részletezve:

- Részletező okirat

Akkreditálási okiratszám:
 NAT-1-1617/2010 Kiadás ideje: 2010-01-27 Érvényesség ideje: 2014-01-26

1119 Budapest, Téliúti út 62. | Postai cím: 1464 Budapest, Pf. 1681 | telefon: +36 (1) 203-3981 | fax: +36 (1) 204-5075 | [nat@nat.hu](http://nat.hu)

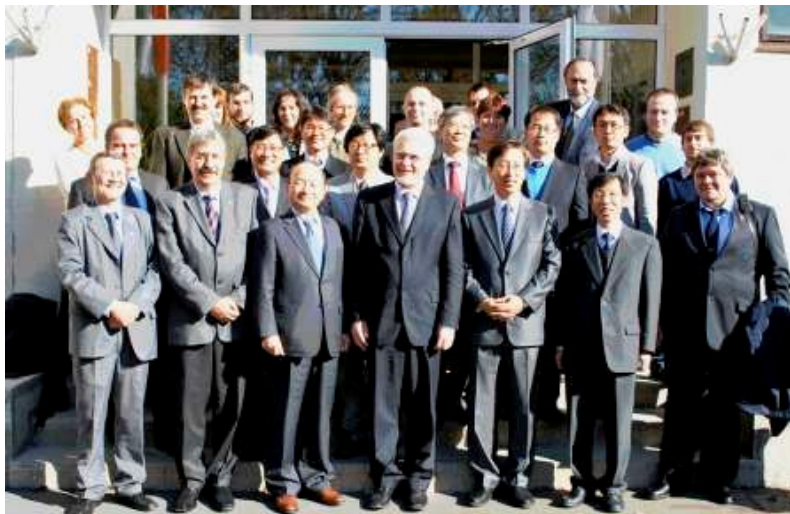


The official opening of the **Joint Korean-Hungarian Laboratory for Nanosciences** took place on 24 October 2010.

The Hungarian and Korean principal investigators, Prof. László P. Biró and Dr. Hwang Chan-Yong introduce the graphene-project to Prof. Park Yong-Ki, the Vice-president of KRISs, Mr. Suh Chung-Ha, the Ambassador of the Republic of Korea in Hungary, Prof. Min Dong-Pil, Chairman of KRCF, and Prof. József Pálinkás, the President of HAS.

Group photo taken in front of the main building of MFA after the official opening ceremony of the Joint Korean-Hungarian Laboratory for Nanosciences at MFA.

In the centre of the front row Prof. J. Pálinkás, the President of HAS, flanked by Prof. Min Dong-Pil, Chairman of KRCF (left) and Mr. Suh Chung-Ha, the Ambassador of the Republic of Korea in Hungary (right).



*On 24 March 2010 Prof. József Pálinkás, the President of the Hungarian Academy of Sciences opened the operation of the **north-wing of the MFA clean-room technology complex** in Building 29. Dr. Tsuneo Morita, the President of Tatemaya Hungary introduced the planned activities of the Tatemaya Satellite Office in this building.*

In the audience the first row from left: Prof. Tamás Roska and Prof. Judit Gaizler-Nyéki (Pázmány Péter Catholic University), Dr. Tsuneo Morita (Tateyama Hungary) and István Krafcsik (BudaSolar Ltd).



*The representatives of the press and the President of HAS were informed about the activities of the new **Thin Film Solar-Lab** operated jointly by MFA and BudaSolar Ltd. by Dr. István Krafcsik.*

High School Relations

MFA always helps talented young scientists become the best possible in their research area. Also, we realize the importance of the propagation of natural sciences to the wider public, especially to secondary school students. We would like to give them a chance to test themselves in science, well before the decision about their future profession. For this purpose we organize open days (called “**MFA Nyílt Nap**”) to show our laboratories to the general public, and a special science camp (called “**MFA Nyári Iskola**”) for selected high school students coming from the whole Carpathian basin. Even after these occasions we do our best to follow (and help) their progress. We see education and learning as an integral process, and in this spirit our most successful young researchers in the previous generations are the mentors of the next generation.



Gábor
Vásárhelyi

Levente
Tapasztó

Péter
Nemes-Ince

Not less than three young scientists of the MFA were awarded by the Junior Prima prize during the last few years in the fields of electro-mechanics and graphene!

Open Days of MFA:

Our open days are more and more popular, so beside the **official** one (held at 12 November 2010) we organized several more for larger groups of students from the high schools Deák Téri Evangélikus Gimnázium, Károlyi István Gimnázium, and Leövey Klára Gimnázium - to name a few. Being a multi-disciplinary research institute, we have exciting laboratories to display for almost anybody!

Also, heartened up by the success of the last year's scientific speeches, we delivered even more of them on various subjects from the evolution of music through the quantum mechanical tunneling effect to nanotechnology (below).

From left: Zoltán Juhász, György Szabó, Géza István Márk, János Volk, István Bársony





MFA summer camp for high school students:

Between June 21-25, 2010 we organized this program already for the 3rd time, under the motto *'Let's learn from each other!'* (organized by Csaba Sándor Daróczi). There were about **23 scientific themes** offered to the **students**, and later to work on them under the guidance of our colleagues. From the Hungarian speaking applicants 23 were selected. MFA fully financed their participation (travelling, subsistence, evening social programs, etc.). Our students looked very busy in the working hours, and happy during the social programs, or both ☺.



Who said that science is boring??



Several of our summer camp students already wrote their first scientific articles about the work they had done at MFA, in the periodical „Élet és tudomány” (Ádám Benedek [15], Kata Ferenc [33], Ágnes Kúsz [75], András Simon [119], Réka Tuza [146].) We also know (from first hand), that since the appearance, there are more regular readers of the ET in their schools...



SCIENTIFIC REPORTS

Nanostructures Department

Head: Prof. László Péter BIRÓ, D.Sc., scientific advisor

Research Staff

- Zsolt Endre HORVÁTH, Ph.D.,
Deputy Head of Department
- Prof. József GYULAI, Member of the
HAS (Professor Emeritus)
- Antal Adolf KOÓS, Ph.D. (on leave)
- Géza István MÁRK, Ph.D.
- Zoltán OSVÁTH, Ph.D. (on leave)
- Levente TAPASZTÓ, Ph.D.
- Krisztián KERTÉSZ, Ph.D.
- Enikő HORVÁTH, Ph.D. (maternity)
- Zofia VÉRTESY, Ph.D.

Ph.D. students / Diploma workers

- Gergely DOBRIK, Ph.D. student
- Péter NEMES-INCZE, Ph.D. student
- Péter Lajos NEUMANN, Ph.D.
student
- Bernadeth PATAKI, Ph.D. student
- István TAMÁSKA, Ph.D. student
- Péter VANCSÓ, Ph.D. student

- Gábor MAGDA, diploma worker
- Vince OBRECZÁN, diploma worker
- Gábor PISZTER, diploma worker

Technical Staff

- Zoltánné SÁRKÁNY, technician

The Nanostructures Department has an almost two decades expertise in the production and characterization of various nanostructures. In recent years in the focus of work were various carbon nanostructures (CNTs, graphene and few layer graphite) their nanoarchitectures, bioinspired photonic nanoarchitectures and applications of these nano-objects in various fields in nanotechnology, nanoelectronics, sensorics and environmental protection. The most relevant results in 2010 are detailed below:

We showed that the color changes of various lepidoptera wings on water vapor condensation, is useful in the identification of the wings colored by photonic nanoarchitectures. Possible applications were identified in display technology.

Using FIB nanomachining and controlled oxidation we produced bioinspired photonic nanoarchitectures from graphite.

Combining experimental data and modeling we explained the visual aspect of the silver butterfly *Argyrophorus argenteus*.

The gas/vapor sensing properties of individual MCNTs and SWCNT ropes were compared with the behavior of random mats of the same materials. The data indicate that the sensing of mats is dominated by the intertube contacts.

In the time sequence of charge spreading in graphene we evidenced two distinct regimes: the first is dominated by molecular spreading, in a later stage switchover takes place to preferential spreading along the zig-zag directions.

Successful experiments were carried out to combine electron beam lithography with the carbothermal etching (CTE) of graphene developed by us.

For more details, please feel free to visit the web page of the Nanostructures Department (link: <http://www.nanotechnology.hu/>).

Colour changes on cooling of Lepidoptera scales containing photonic nanoarchitectures

(OTKA-NKTH K067793)

I. Tamáska, K. Kertész, Z. Vértesy, Zs. Bálint (HNHM, Hungary), A. Kun (HNHM, Hungary), S-H. Yen (LNRC, Taiwan), L. P. Biró

The colour of butterfly wings may be produced by light absorbing pigments (chemical colour) or by photonic crystal type nanoarchitectures built of two components: chitin and air (physical colour), eventually by the combination of these. Most butterfly wings are hydrophobic, this prevents water to penetrate into the photonic nanoarchitecture. We presented a simple method, using a refrigerator, to avoid the hydrophobic effect and to observe the colour change of butterflies coloured by nanoarchitectures (Fig. 1). This method can be used to test easily if the butterfly has photonic crystal type structures or not. It was also shown that when water condensates into the structures, the wings become softened, this allows to set the collected butterflies easier and faster than the technique commonly used today.

Detailed spectroscopic experiments were done in a complete cooling cycle (dry status, below the dew-point where condensation can begin, freezing, melting and the evaporation process (Fig. 2)). The experiments were done on a Peltier cooler to ensure the controllability. It was shown that the duration, the magnitude, and the way in which colour change occurs, is specific for a certain structure (species) but small variations may occur from individual to individual.

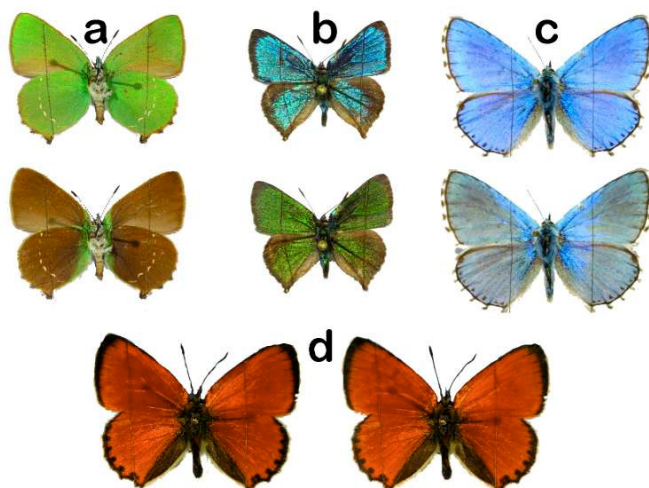


Figure 1 Butterflies cooled in the refrigerator. a), b), c) are species with, and d) without photonic structures in their scales. The colour change can be seen on butterflies with photonic nanostructures. Under identical conditions the butterfly coloured by pigments d) did not change colour.

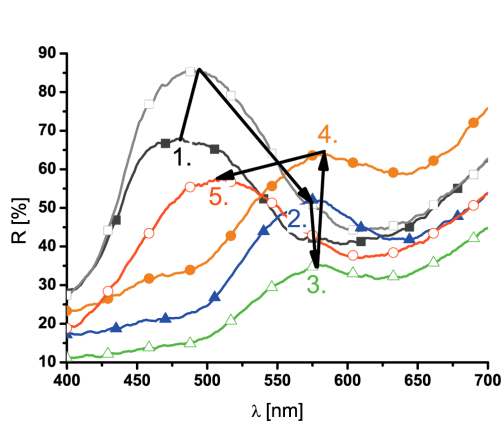


Figure 2 Spectral measurements on the blue (dorsal) surface of the wings of *Cyanophrys remus* butterfly when cooling them. The numbered curves show the stationary reflection maximums in various stages: 1. dry status; 2.: condensation; 3.: freezing; 4.: melting; 5.: evaporation processes.

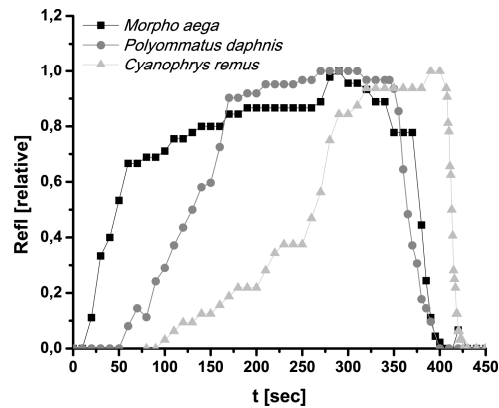


Figure 3 The time dependence of the reflection maximum shift. The cooling was turned off at 350 sec. for *Morpho aega* and *Polyommatus daphnis*, and at 400 sec. for *Cyanophrys remus*. The reflectance of the curves was normalized to see the relative change.

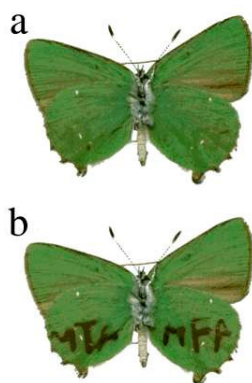


Figure 4 The butterfly *Callophrys rubi* was placed onto cooled wires that were used to form characters (a). After 1 minute (b) the cold wires cool the area around them where the condensation can begin.

Different butterfly wings exhibit differences in the time elapsed from starting the cooling till the colour change is clearly observed. This can be explained if the differences in the nanoarchitectures generating the colour are taken into account. A longer time is needed for the penetration of the air carrying the water vapours into a more closed structure. The colour change of the examined species lasts from a few seconds to even a minute. The shifts of reflectance maximum of the spectroscopic measurements were studied in detail (Fig. 3). Although some difference occurs, the shape of the curves in samples from one butterfly species is very similar. Repeated cooling cycles were also done to examine the long term behaviour of the wings. The colour of the wing during the cycles was slowly faded, because chitin slowly absorbed the water in the structure and became softened. Drying the samples for a few days fully restored the initial conditions of the wings.

If local cooling is provided, for example by thin copper wires, it is possible to “write” on wings possessing structural colours (Fig. 4). This may open up new ways for producing large size flat panel displays operating with photonic nanoarchitectures like those occurring in butterfly scales.

Bioinspired photonic nanoarchitectures from graphitic thin films

(OTKA-NKTH K067793)

I. Tamáska, G. Dobrik, P. Nemes-Incze, K. Kertész, E. Horváth, G. I. Márk, T. Jászi, P. Neumann, Z. E. Horváth, and L. P. Biró

Graphite is a well known material, graphitic samples can be produced at low cost by exfoliation or by chemical vapour deposition. It is black which means it absorbs any stray light without the need of any absorptive pigment that may be needed to enhance the color arising from the structure. Bioinspired, regular, rectangular (with periodicities of 600 nm and 700 nm), and random (with average characteristic distances of 600 nm and 750 nm) two dimensional (2D) photonic nanoarchitectures were produced in graphite. Similar to the structures that were found in a Taiwanese beetle: *Trigonophorus rotschildi varians*. The random pattern was derived from a two dimensional hardcore model, by randomizing the arrangement of spheres with uniform radius on a plane.

Focused Ion Beam (FIB) nanomachining was used to create hole patterns with a well focused Ga^+ ion beam, then the diameter of the holes was increased by four subsequent controlled oxidation steps in 650°C . It is worth pointing out that an extremely thin layer (60 nm) is responsible for the color generation.

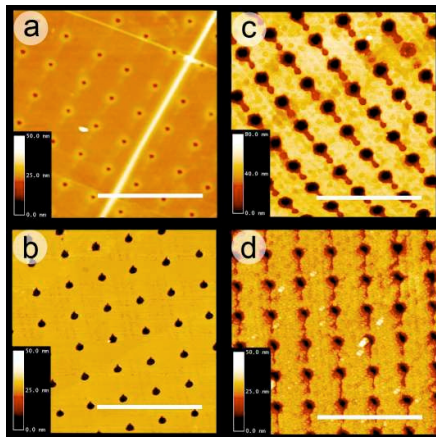


Figure 1 T-AFM images of the larger regular pattern square (rectangular arrangement of holes with lattice distance of 700 nm) after different technological steps: (a) after FIB etching of holes (b) after the 1st oxidation step, (c) after the 4th subsequent oxidation step, (d) after the deposition of 90 nm thick conformal alumina layer by ALD. Scalebar: 2.5 μm .

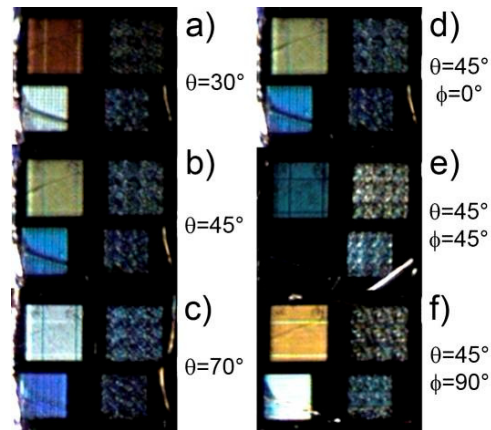


Figure 2 Optical micrographs of the group of four patterned squares (left: rectangular arrangement of holes with lattice distance of 700 nm and 600 nm, right: random arrangement of holes with average hole distance of 750 nm and 600 nm) at different angles of illumination with respect to the sample normal (angle θ), and rotation with respect to the rows of the regular pattern (angle Φ).

After oxidation the patterned structures show different colors in off-specular geometry that depend on the illumination angle, the period, diameter and regular or irregular arrangement of the holes (Fig. 1) while the regular patterns exhibit strong angle dependence, the random ones have fairly constant color under the various illumination conditions. Under the same illumination and observation conditions the random patterns show a significantly weaker dependence of the color on the average periodicity of the pattern as compared with the regular square patterns. Another difference is that when the angle of illumination was fixed and the sample was rotated in its plane, the colors of the regular patterns show a large variation, the random pattern exhibit a remarkable constancy in color. These results clearly show that random two dimensional nanoarchitectures may find applications in achieving structural colors which are not dependent on the direction of illumination and observation, or present only a moderate angular dependence.

A further possibility for the tuning of the color of the nanoarchitectures is given by depositing conformally thin films on the nanopatterned surface. First simulations were carried out to estimate the effect of various layer thicknesses. In the simulations only a 2D model was used, a 70nm blue-shift was found with 90nm alumina layer in agreement with experimental data by the conformal deposition of 90 nm Al_2O_3 with Atomic Layer Deposition technique (Fig. 2).

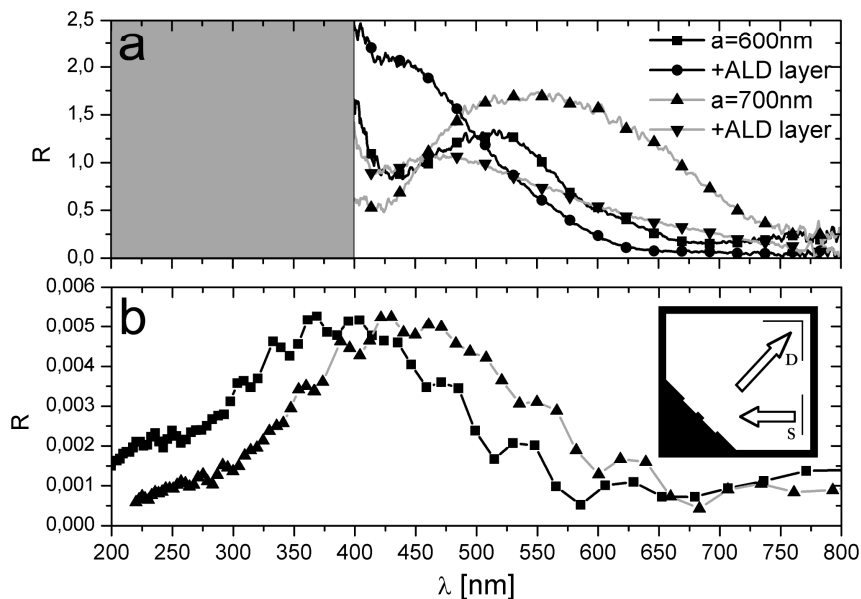


Figure 3 (a) Spectroscopic microreflectance spectra of the rectangular patterns with lattice distance of 600 nm and 700 nm after the 4th oxidation step and after the subsequent alumina deposition (angle of illumination 45°, the optical axis of the microscope is perpendicular to the sample surface). In the gray region the absorption of the measured data. (b) Numerical simulation of the reflectance spectra with the same geometry using a 2D finite-difference time-domain (FDTD) method. Inset shows the applied model sample geometry.

Silver color production by a novel biologic nanoarchitecture

(OTKA-NKTH K067793, EU7 BioPhot-12915)

G. I. Márk, K. Kertész, Z. Vértesy, Zs. Bálint (HNHM, Hungary), and L. P. Biró

Metallic silver and gold appearance is sometimes seen in insects. At a first glance this may be intriguing as their wings and elytra are constituted of chitin, a transparent biopolymer. The structure behind the silvery aspect of beetles may be a so called “chirped” multilayer. When the multilayer periodicity is not uniform, a broadband reflection may occur. The total thickness of the broadband reflector is 10 μm or more in these systems. Silver and gold colors are rare in butterflies. The South Andean butterfly *Argyrophorus argenteus*, Fig. 1, however, has a metallic silver appearance. As shown on Fig. 2, its reflection is unsaturated, independently of the direction of the illumination. Butterfly wing scales, however, have a limited thickness, in the range of 1 μm . Hence the broadband reflection can not be produced by a “classical” chirped multilayer.



Figure 1 Dorsal wing surface of an *Argyrophorus argenteus* exemplar

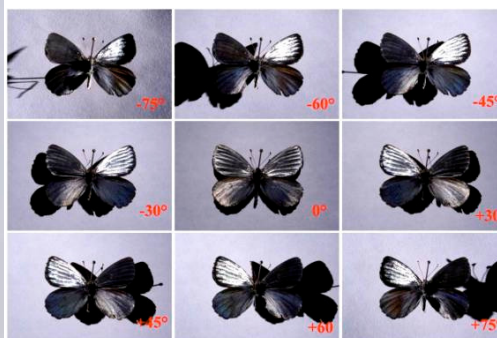


Figure 2 Photograph with changing illumination direction. The light source is moving along a horizontal semicircle and the camera is fixed

The silver reflectance in this case is produced by an optical nanoarchitecture where the lattice periodicity is varying laterally. As seen in the optical micrograph of an individual scale, Fig. 3, there are strips parallel to the ridges and the strips are composed of sections with different colors. The net effect of these microscopic sections gives a broadband reflectance. Based on the SEM and TEM images of Fig. 4 each scale is composed of long channels. Each channel contains a basal chitin sheet and a roof like upper chitin sheet. We model the scale structure with two dielectric sheets of $n=1.56 + 0.06i$ index of refraction (chitin). Because of the small thickness and the small index contrast we can utilize First Born Approximation. The total electric field reflected by the two chitin layers is given by the Fresnel formula as:

$E_2^{tot} = E_{in} (tt're^{-ik(2d-2l)} + tt'tr'e^{-ik(4d-2l)})$, where E_{in} is the electric field of the incoming light, t and r are the transmission and reflection values at the air-chitin interface and t' and r' are the transmissions and reflections at the chitin-air interface, d is the thickness and l is the distance of the chitin sheets.

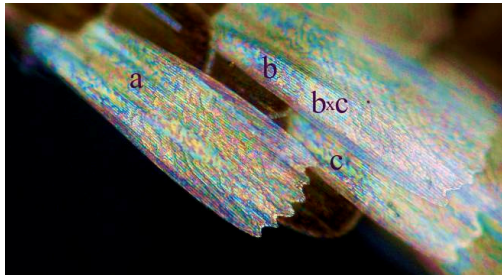


Figure 3 Optical micrograph of individual dorsal wing scales. “bxc” denotes the region where scales b and c overlap. Length of the scale is 200 μm

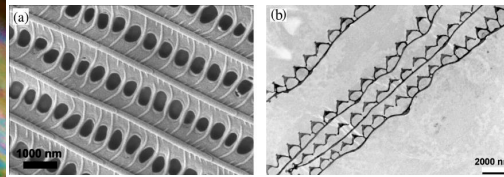


Figure 4 Scanning- and transmission electron micrographs of a dorsal scale (Fig. a, and b, respectively)

Reflectance spectra calculated from the First Born Approximation are shown on Fig. 5. Next we calculated the reflected colors in the CIE 1931 colour space, Fig 6.

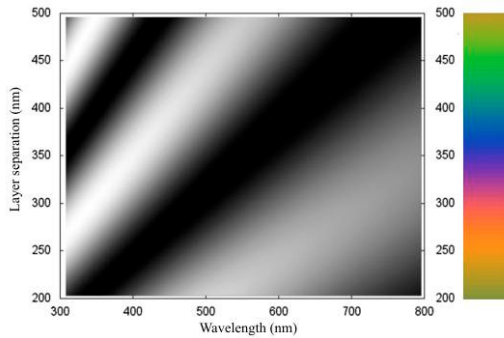


Figure 5 Calculated reflectance spectra for different layer distances. Black corresponds to zero intensity and white to maximum intensity. The colour bar on the right shows the colors calculated from the spectra for the different layer distance

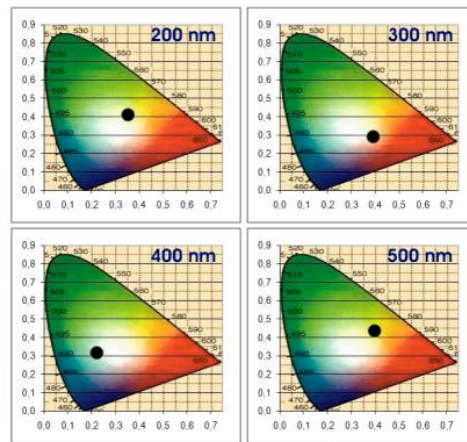


Figure 6 Reflected colors of the two chitin layer model in the CIE 1931 colour diagram for several layer distances. The black dot denotes the calculated colour

The experiments and model calculations show that in a thickness of only 1 μm , natural evolution, using very different “design principles” than human technology, has created a very efficient chirped mirror which generates silver aspect under any angle of observation.

Charge spreading in graphene

(OTKA-NKTH K67793)

G. I. Márk, P. Vancsó, Ph. Lambin (FUNDP, Belgium), and L. P. Biró

The exponential decrease of physical feature size of silicon based integrated circuits over time is expected to reach a physical limit in some years. One of the promising candidates to exchange silicon is graphene. It is a one-atom-thick sheet of sp^2 bonded carbon atoms arranged in a honeycomb lattice. Graphene is different from the semiconductor materials commonly used in microelectronics, because it has a linear energy dispersion relation near the Fermi level. The near-to-Fermi-energy behavior of graphene has been extensively studied in the recent years theoretically and experimentally. Less is known about the high excitation energy range when $E-E_F > 1\text{eV}$. Electron beam splitting, collimation, and beam-guiding can all be realized in the hot-energy region, where the dispersion relation, which is isotropic near the Fermi energy, becomes anisotropic.

By using wave-packet dynamical simulations, we demonstrate that the electronic wave packet, when tunneling from a sharp STM tip into the graphene sheet, selects higher energy states, the lower energy components may tunnel back into the tip. The geometry of the wave packet transport calculation is shown in Fig. 1. We modeled the graphene sheet by a local one electron pseudopotential designed to match the ab-initio band structure of the graphene sheet as best as possible. The STM tip is represented by a jellium background model. The tip is taken as a hyperboloid of 0.5 nm apex radius and 15° aperture angle. The jellium potential is zero outside the effective surface of the tip and -9.81 eV inside. A Gaussian wave packet is injected into the graphene sheet from the simulated metallic STM tip with central energy E_F .

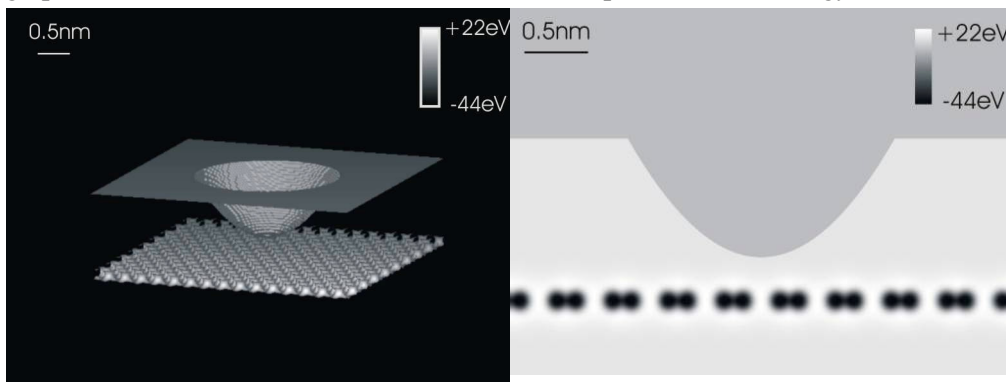


Figure 1 Model geometry of the STM tip – graphene system shown by the -2.7 eV equipotential surface of the potential.

Figure 2 Grayscale image of the 2D cross section of the potential. Black (white) denotes negative (positive) potential values.

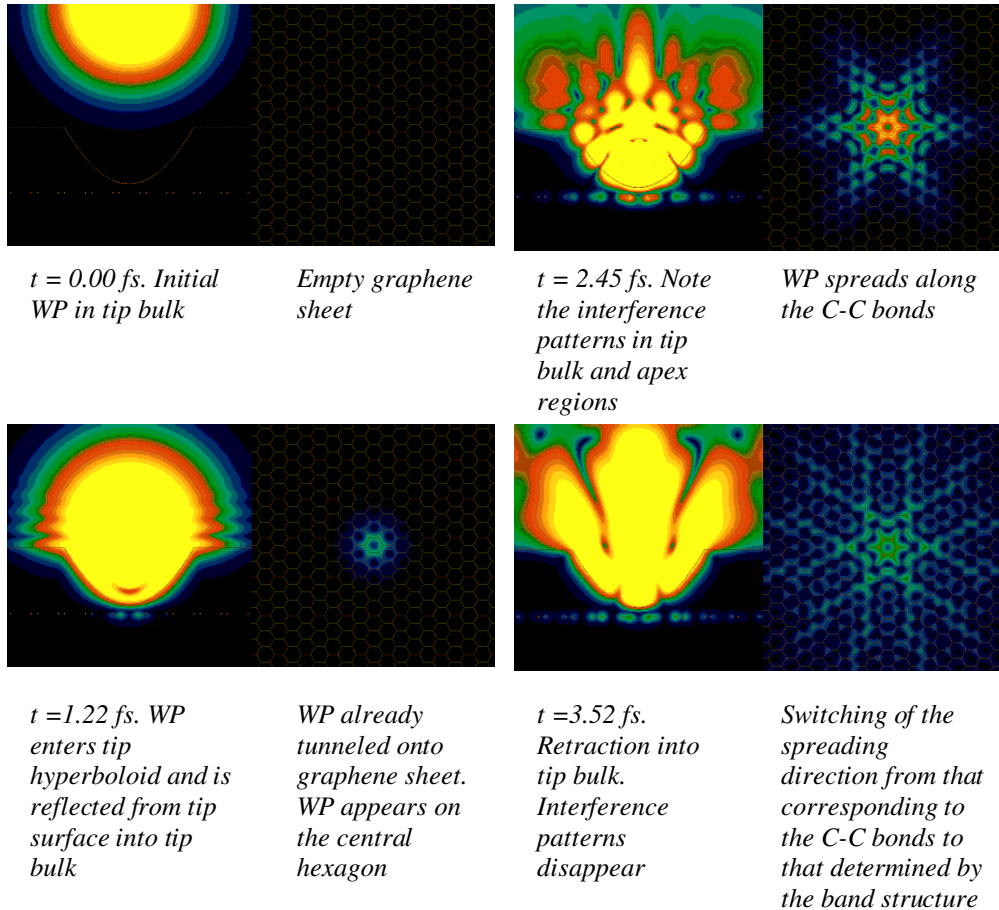


Figure 3. Selected snapshots from the time evolution of the probability density of wave packet shown as color coded 2D sections. Left hand side images are XZ (vertical) 2D sections, right hand side images are YZ (horizontal) 2D sections

Fig. 3. shows the details of the time evolution of the wave packet. As the wave packet reaches the tip apex from inside the tip bulk, it begins to tunnel onto the central hexagon. Then the wave packet begins to spread on the graphene sheet along the C-C bonds, in hexagonal symmetry. At $t = 3.14$ fs, the direction of the spreading is changed. Further spreading occurs along the 6 Γ K directions of the Brillouin zone. Spectral analysis of the spreading state shows a large peak around $E_F + 2.5$ eV. For a sharp tip the width of the tip-sample tunneling channel is approximately 0.1–0.2 nm. From the uncertainty relation we obtain an energy uncertainty 2 eV, which explains the appearance of hot carriers. In summary, our simulations show that it is possible to inject hot carriers into a graphene sheet by the utilization of a localized contact. These hot carriers cause an anisotropic spreading of the electronic wave packet along the zigzag directions. By patterning the graphene sheet into specific ribbons and junctions it is potentially possible to build all-carbon nanoelectronic circuits.

Comparison of the chemical sensing properties of individual carbon nanotubes and their mats

(OTKA T049182, OTKA-NKTH K67793)

G. Dobrik, Z. E. Horváth, V. Obreczán, P. Neumann, and L. P. Biró

The electronic structure of carbon nanotubes (CNT) is very sensitive to the chemical ambient. Transport in CNT is dominated by delocalized π electrons located outside the plane of the carbon-carbon bonds. Therefore, interaction between CNT and ambient molecules is usually strong enough to modify the electronic transport, molecules adsorbed on CNT surface act as scattering centers. This phenomenon is the basis of the chemical sensing properties of CNT. However, CNT sensors in practice are usually made of CNT mats because they can be prepared much easier by conventional methods and tools used in a basic chemical laboratory, while contacting individual CNT is very labor-intensive and needs special nanotechnology equipment. Mats can be regarded as random networks of CNTs. Their transport properties are determined by both individual nanotubes involved in the network and the CNT-CNT junctions. In this study, we compared the chemical sensing properties of two different CNT materials in individual and mat form in order to estimate the contribution of the CNT-CNT junctions to chemical sensing. We prepared resistive elements of individual CNT and CNT mats of the same origin and compared the effect of gas ambient change on them. Two types of CNT were used, an as purified multiwall CNT sample grown by CVD and an arc-grown single wall sample functionalized with carboxylic groups, here the SWCNTs are assembled in bundles. Mat samples were prepared by filtering CNT suspension through a polymer membrane filter. The CNT mat self-assembled on the filter was contacted by evaporating gold through a simple mask on 2 smaller areas on opposite sides of the round shaped mat. For contacting individual CNTs, diluted suspensions of them were spin-coated on marked Si/SiO₂ substrate.

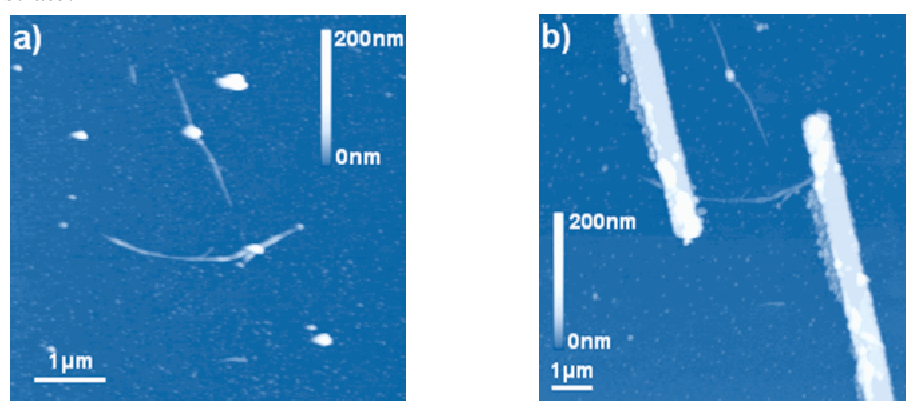


Figure 1 Tapping mode AFM images of SWCNT bundles a): as deposited on marked SiO₂ substrate, b): the same area after contacting one of the bundles with two Cr-Au electrodes prepared by e-beam lithography.

Atomic Force Microscopy (AFM) was used to locate a few separated nanotubes or bundles on the surface. Contacts were deposited on them using a standard electron beam lithography process. Electrodes were prepared from 5 nm thick Cr and 35 nm thick Au films. Fig. 1 shows AFM images of a SWCNT bundle before (left) and after (right) contacting. Responses on six different vapors (ethanol, acetone, toluene, acetic acid, chloroform and water) diluted in pure nitrogen gas were recorded. A few typical response curves are shown in Fig. 2.

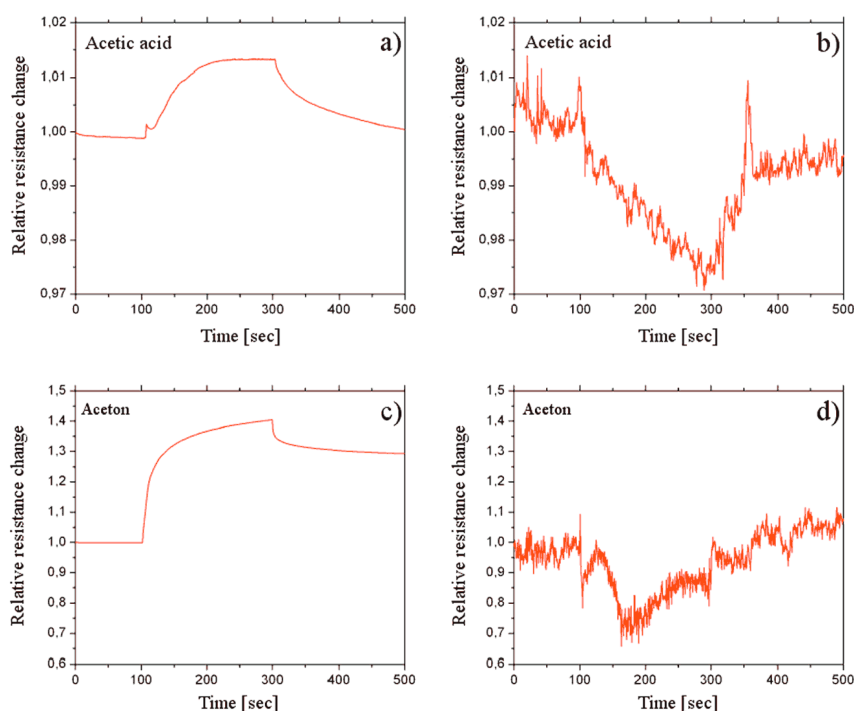


Figure 2 Comparison of relative resistance responses of random network (a: SWCNT network, -COOH functionalized, c: MWCNT network, as purified) and individual CNT (b: single bundle of the same material as a, d: individual tube of the same material as c) sensors on chemical ambient change: pure nitrogen flow was changed to acetic acid vapor (a and b) or acetone vapor (c and d) at 100 sec and changed back to nitrogen at 300 sec.

We used much lower measuring current in case of individual CNT which led to higher noise levels (see Figs. 2b and d) but it was required to prevent their damage. Disregarding the noise, we found substantially different behavior of the individual and mat samples. The increase of the resistance was observed in case of the mat samples for all the vapors, while some of the individual samples exhibited opposite behavior to their mat counterparts. This finding indicates that the role of CNT-CNT junctions in chemical sensing of CNT mats is more important than it has been supposed. We are planning further investigations of this field to clarify the details.

Graphene nanopatterning with EBL and carbothermal etching

(OTKA-NKTH K67793)

P. L. Neumann, E. Tóvári (BME), S. Csonka (BME), P. Nemes-Incze, Z. E. Horváth, and L. P. Biró

Being a zero gap semiconductor, graphene is not suitable for preparation of FET devices because of the missing “off” state [A. K. Geim and K. S. Novoselov, *The rise of graphene*, Nature Materials 6 (2007) 183.]. A straightforward way to overcome this is to cut ribbons of a few nanometers width with controlled edge orientations. In a previous paper, we showed that carbothermal etching (CTE) [98] is a useful technique to make preferentially zigzag oriented ribbons or other formations (SET, Y branch, spin device, etc.) with various sizes. This method was based on the controlled oxidation of graphene in inert atmosphere, where the oxygen source is the SiO₂ substrate. Oxidation takes place at defect sites, including the edges. Defects produced by AFM indentation were starting points of the formation of hexagonal holes with uniform size.

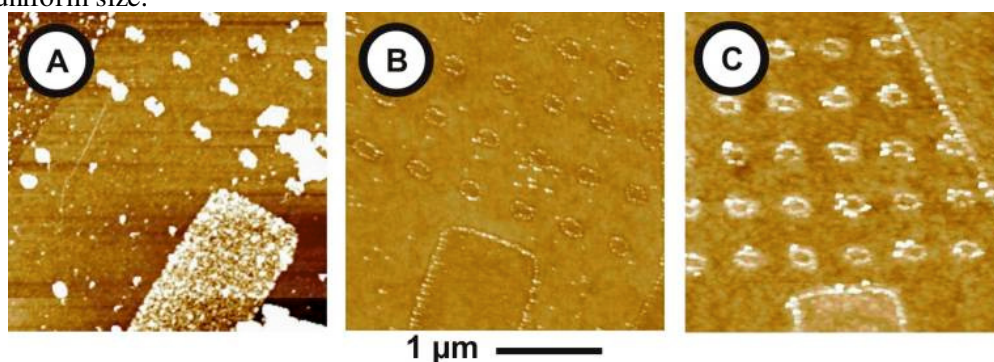


Figure 1 AFM images of a patterned graphene flake on Si/SiO₂ substrate: A) after Ar/O₂ plasma etching; B) after annealing in Ar atmosphere at 300°C; C) after annealing in air at 300°C.

In the present study, we applied electron beam lithography (EBL) followed by O₂/Ar plasma etching for patterning. These methods are more effectively applicable for patterning larger areas but the applied processes can modify the surface chemistry of the samples causing unwanted side effects. Covering the sample with PMMA, the required patterns were shaped by electron beam lithography. The plasma with suitable composition is able to etch the graphene without damaging the PMMA mask layer. The plasma etched areas show protrusions (white spots on AFM image, Fig. 1A) thanks presumably to redeposition of resist material damaged by the plasma treatment. Annealing at 300 °C in inert atmosphere produced the elimination of this residue, besides the decoration of the edges of the plasma treated areas with dust particles (Fig. 1B), connected presumably to the dangling bonds or other defect sites. Annealing at 300 °C in air led to the increase of the dust amount (Fig. 1C).

The extended defect sites prepared by the above described process can be starting points of oxidation in CTE process, similarly to the ones prepared by AFM indentation.

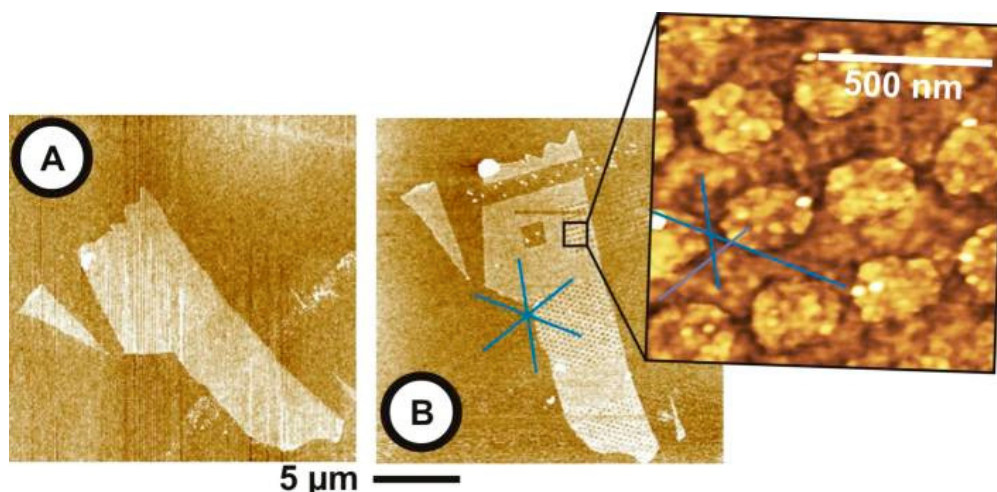


Figure 2 AFM images of a patterned graphene flake (brighter area) on Si/SiO₂ substrate (darker area): A) initial state; B) after tailoring process. The inset shows higher magnification image of the marked region. The holes in the graphene are brighter.

A mechanically exfoliated graphene flake shown on Fig. 2A was patterned with EBL and plasma etching as it was previously described. Two pattern structures with holes in triangular and one in rectangular lattice arrangement were shaped (Fig. 2B bottom and middle). The lattice constant was 300 nm. The blue lines on Fig. 2B show the feasible lattice orientation of the hexagonal graphene structure. Fig. 2B shows AFM image of the shaped sample after a 4 hours annealing at 700 °C in Ar atmosphere. The inset of Fig. 2B shows a higher magnification AFM image with enlarged holes. The average hole size was found to be 200 nm after etching. From this, the etching speed can be estimated as approx. 20 nm per hour. The produced holes have oval form but, in some cases, polygonal edges parallel with the feasible lattice orientation can be recognized.

We expect that the edge quality can be improved by more effective removal of contaminations.



Photonics Department

Head: Miklós FRIED, D.Sc., scientific advisor

Research Staff

- Péter PETRIK, Ph.D., Head of Ellipsometry Laboratory
- Miklós SERÉNYI, C.Sc., Head of Semiconductor Photonics Laboratory
- János BALÁZS, Ph.D. (part-time)
- Antal GASPARICS, Ph.D.
- Norbert NAGY, Ph.D.
- András HÁMORI, dr. Univ.
- Róbert HORVÁTH, Ph.D.
- Csaba MAJOR, Ph.D.
- György JUHÁSZ, dr. Univ.
- Zsolt LACZIK, Ph.D. (on leave)

Technical Staff

- Rózsa Mária JANKÓNÉ, technician

- Tivadar LOHNER, C.Sc.
- János MAKAI, C.Sc. (part-time)
- György KÁDÁR, D.Sc.
- Sándor KURUNCZI, Ph.D.
- Olivér POLGÁR, Ph.D.
- Miklós RÁCZ, Ph.D. (part-time)
- Ferenc RIESZ, C.Sc.
- Gábor VÉRTESY, D.Sc.
- Péter TÖRÖK, D.Sc. (on leave)

Ph.D. students / Diploma workers

- Dániel PATKÓ, Ph.D. student
- Péter KOZMA, Ph.D. student
- Emil AGÓCS, Ph.D. student
- Andrea NÉMETH, BSc student
- Bálint FODOR, BSc student

MFA is involved in the NANOMAGDYE (EU FP7) project with the aim to develop tailored biocompatible magneto-optical nanosystems and to apply them in medical practice. A magneto-optical probe is being fabricated for oncology imaging. In the project, MFA's role was to develop a magnetic sensing system capable of indicating the presence and distribution of the submicron sized magnetic particles. The real challenge of the detection was the very low concentration of the accumulated particles in a typical lymph node. Novel Fluxset sensor and electronics was developed to detect even 0.7 mg of magnetic particles with 2.5 mm of the probe.

A phase shifting optical waveguide interferometer, the so-called Grating Coupled Interferometry (GCI), was demonstrated for label-free evanescent wave biosensing in aqueous solutions. The sensitivity of the instrument for bulk refractive index was proven being below 10^{-6} . The high phase resolution allows the detection of surface adsorbed molecule densities below 1 pg/mm^2 without using any labeling or on-chip referencing.

In Bioellipsometry we have made a significant progress by developing new optical models and flow cells, as well as investigating the adsorption on different substrates, building a new measurement tool combining spectroscopic ellipsometry and grating coupled interferometry, and creating 3D structural and kinetic models. We have developed numerical models in MATLAB programming language to follow the structural change of the flagellar filament structure during adsorption.

Magnetic Adaptive Testing (MAT) is a recently developed nondestructive magnetic measurement method, which is based on systematic measurement and evaluation of minor magnetic hysteresis loops. Very good correlation was found between the optimally chosen MAT parameters and the independently measured other quantities (Brinell hardness and conductivity). MAT seems to be a good method for replacing the destructive hardness measurements by nondestructive magnetic measurements.

Makyoh topography is an optical tool for the qualitative flatness testing of specular surfaces, based on the defocused detection of a collimated light beam reflected from the tested surface. Based on our earlier work, a generalised model of the sensitivity of Makyoh topography was developed for a general surface model, including vision physiological effects. The model gives the amount of observed contrast for periodic surface morphology and isolated defects.

We are involved in two “National technology development” projects: “Development of integrated process monitoring metrology for the 32 nm technology node of IC processes” and “Development of metrology tools based on electrical and optical techniques for in-line and laboratory qualification of thin film solar cells”

Since January 2010 the Ellipsometry Laboratory of MFA is working according to ISO 17025 accredited by the National Accreditation Board. Further details about the laboratory can be found under <http://www.ellipsometry.hu>. Joined to an international consortium in frame of the ANNA project (<http://www.i3-anna.org/>) the Ellipsometry Laboratory provided in total more than 100 units (days) of transnational access (http://www.i3-anna.org/context.jsp?ID_LINK=2&area=8) to the infrastructures of ellipsometry and Makyoh topography. Based on the Transnational Access projects and on the Joint Research Activities the Ellipsometry Laboratory had almost 40 presentations or publications from the ANNA cooperations during the four years of the project.

MFA is involved in a multidisciplinary research project (including photonics, microfluidics, biochemistry and materials science) called P3SENS (www.p3sens-project.eu) which is funded by EU. This Pan-European cooperation aims to develop high-performance, multichannel optical biosensors for the early detection of brain diseases (for instance, to prevent the occurrence of ischemic damage as a result of stroke) from human blood. Among many other tasks MFA functionalizes the photonic biochips with appropriate surface chemistry and tests the receptor performances by a high resolution label-free optical biosensor called OWLS (Optical Waveguide Lightmode Spectroscopy).

New patent measuring arrangement and technique to measure impurities floating on liquid surfaces, especially for water wells was filed “*Mérési elrendezés és eljárás folyadékfelszínen úszó szennyeződések kimutatására, elsősorban monitoring kutakhoz*”. Rácz Miklós 35%, Bársony István 10%, Hámori András 15%, Hidasi János 10%, Makai János 15%, Serényi Miklós 15%. Szabadalmi Közlöny és Védjegyértesítő, 2010. 8. szám, II. kötet. 2010, aug. 30.

NANOMAGDYE

Magnetic nanoparticles combined with submicronic bubbles and dye for oncology imaging

(EU FP7 – GA No 214032)

G. Vértesy, and A. Gasparics

The objective of NANOMAGDYE project is to develop tailored biocompatible magneto-optical nanosystems and to apply them in medical practice. A magneto-optical probe is being fabricated for oncology imaging. Combining optical and magnetic labeling techniques into a single biocompatible nanosystem will provide increased spatial resolution and will avoid currently used ionising radiation based method in order to improve patient safety and medical effectiveness this way.

In the framework of the project MFA has the role to develop suitable magnetic sensing technology for indicating the presence of the submicron sized magnetic particles. These iron-oxide based particles are close to (or already in) super-paramagnetic state due to their dimension. However, the real challenge of the detection is the very low mass of the accumulated particles in a typical lymph node. Novel Fluxset sensor based method has been used to detect the particles with acceptable signal/noise ratio. Fluxset sensor is a high sensitivity magnetic field sensor, developed formerly in MFA, and in this application the sensor is assembled into a measuring head, which generates AC exciting magnetic field. The response of magnetic particles to this field is detected by magnetic field measurement.

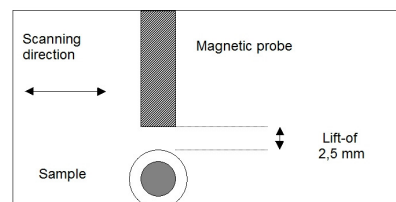
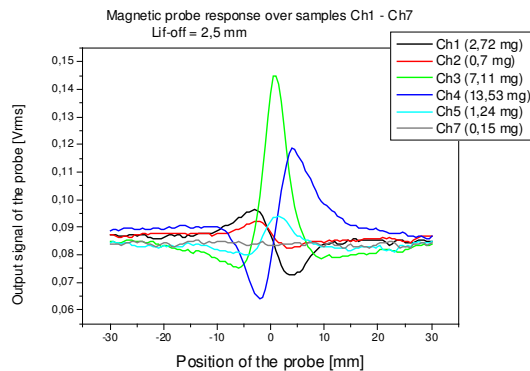


Figure 1 Detection of magnetic particles by moving the probe over samples containing different amount of ferromagnetic particles.

In the first year of the project a magnetic probe has already built and tested, with satisfactory results. To improve the sensitivity of the magnetic probe, an improved version of the device was designed and built. In this version the magnetic excitation is performed by two coils and the magnetic sensor is balanced between the two exciting coils. Such a way significantly higher sensitivity can be reached. The result of the test measurement is given in Figure 1. The magnetic probe was moved over the sample

holder capsules containing magnetic particles according to the scheme of Figure 1 and the output signal of the probe for several different samples is given. As it can be seen on the Figure, even 0.7 mg of magnetic particles can be detected with reasonable signal/noise ratio with 2.5 mm lift-off of the probe.

In order to obtain signal to be evaluated from the magnetic probe response, signal processing chain is also needed to be established. This chain processes the electric signal in both directions. In forward direction it generates exciting signal and magnetic field for exciting the target magnetic nanopartricles to be detected, as well as, for the operation of the applied Fluxset sensor. In backward direction the Fluxset sensor output is processed in two phases: first the sensor pick-up signal is demodulated by the Front-End Electronics and analogue signal as probe response is produced which is proportional to the actual value of the measured alternating magnetic field. Following that the parameters (like amplitude and phase, or real and imaginary part of its complex representation) of this demodulated signal is determined by the Digital Signal Processing (DSP) module. Finally, the DSP provides analogue output according to the requirements of final practical application. The magnetic probe together with DSP module is shown in Figure 2. This is the complete unit, which is ready for in-vivo measurements of small animals.



Figure 2 The magnetic probe and the digital signal processing unit.

Nondestructive characterization of cast iron by Magnetic Adaptive Testing

(OTKA K62466)

G. Vértesy

Cast iron is one of the most frequently used industrial construction materials. Low cost of production, good machinability, and excellent possibilities of shaping the details by casting bring about an intense interest of industry. The cast irons are generally many-component alloys of iron with large content of carbon. The mechanical properties are fundamentally dependent both on the matrix and on the graphite, its shape, size and density. There is a strong demand from the industry to develop reliable, fast and simple ways for non-destructive characterization of this common and frequently used type of structural material. In the present work Magnetic Adaptive Testing (MAT) has been applied for a special series of ductile cast iron. MAT is a recently developed nondestructive magnetic measurement method, which is based on systematic measurement and evaluation of minor magnetic hysteresis loops. It has been shown previously that this method is significantly more helpful than that of the traditional major loop studies.

Four staircase-shaped block specimens with 5 steps each were prepared, as shown in Fig. 1. Pig iron, ferrosilicon (Fe-75%Si) and commercial pure iron were used as raw materials. The melt was cast into shell moulds with staircase shape, and different thickness of each step brought about difference in cooling rate during solidification, which led to different matrices and graphite sizes.

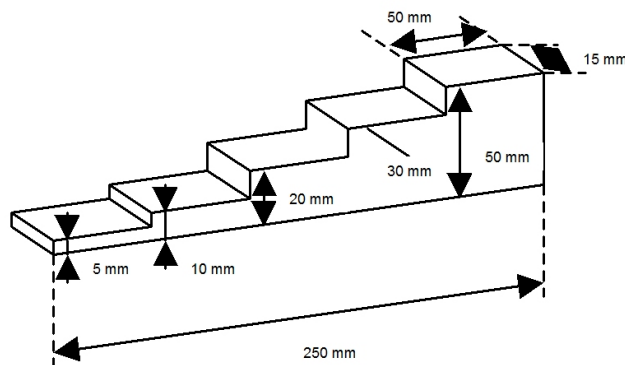


Figure 1 Staircase-shaped specimens of cast irons

The amount of ferrosilicon and of commercial pure iron in the melt was controlled, in order to get different carbon equivalents, C (mass%) $+1/3$ Si (mass%). The targeted carbon equivalent of sample 1 was set to a low value (3.7), in order to have cementite (ledeburite and free cementite) in the matrix. The targeted chemical compositions of samples 2, 3 and 4 were the same, but they were given different heat treatments, in order to have different matrices. Sample 2 was normalized for getting a pearlitic matrix: it was reheated up to 1173 K in an electric furnace, kept there for three hours,

and then cooled in air. Samples 3 and 4 were annealed in different ways to have ferritic matrices. Both samples were reheated up to 1173 K in an electric furnace, and kept there for three hours. After that, sample 3 was cooled in the furnace down to the room temperature, whereas sample 4 was cooled down to 1048 K in the furnace and then brought out to air. The correlation of the nondestructively measured MAT parameters with the destructively determined Brinell hardness and also with the electrical conductivity of samples was studied.

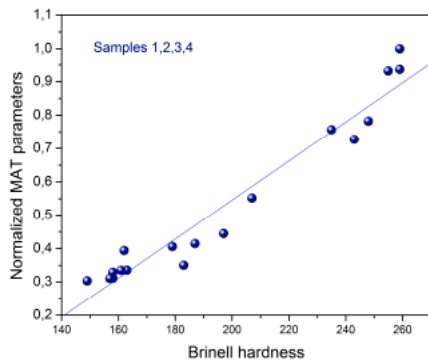


Figure 2 The optimal MAT parameters vs. Brinell hardness.

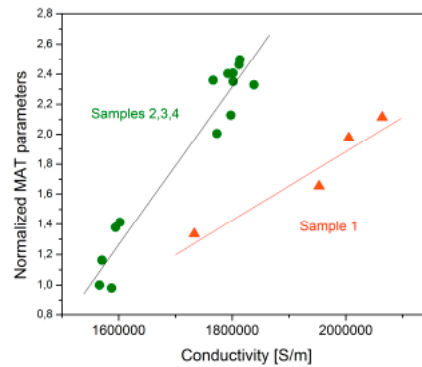


Figure 3 The optimal MAT parameters vs. Conductivity.

Very good correlation was found between the optimally chosen MAT parameters and the independently measured other quantities. In all cases Brinell hardness and MAT parameters correspond to each other very well, linear correlation was found between hardness and the properly chosen magnetic descriptors, as shown in Fig. 2. The presented relationship was found if all the samples (with different chemical compositions and preparation conditions) were considered for the evaluation. A very good correlation was also found between the MAT descriptors and conductivity, but in this case the samples with different chemical composition should be handled separately, as can be seen in Fig. 3. The optimally chosen MAT descriptors of samples 2, 3 and 4, which have rather similar compositions, lie more-or-less on a straight line as a function of conductivity. This is also valid for sample 1, but with a different slope.

This result shows the capability of Magnetic Adaptive Testing very well: MAT parameters reflect modifications of the investigated material. The presented figures demonstrate, that this method feels the difference between the samples, which were produced by different cooling rates, consequently having different matrix structure. Regular correlations were found, with low scatter of the points between the MAT descriptors and other parameters, which are frequently used in industry for characterization of the material integrity. MAT seems to be a good method for replacing the destructive hardness measurements by nondestructive magnetic measurements [148,149].

Makyoh topography

(OTKA K 68534; ANNA, EU 026134 (RII3); MORGaN, EU 214610)

F. Riesz, and J. P. Makai

Makyoh topography is an optical tool for qualitative flatness testing of specular surfaces, based on defocused detection of a collimated light beam reflected from the tested surface. By inserting a square grid into the path of the illuminating beam, the height map can be calculated by integrating the gradients from the grid's distorted image. The spectra of Makyoh imaging of periodic and quasi-periodic surfaces were investigated. We found, that in spite of the non-linear nature of imaging, Fourier representation can still be applied. A criterion was given for the dominant spectral component. Ray-tracing simulations confirmed our predictions. Based on our earlier work, a generalised model of the sensitivity was developed for a surface, including vision physiological effects. The model gives the amount of observed contrast for periodic surfaces and isolated defects. The microscopic roughness of the studied surface causes speckle image pattern. Criteria for the discrimination of the speckle and Makyoh patterns were given and the sensitivity were analysed.

Deformation and surface morphology measurements were also performed on SiC/Si heterostructures, grown by vapour phase epitaxy at IMEM-CNR (Parma), with the final aim to find the optimum growth parameters to obtain stress-free layers having low surface defect density and appropriate flatness. Effects of the substrate's orientation and the pre-growth preparation on the sample deformation were studied. The orientation of the substrate plays an important role in the resulting deformation: the addition of SiH₄ during the carburisation ramp leads to increased deformation for (001) orientation, while decreased for (111). Deformation and morphology measurements were also done on diamond/Si, AlN/Si and GaN/AlGaN/AlN/Si composite substrates. The deformation and interface defects of wafer bonded Si/glass structures and the used substrates were investigated for process optimisation. As an example, Fig. 1 shows the Makyoh image of a bonded structure. The black dots indicate hillocks due to interface imperfections. A middle area of different surface morphology is clearly delineated. In addition, the mechanical stress of hydrogenated amorphous Ge and Si layers, as well as Si/Ge multilayers sputtered onto Si substrates was studied.

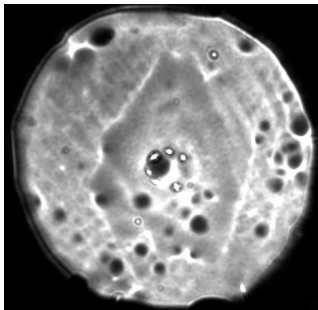


Figure 1 Makyoh image of a wafer bonded Si/glass structure

Study of nanocrystalline diamond films fabricated by Microwave Plasma Enhanced Chemical Vapor Deposition

(OTKA-NKTH-K-68688)

T. Lohner, P. Csíkvári, N. Q. Khánh, S. Dávid, Z. E. Horváth, P. Petrik, and G. Hárs

Optical properties of ultrananocrystalline diamond films were studied by ex-situ variable angle spectroscopic ellipsometry (SE). The films were prepared by Microwave Plasma Enhanced Chemical Vapor Deposition method in the laboratory of Department of Atomic Physics of the Budapest University of Technology and Economics. In the experiments Ar, CH₄, and H₂ gases were used as source gases. Elastic recoil detection analysis (ERDA) was applied to measure the hydrogen content of the deposited layers. Three-layer optical models were constructed for the evaluation of the measured SE spectra. Besides the Cauchy relation, the effective medium approximation and the Tauc-Lorentz dispersion relation was also used for the modeling of the optical properties of the diamond films. Atomic force microscopy was applied to investigate the surface roughness in function of the deposition conditions. The average crystallite size has been estimated from the XRD spectra using the Scherrer formula, values between 11 and 24 nm were obtained for films deposited using various argon concentration in the gas mixture.

The three-layer optical model based on effective medium approximation and on the Tauc-Lorentz dispersion model (Fig. 1.) proved to be the best evaluation method yielding satisfactory agreement between the measured and calculated ellipsometric data in the whole wavelength range. From the experiments we have extracted the thickness of sublayers and the refractive index. The layer growth rate decreases as the argon concentration increases in the gas mixture during the deposition. Evaluation of SE data showed the presence of a considerable amount of non-diamond carbon phase in the sublayer adjacent to the single crystalline silicon substrate. The refractive index of sublayer-2 is plotted in Fig. 2 in function of wavelength for samples prepared in gas mixture with 10%, 70% and 95% argon content, respectively.

Fig. 3 displays the measured and simulated ERDA spectra of sample deposited in gas mixture containing 90% argon. According to Rutherford Backscattering spectra the argon content in the deposited films is below 0.1 atomic percent.

The results were presented on the 5th Int. Conf. on Spectroscopic Ellipsometry, 23-28 May 2010, Albany, NY USA, as poster with author list of T. Lohner, P. Csíkvári, N.Q. Khánh, S. Dávid, Z.E. Horváth, P. Petrik, G. Hárs and with title „Spectroellipsometric and ion beam analytical investigation of nanocrystalline diamond layers”. The paper is in press in Thin Solid Films [<http://dx.doi.org/10.1016/j.tsf.2010.12.061>].

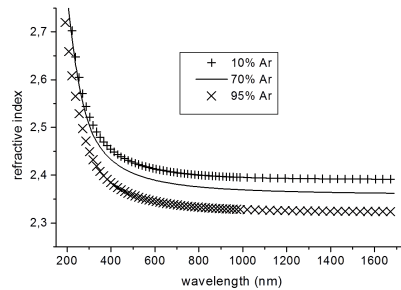
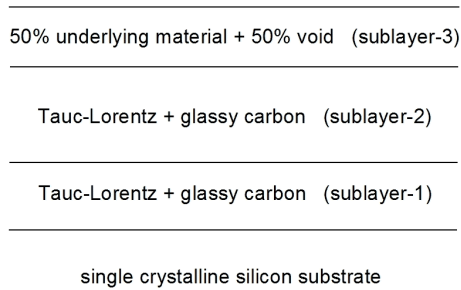


Figure 1 Three-layer optical model based on the use of effective medium approximation and the Tauc-Lorentz dispersion model.

Figure 2 The refractive index of sublayer-2 in function of wavelength for samples prepared in gas mixture with 10%, 70% and 95% argon content, respectively.

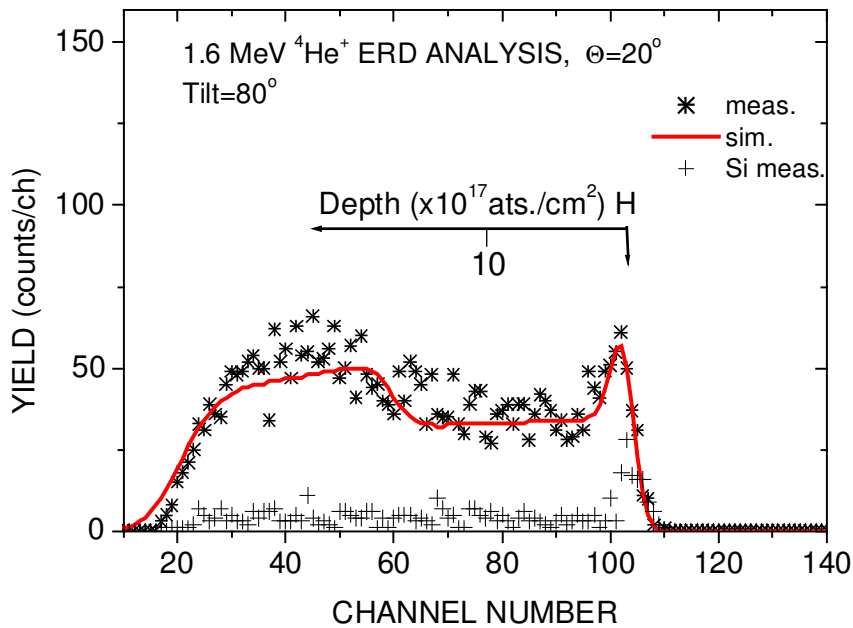


Figure 3 The measured and simulated ERDA spectra of sample deposited in gas mixture containing 1% methane, 9% hydrogen and 90% argon. The spectrum of a clean single crystalline silicon substrate (symbols "+") is also shown for comparison. The average hydrogen content in this sample is about 4 atomic percent.

Fabrication and Investigation of Diffractive Optical Elements Using Ion Implantation

(Hungarian Scientific Research Fund under Grant No. K68688)

T. Lohner, I. Bányász, M. Fried, C. Major, F. Pásztai, and A. Watterich

Tellurite glasses have gained a widespread attention due to their potential as hosts of rare-earth elements for the development of fiber and integrated optic amplifiers and lasers covering all the main telecommunication bands. Er^{3+} doped tellurite glasses in particular are very attractive materials for the fabrication of broadband amplifiers in wavelength division multiplexing around $1.55 \mu\text{m}$, as they exhibit large stimulated cross sections and broad emission bandwidth. Furthermore, tellurite glasses have low process temperature, good chemical durability and nonlinear properties.

Fabrication of channel waveguides in Er-doped tungsten-tellurite glasses using ion implantation was recently demonstrated. In order to get a deeper understanding of the process and to optimize the characteristics of the waveguides, we fabricated a set of planar waveguides, in an Er-doped tellurite glass sample by implantation of (last year) 1.5 MeV and (present year) 3.5 MeV nitrogen ions. Doses of the implanted ions ranged from $1\text{-}8 \times 10^{16} \text{ ions/cm}^2$. Refractive index changes of the waveguides were measured by spectroscopic ellipsometry (SE). Functionality of the waveguides was tested by m-line (dark-line) spectroscopy and prism coupling technique. The results show that a waveguiding (even at the $1.55 \mu\text{m}$ telecom-window) layer was created at every dose. Thicknesses of the guiding layer and of the implanted barrier obtained by SE correspond well to SRIM – “The Stopping and Range of Ions in Matter” simulations. It is hoped that combination of the results obtained in these experiments with simulations for channel waveguides will make it possible to optimize ion-implanted fabrication of integrated optical components in this tellurite glass.

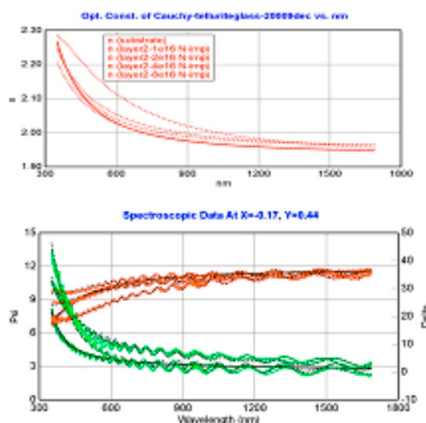


Figure 1 Measured + fitted ellipsometric spectra and determined (refractive index curves of the implanted tellurite-glass

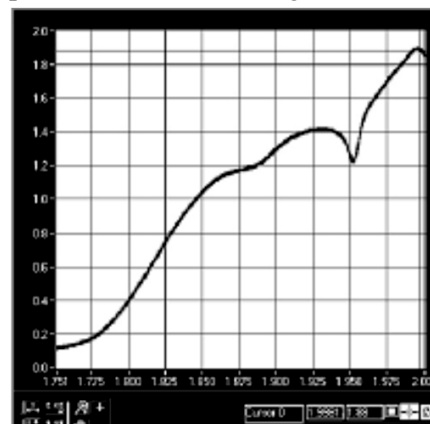


Figure 2 Dark-line result (wl: 1550 nm , dose: $8 \times 10^{16} \text{ N}^+/\text{cm}^2$). Y-axis: intensity (arb. unit) X-axis: N_{eff}

Optical critical dimension measurement of photonic structures

(OTKA 81842, PVMET_08)

P. Kozma, B. Fodor, A. Deak, and P. Petrik

Optical models for the characterization of ordered silica nanospheres using spectroscopic ellipsometry (SE) were developed. Out of silica nanospheres in the size range of 40-1000 nm an ordered layer can be created using Langmuir-Blodgett method. We present a series of physical models of increasing complexity to find the connection between properties of the layers. A method, fitting the whole spectra at different wavelength ranges was developed to detect with high sensitivity the threshold wavelength of the quasi-static regime, i.e., the limit of the applicability of the effective medium approximation. This method allows the user apply the widest possible wavelength range at a minimal error caused by light scattering. D/λ_T values of 0.298 ± 0.004 were found, where D and λ_T are the diameter of the spheres and the threshold wavelength, respectively. Using this method, the critical dimension of ordered structures can be measured in a simple and robust way, using only the effective medium method, avoiding the use of complicated scattering models. The advanced analytical parametrizations allow sensitive determination of not only the layer thickness, the size, and the packing density of the spheres, but also the size distribution and the quasi-continuous depth density profile within the ordered monolayer of silica spheres. Our results were published in *Langmuir* [70].

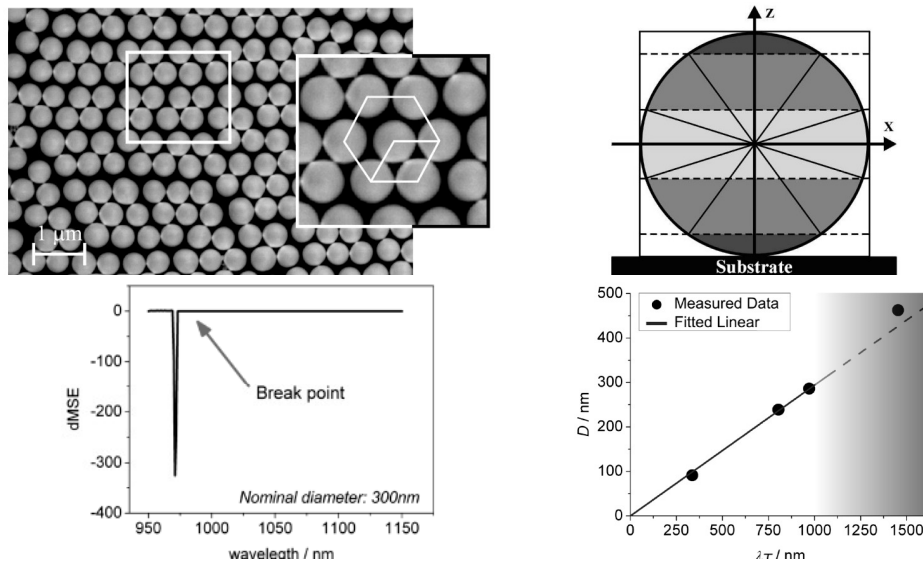


Figure 1 Silica nanospheres with a diameter of 460 nm created by the Langmuir-Blodgett method (top left); optical model using sublayers determined by the “equal angle” method (top right); cut off wavelength showing the boundary of applicability of the effective medium method (bottom left); correlation between the cut-off wavelength and the diameter of the spheres (bottom right).

Development of models and instruments to monitor protein adsorption

(OTKA 81842)

A. Németh, P. Kozma, S. Kurunczi, P. Petrik, R. Horváth, M. Fried, and F. Vonderviszt

Last year, bioellipsometry as a new research direction in the Ellipsometry Laboratory of MFA (<http://www.ellipsometry.hu>) was reported. The topic became by now as one of our main research fields. In 2010 we have made a significant progress by developing new optical models [74] and flow cells, as well as investigating the adsorption on different substrates [99], building new measurement tool combining spectroscopic ellipsometry and grating coupled interferometry [P. Kozma, R. Horvath, A. Hamori, P. Petrik, S. Kurunczi, and M. Fried; A combined tool for simultaneous measurement by spectroscopic ellipsometry and grating coupled interferometry, 5th Int. Conf. on Spectroscopic Ellipsometry, 23-28 May 2010, Albany, NY USA, poster presentation], and creating 3D structural and kinetic models [A. Nemeth, S. Kurunczi, P. Petrik, R. Horváth, H. Jankovics, F. Vonderviszt and M. Fried, “Adsorption of flagellar filaments with two different length distributions”, Third International NanoBio Conference, ETH Zurich, August 24-27, 2010, poster presentation], and [A. Nemeth, P. Kozma, S. Kurunczi, R. Horvath, P. Petrik, H. Jankovics, M. Fried, and F. Vonderviszt, “Optical models for in situ measurement of the adsorption of flagellar filaments in a liquid cell using spectroscopic ellipsometry”, 5th International Conference on Spectroscopic Ellipsometry May 23-28, 2010, Albany, OH, USA, poster presentation]. We have created numerical models in MATLAB to follow the structural change of the flagellar filament structure during adsorption.

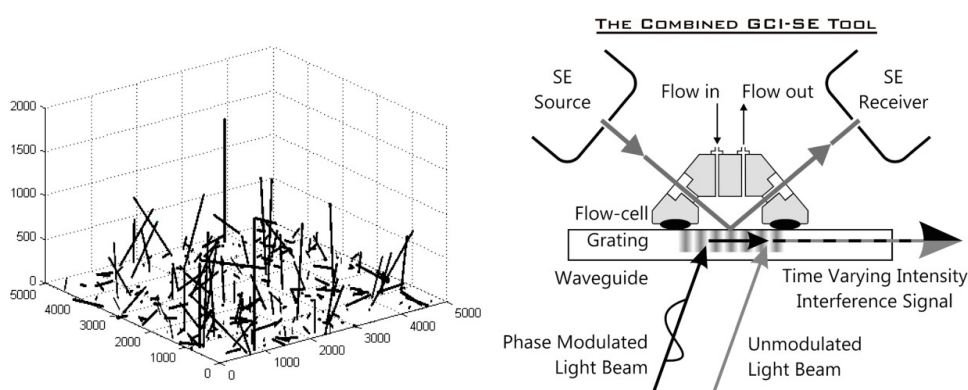


Figure 1 Numerical simulation of the distribution of flagellar filaments on the sample surface (left); tool for the simultaneous measurement using spectroscopic ellipsometry and grating coupled interferometry (right).

Accredited Ellipsometry Laboratory in frame of a European Intergated Activity

(EU I3, ANNA Project Nr. 026134)

P. Petrik, T. Lohner, M. Fried, A. Bolgár, and F. Riesz

Since January 2010 the Ellipsometry Laboratory of MFA is working according to ISO 17025 accredited by the National Accreditation Board (<http://nat.hu/adatbazis/reszletes-oldal.php?azon=2695>).

Further details about the laboratory can be found under <http://www.ellipsometry.hu/>. Joined to an international consortium in frame of the ANNA project (<http://www.i3-anna.org/>) the Ellipsometry Laboratory provided a total of more than 100 units (days) of transnational access (http://www.i3-anna.org/context.jsp?ID_LINK=2&area=8) to the infrastructures of ellipsometry and Makyoh topography. Based on the Transnational Access projects and on the Joint Research Activities the Ellipsometry Laboratory had almost 40 presentations or publications from the ANNA co-operations during the four years of the project.



A distributed multi-technique analytical lab available under the Transnational Access Activities program

Figure 1 Accreditation certificate of the Ellipsometry Laboratory (left); Logo of the ANNA consortium (right).

Synchrotron ellipsometry at high photon energies

(*BESSY II synchrotron facility, Berlin*)

P. Petrik, Z. Zolnai, O. Polgar, M. Fried, Z. Betyak, E. Agocs, and T. Lohner

The optical characterization of wide band gap semiconductors requires the use of the vacuum UV range. The characteristic interband transitions in SiC are located between 5 and 8 eV. In this study we used synchrotron radiation in the photon energy range from 5 to 9 eV at the BESSY II synchrotron facility in Berlin that enabled the sensitive measurement of disorder created by ion implantation. We have characterized the damage structure in ion implanted SiC using high photon energy synchrotron ellipsometry. We have determined the reference dielectric function (i-a-SiC) of SiC amorphized using 100-keV Xe ions at a fluence of $1.6 \times 10^{14} \text{ cm}^{-2}$. Using the effective medium approximation combining single-crystalline SiC and i-a-SiC we measured the damage depth profiles caused by the 100-keV Xe ions at different doses. We found a good agreement with Rutherford backscattering and Monte Carlo simulations. Analyzing the pseudo-dielectric function and the relative damage vs. fluence curves we determined the ion track size with good agreement between the two independent methods. Using a physical model with random ion track positions we could simulate the evolution of the buildup of damage and the size of the remaining crystalline parts as a function of fluence [P. Petrik, Z. Zolnai, O. Polgar, M. Fried, Z. Betyak, E. Agocs, T. Lohner, C. Werner, M. Röppischer, C. Cobet, "Characterization of damage structure in ion implanted SiC using high photon energy synchrotron ellipsometry", Thin Solid Films doi:10.1016/j.tsf.2010.12.070].

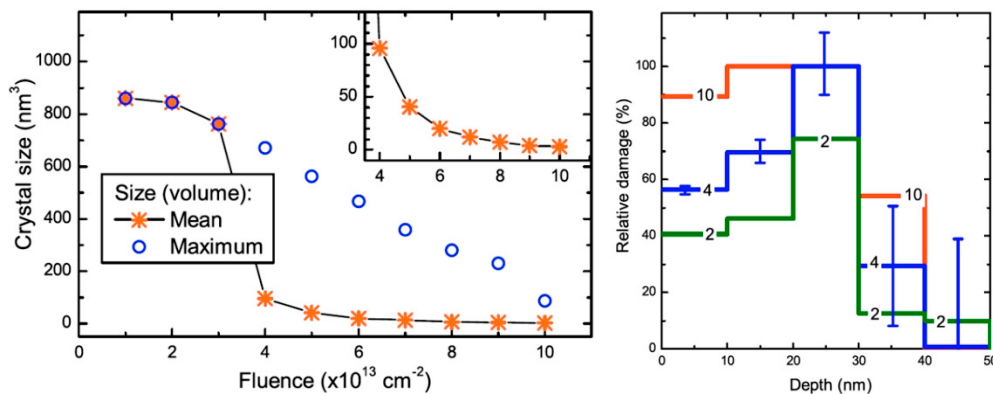


Figure 1 Mean and maximum crystal size as a function of the fluence (on the left); Damage profiles measured by SE using 5 sublayers of equal thickness but independently fitted volume fraction of i-a-SiC, i.e. relative amount of damage. The numbers on the lines show the fluence in units of 10^{13} cm^{-2} (on the right).

Flagellin Based Protein Layers for Label-free Biosensing Monitored by OWLS

(OTKA PD 73084, FP7 OPTIBIO)

N. Kovács, D. Patkó, N. Orgován, S. Kurunczi, R. Horváth, J. J. Ramsden, and F. Vonderviszt

Genetically modified bacterial flagellar filaments with thousands of possible binding sites are promising candidates as novel sensing matrixes in affinity biosensors. In our research optical waveguide lightmode spectroscopy (OWLS) is applied to in-situ monitor the surface deposition of flagellar filaments and the optical structure of the layers. Reconstructed flagellar filaments with a diameter of 24 nm as well as flagellin monomers and filaments with various lengths are used in the experiments.

The basic building block of these filaments is the 51.5 kDa molecular weight flagellin protein (see Fig. 1.). In 2010 we have been mainly focusing on the label-free monitoring of the surface deposition of the monomer subunits using OWLS. The effect of substrate hydrophobicity, solution concentration, ionic strength and pH on the protein adsorption was investigated. Comparing the different surfaces we found that significantly more monomers deposit on the hydrophobic surface than on the hydrophilic one at pH 7.4. But, highest adsorbed amount is reached on the hydrophilic surface and in water, possibly due to its lower pH. Moreover, the deposition experiments of the flagellin monomers revealed a significantly faster adsorption kinetics compared to the filamentous form (see Fig. 2.), but resulting in a 2 dimensional (conventional) sensing layer, compared to the novel 3 dimensional matrix obtained using the filamentous form.

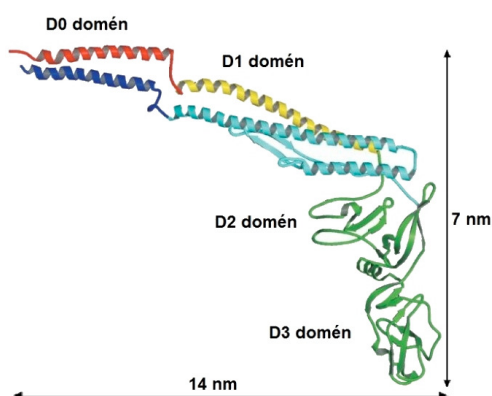


Figure 1 The flagellin monomer, building blocks of the flagellar filaments.

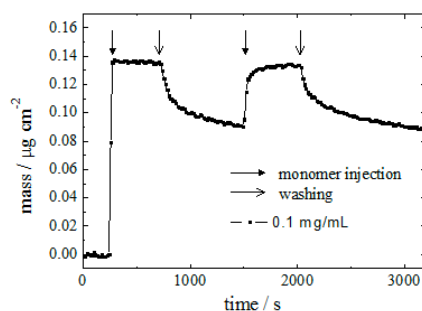


Figure 2 Mass of flagellin deposited on the bare OWLS sensing surface. After washing off the reversible bound monomers the deposition was repeated resulting in a slower adsorption kinetics.

Grating Coupled Optical Waveguide Interferometer for Label-free Biosensing

(FP7 OPTIBIO, OTKA PD 73084)

P. Kozma, A. Hámori, D. Patkó, S. Kurunczi, K. Cottier*, and R. Horváth
*Creoptix GmbH, Wädenswil, Switzerland

A phase shifting optical waveguide interferometer, the so-called Grating Coupled Interferometry (GCI), is demonstrated for label-free evanescent wave biosensing in aqueous solutions. In the proposed configuration, the reference and measurement arms of the interferometer are combined inside an integrated optical Ta_2O_5 waveguide using an ion implanted grating. Biomolecules adsorbing on the waveguide surface shift the phase in the measurement arm, which is modulated at the same time by a periodically relaxing liquid crystal phase modulator (Fig. 1.). It is demonstrated that by analyzing the periodic intensity response at the end facet of the waveguide, the phase shifts in the measurement arm can be monitored in real-time with a precision of 10^{-4} radians, corresponding to bulk refractive index sensitivity below 10^{-6} .

The high phase resolution allows the detection of surface adsorbed molecule densities below 1 pg/mm^2 without using any labeling or on-chip referencing. The instrument performance is demonstrated by monitoring in-situ protein adsorption and affinity binding of low molecular weight pure biotin to an immobilized avidin layer (Fig. 2.). Our results are under publication in *Sensors and Actuators B – Chemical*.

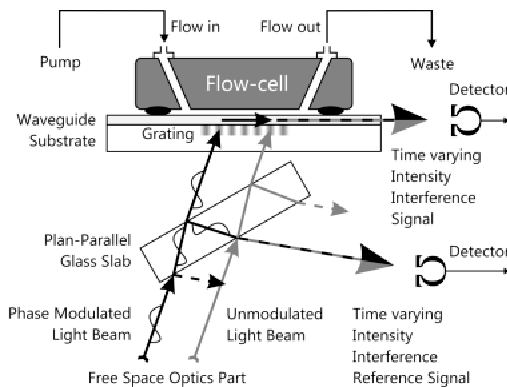


Figure 1 The basics of the GCI setup.

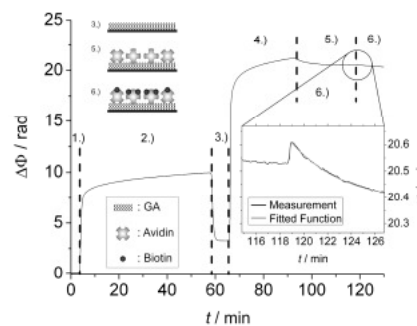


Figure 2 Avidin-biotin affinity binding monitored by GCI.

Fluid Handling in OWLS Experiments – Injections of Serum Samples

(FP7 P3SENS, FP7 OPTIBIO, OTKA PD 73084)

N. Orgován, D. Patkó, A. Hámori, S. Kurunczi and R. Horváth

P3SENS (www.p3sens-project.eu) is a multidisciplinary research project (including photonics, microfluidics, biochemistry and materials science) funded by the European Commission. This Pan-European cooperation aims to develop high-performance, multichannel optical biosensors for the early detection of brain diseases (for instance, to prevent the occurrence of ischemic damage as a result of stroke) from human blood. Among many other tasks MFA functionalizes the photonic biochips with appropriate surface chemistry and tests the receptor performances by a high resolution label-free optical biosensor called OWLS (Optical Waveguide Lightmode Spectroscopy).

Considering the limited availability of the sample materials (human blood, serum, costly chemicals) in 2010 we have been extensively studied the flashing of the OWLS cuvette with model solutions and worked out an injection strategy to reduce the sample volume needed for a single test. We successfully injected serum samples and monitored the optogeometrical parameters of the adsorbed protein layers.

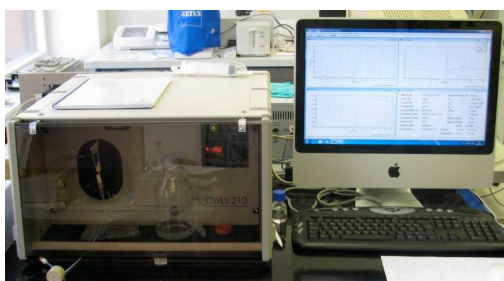


Figure 1 OWLS 210 biosensor instrument.

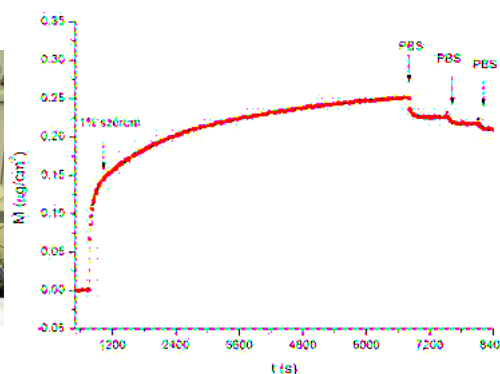


Figure 2 Mass of surface adsorbed serum proteins monitored by OWLS.

Development of integrated process monitoring metrology for the 32 nm technology node of IC processes

(NKFP-07-A2-ICMET_07)

M. Fried, G. Juhász, P. Petrik, and I. Mohácsi

The aim of this project (led by Semilab, Inc.) is to develop a measurement technology and equipment, which would enable the process control of production of integrated circuits of the 32-65nm generation, an equipment complying with clean room and automatization standards. The equipment, which will be delivered by the project, enables one of the most important technological processes in the semiconductor dopant monitoring (resistance and conduction type adjustment) in several steps: after the implantation and thermal activation of the dopant species.

MFA's task in the project was to prepare ion-implanted reference samples (ultra-low-energy implantation, ULE-imp), and to perform reference measurements.

Spectroscopic Ellipsometry (SE) is very sensitive for changes but the detection is limited from two directions. The lower limit is the minimum detectable lattice-disorder depending on the atomic mass of ions and the implantation energy. The upper limit is the full amorphization, also depending on the atomic mass and energy, two orders of magnitude higher than the lower limit. The precision is better than 1 % between the two limits if it is calibrated with ion-backscattering technique (MEIS, Medium Energy Ion Scattering). MEIS needs expensive accelerator and vacuum system but ellipsometry being an optical method can be used in-situ or in-line. Note, that ellipsometry cannot be applied for the determination of electrically active dopants after high temperature annealing.

After appropriate modeling, SE can determine damage depth profile with high precision. Determined depth profiles can be compared with MEIS measurements.

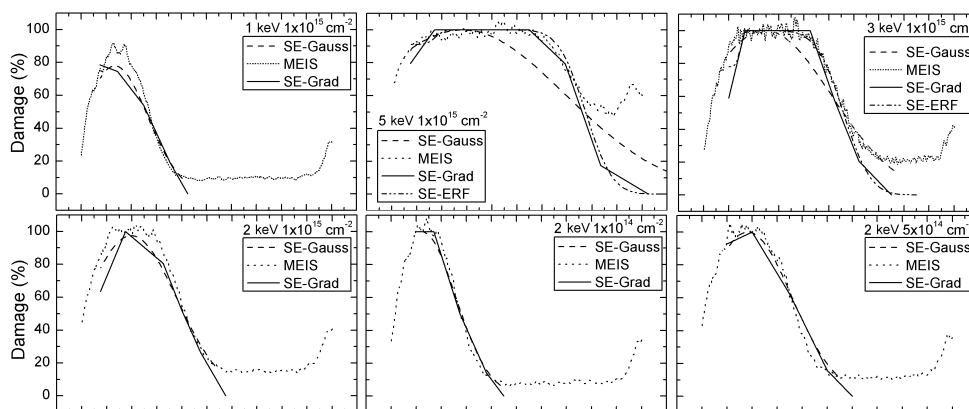


Figure 1 SE and MEIS depth profiles of low energy As implanted samples Si.

Development of metrology tools based on electrical and optical techniques for in-line and laboratory qualification of thin film solar cells

(TECH_08_D2(2008) PVMET_08)

M. Fried, C. Major, G. Juhász, and P. Petrik

The aim of this project (led by Semilab, Inc.) is to develop an equipment and measurement technology family, which is capable to perform electrical and optical measurements for in-line and laboratory qualification of thin film solar cells. MFA's task in the project was to make spectroscopic ellipsometry capable for this task.

We have developed optical models for different types of amorphous silicon (p-a-Si, n-a-Si, i-a-Si). The Cody-Lorentz function was used, as suggested by R. W. Collins's group (A. S. Ferlauto, G. M. Ferreira, J. M. Pearce, C. R. Wronski, R. W. Collins, Xunming Deng, Gautam Ganguly: "Analytical model for the optical functions of amorphous semiconductors from the near-infrared to ultraviolet" Applications in thin film photovoltaics, Journal of Applied Physics v92(5) p.2424, (2002).

As it is shown in Fig. 1, the measured spectra are fitted very well in the whole spectral region (1.1-5 eV) on a very thin (appr. 9 nm) a-Si layer on glass with no other preparation step applied. In Fig. 2, results on the same sample after a mechanical roughening is shown. The resulted thickness value of the a-Si layer is within the error limit but the measurement error is reduced.

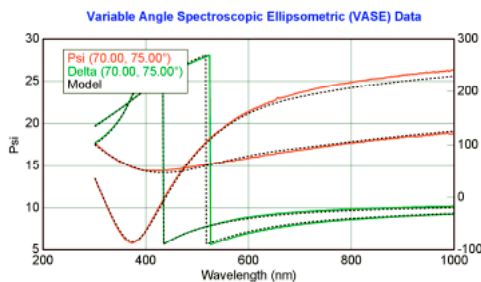


Figure 1 Very thin (9 nm) a-Si layer on glass

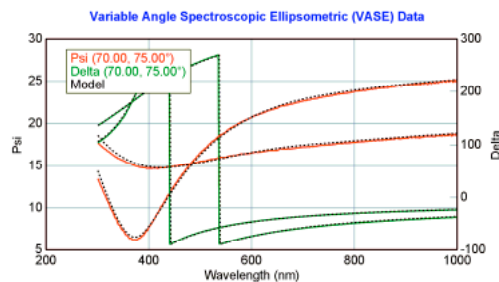


Figure 2 Same sample as on Fig.1 but with reduced back-reflection

Nanopatterning of macroscopic surfaces by tunable ion-swelling

N. Nagy, A. Deák, Z. Zolnai, G. Battistig, and M. Fried

Various nanostructures were fabricated by ion irradiation on large area (100) Si surfaces covered by colloidal Langmuir-Blodgett films as nanolithographic masks. The ordered structure of the Langmuir-Blodgett monolayer composed from spherical Stöber silica particles of 200nm and 450nm diameter offer the possibility to form local surface swelling patterns during the ion bombardment step. Utilizing the dependence of the surface morphology on the irradiation parameters the tunability of nanostructuring was studied for 40 keV Ar⁺ and 500 keV Xe²⁺ ions.

We showed that the periodicity of the resulted surface pattern is determined by the size of the masking particles, while the height of nanostructures can be tuned by the ion fluence. The quality of projection of the nanomask contours to the substrate – the contrast of masking – can be set by choosing appropriate ion energy, thereby determining the curvature of the surface pattern. Moreover, deformation of the nanomask due to ion–nanoparticle interactions should be taken into account since these effects can be also utilized for tailoring various structures.

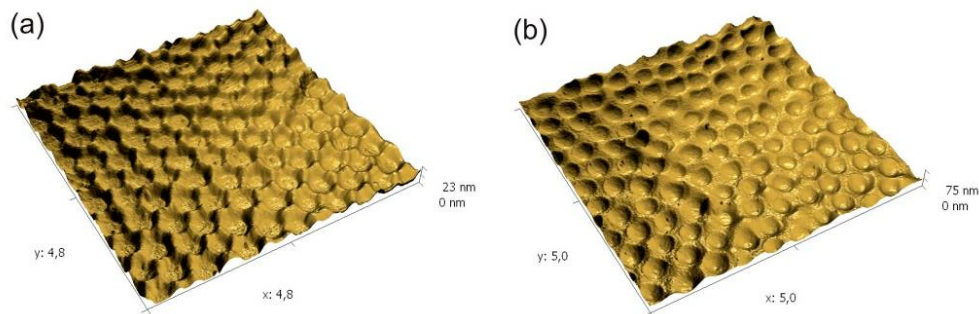


Figure 1 AFM images of the Si surface after irradiation with 500 keV Xe²⁺ ions carried out at fluences of (a) $3 \times 10^{15} \text{ cm}^{-2}$ and (b) $2.4 \times 10^{16} \text{ cm}^{-2}$ through a mask of ordered silica particles with the diameter of 450 nm

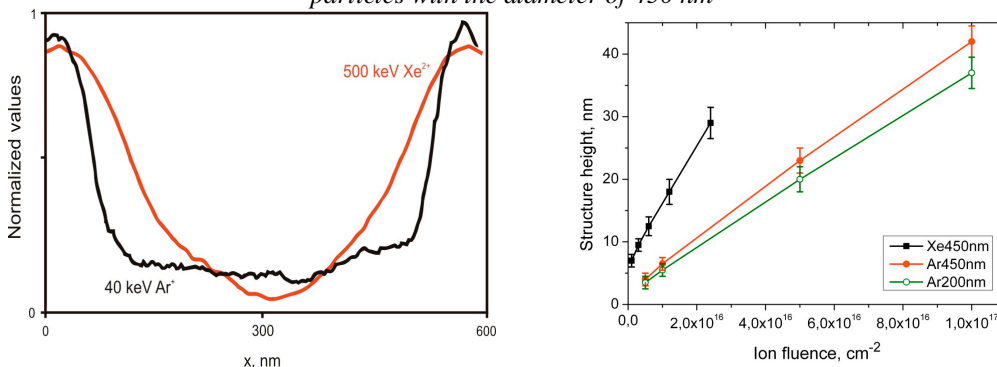


Figure 2 Measured cross-section profiles (left) on 40keV Ar⁺ and 500keV Xe²⁺ implanted substrates and measured structure height vs. the applied ion fluence (right)

Relationship between structural changes, hydrogen content and annealing in stacks of ultrathin Si/Ge amorphous layers

M. Serényi, N. Q. Khánh, A. Csik¹, and C. Frigeri²

¹ Institute of Nuclear Research of the HAS, P.O. Box 51, H-4001 Debrecen

² CNR-IMEM Institute, Parco Area delle Scienze 37/A, 43100 Parma, Italy

Hydrogenated a-Si and a-Ge layers are key materials for employment in (nano) structures to be applied, e.g., in the technology of multi-junction solar cells since a-Ge acts as the low band gap absorber while a-Si acts as the high band gap one thus allowing a better exploitation of the solar spectrum and the achievement of higher efficiencies. However, the a-SiGe alloy is now the material of choice as the low band gap absorber. It allows a higher degree of freedom as regards the choice of the band gap as the latter one can be tailored over some range by changing the Si/Ge ratio. The a-SiGe alloy can be realized from a sequence of thin a-Si and a-Ge layers by intermixing them which is obtained by heat treatments.

In previous works it was shown how the hydrogen content and annealing conditions can dramatically influence the structural stability of the a-Si/a-Ge multilayers (MLs) produced by sputtering and then annealed in order to produce intermixing (see in [C. Frigeri et.al., *Superlatt. Microstru.* 45, 475 (2009)], [C. Frigeri et.al., *J. Mater. Sci.: Mater. Electron.* 19, S289 (2008)], [A. Csik et.al., *Vacuum* 84, 137 (2009)]). We reported that surface bumps formed whose size and height increased with increasing H content and/or annealing temperature and time. It was hypothesized that H could be first released from the Ge layers because of the lower binding energy of the Ge-H bond with respect to the Si-H one. To check this hypothesis an analysis of the structural behaviour of single films of a-Si and a-Ge submitted to the same anneal as the MLs previously studied was performed.

The investigated samples were single layers of a-Si and of a-Ge having a thickness of 40 nm. Both types were RF sputtered from high purity crystalline silicon and germanium targets. Sputtering was done with a mixture of high purity argon and hydrogen gases. Hydrogenation was carried out by letting hydrogen to flow into the deposition chamber at flow rates of 0.4, 0.8, and 1.5 ml/min. The samples were annealed in high purity argon at 350 °C or 400 °C for 1, 4 and 10 hours.

The samples were analysed by Elastic Recoil Detection Analysis (ERDA) and Atomic Force Microscopy (AFM). For ERDA the 1.6 MeV ⁴He⁺ beam available at the 5 MeV Van de Graaff accelerator has been applied to measure the hydrogen in the samples. By using the simulation program the calibration curves of Fig. 1 giving the incorporated at % of H as a function of the H flow rate was obtained. The H concentration increase in a-Si already tends to slow down significantly between 1 and 1.5 ml/min flow rate reaching a maximum value of 17 at %. In a-Ge the same slowing down trend is observed for the same flow rate values reaching a maximum value of only about 7 at %.

The different release efficiency of H in a-Si and a-Ge studied with ERDA are summarized in Fig. 2 for the case of annealing at 350 °C for times of 1 and 4 h. Irrespective of the initial H content in the as-deposited films a decrease of the H

concentration upon annealing is observed which is greater for longer annealing time. However, such decrease is more effective in the case of the a-Ge film. This indicates that the release of H in the a-Ge layer was highly effective and that its escape from the layer was very fast. Evidence for this is given by Fig. 3 which shows the surface morphology of the 2 types of layer after annealing. For the same annealing time, either of 1 or 4 h, the Si layer mainly exhibits surface bumps after annealing, indicating that H is still in the film, though partially gathered in bubbles, whilst the Ge layer exhibits mostly craters, i.e., exploded H bubbles, suggesting that H has almost all escaped in agreement with the ERDA.

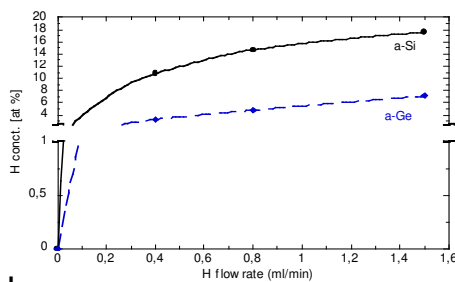


Figure 1 Total H concentration in a-Si (solid black line) and a-Ge (dash blue line) layers as a function of the H flow rate as determined by ERDA.

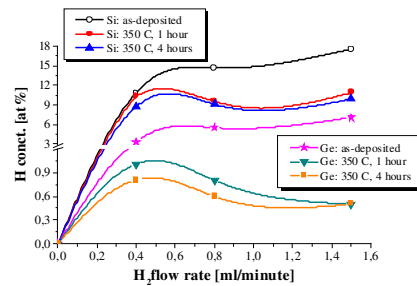


Figure 2 H concentration, as determined with ERDA, as a function of the H flow rate in a-Si and a-Ge single layers before and after annealing at 350 °C for 1 and 4 h.

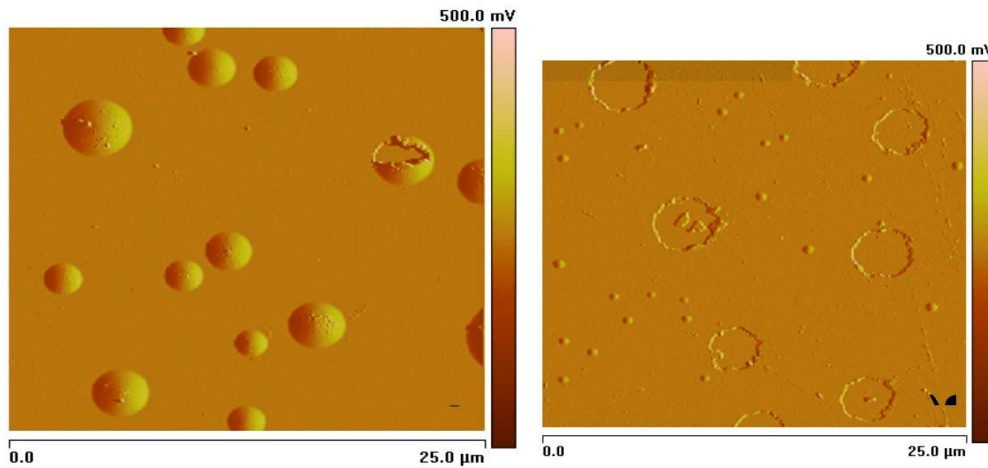


Figure 3 AFM topographic image of a) (left) a-Si and b) (right) a-Ge single layer after annealing at 350 °C for 4 h. H flow rate 1.5 ml/min.

In a) bumps are predominant. In b) large craters, i.e. exploded bumps with escape of H, are by far predominant.



Microtechnology Department

| Head: Gábor BATTISTIG Ph.D. | |
|--|--|
| <p>Research Staff</p> <ul style="list-style-type: none"> • István BÁRSONY, Member of HAS., • László DÓZSA, Ph.D., • Péter FÜRJES, Ph.D., • Zoltán LÁBADI, Ph.D., • György MOLNÁR, Ph.D., • Anita PONGRÁCZ, Ph.d., • Vilmos RAKOVICS, Ph.D., • Zsolt ZOLNAI, Ph.D. • Ágoston NÉMETH, Ph.D., (on leave) • Péter BASA, Ph.D., (left) • Andrea Edit PAP, Ph.D., (part time) • Antalné ADÁM, M.Sc., (part time) • Albert KARACS, M.Sc., (part time) • Tibor MOHÁCSY, M.Sc., (part time) • Ákos NEMCSICS, Ph.D. (part time) • Gábor PETŐ, D.Sc., Prof. Emeritus • István PINTÉR, Ph.D., (part time) • Bálint PÖDÖR, Ph.D. (part time) • Zsolt József HORVÁTH, D.Sc., (part time) • Béla SZENTPÁLI, Ph.D., (part time) • Éva VÁZSONYI, M.Sc., (part time) | <p>Technical Staff</p> <ul style="list-style-type: none"> • György ALTMANN, technician • Edvard BADALJÁN, engineer • Gabriella BIRÓ, technician • Sándor CSARNAI, technician • Ábel DEBRECZENY, engineer • Magdolna ERŐS, technician • Csilla ARIAS-SOTONÉ FARAGÓ, technician • János FERENCZ, engineer • Róbert HODOVÁN, engineer • Csaba LÁZÁR, engineer • András LŐRINCZ, engineer • Ákos MAJOROS, engineer • Attila NAGY, technician • Károlyné PÁYER, technician • István RÉTI, engineer • Ádám SZENDREY, engineer • Magda VARGA, technician • Katalin Veresné-VÖRÖS, engineer • Tamás JÁSZI, engineer (left) • Sándor PÜSPÖKI, engineer (part time) • Zsuzsa PÜSPÖKI, engineer (part time) • Imre SZABÓ, engineer, dr. Univ. (part time) • Tamás SZABÓ, engineer (part time) |
| <p>Ph.D. students / Diploma workers</p> <ul style="list-style-type: none"> • Zsófia BAJI, Ph.D. student • Zoltán FEKETE, Ph.D. student • László GRAND, Ph.D. student • Tamás KÁRPÁTI, Ph.D. student • Endre LÁSZLÓ, Ph.D. student • Dorottya GUBÁN, M.Sc. diploma w. • Gergely MÁRTON, M.Sc. diploma w. • Péter NAGY, M.Sc. diploma w. • Tamás RETKES, M.Sc. diploma w. • Tamás WEIDISCH, M.Sc. diploma w. | |

The main task of the Microtechnology Department is the research, development and system integration of physical, chemical/biochemical sensors and systems:

- MEMS and MEMS related technologies, with special emphasis on development of Si MOS embedding circuits;
- Development and functional testing of different MEMS gas, chemical, 3D force, thermal, biology related sensors and sensor systems;
- Development of microfluidic systems;
- Development and applications of near IR light emitting diodes and detectors;
- Development of solar cells and their competitive technology.

Fundamental research on:

- sensing principles;
- novel materials and nanostructures;
- novel 3D fabrication techniques;
- ion-solid interaction for supporting MEMS development.

Device and material characterizations widely used in our projects:

- Ion beam analysis methods;
- IR and Raman scattering;
- Scanning Microprobes;
- Optical and Electron Microscopy, SEM, TEM, EDX;
- Spectroscopic Ellipsometry;
- Electrical characterisations.

The Microtechnology Department of MFA runs the 300 sqm clean lab (Class 100-10000) with the complete Si-CMOS technology together with a mask shop, unique in Hungary. A rather new and developing large facility of the Department is the CIGS solar cell technology laboratory equipped with a pilot line of sputtering, evaporation and laser scribing modules for 30×30 cm² glass substrates.

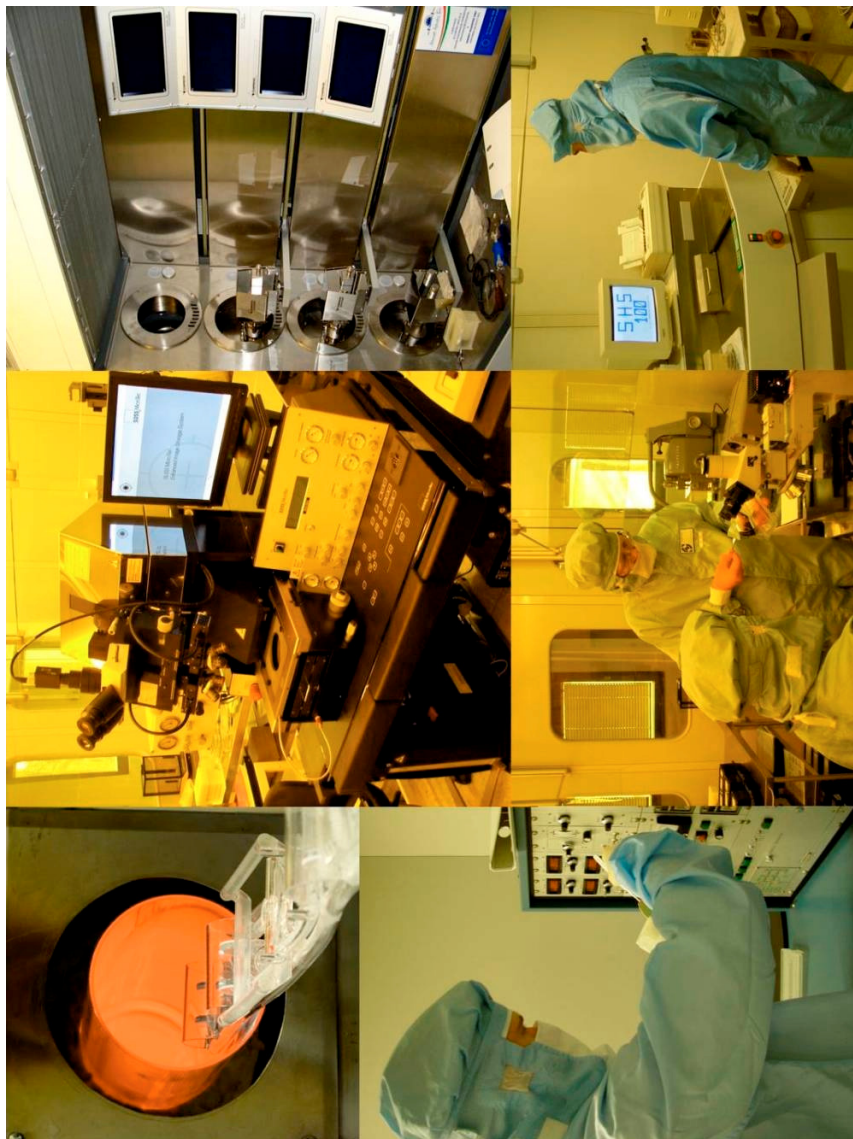
The technology base of the clean lab has been further improved in the recent years. A basic new technology – DRIE– was installed in 2010 into our Si technology line: Oxford Instruments Plasmalab 100 type deep reactive ion etching system was introduced in order to facilitate the works on 3D Si based MEMS devices.

Main technologies available in the Microtechnology lab for our partners and customers:

- High temperature annealing, diffusion and oxidation
- Rapid Thermal Treatment
- Low Pressure Chemical Vapor Deposition of poly-Si, SiO₂ and Si₃N₄ layers
- Low Temperature Chemical Vapor Deposition
- Ion implantation
- Thin film depositions – Electron beam evaporation, DC and RF Sputtering
- Atomic Layer Deposition
- Deep Reactive Ion Etching

- Photolithography with back-side alignment and Nanoimprinting
- Wafer Bonding
- Wet chemical treatments
- Electro-chemical porous Silicon formation
- Mask design, Pattern generator and Step-and-Repeat Camera
- Electrical and functional characterizations

Overview of the MFA Microtechnology clean lab



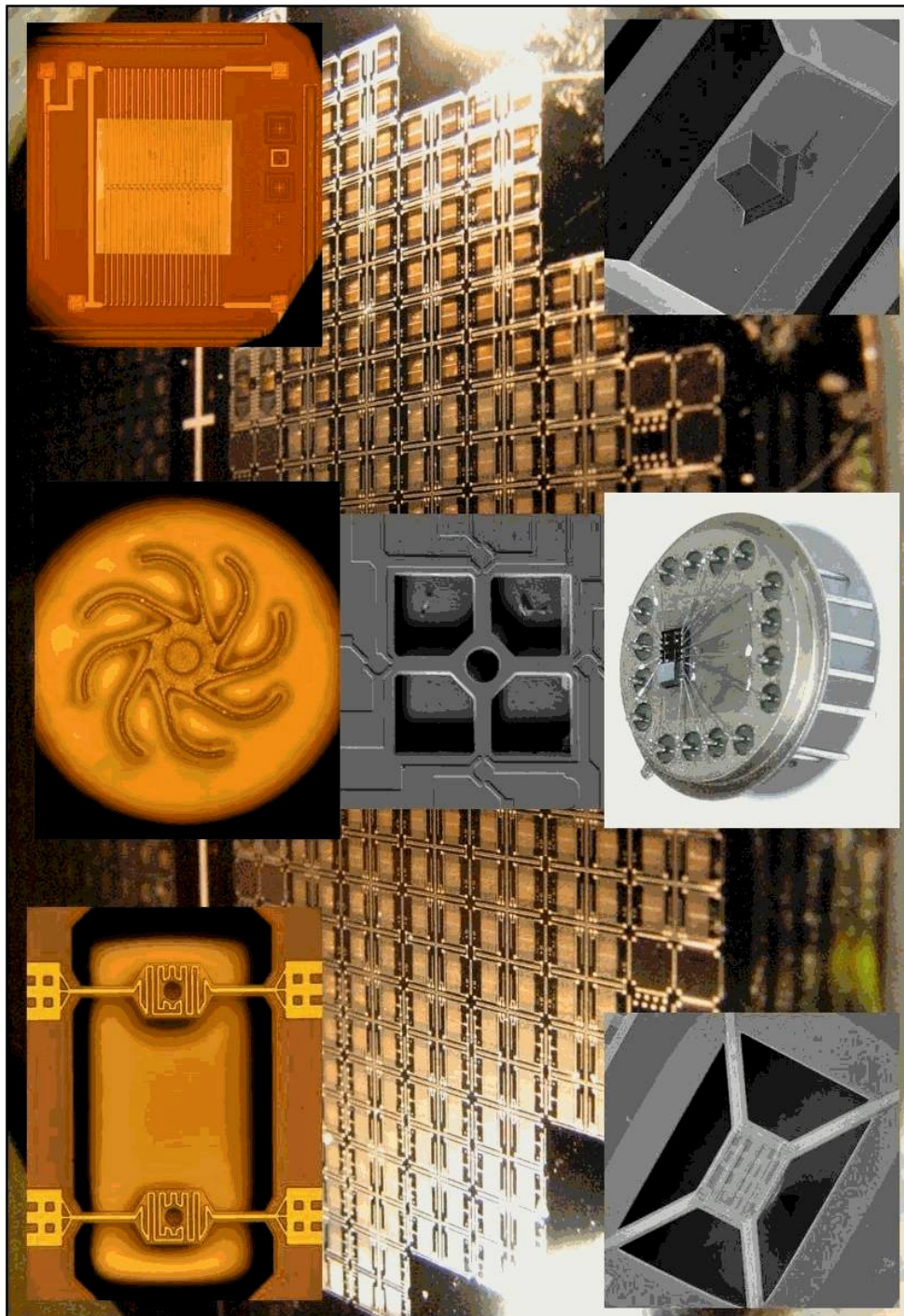
The recently installed Oxford Plasmalab 100 DRIE system



The load-lock and computer control of Oxford Plasmalab 100 DRIE system



MEMS devices developed in the MFA MEMS lab.



Sensitivity tuning of a three-axial force sensor

(ENIAC SE2A)

D. Molnár, A. Pongrácz, M. Ádám, Z. Hajnal, V. Timár-Horváth, A. Nagy, and G. Battistig

In the frame of ENIAC SE2A project a Si mono-block, full-membrane, and three-axial force sensor is developed and optimized. In the Si element, a column like rod at the centre of a deforming membrane protrudes over the top surface of the device. Piezoresistors placed on the backside of the membrane, provide the signals for resolving the vector components of the load. The mono-block Si structure guarantees the perfect transmission of the attacking force to the sensing elements.

The developed fabrication technology allows us to tune the sensitivity of the sensor easily by adjusting two lithographic steps defining the geometry of the sensor.

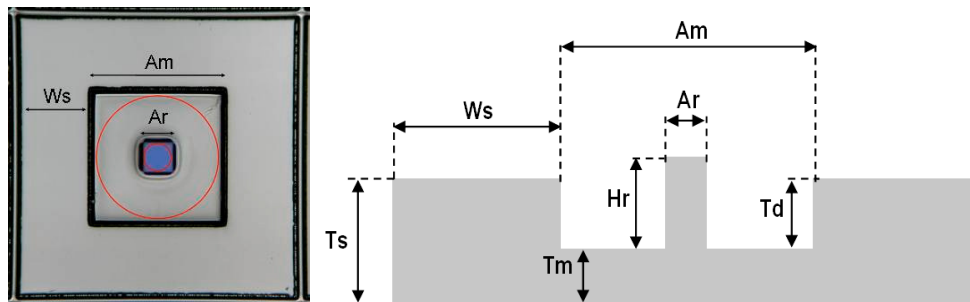


Figure 1 Top and cross sectional schematic view of the simulated and realized sensors. Membrane with square shape and its circular equivalent is marked by dotted and continuous lines, respectively.

Effect of membrane thickness, shape of the membrane and fill factor (the area of the rod/area of the membrane) on the sensitivity of the sensor is analyzed systematically by finite element methods using the COMSOL Multiphysics 3.5 software package.

Sensitivity of a resistor was analyzed as a function of membrane thickness (50-230 μm) while applying 1N normal and 45° shear force load. The sensitivity decreases with increasing the membrane thickness, as the resistivity change is inversely proportional to the square of the membrane thickness. It means that just by varying the thickness of the membrane, we could tune the sensitivity of a chip by one order of magnitude. Another important conclusion is that the square shaped sensors are more sensitive, than their circle shaped equivalents.

Based on the simulation results new layouts were designed and force sensor elements were realized. Experimental results were compared to simulations and good agreement was found.

Comparison of the characteristics of the different sensor designs obtained from simulations and from experimental measurements is also presented.

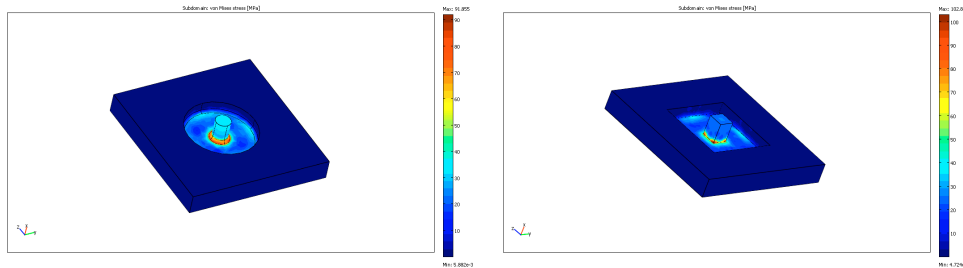


Figure 2 Overview of the equivalent stress on the circular (left) and square shaped (right) sensors to the resistance change

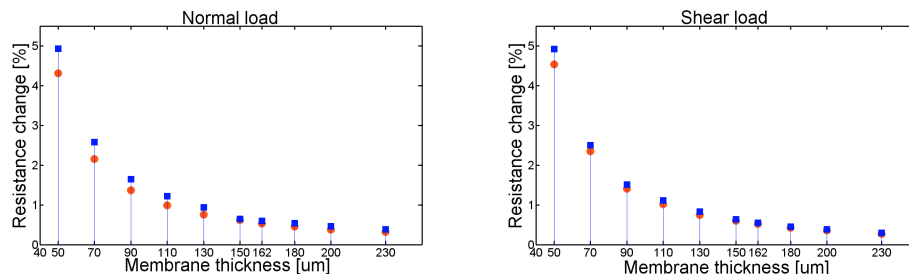


Figure 3 Relative resistance change versus membrane thickness for 1N normal (left) and shear (right) load on square shaped (marked with blue squares) and circular (marked with red circles) sensors

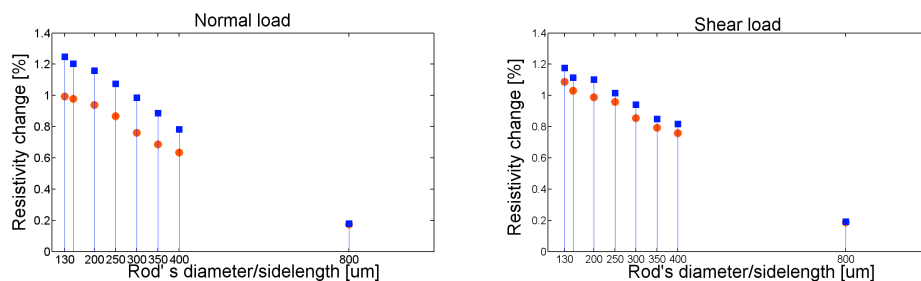


Figure 4 Relative resistance change versus fill factor for 1N normal (left) and shear (right) load on square shaped (marked with blue squares) and circular (marked with red circles) sensors

The experimental setup consisted of a loading instrument, signal measuring system and data processing. Piezoresistors with their reference pairs were arranged in a half-bridge configuration to provide a direct voltage reading proportional to the strain. Responses to the normal loading in all four elements are approximately equal, since the stress and the arising strain at the position of all the symmetrically arranged piezoresistors in the membrane is similar.

Sensors realized with the following parameters were tested using Andilog Centor force gauge: side length of the membrane is $940\ \mu\text{m}$, side length of the transmitting rod is $200\ \mu\text{m}$, thickness of the membrane is $162\ \mu\text{m}$, and height of the rod is $310\ \mu\text{m}$. In response to normal loading, the sensor outputs were recorded at different force magnitudes in the 0-2.5 N range.

As expected the input-output characteristics was linear and resulted in a sensitivity of $5.98\ \text{mV/V/N}$. Note, the calculated value is $6.01\ \text{mV/V/N}$, for a sensor with $162\ \mu\text{m}$ thick square shaped membrane, which is in good agreement with the measurements. Sensitivity tuning of a full membrane mono-block 3D force sensor was shown by varying geometrical parameters of the structure. Finite element simulations show that sensitivity depends on the membrane thickness, the shape of the membrane and the ratio of the transmitting rod/membrane area, too. Calculated sensitivity forecasted by FE analysis was compared with experiments on realized sensors.

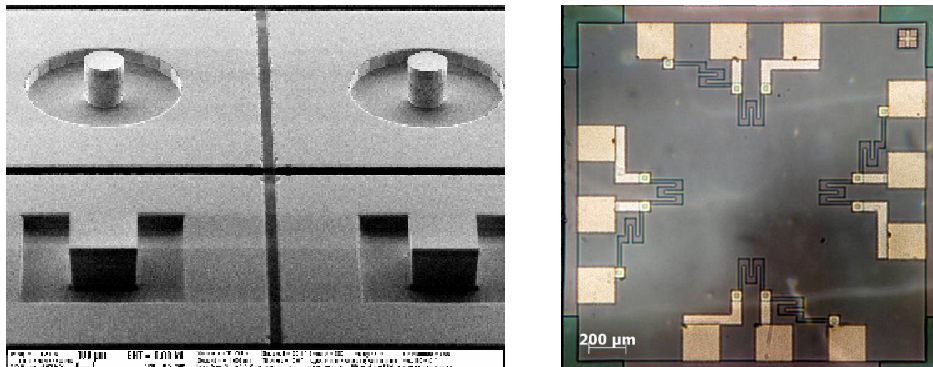


Figure 5 Front (left) and back-side (right) images of the fabricated sensors.



Figure 6 The measurement set-up with the force gauge and the chip

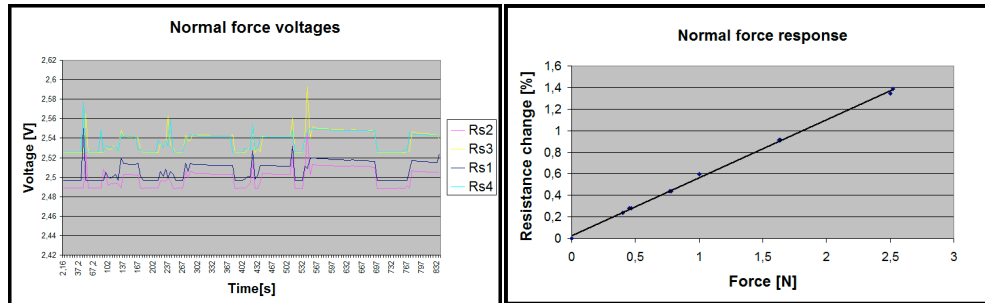


Figure 7 Voltage response of the resistors to normal loadings versus time. b) The linear input–output characteristics of the sensor with square shaped $162\ \mu\text{m}$ thick membrane and rod with side length of $200\ \mu\text{m}$

Thermal behaviour of 3-dimensional single crystalline force sensor (ENIAC SE2A)

G. Battistig, T. Weidisch, T. Retkes, M. Ádám, I. Bársony, A. Nagy, and T. Mohácsy

A piezoresistive-type integrable single-crystalline sensor was developed for 3D force sensing. The piezoresistance effect is inherently temperature-dependent; therefore thermal properties of the device were studied. Furthermore, the elastic cover and the packaging strongly affect the thermal behaviour of the sensor. The temperature dependence of the offset and the sensitivity were measured and the value of temperature coefficient of offset and sensitivity were calculated. In sensitivity we found a nonlinear relationship and a remarkable drop over the temperature of $45\ ^\circ\text{C}$. There are less demanding applications, where - in spite of their temperature sensitivity - the force sensors are appropriate, however, for precise tasks temperature compensation is indispensable. On this reason a new perforated membrane force sensor design was proposed and manufactured, providing the necessary signals for obtaining temperature compensated outputs.

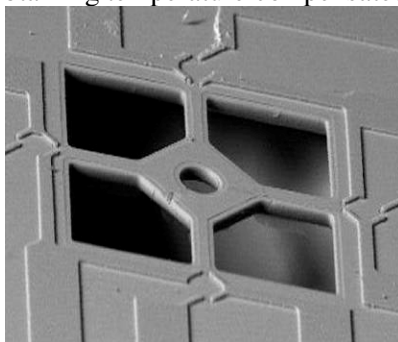


Figure 1 Previous design: SEM micrograph of the bare sensor (on the left) and the mounted and covered chip (on the right).

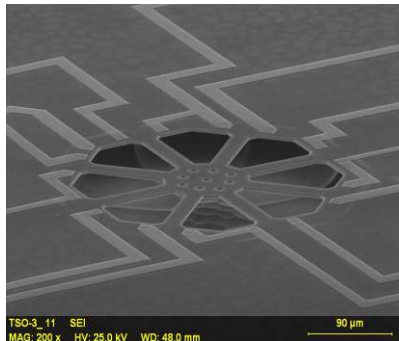
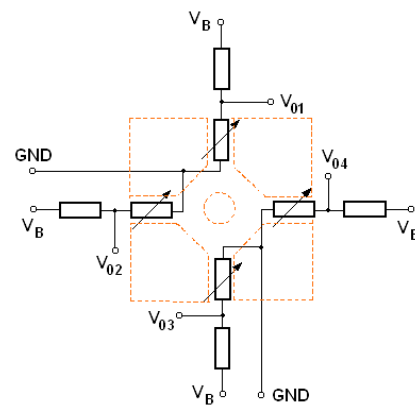
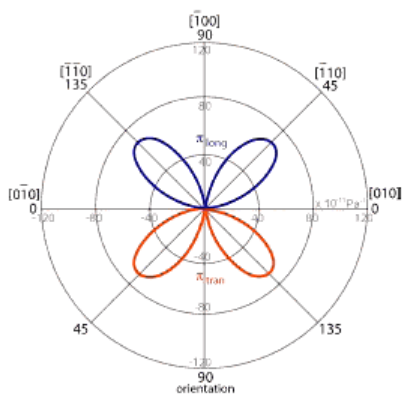
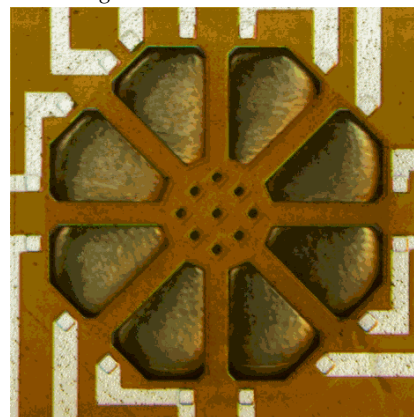
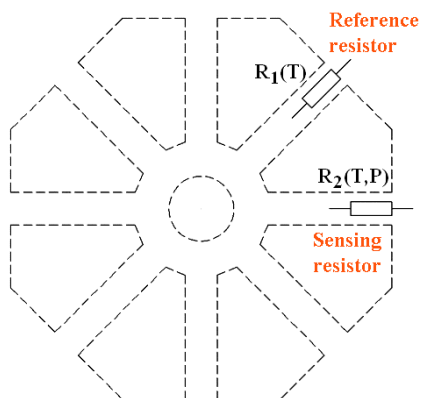


Figure 2 New design: for thermal compensation.



Strong orientation dependence of piezoresistivity in silicon

Scheme of a piezoresistive-type 3D force sensing element



Schematic top view and optical microscope image of the proposed and manufactured new 3D force sensor design.

Figure 3

Temperature sensitivity is a major concern for piezoresistive sensors. To eliminate the effects originating from different thermal boundary conditions in the reference and sensor elements, a new structure was proposed. The reference resistors are aligned to [100] or equivalent directions and they remain insensitive to mechanical stress. Therefore, they can be formed in thin bridges, where they operate at identical thermal conditions with the sensor elements on the same perforated membrane.

As our measurements show the Non-covered chips have a positive, while the elastic rubber covered ones a negative offset warm-up shift. Up to 5V bias the rate of change is nearly equal for both sensor types.

The reason for the thermal response in bare sensors is based on the temperature difference of the sensing and reference resistors. Reference resistors are placed in the heat-sinking bulk Si, while the sensing resistors lie on the thermally more isolated membrane so thus they are exposed to different thermal conditions.

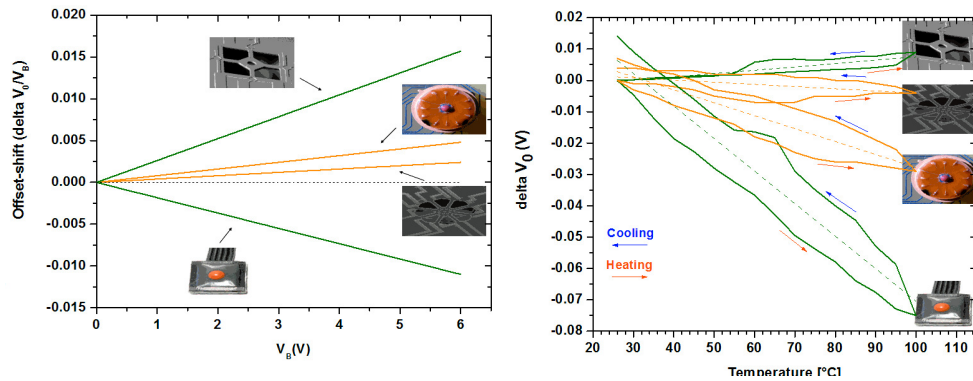


Figure 4 Offset-shifts of bare and covered sensors (left) vs. power supply and (right) vs. ambient temperature.

In order to calculate the thermally independent pressure sensitive component of the sensor element, the continuous measurement of the voltages $V_1(T)$ and $V_2(T,P)$, and the storage of $V_1(T_0)$ and $I(T_0)$ – both measured at T_0 – is required.

$$R_2(T_0, P) = \frac{V_2(T, P) V_1(T_0)}{V_1(T) I(T_0)}$$

A thermally compensated bulk micromachined 3D force sensor is developed. A novel approach is proposed based on the utilization of the anisotropic piezo-sensitivity in silicon, appropriate for realization by perforated thin Si membrane technology.

Separation of biological samples in microscale

(Projects EU FP7 P3SENS, ENIAC JTI, CAJAL4EU project via the National Office for Research and Technology)

Z. Fekete, P. Nagy, and P. Fürjes

Demands for analytical devices applicable for in situ diagnostics far from clinical environment using small sample volumes and not requiring professional staff is apparently increasing in the clinical practice. Such requirements can be fulfilled by microfluidic systems. This miniaturization effort enables, for example, the acceleration of low-cost clinical tests by largely decreasing sample amount needed for a single test and realizing High-Throughput (HT) quick and cost effective analytical systems.

One of the first preparation steps of blood sample tests is the separation of the blood plasma from whole blood, since the detection of specific blood markers in the blood plasma may prove the presence of several cardiovascular diseases. To establish fast diagnosis, the realization of that function in today's microfluidic systems is therefore essential. Special microfluidic structures can be applied for hydrodynamic focusing and positioning the solution in the microchannels, or for inertial separation of dissolved particles by size. Utilizing the Zweifach-Fung effect the highly polarised blood cells can be transported separately from the plasma.

Our group aimed the investigation of the Zweifach-Fung separation phenomenon. In order to analyse the geometric effects and biomechanics of red blood cell flow, special microstructures (see Figure 1) were fabricated in single-crystalline silicon by Deep Reactive Ion Etching (DRIE). The sealing cap and connections of the fluidic system was realized by a Nd:YAG laser in Pyrex glass. The leak-free alignment of the substrates was carried out by anodic bonding.

The results of the promising measurements, directed to the determination of the efficiency and quality of the above mentioned separation technique, are being evaluated.

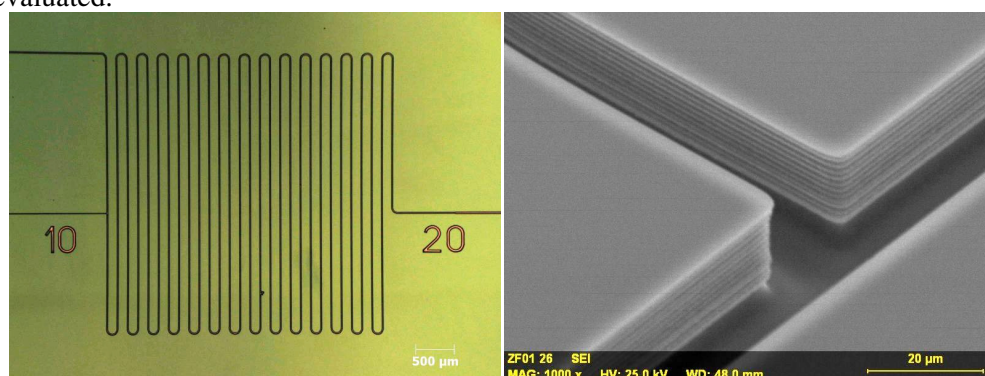


Figure 1 Representative silicon test structure for Zweifach-Fung plasma filtering fabricated by DRIE.

Sample transport in polymer based microfluidic system

(EU FP7 P3SENS project)

P. Fürjes, Z. Fekete, E. Tóth, and E. Holczer

Manipulation of fluids (e.g. biological samples) in analytical systems is a key issue in terms of the final applicability of these devices. In novel analytical microsystems the sample manipulation is executed by complex micro-fluidic structures, which can perform the main sample preparation tasks such as mixing, dilution, transportation, and separation; all of these complex tasks realized in a single integrated structure. Complex fluidic devices integrating active and passive micro-systems, as well as combining silicon micromechanics and polymer technology can be applied for fast, low cost and intelligent sample control at the microscopic scale.

The basic function of the fluidic structure is the transportation of the diluted sample from the inlets to the sensing area of the device. Another important function of the fluidic structure is the dilution and complete mixing of blood sample with an adequate buffer solution. Several possible mixing strategies can be found in macroscale as molecular diffusion, turbulent diffusion, advection and Taylor-dispersion. Due to the small dimensions of the microfluidic systems usually the flows are laminar and the component streams mix only by diffusion, creating a dynamic diffusive interface with predictable geometry. The advection generated by the fluid flow which results in a chaotic distribution of the molecules, could be an ideal mixing method in the case of microfluidics considering stable and laminar flow.

The mixing behaviour of the microfluidic structures was analysed by numerical modelling to determine the mixing efficiencies. For reference a simple T-mixer structure was implemented with rectangular cross-section. In addition, an advanced T-mixer staggered by blocks and a Herringbone type chaotic mixer structure were also investigated.

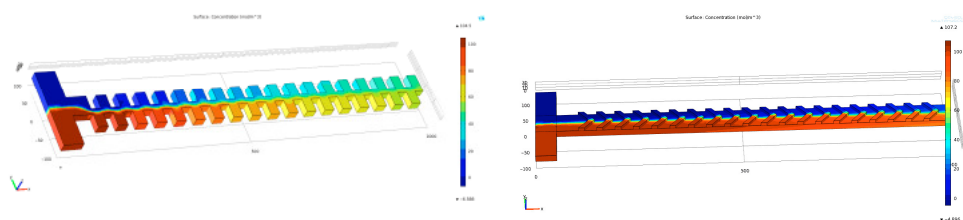


Figure 1 Representative concentration distribution in staggered blocks T-mixer and Herringbone mixer structure.

When micro-fluidic structures transport biological samples (like blood, serum, saliva, etc.) the material selection and the determination and control of surface effects taking place on the channel walls have crucial importance. Beyond the conventional materials applied in micromechanics like silicon and glass low cost polymer based systems gain increasing interest. The wetting effects of these materials have significant influence on the behavior of the flow. Moreover, from biological samples

the non-specific binding of proteins or other molecules on the channel surfaces is also critical and can influence the analytical results affecting the final applicability of the system. All of these effects have to be carefully considered and investigated in detail in order to find the most suitable materials for a given application.

Among the polymer materials the most attractive candidates to realize simple microfluidic systems are Polydimethylsiloxane (PDMS) and the epoxy-based negative photoresist*. These materials are relatively cheap (especially PDMS) and can be easily microstructured using standard photolithographic processes (with resolution of 1 μm at MFA). PDMS is also well suited for mass production, since it can be replicated from photoresist microstructures serving as replication masters. Using the above mentioned processes microfluidic channels in the thickness range of 5-100 μm can be fabricated at MFA. To form the microfluidics in different polymer materials (SU-8 and PDMS) two variations of the realization processes were developed. Both of them apply the described multilayer SU-8 technology to form the moulding form for PDMS or directly the microfluidic structure.

The transport fluidic systems subscribed further – containing 3 different mixer components – were realized in both PDMS and SU-8 polymer materials. The realized structures are presented in Fig. 2.

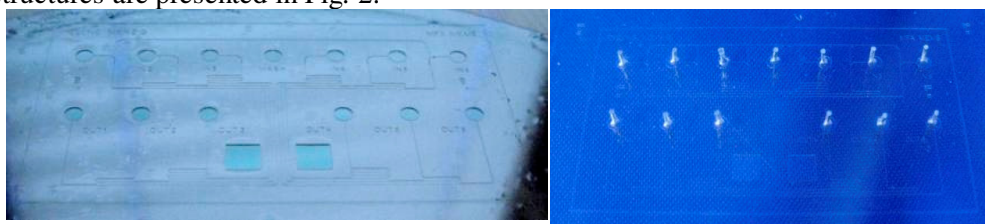


Figure 2 The microfluidic layouts realised in SU-8 (left) and PDMS (right) polymers.

The permeability and sealing of the fluidic channels are adequate although the pressure sustainability and washing and mixing efficiencies in case of the different mixer structure are to be evaluated. Fig. 3 represents the applicability of the realized structure containing the parallel channels.



Figure 3 Fluid flow in the 6 parallel channels over the sensing area of the optical structure.

*SU-8, MicroChem Corp.:

http://www.microchem.com/products/su_eight.htm

Chemically Modified Solid-State Nanopores for Sensing

(ENIAC JTI, CAJAL4EU via the National Office for Research and Technology, OTKA No. NF69262)

P. Fürjes, A. L. Tóth, and R. E. Gyurcsányi

Sensing with chemically-modified nanopores is an emerging field that is expected to have major impact on bioanalysis and fundamental understanding of chemical interactions on nanoscale down to the single-molecule level. The main strength of nanopore sensing [R. E. Gyurcsányi, *Trac-Trends In Anal. Chem.* 27 627-639 (2008)] is that it implies the prospect of label-free single-molecule detection by taking advantage of the built-in transport-modulation-based amplification mechanism. Here we present the development of nanopore based sensors, including methodologies for fabrication of single- and multichannel nanopores in solid-state membranes with diameters ranging from 5 to 100 nm, their chemical modification and application for bio(chemical) sensing (Fig. 1).

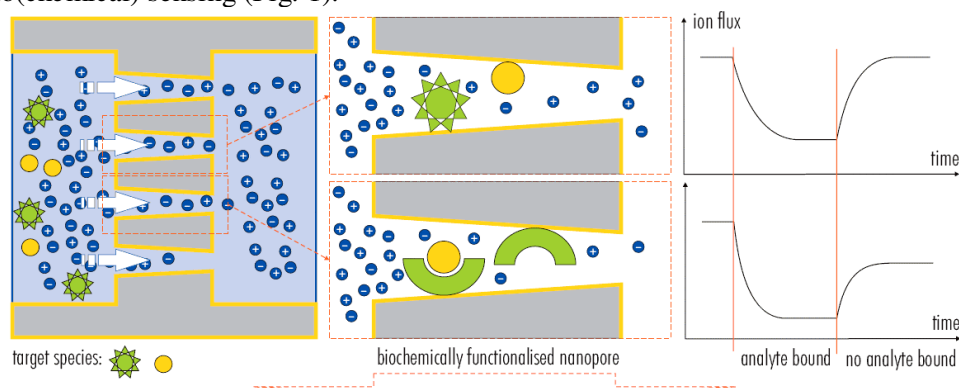


Figure 1 Application of the nanopores for sensing

Solid-state single gold nanopore structures were fabricated by the combination of the silicon based 3D MEMS/NEMS technology, and special subsequent nanofabrication techniques, such as subtractive nanoscale modification of the existing microstructure by focused ion beam etching. (Fig. 2.a) **Multichannel gold impregnated nanopore membranes** (Fig. 2.b) were also fabricated and characterized. For interfacing the nanopore membranes a special crossing microchannel structure was designed combining the silicon 3D micromachining with both SU-8 and PDMS polymer structuring.

In order to use nanopores as selective detectors, their surfaces must be chemically modified. The functionalization of the nanochannels passing through the gold layer and the method of transport-modulation-based selective molecule detection were developed by the Research Group for Technical Analytical Chemistry of the Hungarian Academy of Sciences at Budapest University of Technology and Economics.

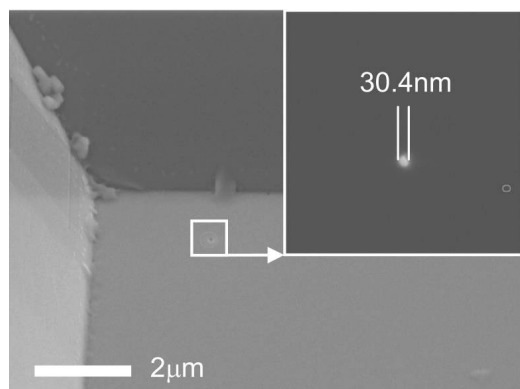


Figure 2a Single nanopore in solid-membrane.

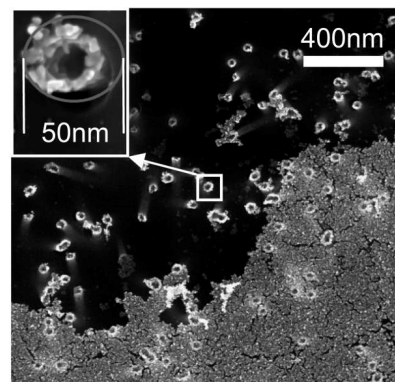


Figure 2b Multichannel nanopore membrane

The capabilities of nanopore based sensors in terms of detection limit are explored by using random walk simulation and multiphysics modeling. Apparently, the detection limit of single nanopore based affinity sensor is determined by the probability of a successful encounter between the nanosensor and analyzer. Since in principle even a single molecule can be detected by nanopore sensors, the detection limit of such sensors was also explored in terms of concentration. However, significant improvements are obtained upon directing the analyte into the sensing zone of the nanopore by means of an electric-field or pressure gradient.

Besides introducing specific receptors chemical modification can be also used to protect surfaces from biofouling, or to induce specific transport modulation effects. Aspects of thiol (dithiolan, disulfide) chemistries for building up self-assembled molecular architectures with molecular recognition capabilities (Fig. 3) are demonstrated [50].

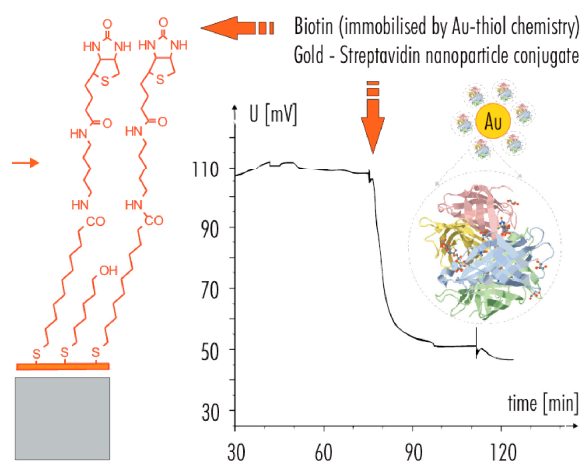


Figure 3 Selective molecule recognition by a chemically modified gold nanopore

Investigation of silicon-based superhydrophobic surfaces

(EU FP7 P3SENS project)

P. Fürjes, Z. Fekete, and T. Pardy

Recently there was a significant progress in the development of water-repellent surfaces regarding biomimetics or ElectroWetting on Dielectric (EWOD) for digital microfluidics. Bioinspired surface topographies are of key importance, therefore a range of micromachining concepts have been demonstrated. The fabrication of superhydrophobic surfaces has involved a wide variety of techniques including surface preparation, micromachining and the application of several surfactants. In spite of the rapid development of dry etching techniques, like deep reactive ion etching (DRIE), there is still room for further investigation as regards the combination of less expensive wet etching techniques.

The functionality of the micro- or nanofluidic structures is significantly influenced by the surface properties of the applied structural materials. The fluidic behaviour can be modified by micro- and nanoscale surface structuring and deposition of additional coatings. In our work, the effects of 3D surface topography, nanoscale roughness and additive chemical layers were discussed.

MEMS compatible processes, as two-step wet chemical etching and Deep Reactive Ion Etching was elaborated and characterised for modification of surface properties of silicon combined with subsequently deposited dielectric layers (Hexamethyl-disilazane - HMDS or plasma-polymerised fluorocarbon). The feasibility of the combined technique was demonstrated by the analysis of the wetting behaviour of the realised structures applying contact angle measurements. The developed micro- and nanoscale surface topographies by wet and dry etching techniques was also characterised by AFM and SEM.

In our laboratory, a two-component alkaline etching (NaOH, NaOCl) in case of different substrate orientation and subsequent polishing ($\text{HF}:\text{HNO}_3:\text{H}_3\text{PO}_4$) with varied mol-ratio was investigated. The proposed alkaline etching was successfully applicable for the formation of high aspect ratio microstructures, see Figs. 1(a) and (b). To evaluate the feasibility of the technique microstructures of similar patterns were also produced by DRIE (Fig. 1(c)).

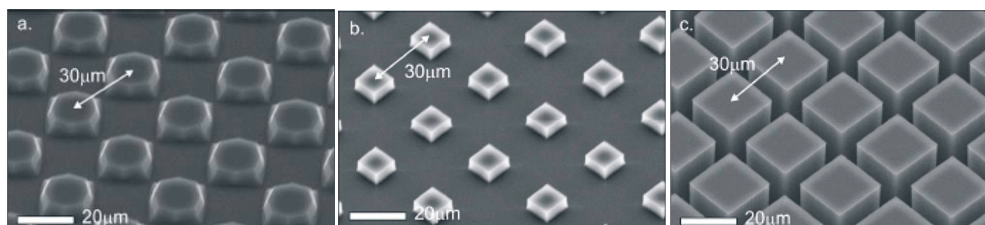


Figure 1 3D silicon microstructure array formed by two component alkaline etching (a, b) and deep reactive ion etching (c.)

The combination of the 3D bulk micromachining and the subsequent chemical layer deposition steps is expected to modify the surface behaviour of the silicon radically. The microstructured silicon surfaces coated by plasma-polymerised poly-fluoro-carbon represented excellent hydrophobicity (see Fig. 2).

Contact angle measurements in case of the different structures (geometric parameters are listed in Table I) coated by poly-fluoro-carbon deposited by DRIE proved the feasibility of the fabrication process. Results for two-component alkaline etching solution (at the orientation of 45°) are illustrated in Fig. 3.

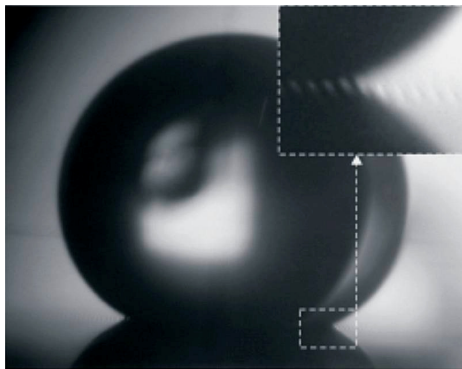


Figure 2 Superhydrophobic behaviour demonstrated on solid-air composite surface fabricated by two-component alkaline etching and subsequent plasma-polymerisation of poly-fluoro-carbon layer. Air cushions are clearly shown in the enlarged area.

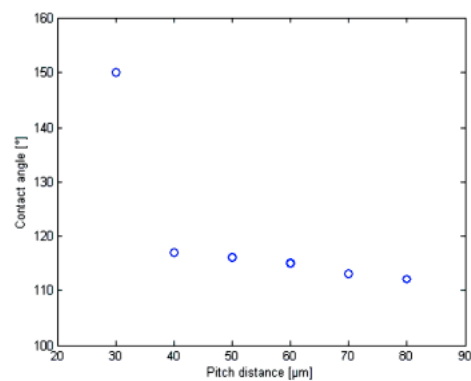


Figure 3 Measured contact angles at different pitch distances in case of chips fabricated by alkaline etching. Cassie-Wenzel transition is apparently noticeable on the figure.

Integration of buried channels in cerebral silicon microprobes

Z. Fekete, A. Pongrácz, and Á. Szendrey

Studying physiological processes at the neuronal population level is essential in order to elucidate the complex neural mechanisms of information processing in the brain. Our group's previously developed probe shaft (Fig. 1) is being modified in order to involve the integration of microchannel systems. However, several probe designs were reported in literature according to the experimental needs, during surgical implantation the injection technique in such microprobes does still not meet the demands of accuracy and reliability established by researchers in this field.

The production technology of buried channels is based on Deep Reactive Ion Etching (DRIE). The subsequent using of Bosch process, anisotropic oxide and isotropic silicon etching recipes results in microchannels well below the wafer's surface (Fig. 2). By the deposition of LPCVD poly-silicon sealed channels are created which can be used as part of injection systems in microcantilevers used as i.e. cerebral probes. The technological parameters of the process are still being tuned, and the effects of the plasma etching mechanisms are investigated in order to establish design rules.

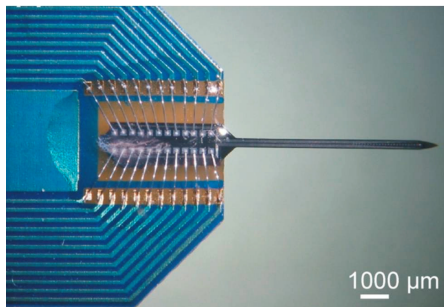


Figure 1 Ready-to-use in-plane silicon microprobe developed in MFA

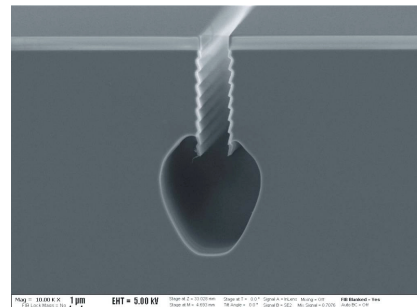


Figure 2 „Almost buried” microchannel in silicon before the last step of LPCVD poly-Si deposition

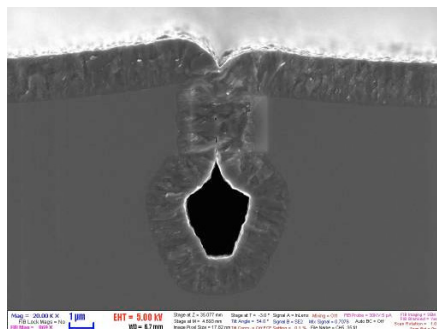


Figure 3 Buried microchannel after the SiO_2 removal and LPCVD poly-Si deposition.

Development of THz detectors

(OTKA No 77843, 77997, and 73424 NK)

B. Szentpáli, P. Fürjes, E. László, P. Basa, G. Battistig, I. Bársony,
G. Károlyi (BME), and T. Bercei (BME)

Recently THz and mm wave radiations find widespread application, albeit their management is more difficult than that of microwaves. A serious bottleneck is the lack of choice of appropriate detectors. Even the best microwave Schottky diodes have their cut-off frequency within these bands. Micromachined thermopiles are widely exploited for measuring the intensity of the infrared radiation, etc. A novel MEMS thermopile structure is proposed, which consist of linearly arranged p- and n-type polysilicon strips instead of the conventional loop-like configuration [129]. The traditional thermopile and the novel structure are shown in Fig. 1 (a) and (b).

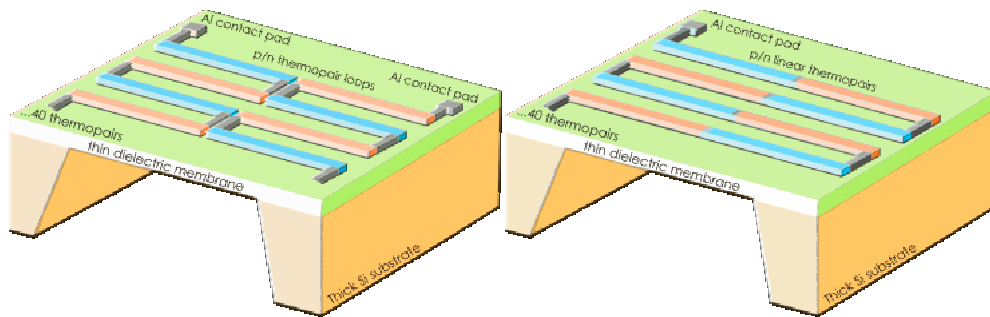


Figure 1 (a) The outline of a MEMS thermopile for measuring the infrared radiation. The good heat isolation on the membrane makes possible the formation of temperature difference between the hot and cold ends of the thermocouples.

Figure 1 (b) The proposed linear arrangement of the thermopairs. Here the thermocouple lines act as short circuited dipole antennas, in which the distribution of the induced current is sinusoidal, having the maximum value at the centre. Therefore the heat formation peaks around the middle of the lines, exactly where it generates the highest thermoelectric effect.

The conventional poly-silicon thermopile technology was combined and improved by double side bulk silicon micromachining for the realization of the designed structure [131], [M. Graf et al, Meas. Sci. Technol. 18 R59-R75 (2007)], [H. Seidel et al, J. Electrochem. Soc. 137 3612-3638 (1990)]. Towards reducing the residual stress of the suspended membrane a stacked layer structure was applied containing non-stoichiometric silicon-nitride (SiN_x) and silicon-oxide (SiO_2) as structural materials with adequate thickness ratio. The sheet resistivities of the n and p type poly-silicon were $23.7\Omega/\square$ and $37\Omega/\square$, respectively.



Four types of measurements were performed on the devices. The responsivity against direct heating was investigated on loop-like structures with the integrated heater placed between the hot ends of the loops. The thermal coefficient of the heater resistance was obtained from independent measurement, and using this value the temperature of the heated resistor was calculated. On this way the thermopower was determined to be 18 mV/K for the 40 p-n pairs, while the responsivity was found to be 90 V/W. The responsivity to infrared radiation was measured with the help of a black body heated gradually up to 100 °C. There is no information about the reflected and transmitted power; the responsivity was calculated as the total black-body radiation impinging the sensor, which was not covered by any absorbing medium. No significant difference was observed between the behavior of the linear and the loop-like structures.

The responsivities in the microwave and millimeter wave bands were measured in the K_u -band, at 13 GHz and in the W-band at 100 GHz. In the K_u -band the radiation emitted by the open end of the rectangular waveguide was used, while at W-band the beam was expanded by a small horn antenna. In these experiments there was no any information on the reflected and transmitted signal and the responsivities were calculated from the full power. The polarity dependence was very significant at both frequencies. The maximum of the output was obtained when the E field was parallel to the lines and it falls to the level of the background noise in the orthogonal case. The loop-like structures did not produce any significant output over the background. Table I summarizes the measured responsivities.

| Method | Responsivity [V/W] |
|--------------------|--------------------|
| electrical heating | 90 |
| thermal radiation | 20 |
| 13 GHz | 0.2 |
| 100 GHz | 5.58 |

Table I

It is obvious that electric heating results in the largest responsivity. In this case all the power is directly introduced into the thermopile, close to the hot point. The infrared radiation is absorbed only partly and it is uniformly distributed along the surface. The responsivity at 100 GHz is reasonably greater than at 13 GHz. This fact supports the antenna-like operation of the device; the 1.6 mm long antenna should have a resonance at around 100 GHz, while at 13 GHz it is a short dipole with low efficiency.

The measurements at 100 GHz were made at the Universität Duisburg-Essen, with the kind help of Vitaly Rymanov and Prof. Andreas Stöhr. Their contribution is acknowledged.

Deposition of Al doped ZnO layers by Atomic Layer Deposition

(OTKA NK 73424, TFSOLAR02)

Z. Baji, Z. Lábadı, Z. E. Horváth, M. Fried, B. Szentpáli, and I. Bársony

In the field of thin film solar applications there is a stringent need for limitation of thermal budget given by the substrate and the active layer alike. Recent advancement in polymer-based solar cells restrict the maximum applicable temperature to $< 250^{\circ}\text{C}$. A vacuum-compatible low temperature method for TCO ZnO deposition could be the use of Atomic Layer Deposition (ALD) especially when the requirements for conformality are substantial, as in the case of e.g. thin buffer layers. Setting the conductivity of this TCO or buffer layer is, however, not obvious, since the introduction of substitutional Al dopants into the ZnO matrix is a thermal budget influencing step as well.

Our work was aimed at the study of a combined deposition of a controlled level of Al content in ALD grown ZnO by using alternate precursor pulse method. The source of Al dopants in this case is the AlO_x interlayer. The ALD temperature window for Al_2O_3 is, however, around 300°C , above the optimum ZnO temperature window of around 170°C . We analysed the incorporation and activation of a controlled amount of Al around this optimum temperature of the ZnO ALD growth.

We examined both the effects of different Al contents and deposition temperature on the conductivity and structure of the layers, in a wider doping and temperature range.

Results:

- (i) specific resistivity of the layer as a function of Al content shows a minimum curve
- (ii) incorporation of Al into the layer is proven by EDS spectra
- (iii) even 0.1 at % Al decreases the specific resistivity
- (iv) XRD spectra of the samples show that Al incorporation changes the preferred orientation of the polycrystalline layer
- (v) layers with resistivity of $10^{-3} \Omega\text{cm}$ can be deposited at 150°C substrate temperature

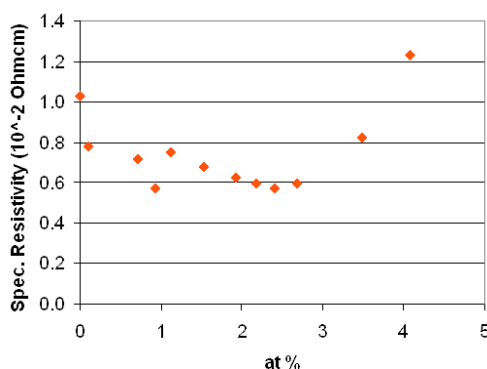


Figure 1 Specific resistivity vs. Al content of Al:ZnO layers deposited at 150°C

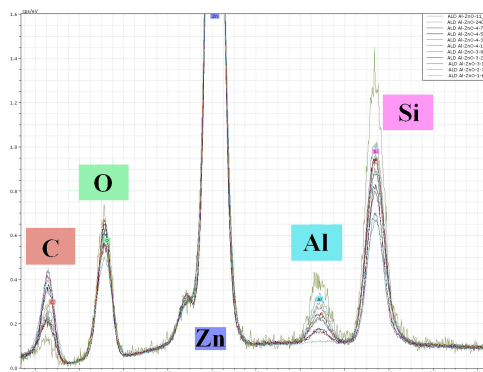


Figure 2 EDS spectra of the ALD Al:ZnO layers showing the Al incorporation

Growth of CIGS layers by post-selenization of metal precursors

(OTKA NK73424, TFSOLAR02)

Z. Baji, Z. Lábadi, G. Molnár, A. L. Tóth, and I. Bársony

The post-selenization of CuInGa metal precursor layers is a possible way to form CuInGaSe₂ active layers for solar cells, but it is relatively less developed and less extensively studied area. Our method to form CIGS layers is based on precursor evaporation from an alloy source (alloying takes place during the heating of the evaporation sources). Metal precursors were weighed in to provide CuIn_{0.8}Ga_{0.2}Se₂ compound. Evaporation of metals was made from Ta boat at 1500–2000 °C and the full load was evaporated from the boat. Metal precursors were subsequently selenized in sealed glass ampoules under Se vapour pressure at 500°C.

XRD spectra of the layers showed that the whole layer consisted of CuIn_{0.8}Ga_{0.2}Se₂ phase. Fig. 1 shows the morphology of the layer after 5 min post-selenization.

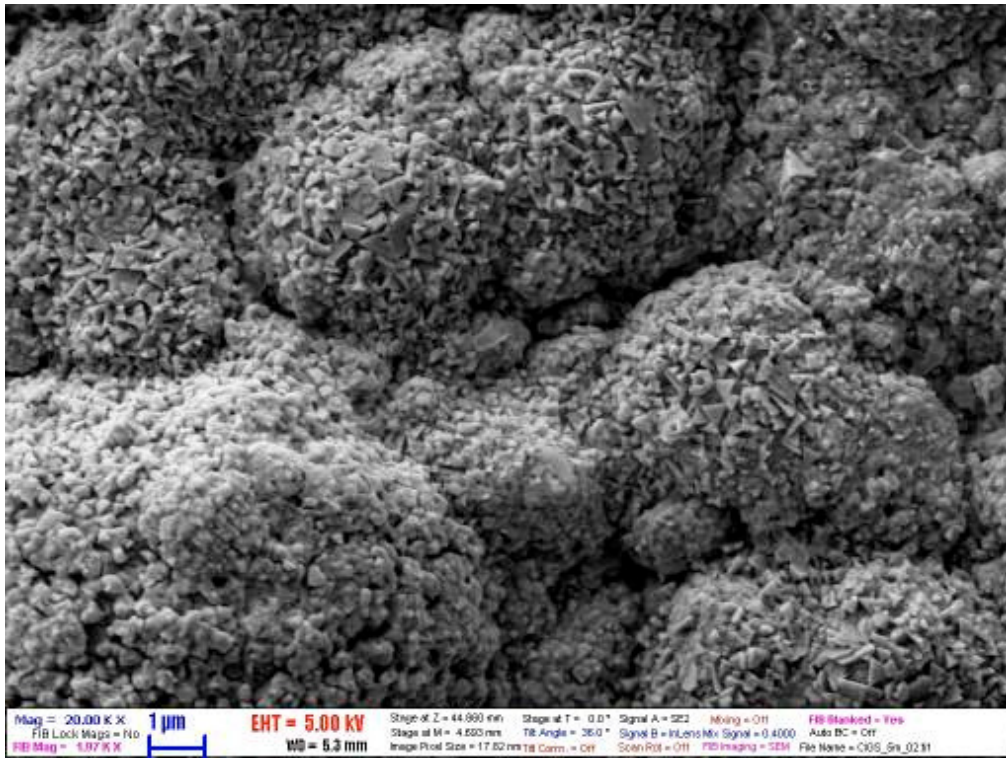


Figure 1 SEM morphology of a CIGS layer formed by 5 min post-selenization at 500 °C

Wafer bonding for microelectronics

T. Kárpáti, and A. E. Pap

The wafer bonding technology is of great importance in microelectronics (for example packaging) and micromachining. Wafer bonding refers to the mechanical fixation of two or more wafers to each other. It is of great account that the whole bonding process is compatible to microelectronics technology. The SüSS MicroTech SB6L Wafer Bonder at MTA MFA allows low temperature bonding (max. 500°C). Also, both electro-assisted and wafer bonding by thermocompression is possible. We can bond several kinds of materials and wafers of various sizes (max. 4"), see Table I. Some of our results for wafer bonding are shown in Figs. 1-3.

| Materials | | Type of wafer bonding | | Details |
|-----------------------|------------------|-----------------------|--------|------------------|
| Type A | Type B | Thermocompression | Anodic | Bonding strength |
| Si | Si | + | | Strong |
| Si | Glass* | | + | very strong |
| Si + SiO ₂ | Glass* | | + | strong |
| Si + SiN _x | Glass* | | + | weak |
| Glass* | Glass* | + | | strong |
| Glass** | Glass** | + | | strong |
| Glass* + dep. Si | Glass* | | + | very strong |
| SiN _x | SiN _x | + | | weak |
| Al | SiN _x | + | | weak |
| Al | Al | + | | weak |

Glass* - Schott Borofloat® 33; Glass** - quartz glass

Table I Different materials and their nature of bonding.

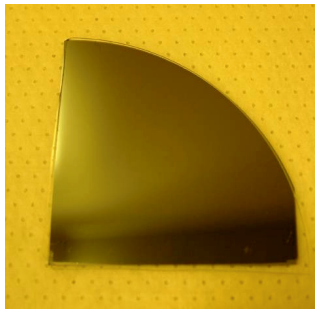


Figure 1 Si and Borofloat® 33 anodic bond

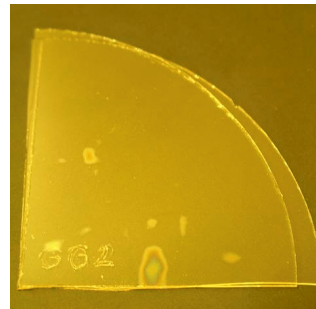


Figure 2 Glass to glass thermocompression bond



Figure 3 Glass to glass anodic bond with deposited Si intermediate layer

The great advantage of wafer bonding is its flexibility and wide range applicability in the development of different MEMS structures. It could form simple hermetically closed cavities or create mechanically fix substrates for chips. By means of bonding it is easy to develop microfluidic devices with structured wafers. Another application is to create back side electrical contacts for sensors, see Figs. 4-5. In addition, Fig. 6 shows how a closed pressure of 500 mbar can unsharpen a thick Si membrane.

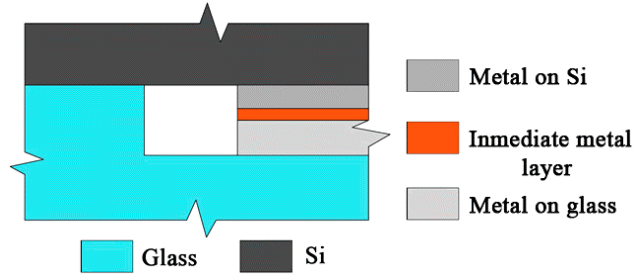


Figure 4 Schematic draw of electrical contacts and mechanical fixation between two wafers

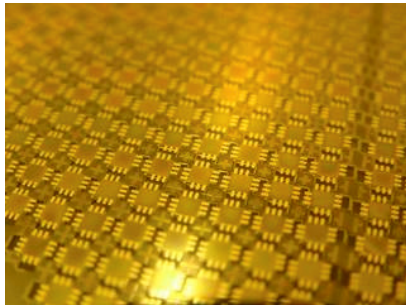


Figure 5 Electrical contacts between two wafers.

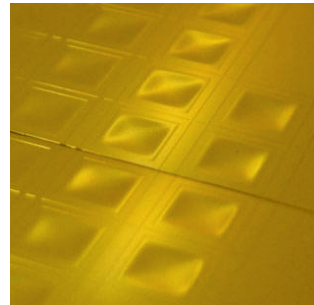


Figure 6 A pressure of 500 mbar closed in a cavity

One of our completed projects with wafer bonding technology is the silicon based capacitance pressure sensor. The device can measure in the 0-1000 mbar pressure range. The geometrical size of the sensor is 5 mm × 6 mm with 1 mm thickness. The integrated membrane thickness is 10 μm and the sensing area is 11.56 mm², see Fig. 7). Fig. 8 shows measurements performed with capacitive pressure sensors.

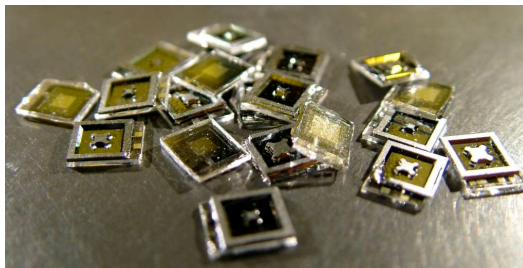


Figure 7 MEMS capacitive pressure sensors.

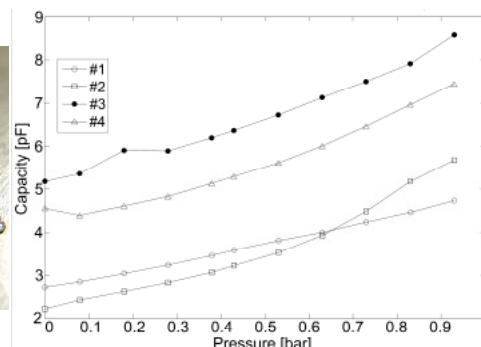


Figure 8 Measurements performed with MEMS capacitive pressure sensors.

MBE related research and development in MFA

(OMFB-01109/2009, OTKA K75735, OTKA K77331)

Á. Nemcsics, I. Réti, G. Tényi, P. Kucsera, P. Harmat, L. Tóth, R. Hodován,
Á. Szendrey, B. Pődör, J. Balázs, L. Dobos, and J. Makai

The main part of our MBE equipment is originated from a donation, which was a consequence of a long time scientific cooperation led by Á. Nemcsics. The MBE Laboratory (Joint Research Laboratory of MTA-MFA and ÓE-MTI) shared between our Research Institute and the Óbuda University, Institute for Microelectronics and Technology was inaugurated in 2009 November [Á. Nemcsics *et al*, *El. Tech. Mikrotech.* 48 33-35 (2009)]. Our MBE equipment has three UHV chambers such as a reactor-, a supplement-, and a load-lock chamber. The reactor chamber is equipped with 4 effusion cells (Ga, As, In, Al). The sample holder is mounted on a precision manipulator. The electron beam sample heating arrangement provides a quickly changeable temperature control, which is important at the production of multi quantum well structures. A 10 kV RHEED is provided for in-situ monitoring of the process. A sample chamber is joined to the main chamber with a vacuum shut-off valve where the manipulation of the sample is facilitated by magnetic rods. The RHEED picture can be viewed on a fluorescent screen opposite of the electron gun. Since the fluorescent screen is not suitable for the accurate measurement of the intensity change, a Faraday-cup, mounted on a precision manipulator, measures the electron current directly, which is the speciality of our equipment. A turbo pump and an ion-getter pump provide for the evacuation of the two chambers. The load-lock chamber with the manipulator and with four sample containers is our own development [90]. Furthermore, the equipment was supplied by PLC controlled heatings and shutter moving and also by RHEED evaluation with image processing [72, 89].

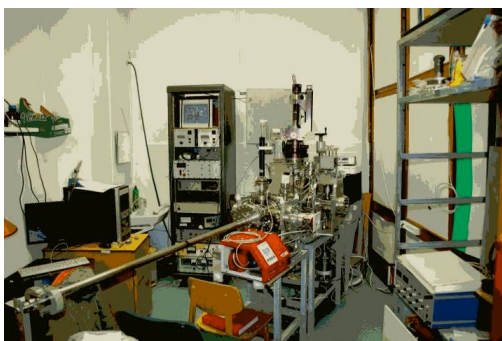


Figure 1 View of our MBE equipment.

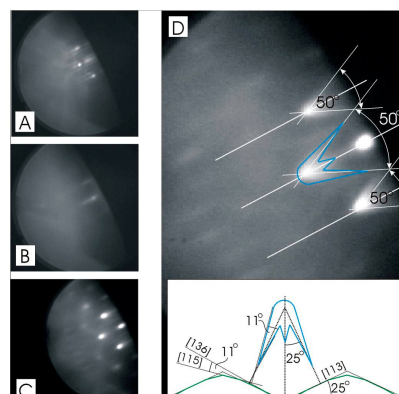


Figure 2 The change of the RHEED pattern during the QD formation



Investigation of MBE grown quantum structures.

Recently, the growth of self-assembled quantum structures has been intensively investigated for basic physics and device applications. It is very important to understand their growth process and to know their particular shape. The archetypal system of these nano structures is the lattice-mismatched system, where the strain-induced process leads to the formation of QDs. The detailed electronic structure of a QD, which governs electronic and optical properties, depends on its shape. It is generally agreed that the essential driving force for coherent lattice mismatched QD formation is strain relaxation. In this field, the self-assembled lattice matched quantum structures employing droplet epitaxy is an interesting and novel alternative against the established technology of strain-driven QD formation. With this method, we can prepare not only QDs but quantum rings (QRs) and other various quantum structures. Today, a theoretical description is not yet available for the underlying growth mechanism, i.e. the development of faceting in the case of droplet epitaxy even so it is very important to understand the growth kinetics. We have given explanation of the RHEED pattern for different quantum structures [Á. Nemesics *et al*, *Mat. Sci. Eng. B* **165** 118-121 (2009)]. Few particular behavior of their growth kinetics is also explained [93], [Á. Nemesics *et al*, *Microel. Reliab.* (2010) in press]. The QD and QR structures are also investigated by photoluminescence (PL) method [Á. Nemesics *et al*, *phys. stat. sol. c* (2010) in press].

LPE growth and optical investigation of InGaAsP/InP double heterostructure wafers

V. Rakovics

GaInAsP/InP is an ideal material system for the fabrication of double heterostructure devices. As InP has higher bandgap than the lattice-matched GaInAsP active layer, absorption losses inside the device structure can be minimized. Liquid phase epitaxy (LPE) was used for the development of device structures, as the composition of the active layer can be relatively easily adjusted by weighing appropriate amount of the materials into the growing melts.

Photoluminescence (PL) is widely employed as a non-destructive characterization technique for epitaxial device structures, yielding measurements that may be correlated with final device performance. In order to obtain useful correlations, however, a number of experimental factors must be considered. We discuss herein the effect of probe source wavelength on the results of experiments. InGaAsP/InP double heterostructure diode wafers (Fig. 1.) grown by liquid phase epitaxy were characterized by photoluminescence and infrared transmission measurements.

Double heterostructure InGaAsP/InP diodes were grown in a computer-controlled LPE apparatus equipped with a multibin slider boat. Single-phase melts with relatively high supersaturations were used for all growth experiments. Four-layer structures were grown on (100) oriented InP substrate consisting of an n-InP buffer layer (3–4 μm), an undoped GaInAsP active layer (1–2 μm), a p-InP confinement layer (6–10 μm), and a p⁺ InGaAsP contact layer (0.5–1 μm). PL and IR transmission spectra have been measured by a fiber optic diode array spectrometer. Tungsten halogen lamp source was used for transmission measurements.



Figure 1 Schematic cross-section of an InGaAsP/InP double heterostructure diode.

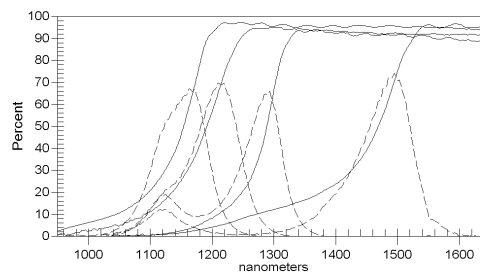


Figure 2 IR transmission and photoluminescence spectra of 1180, 1220, 1290, and 1500 nm LED wafers. The dashed lines show the luminescent spectra at 1120 nm excitation wavelength.

Fig. 2. shows that information obtained from luminescence and infrared transmission are compatible regarding active layer compositions, but in the case of thick active

layers the thickness and compositions of quaternary contact layers remain hidden in transmission measurements, as the active layer is not transparent for higher energy photons.

The optical band gap of direct band gap semiconductors can be obtained from their optical absorption spectrum using $\alpha = A((h\nu - E_g)^{1/2})/h\nu$, where α is the absorption coefficient, A is a constant, $h\nu$ is the energy of the absorbed light, and E_g is the band gap. PL peaks corresponding to 1180 nm contact layer are also not appearing in the spectra. As it is shown in Fig. 3, complex and informative luminescent spectra have been obtained by using visible sources for excitation of InGaAsP/InP double heterostructure diode wafers. The thin contact layer transforms the high energy exciting light to lower energy photons which can excite the active layer, although the InP confining layers are not transparent for primary exciting photons. The peaks corresponding to the active and the contact layers are clearly seen, but with smaller intensity. Intensity ratio of the corresponding active and contact layers is influenced by their thicknesses, and is also affected by the excitation wavelength. Fig. 4 shows the PL spectra of 1510 nm LED wafer at three different excitation wavelengths.

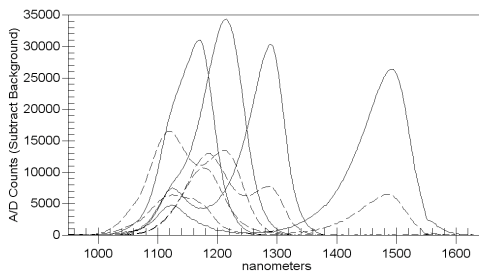


Figure 3 PL spectra of InGaAsP/InP heterostructure wafers. Solid (dashed) lines show the spectra with 1120 nm (525 nm) excitation wavelength.

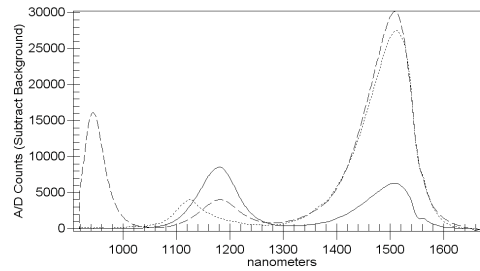


Figure 4 PL spectra of InGaAsP/InP double heterostructure LEDs with 1510 nm active and 1180 nm contact layers. Excitation wavelengths: 1120, 940, and 525 nm for dotted, dashed, and solid lines, respectively.

The two short wavelength peaks are only side effect of the scattering excitation light from the back side of the wafer, but both characteristic peaks can be observed at visible and near infrared excitation. The peak wavelengths obtained by the evaluation of the PL spectra measured with two different excitation sources are practically the same values. In summary, PL intensity spectra are influenced by absorption and energy transfer between the quaternary layers. The peak positions are precisely indicating the composition of the lattice-matched quaternary layers, but for determination of the layer thicknesses an additional measurement, such as optical transmission, is necessary. After the calibration of the PL peak intensity ratios with the quaternary layer thicknesses, the PL measurement is suitable for the quality control of InGaAsP/InP double heterostructure wafers.

Reactive deposition epitaxy growth and electronic properties of iron silicide nanoparticles on Si(001)

(OTKA K81998)

G. Molnár, L. Dózsa, and Z. Vértesy

Future generation thin film solar cells have to use abundantly available, non toxic and environmentally friendly chemical elements. Semiconducting β -FeSi₂ is a possible material which has 23% theoretical efficiency in solar cells, and both its layer and nanoparticle forms have potential applications in photovoltaic technology. Recently, a composite β -FeSi₂/Si film was proposed for photovoltaic use, where charge carriers are generated in the iron silicide particles, which has high photoabsorption coefficient, and the carrier transport takes place in silicon. The motivation of our research was to find proper methods for the preparation of β -FeSi₂ nanostructures.

The iron silicide samples were prepared by reactive deposition epitaxy (RDE), where iron particles were deposited onto heated substrates. The phases and structures were characterized by reflection high energy electron diffraction (RHEED), scanning-SEM and transmission electron microscopy (TEM), atomic force microscopy (AFM), and by Fourier transform infrared spectroscopy (FTIR). The electrical characteristics were investigated by I-V and C-V measurements and the defects were measured by DLTS [Vouroutzis N *et al*, J. Alloys Comp. **448** 202 (2008), and Tsormpatzoglou A *et al*, J. Appl. Phys. **100** 074313 (2006)].

The iron silicide nanoislands were successfully grown by RDE on Si(001) substrate. The size distribution and shape of the formed islands depend on the amount of deposited iron and on the annealing after deposition. Using higher temperature and longer time annealing a greater fraction of iron silicide transforms into the β -FeSi₂ phase.

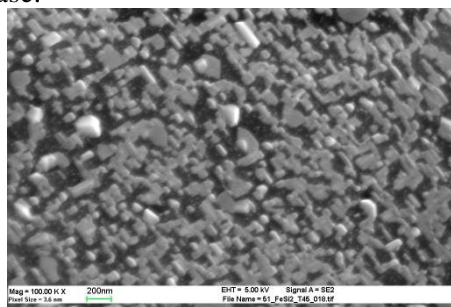


Figure 1 SEM image of a sample with 3 nm deposited Fe thickness.

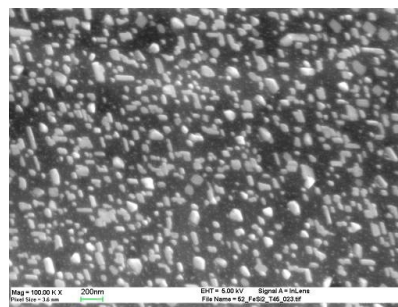


Figure 2 SEM image of a sample with 1 nm deposited Fe thickness.

The size of the dots increases with the annealing time as a consequence of Ostwald ripening and coalescence. To optimize the islands size and β -FeSi₂ phase content further experiments are needed. In case of successful experiments, iron silicide nanostructures may be used as environmentally friendly more effective solar cells.

The detection and identification of contamination in silicon is of technological importance. For understand the electrical properties of nanostructures high spatial resolution is necessary. In this work we used a new method of point defect identification [Dózsa L *et al*: Scanning tip measurement for identification of point defects, accepted for publication in *Nanoscale Research Letters*]. The electrical characteristics are measured by a DLTS system using a preamplifier. The method is illustrated by measurements performed on iron silicide nanostructures. Fig. 3 shows the detection of Fe-related deep level defects through a series of frequency scan DLTS spectra measured on large-area Schottky junctions.

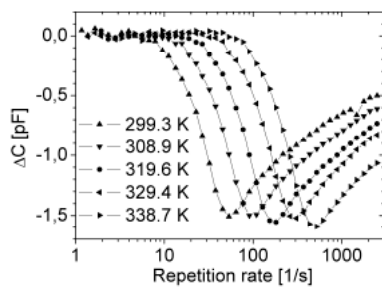


Figure 3 DLTS frequency scan spectra measured in a DLS-83D system at different temperatures.

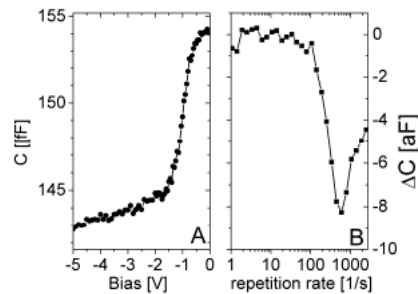


Figure 4 C-V characteristics (A) and DLTS frequency scan (B) measured on a tungsten tip positioned at tunneling distance from the surface.

Capacitance-voltage characteristics and capacitance DLTS frequency scan of the measuring tip positioned at tunneling distance from the silicon surface is shown in Fig. 4. Both the C-V and DLTS characteristics are analogous to characteristics measured in macroscopic Schottky junctions. The preamplifier increases the capacitance sensitivity 200 times, while the current sensitivity increases 1000 times, which enables DLTS measurements on scanning tip-semiconductor junctions.

Reorganization of silica nanoparticles under ion irradiation

(Bilateral project HR-20/08)

Z. Zolnai, S. Lugomer, A. L. Tóth, and I. Bársony

Recent modern topics of nanoscience and nanotechnology relate to the hexagonally ordered mono- and multilayers of silica nanoparticles, which can be considered as e.g. tunable photonic crystals or nanomasks used for modification of the optical, electrical, magnetic or structural properties of macroscopic surfaces at the nanoscale by low energy ion bombardment [N. Nagy *et al*, Appl. Phys. Lett. **89** 063104 (2006)]. Beyond surface patterning, these nanofabrication processes are accompanied by the reorganization of the silica monolayer due to ion-particle and particle-particle interactions, see Fig. 1. Our motivation was to shed more light on this process observed under ion bombardment, and its dependence on the nanoparticle size and ion fluence. The low energy (30 keV) scanning focused Ga⁺ ion beam (FIB), as a commonly applied nanofabrication tool, has been used to irradiate the silica monolayers.

We show that the induced patterning of silica particles can be associated with their charging, Coulomb repulsion and motion, heating/surface melting, discharging, particle-particle and particle-substrate adhesive interactions, and causing their reorganization into chain-like clusters [S. Lugomer *et al*: Self-organization of silica nanoparticles induced by the ion beam, to be published in phys. stat. sol. a (2011)]. The calculation of charge accumulation is based on a previous experiment [S. Yogev *et al*, J. Appl. Phys. **103** 064107 (2008)] where the surface potential change induced by FIB was measured with Kelvin probe microscopy on planar silica layers.

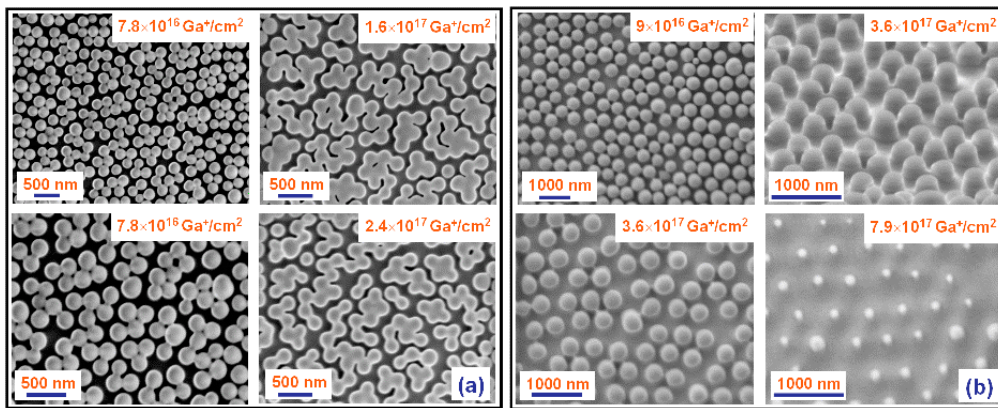


Figure 1 Reorganization of silica nanoparticles under ion irradiation. (a) $D = 220$ nm; Hexagonal layer restructured into isolated clusters (top left); □ Characteristics of chain-clusters (bottom left); Short chain-clusters (top and bottom right); Significant rearrangement occurs. (b) $D = 450$ nm; Disturbed hexagonal layer (□ top left); Characteristics of disturbed layer (bottom left); Buckling (side view, top right) and sputtering (bottom right) of particles. Significant rearrangement does not occur.

The high local ion flux of FIB with an input power density of about $1\text{-}10\text{ kW cm}^{-2}$ causes the fast heating of the particles so that the temperature of 2D surface melting of silica is reached within a short time. At high temperature the particles are softened and they can establish significant adhesion contact with each other and with the substrate. The number of particles N , connected into a chain-cluster strongly decreases with the particle diameter D , in the sub-micron size region, see Fig. 2(b). Note further experiments performed by low energy Ar^+ bombardment are under evaluation in order to see the role of the heating rate in final pattern formation.

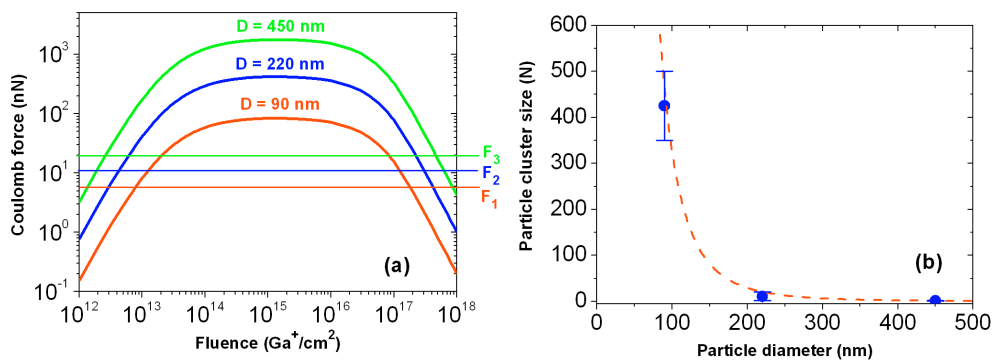


Figure 2 (a) Calculated irradiation-induced Coulomb force vs. ion fluence for $D = 90$, 220 and 450 nm silica particles. F_1 , F_2 , and F_3 denote the corresponding threshold forces (particle-substrate adhesion shear forces) for the motion of silica spheres due to Coulomb repulsion. (b) Cluster-size distribution as function of particle diameter.

Thin Film Physics Department

Head: János L. LÁBÁR, D.Sc., scientific advisor

Research Staff

- György SÁFRÁN, C.Sc., Deputy Head of Department
- Árpád BARNA, D.Sc., Emeritus
- Péter B. BARNA, D.Sc., Emeritus
- György GERGELY, D.Sc., Emeritus
- Miklós MENYHÁRD, D.Sc.
- Béla PÉCZ, D.Sc, Deputy Director
- Görgy RADNÓCZI, D.Sc
- Katalin BALÁZSI, Ph.D. (on leave)
- Zsolt CZIGÁNY, Ph.D.
- László DOBOS, Ph.D.
- Olga GESZTI, M.Sc.
- Sándor GURBÁN, M.Sc.
- Viktória KOVÁCSNÉ KIS, Ph.D.
- Fanni MISJÁK, Ph.D.
- György Zoltán RADNÓCZI, Ph.D.
- Attila SULYOK, Ph.D.
- Péter SÜLE, Ph.D.
- Lajos TÓTH, C.Sc.

Technical Staff

- Sándor CSEPREGHY, engineer
- Ferenc GLÁZERNE, lab . assistant
- Andrea FENYVESI-JAKAB, engineer
- Valéria OSVÁTH, engineer
- Andor KOVÁCS, engineer
- István KOVÁCS, engineer
- László PUSKÁS, technician

Ph.D. students / Diploma workers

- Zsolt FOGARASSY, Ph.D. student
- László KÓTIS, Ph.D. student
- Marianna SZERENCSI, Ph.D. student
- Lajos SZÉKELY, Ph.D. student
- Mohamed FATHY, Ph.D. student
- Ákos Koppány KISS, diploma worker

The Department has half a century tradition in the research of thin film phenomena. That tradition, which embraces construction of models for structure forming phenomena and experimental verification, together with developing both methods and instrumentation for those experiments is continued in the activity of 2010. A new OTKA project aims at understanding phase formation in the Cu-Mn system and a new method is being developed for complete characterization of grain boundary structure, including identification of grain boundary planes, based on TEM measurements. Practical application of scientific results was targeted in 4 European projects, 6 National projects, 1 industrial contract and 1 submitted patent.

The Department produced 46 referenced publications (cumulative impact factor 69.475) and received 530+ independent citations for their previous publications. One PhD was defended in 2010 and P. B. Barna received the very prestigious Science Prize of IUVSTA. Four members are founding members of Ph.D. Schools and the Department gave the President of the Hungarian Microscopy Society, the Vice President of the European Microbeam Analysis Society and two (out of 200) D.Sc. Representatives at the General Assembly of the Hungarian Academy of Sciences.

Composition dependence of film structure and morphology in Cu-Mn sputtered alloy films

(OTKA K81808)

F. Misják, Zs. Czigány, O. Geszti, and G. Radnóczy

The scope of this work is to substantially contribute to the basic knowledge of atomic mechanisms and kinetics of self-organized interfacial layer formation in order to facilitate their use in technological processes. In the current technology for advanced semiconductor devices, copper is the material of choice for transistor interconnects. The high diffusion rates for elemental copper in silicon and silicon oxides have required the development of diffusion barriers to prevent interdiffusion across the interface. As the semiconductor industry moves from the 45 nm technology node to 32 nm and beyond, the currently used barrier layers will not be a viable option, because of their thickness. The International Technology Roadmap for Semiconductors (ITRS) 2007 has targeted a 5.4 nm barrier for the 32 nm technology node and for future technologies; there will be a need to reduce the barrier width below 4 nm while retaining its diffusion integrity and adhesion properties. One possible way for meeting these requirements can be the utilization of self-organized processes for meeting preconditions like conformal coating, small thickness of the barrier layer and small lateral sizes simultaneously. The most promising results in the literature relate to copper-manganese (Cu-Mn) as contact and self-forming barrier material.

In this aspect, a detailed investigation of the Cu-Mn system is aimed at background knowledge for technological developments. Our basic intention is the detailed understanding of the Cu-Mn phase diagram and how the microstructure of the alloys depends on the composition. The kinetics of the alloy segregation process on dielectric substrates for the Cu-Mn alloy and its role in the development of film morphology is also a key issue.

Cu-Mn films were prepared by DC magnetron sputtering from two separate sources by co-deposition of the components. Thin SiO_x layers were used as substrates. The composition of the film was determined by the variation of the power of Cu and Mn sources and the whole composition range was covered. Combinatorial samples have been grown at room temperature on composition in order to survey the dependence of the structure and morphology of the films. The thickness of the films ranged from 50 nm to 500 nm. TEM and EDS were used to determine the morphology and texture as well as the chemical composition of the films. The Process Diffraction program [J. L. Lábár: *Ultramicroscopy* 103 (2005) 237] was used to evaluate the phase state of the films.

As a first step, the structure and morphology of the films has been investigated in the composition range of 8-80 at% of Mn. TEM images revealed that Cu-Mn films show extremely small grain size in the whole composition region. The minimum of the grain size is at 70 at% Mn (Fig. 1). Evaluation of the diffraction patterns shows the changes of the phase state of films as the function of their composition (Fig. 2). For

Mn content 8 - 33 at.% the diffraction pattern is characteristic of a fcc phase. The measurement of the lattice parameters in this composition range shows an agreement with Vegard's law (for fcc Cu ($a=0.361$ nm) and fcc γ -Mn ($a=0.384$ nm) phases), proving that the film is single phase fcc solid solution. For compositions from 37 at.% of Mn and above the structure is cubic α -Mn ($a=0.891$ nm) and also appears to be single phase. This shows the existence of a solid solution also in this composition range.

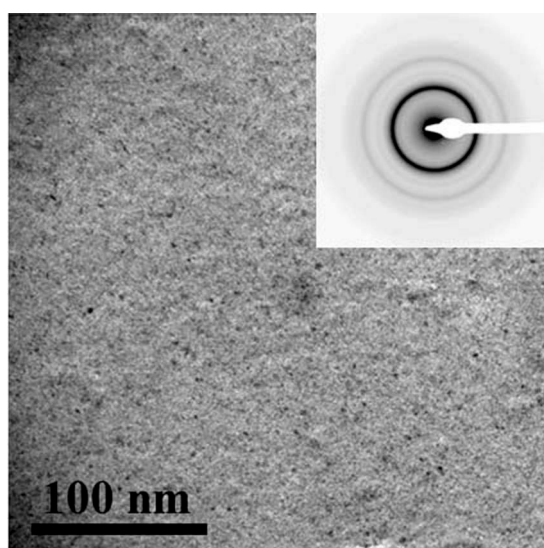


Figure 1 Morphology and electron diffraction pattern of the film with grain size corresponding to the minimum at 70 at% of Mn content.

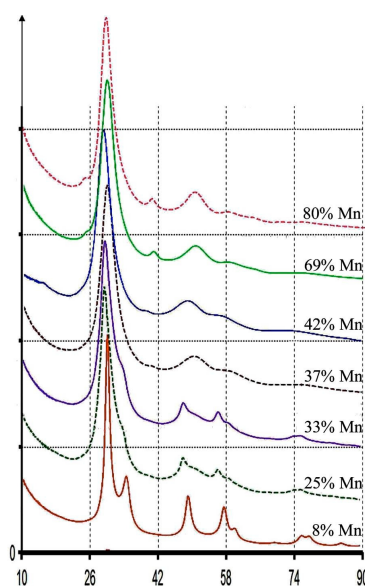


Figure 2 Comparison of electron diffraction patterns as the function of composition.

Between the two (Cu and Mn based) solid solutions we have not found the two phase region expected according to equilibrium phase diagram. As a consequence, the Cu-Mn films form metastable structures. Their metastability is apparent in the formation of the broad composition ranges of solid solutions i.e. in phase state and in the morphology of the films. This may suggest that phase separation is kinetically hindered in these films and even if a two phase region exists it must be very narrow. The clarification of this detail needs further investigations.

The circumstances of phase separation and its conditions can provide important information for understanding and achieving the formation of self-organized barrier layers in the Cu-Mn- SiO_x system. Investigation of structural details on nm scale can open the way to technologically direct these processes to intentionally form multifunctional structures by selforganization processes.

Spinodal Decomposition as Phase Separation Mechanism in Thin Films

(OTKA K81808)

F. Misják, P. B. Barna, L. Székely, V. Kis, and G. Radnóczy

A smart way of producing functional nanostructures is their creation through self-organized processes. These processes can be controlled by technological parameters only if the atomic movements during their formation are known. The key to the understanding of self-organization could be the mapping of the phase separation kinetics.

Concerning the existing atomic mechanisms/models of thin film formation they are restricted to the surface diffusion processes, namely kinetic segregation due to high activation energy of bulk nucleation processes. However, there is a process needing no activation energy for considerable change of structure and morphology, well established in bulk alloys. This is spinodal decomposition of supersaturated solid solutions by short range atomic rearrangements resulting in separation of components. In the spinodal decomposition process phase separation takes place to the stages preceding nucleation. Instead of sharp phase boundaries fluctuation of composition occurs. Nevertheless, these fluctuations can be large enough to identify two structurally identical compositions in building a nanocomposite. The wavelength of compositional fluctuations is really on the nanoscale, i.e. 2-3 nm.

In two different eutectic systems, namely in the Cu-Ag and in the TiN-AlN systems spinodal decomposition in the growing film has been observed as the beginning mechanism of phase separation. Since spinodal decomposition occurs on nanoscale, the relevant method for documentation of the structural evidences is high resolution transmission electron microscopy in conjunction with image simulation. In both systems the growth morphology of the films was columnar and the nanostructure of the columns consisted of epitaxial 2-4 nm size domains with semicoherent boundaries. For the interpretation of the structure of the boundaries and the identification of the appearing lattices (phases) structural models were built and image simulation on these models was performed by the JEMS program [P.J. Stadelman, Ultramicroscopy 21 (1987) 131]. Matching of the computed and observed HREM images in the Cu-Ag system shows (fig. 1) that the parent eutectic solid solution (60 at% of Ag) separated by spinodal decomposition into two solid solutions of about 10 at% dissolved component. By this a three dimensional compositional nanocomposite occurred, composed from epitaxial domains. According to the detailed structural investigation the phase separation process stopped in the spinodal region due to the increasing misfit strain energy during separation between the Ag and Cu rich domains.

In the case of the TiAlN system (fig. 2) the parent cubic TiAlN phase decomposed on the {111} planes into cubic Ti rich and hexagonal Al rich nitrides. These phases differ only on the stacking sequence of the close packed planes, so the separation could start without nucleation. The occurrence of the hexagonal phase, however,

points to the fact that spinodal decomposition might have overrunning to the state, close to nucleation. The coherency of the interfaces on the close packed planes is maintained, but in other directions it should be replaced by phase boundaries.

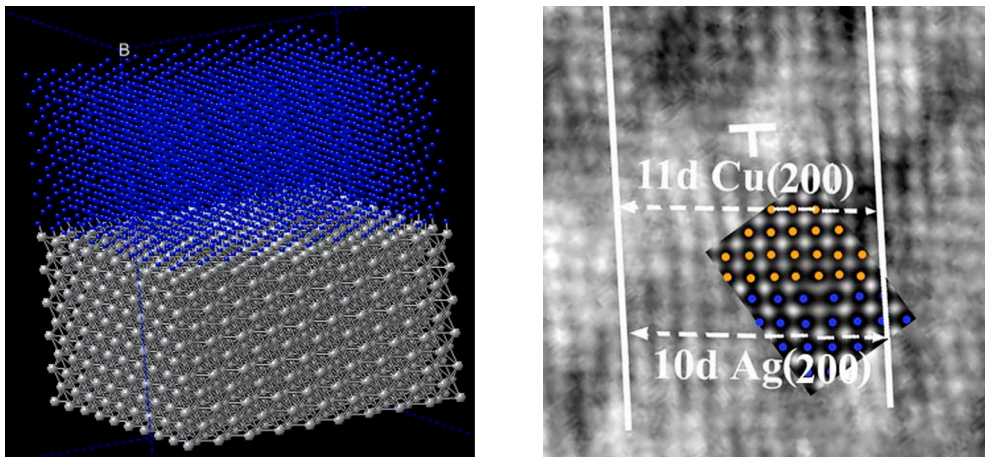


Figure 1 Atomic model and semicoherent matching of Cu rich and Ag rich domains after spinodal decomposition of Cu-Ag solid solution. The insert shows the projected atomic arrangement and simulated image. Yellow dots Cu+10at%Ag alloy and blue dots Ag+10at%Cu.

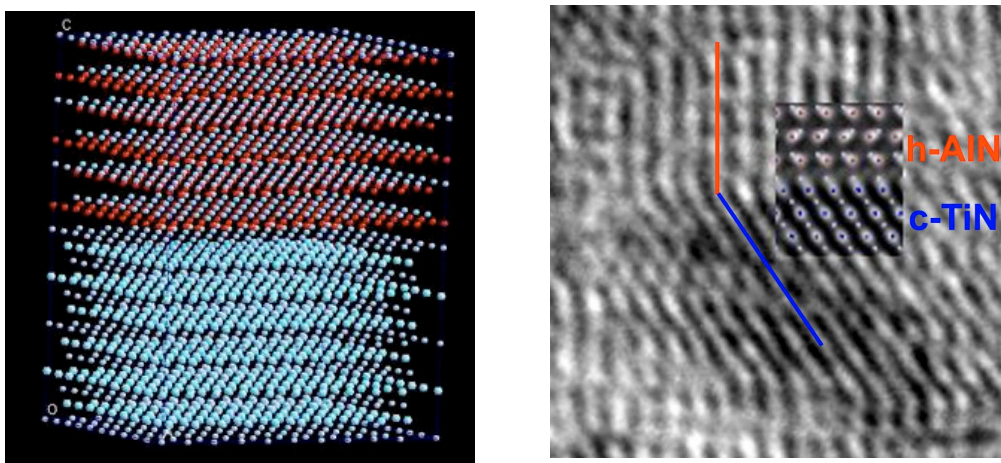


Figure 2 Atomic model and coherent matching of cubic TiN and hexagonal AlN nanocrystallites, formed as a result of spinodal decomposition of a cubic TiAlN solid solution as parent phase. The insert shows the corresponding atomic arrangement.

These examples point to the possibility that spinodal decomposition can be a rather general mechanism of phase separation in non-equilibrium structures obtained by fast deposition techniques eliminating effective surface processes.

Pressure-dependent stability of cubic and wurzite phases within the TiN-AlN and CrN-AlN systems

(Cooperative research with Department of Physical Metallurgy and Materials Testing, Montanuniversität Leoben, Leoben, Austria*)

D. Holec*, F. Rovere*, P. H. Mayrhofer*, and P. B. Barna

The $Ti_{1-x}Al_xN$ and $Cr_{1-x}Al_xN$ coatings are widely used in industrial applications due to their superior mechanical and chemical properties. These excellent properties, which improve with increasing Al content, are, however, obtained only for the metastable cubic structure (B1, NaCl-like). Al rich phases prefer the hexagonal (wurzite B4, ZnS-like) structure which possess significantly poorer mechanical properties. Knowledge of maximum AlN mole fraction in the cubic phase is of basic interest. The experimental observations of the maximum AlN fraction in the cubic phase in $Cr_{1-x}Al_xN$ and $Ti_{1-x}Al_xN$ are not conclusive. The solubility limit for $Ti_{1-x}Al_xN$ varies from 0,4 to 0,68, 0,8 and 0,91, while for $Cr_{1-x}Al_xN$ in the range of 0,6–0,8. In experiments applying increasing bias potential (which is generally connected with increasing compressive stresses), higher maximum mole fractions of AlN in the cubic phase of $Ti_{1-x}Al_xN$ based materials are obtained ¹. In the present work the effect of the pressure on the solubility of AlN was studied. The Vienna Ab Initio Simulation Package together with the PAW pseudopotentials were employed to determine the enthalpies of the cubic and wurzite phases of the $Cr_{1-x}Al_xN$ and $Ti_{1-x}Al_xN$ phases in dependence of the AlN fraction and pressure ². The variation of the solubility in the dependence of the pressure for the two systems are shown in Figs. 1 and 2.

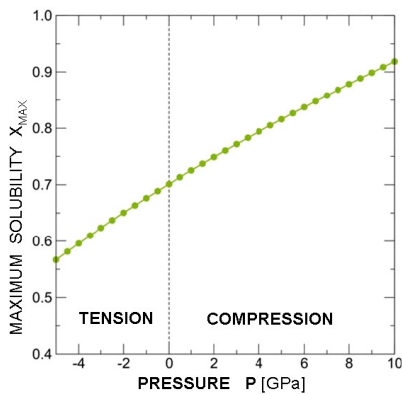


Figure 1 Calculated maximum mole fraction of AlN in the cubic B1 phase of $Ti_{1-x}Al_xN$ system

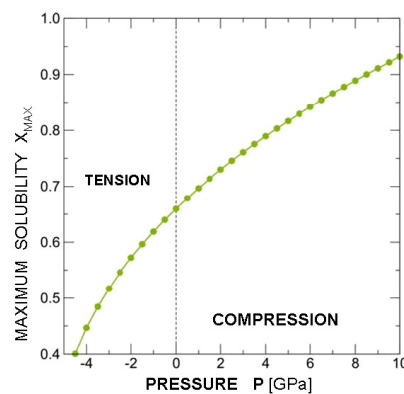


Figure 2 Calculated maximum mole fraction of AlN in the cubic B1 phase of $Cr_{1-x}Al_xN$ system

Determination of grain boundary plane in the TEM exemplified in Si

(HIGH-EF: EU FP7-ENERGY-2007-1-RTD 213303)

Á. K. Kiss, Zs. Fogarassy, J. L. Lábár, S. Christiansen (IPHT), and F. Falk (IPHT)

It has been long observed that phenomena associated with grain boundaries (GB) in metals (e.g. corrosion, energy, segregation, etc) are influenced by the grain boundary geometry. For many years the coincidence site lattice (CSL) model, which describes the grain boundary in terms of the misorientation between neighboring grains, has been a cornerstone of grain boundary research and formation of special boundaries with low- Σ (assumed to result in better material properties) was pursued. Further work subsequently indicated that a low- Σ CSL was a necessary but not sufficient criterion for specialness, but the interpretation of similar results is complicated by the effect of impurities on boundary energies. The structure of the GB is more related to the orientation of the GB plane (planar density of coincidence sites), which is difficult to determine experimentally. Bicrystals with known misorientation and GB plane indices were artificially fabricated and studied both by HRTEM and other characterization methods from the 80's. Structural characterization (including indexing the GB plane) in real-life polycrystalline materials proved to be more challenging. One approach involves following the change in the location of GB traces in a scanning electron microscope (SEM) while thin layers of material are removed mechanically (either by polishing or by focused ion beam, FIB). The other approach, reported here, records the projections of the GB at two different tilt values in a transmission electron microscope (TEM) and deduces the orientation of the GB plane from them.

The method relies on calibrating rotation of the image as compared to the diffraction and determining orientations of both neighboring grains from the Kikuchi-bands (or Kikuchi-lines) seen in convergent beam electron diffraction (CBED) patterns, recorded with low camera length (to include the maximum available angular range in the TEM). The direction of the trace is determined from its direction as related to the diffraction axes and the elevation (tilt) of the GB plane from the beam-direction is determined from the width of its trace as compared to local sample thickness (determined from 2-beam CBED).

A self-supporting thin (100-150 nm) sheet of polycrystalline Silicon (with grain size of tens of micrometer) was used to demonstrate the power of the new method. Neighboring grains with $\Sigma 3$ orientation relation were selected to characterize the GB plane. Figures 1 and 2 show the CBED patterns used for the orientation measurement. Table 1 summarizes the measured misorientation variants (due to symmetry relations); all prove the same $\Sigma 3$ misorientation relation. Figure 3 is a bright-field (BF) image of the projection of the GB plane (and of another one at the other side of the twin lamella), recorded at the same goniometer position as the CBED patterns. The indicated boundary separates the two measured grains (the big one to the left and the thin lamella to the right side of the marked boundary). Local sample thickness of

120 nm was determined from the central part of the CBED in Figure 1. Using the 20 nm measured thickness of the GB plane projection, a plane-beam angle of $9^\circ (\pm 5^\circ)$ was determined from it. (The large error originates from the errors of measuring both the width of the GB projection and of determining the local sample thickness.) The Miller indices of the GB plane were determined as $\{211\}$ type from these data. The observation is consistent with expectation.

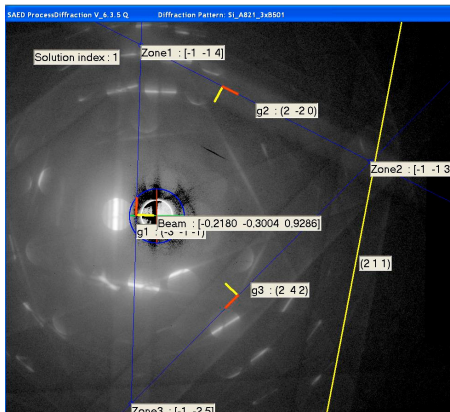


Figure 1 Indexed Kikuchi-bands in CBED pattern recorded in grain 1. Location of the final solution for the GB plane (211) is marked.

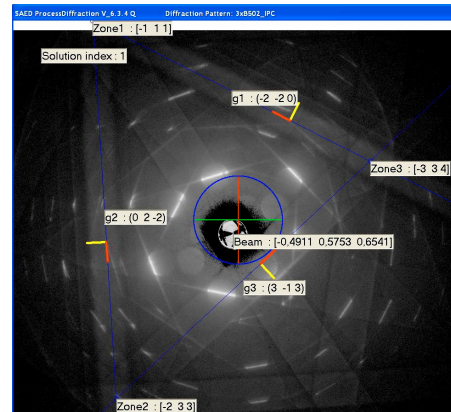
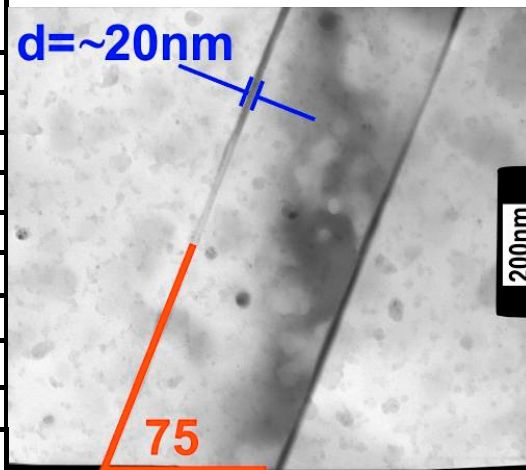


Figure 2 Indexed Kikuchi-bands in CBED pattern recorded in grain 2.

Table 1: Symmetry equivalent solutions from Figs 1 and 2.

| Rotation Axis | Rotation angle |
|-----------------------|----------------|
| $\langle 110 \rangle$ | 70.4° |
| $\langle 110 \rangle$ | 109.3° |
| $\langle 111 \rangle$ | 60.0° |
| $\langle 111 \rangle$ | 180.0° |
| $\langle 210 \rangle$ | 180.0° |
| $\langle 311 \rangle$ | 145.6° |
| | |
| | |
| | |
| | |

Figure 3 BF image of two GB planes on both sides of a twin lamella. The measured boundary is indicated.



Progress in producing large grained, low stress multi-crystalline silicon thin films for solar cell application

(HIGH-EF: EU FP7-ENERGY-2007-1-RTD 213303)

J. L. Lábár, G. Sáfrán, B. Pécz, A. Jakab, Zs. Fogarassy, M. Menyhárd, L. Kótis, S. Gurbán, S. Christiansen (IPHT), F. Falk (IPHT), J. Schneider (CSG Solar), J. Dore (CSG Solar)

Sustainable development requires utilization of green and renewable energy sources, like exploitation of sunshine. The HIGH-EF project aims to improve electricity production by providing improved quality, economically produced Si material for the photovoltaic (PV) industry. In contrast to the high quality (but expensive) Si single crystal solar cells (SC), less expensive, acceptable quality Si material (used in thin films) seems to be the choice for large-scale SC production of the future. HIGH-EF promises to provide a technology for producing better quality thin film (TF) SCs by reducing the density of both grain boundaries (by increased grain size) and of other defects (like dislocation) and reducing stress within the Si layer. Efficiency is expected to increase as a consequence of reduced defect density.

The large (=multi-) crystalline Si layer is produced in two step in the HIGH-EF process. First a thin ($\cong 200\text{nm}$) amorphous Si (a-Si) layer is transformed into a thin layer of laterally large ($>50\mu\text{m}$) crystals by laser crystallization (LC). This LC Si serves as seed layer for the subsequently deposited thicker ($>1.5\mu\text{m}$) a-Si layer, which grows epitaxially over the large seed crystals during an oven heat treatment (solid phase crystallization, SPE).

One of the several results of the project in 2010 was the localization (identification) of the main source of defects in the SPE layer and subsequent elimination of that source.

TEM examinations showed that dislocation density is abruptly increased at the interface between the LC seed and the SPE absorber (Fig. 1). High resolution TEM (HRTEM) demonstrated that there is an amorphous contamination layer at certain locations of that interface. Lattice images are seen in Fig. 2 both in the seed and in the absorber, however, there is an amorphous layer between them.

A systematic study was carried out to reveal the effect of different deposition technologies of the Nitride layer (below the seed) and of the different cleaning methods applied between the laser crystallization step of the seed layer and the deposition of the thicker a-Si on top of it. The appearance of an (oxy)Nitride contamination layer on top of the seed was unexpected, but unambiguously proved by surface analytical technique (Auger electron spectroscopy, AES) depth profiling. The Nitrogen in the contamination can originate from the air, since laser crystallization was performed in air. The previously observed contamination layer resulted from the imperfect removal of this oxy(Nitride) layer by the previously used HF cleaning step. After identification, the contaminant layer was perfectly removed by RCA cleaning from areas of single laser treatment. The structure of the Nitride was different in thin lines of overlapping laser stripes, resulting in imperfect removal of the Nitride from

the doubly-melted lines. That is why a broad line laser was developed within the HIGH-EF project to perform the LC in a single step, without overlapping regions of repeated scans. The results helped to optimize both the laser treatment step and the cleaning step. Both twin density and dislocation density were reduced as a result of the optimized technology. The improvement of Solar Cell parameters prepared from the improved Si-material is tested in a separate study.

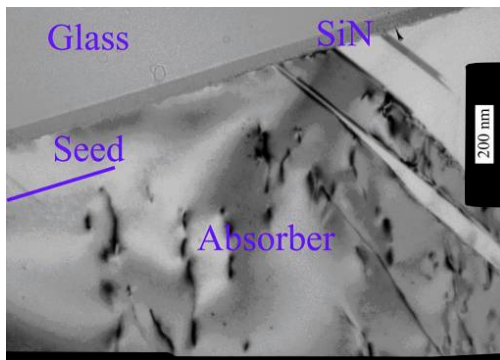


Figure 1 XTEM image, showing the increase of defect density in the SPE layer (as compared to the seed layer).

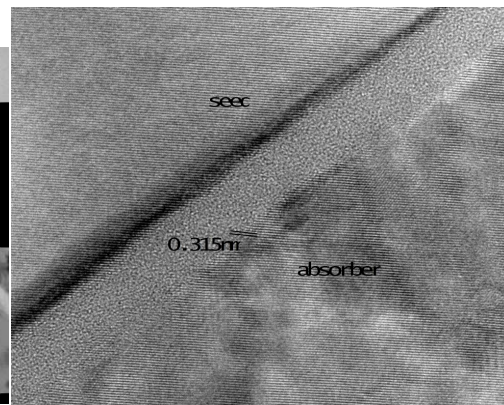


Figure 2 HRTEM image demonstrating the presence of an amorphous contaminant layer at the seed/SPE interface.

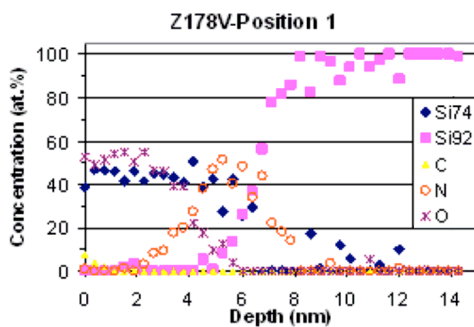


Figure 3 Auger electron spectroscopy (AES) depth profile, proving the presence of an (oxy)Nitride layer on top of the seed layer prior to the cleaning step.

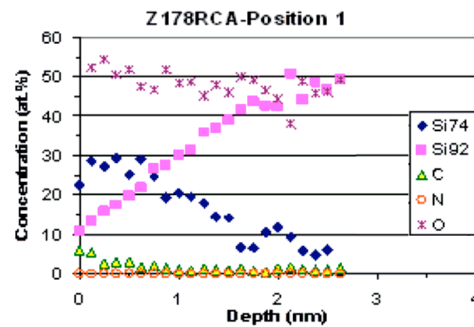


Figure 4 AES depth profile, proving that the (oxy)Nitride layer has been successfully removed from the surface by RCA cleaning.

Microstructure of diamond films grown on nitride HEMT devices

(EU-FP7-NMP- 214610)

L. Tóth (MFA), Á Barna (MFA), B. Pécz (MFA), M. Alomari (Ulm), M. Dipalo (Ulm), S. Rossi (Ulm), E. Kohn (Ulm), M-A. di Forte-Poisson (3-5 Lab), S. Delage (3-5 Lab), J-F. Carlin (EPFL), and N. Grandjean (EPFL)

One of the main limitations of high power density GaN based field effect transistors working at microwave frequencies is self heating during operation. This heat needs to be extracted effectively from the bottom as well as top of the device and due to its extremely high heat conductivity diamond is regarded as the most attractive heat spreading material. One solution could be the direct growth of nanocrystalline diamond on top of the GaN based HEMT (High electron-mobility transistor) structure, putting the heat sink very close to the channel.

Due to their high chemical/thermal stability the lattice matched InAlN/GaN heterostructures can be overgrown with nanocrystalline diamond film at high temperature without degrading the characteristics of HEMT structures. In this paper the microstructure of diamond heat spreader films deposited by hot filament CVD technique at temperatures above 750 °C will be presented. InAlN/GaN HEMT structures were used as substrates formerly passivated by a thin SiO₂ layer. To enhance the bond strength to the substrate the bias enhanced nucleation technique (BEN) has been chosen to initiate diamond growth over a sputtered silicon film covering the SiO₂ layer. The deposited layers have been characterized by transmission electron microscopy (TEM) for what the cross sections were prepared by Ar ion milling. Conventional microscopy was carried out on a Philips CM 20 microscope at 200 keV, while high resolution images were taken at 300 keV on a JEOL 3010 electron microscope equipped with a Gatan imaging filter (GIF) used in an energy filtered mode.

Transmission electron micrographs (Fig. 1) taken on the cross sectional samples have proved that the thin amorphous Si layer deposited prior to diamond has crystallized during the further growth process. The formation of diamond nuclei took place on the surface of this polycrystalline silicon which was also covered by a thin native oxide layer.

High resolution observation (Fig. 2) also revealed a region between the diamond and the silicon films exhibiting a large number of nanosized particles which were identified as cubic SiC. Diamond growth by CVD usually starts with this phase on silicon surface. The observed SiC particles are embedded into other amorphous phase(s) but above this thin nucleation zone the 250 nm thick diamond film was found to be grown as single phase with polycrystalline, columnar microstructure. No crystal defects other than grain boundaries were observed within the diamond. However, with the typical grain size in the order of 100 nm the expected heat conductivity should be inferior to that of the bulk diamond.

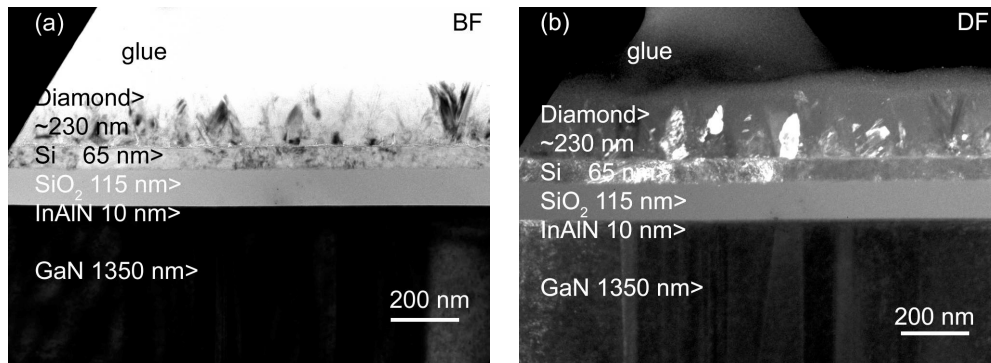


Fig.1: Cross sectional bright field (a) and dark field electron micrographs (b) of the InAlN/GaN HEMT structure covered by a thin SiO₂ and Si layer and the CVD grown diamond coating. The columnar polycrystalline microstructure of the diamond film is well visible on the dark field image.

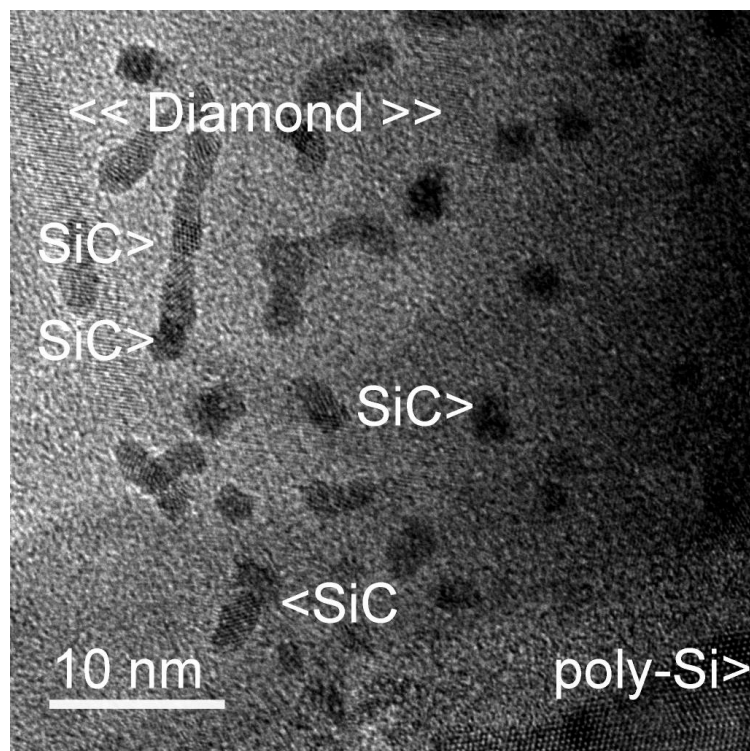


Figure 2 High resolution TEM shows that the growth of the diamond phase starts with the formation of cubic SiC nanocrystals. These particles are embedded in an amorphous phase within a 10-20 nm thick layer on the surface of the crystallized Si film.

Nitride nanowires grown by MOCVD for solar cells

(Seventh Framework Programme (FP7) 227497)

B. Pécz, G. Z. Radnóczy, J-P. Ahl (AIXTRON), H. Behmenburg (AIXTRON), C. Giesen (AIXTRON), I. Regolin (Univ. of Duisburg-Essen), W. Prost (Univ. of Duisburg-Essen), F. J. Tegude (Univ. of Duisburg-Essen), H. Kalisch (RWTH Aachen), R. H. Jansen (RWTH Aachen), and M. Heuken (RWTH Aachen)

Semiconductor nanowires (NW) received lots of attention in recent years due to their optical and electrical properties. In the case of GaN, which is grown generally on substrates with large misfit, NWs offer an alternative with far less threading dislocations. On the other hand nitrides are going to be important solar cell materials as well, thanks to the relatively low band gap of InN, which makes possible to tune the band gap into the required range by the growth of InGaN. Among other reasons this is a motivation of a demand for high quality GaN nanowires.

In our RODSOL project (coordinated by IPHT Jena), beside research and development of Si nanowires, there is an exploratory research task on nitride wires. Here we report on the microstructure of the first set of GaN NW's grown by MOCVD.

The wires were grown using VLS mechanism initiated by a gold catalyst. The NW were grown in AIXTRON MOCVD reactors at low V/III ratios and surface temperatures of about 900 °C on a sapphire substrate previously coated with a 1 nm thick gold film. The grown structures were characterized by scanning/transmission electron microscopy (SEM/TEM) and X-ray diffraction (XRD).

SEM images showed a high density ($\sim 3 \cdot 10^9/\text{cm}^2$) of hexagonally faceted nanowires, which are aligned vertically to the substrate on the whole sample with an average diameter of 60 ± 9 nm and lengths of approximately 400 nm.

Both XRD and TEM measurements confirmed the growth of c-plane GaN with the usual orientation (30° GaN unit cell twist) to the sapphire substrate. TEM analysis (performed at 300 kV in a JEOL 3010 microscope) revealed single crystalline and perfectly straight NWs without any threading dislocations and only a small number of stacking faults (Fig. 1). Some of the stacking faults that are shown in Fig. 2 in high resolution were identified as II type stacking faults [V. Potin, B. Gil, S. Charar, P. Ruterana, G. Nouet, Mater. Sci. Eng. B, 82 (2001)] with stacking sequence: cCaAcCaAbBaAbB and burgers vector $b=1/6 \langle 20-23 \rangle$.

Each wire exhibits a droplet on top of its tip, which was identified as gold by electron energy loss spectroscopy (EELS) confirming the VLS mechanism. Interestingly, the size of each droplet is significantly lower than the corresponding nanowire diameter but still depends linearly on the NW cross section. This was explained in [J.-P. Ahl, H. Behmenburg, C. Giesen, I. Regolin, W. Prost, F. J. Tegude, G. Z. Radnóczy, B. Pécz, H. Kalisch, R. H. Jansen, M. Heuken: "Gold catalyst initiated growth of GaN nanowires by MOCVD", physica status solidi c, in press], where details on the effects

of the initial gold film thickness on the gold catalyst droplet formation were also published.

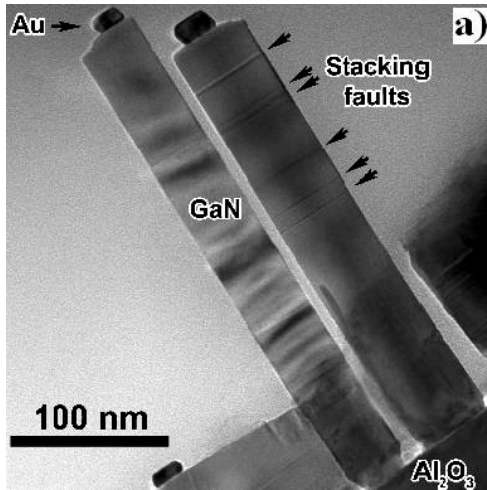


Figure 1 BF image of the nanowires.

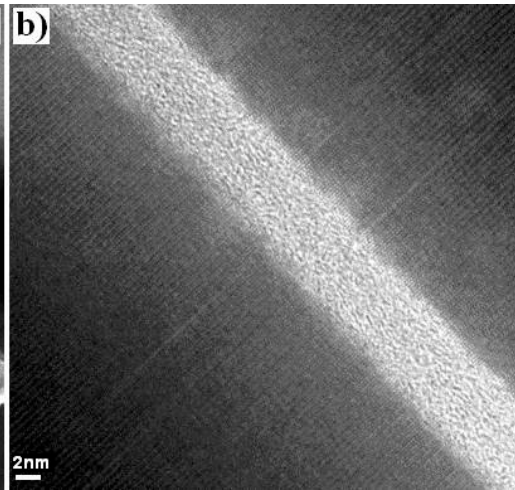


Figure 2 Stacking faults shown in high resolution.

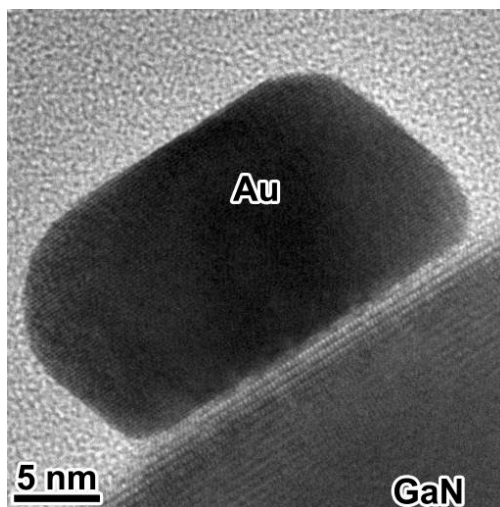


Figure 3 Gold droplet on the top of a GaN nanowire.

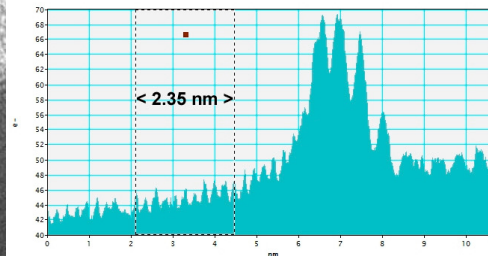


Figure 4 Ten lattice fringes are measured on the HREM image of the gold droplet. This shows clearly the distance between the (111) planes of fcc gold.

The next growth experiments were also carried out depositing about 5 nm InGaN onto the GaN wires. The investigation of those coated wires is in progress at MFA.

Aluminium Oxide Films Deposited by Plasma-Enhanced Atomic Layer Deposition for Corrosion Protection

(CORRAL, FP7, CPFP213996-1)

S. E. Potts (UT Eindhoven), L. Schmalz (FEM), M. Fenker (FEM), B. Diaz (CNRS Paris), J. Świątowska (CNRS Paris), V. Maurice (CNRS Paris), P. Marcus (CNRS Paris), G. Radnóczy, L. Tóth, M. C. M. van de Sanden (UT Eindhoven), and W. M. M. Kessels (UT Eindhoven)

Corrosion is a persistent problem for many modern high-precision applications, such as automotive and aerospace components or speciality gas equipment. These require many high-purity precision parts and instruments of rather complicated form which are commonly manufactured from steel or aluminium alloys. As such, dense and defect-free protective coatings are necessary to prevent corrosion of these parts. Ideally, the films should form a complete sealing barrier to prevent contact between the metal substrates and aggressive environment. Atomic layer deposition (ALD) is an ideal candidate for this application, as it gives high-quality films with excellent conformality, and provides precise thickness control.

Transmission electron microscopy has been used to document the quality of the coatings. High resolution TEM images showed that the Al_2O_3 deposited by both plasma-enhanced and thermal ALD were conformal on ground Al2024-T3 and lapped 100Cr6.

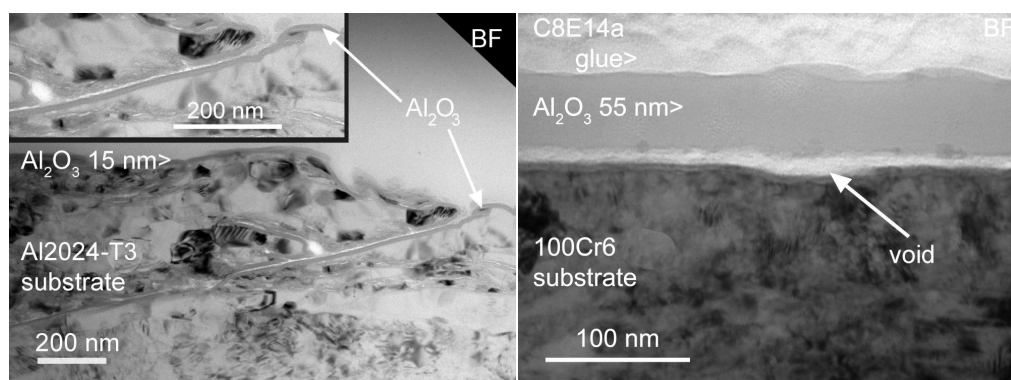


Figure 1. Bright-field TEM image of ~20 nm Al_2O_3 deposited on Al2024-T3 by plasma enhanced ALD. Inset: close-up of the trench area..

Figure 2. Bright-field TEM image of ~55 nm Al_2O_3 coating deposited on 100Cr6 by thermal ALD, showing a void filled with glue between the coating and the substrate.

For the films deposited by plasma-enhanced ALD on Al2024-T3, the coating was present even in deep cracks in the substrate (Fig. 1). For the thermal ALD process, there was a void present (~20 nm) between the substrate and coating (filled with glue used in the TEM preparation), suggesting that the Al_2O_3 coating was not well adhered. The same was the case on 100Cr6 substrates (Fig. 2), where the film was separated from the substrate by ~8 nm.

Silica/nontronite intergrowth in chloropal

(OTKA PF 63973)

I Dódony, T. Németh, E. Vass, and V. K. Kis

Diocahedral ferric smectites (e.g. nontronite) have a general formula $(\text{Si}_{8-x-y}\text{Al}_x\text{Fe}^{3+}_y)(\text{Fe}^{3+}_{4-z}\text{Al}_z)\text{Ex}^{x+y}\text{O}_{20}(\text{OH})_4 \cdot n\text{H}_2\text{O}$, where Ex represents the interlayer cation. In the smectite structure which is a 2:1 layer structure, two layers of $(\text{Si}, \text{Fe}, \text{Al})\text{O}_4$ tetrahedra (T) with a layer of $(\text{Fe}, \text{Al})\text{O}_6$ octahedra (O) between them form the building unit (TOT).

According to the nowadays used smectite structural model, the vertices of the tetrahedra are pointing towards the octahedral layer resulting an interlayer space between the basal planes of two neighbouring tetrahedral sheets. In the interlayer space there are hydrated exchangeable cations.

SAED and HRTEM studies on chloropal from Gönc, Hungary revealed the oriented intergrowth of silica and nontronite. However the silica/smectite association in fine grained smectitic materials (e.g. bentonite) is frequently reported in XRD studies, to our knowledge this is the first time it was observed directly by HRTEM. Based on the idea of reversed tetrahedra by Edelman and Favejee we propose a structural model for this epitaxial intergrowth. Our model has a formula $\text{Ex}_x\text{Fe}_4[\text{Si}_8\text{O}_{18}(\text{OH})_8]$ and implies 2 excess oxygen positions per formula unit with respect to the widely accepted and used Hoffmann-model. The charge balance is maintained with hydroxyl substitution. TEM-EDS analysis proved the excess oxygen in Gönc nontronite, and IR spectrum of the hydroxyl stretching vibration supports the enhanced role of OH in the structure. The varying amount of excess negative charge (3.5-12.4 per formula unit) suggests a chemical and structural heterogeneity on the nanometer scale in Gönc nontronite. The validity of the proposed model with respect to the swelling properties of nontronite is also discussed.

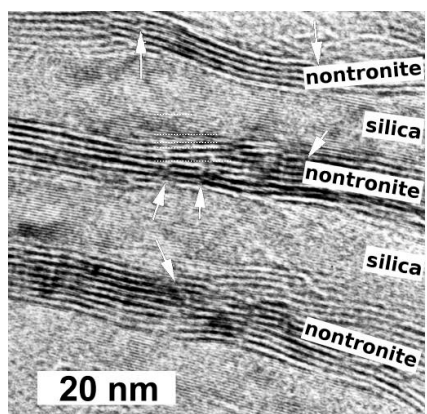


Figure 1 HRTEM of chloropal, electron beam is parallel to the structural layers. Arrows show layer terminations.

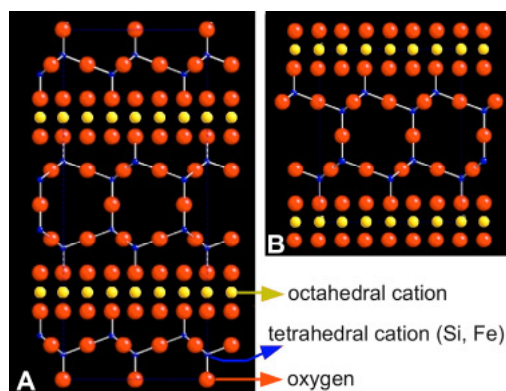


Figure 2 Structural models proposed for the silica/nontronite intergrowth (A) hcp silica stacking (B) fcc silica stacking

Structure and thermal stability of sputtered $\text{Sc}_{1-x}\text{Al}_x\text{N}$

C. Höglund, Zs. Czigány, B. Alling, J. Birch, and L. Hultman

Thin films of $\text{Sc}_{1-x}\text{Al}_x\text{N}$, were deposited by reactive magnetron sputter epitaxy onto $\text{MgO}(111)$ and $\text{Al}_2\text{O}_3(0001)$ substrates at $800\text{ }^\circ\text{C}$ from Al and Sc targets, under conditions optimal for growth of w-AlN(0001) [56]. ScN molar fractions of 22% have been dissolved into AlN, forming a disordered single-crystal solid solution of w- $\text{Sc}_{1-x}\text{Al}_x\text{N}(0001)$. The measured lattice parameters agree with calculated values: the a -parameter increases almost linearly from 3.11 to 3.21 \AA for x varied between 1.0 and 0.8 , while no significant change in the c -parameter is observed. ScN contents between 23% and 50% yield a nanocrystalline mixture of ScN and AlN phases and even higher ScN contents result in solid solutions of c- $\text{Sc}_{1-x}\text{Al}_x\text{N}$.

We have studied the decomposition behaviour and resulting morphology in the metastable rocksalt c- $\text{Sc}_{1-x}\text{Al}_x\text{N}$ by thin-film deposition and stepwise annealing [57]. Reactive magnetron sputter-deposited $\text{Sc}_{0.57}\text{Al}_{0.43}\text{N}(111)$ films phase separate at $1000\text{--}1100\text{ }^\circ\text{C}$, by nucleation and growth at the domain boundaries into coherent c-ScN and w-AlN (Fig. 1) due to volume and electronic-structure mismatch of the respective binaries (determined by *ab initio* calculations). The topotaxial relationship is $\text{AlN}(0001) \parallel \text{ScN}(001)$ and $\text{AlN}(01\bar{1}0) \parallel \text{ScN}(1\bar{1}0)$.

First-principles calculations of mixing energy-lattice spacing curves explain the results and open a route for design of novel metastable pseudobinary phases based on an understanding of the physics of functional materials systems on the most fundamental level.

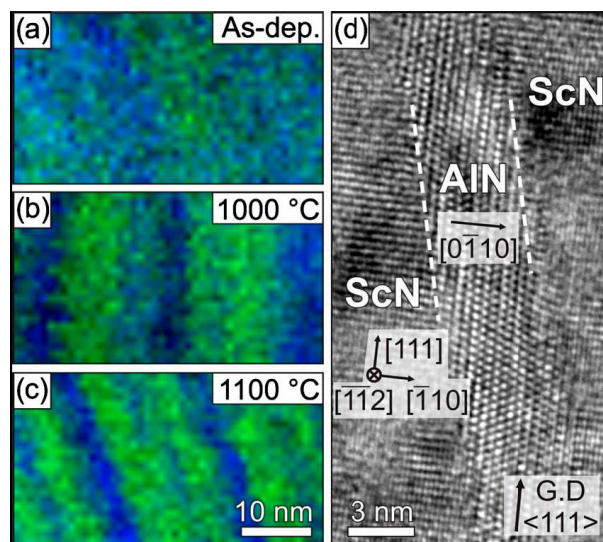


Figure 1 Cross-sectional transmission electron microscopy images showing (a)–(c) EDX maps with Sc-rich (green) and Al-rich (blue) regions of (a) the as-deposited, (b) $1000\text{ }^\circ\text{C}$ annealed, and (c) $1100\text{ }^\circ\text{C}$ annealed $\text{Sc}_{0.57}\text{Al}_{0.43}\text{N}$ films, together with (d) a lattice-resolved image from the same film annealed at $1100\text{ }^\circ\text{C}$ with indexing of AlN and ScN domains.

Experimental determination of the electron elastic backscattering probability and the surface excitation parameter for Si, Ni, Cu and Ag at 0.5 and 1 keV energies

(PL-15 Project between the Polish and Hungarian Academy of Science)

G. Gergely, S. Gurban, M. Menyhard, A. Jablonski (IPC), J. Zemek (IP), and K. Goto (AIST)

Experimental angular resolved (AREPES) spectra measured in arbitrary units on Ni, Cu and Ag samples have been converted to absolute units (%). The experimental elastic peak intensities measured by Zemek have been quantified (I_e), converted to backscattering probability values, applying the database of Goto. Goto's elastic peak intensities have been transformed to the conical solid angle and 4.1° semi-angle with respect to $\alpha_d = 42^\circ$ angle of detection, using the small CMA of Zemek, adjustable between $\alpha_d = 35\text{--}74^\circ$ angular range. AREPES spectra were calculated (I_{ec}) using Monte Carlo simulation applying the EPESWIN software of Jablonski, with the NIST SRD 64 (elastic scattering cross-section) and SRD 71 (IMFP TPP-2M) databases. The Tanuma parameter, the ratio of $I_{e,exp}/I_{ec}$ was compensated using the surface excitation correction and parameter (SEP) $P_e(E, \alpha_d)$. $I_{ec}(E, \alpha_d) = I_e/\exp(-P_{se})$. The SEP parameter was determined using the formulae of Chen and Werner. Material parameters of Chen, our modified Chen values, Werner, Nagatomi, Ding and Kwei have been tested. The quality factor for surface excitation correction defined by Jablonski was applied. For Ni and Cu, reasonable quality factors were found using a single material parameter. Results are presented in Figs 1 ($E = 0.5$ keV) and 2 ($E = 1$ keV), comparing the experimental, the calculated (MC) AREPES spectra and testing material parameters of Werner, our modified Chen, Nagatomi (for Ni), Ding, Kwei and JZ, deduced from the shape of the spectra.

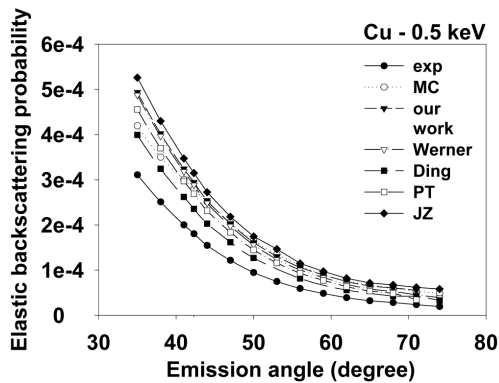


Figure 1 The backscattering probabilities derived from experiments (exp), calculated (MC). SEP corrected

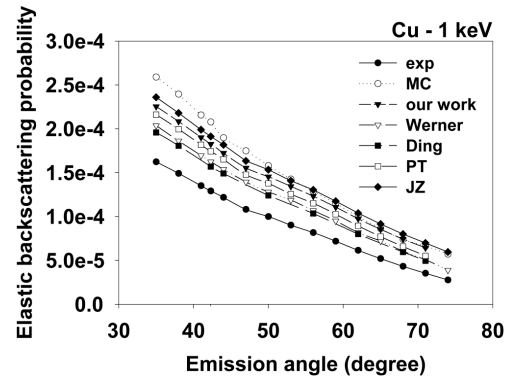


Figure 2 With the exception of 1 keV primary energy, same as Figure 1.

Growing embedded layer with sharp interfaces by means of ion beam mixing of C/Ni layer

(SI-3/2008 Bilateral contact between Slovenia and Hungary)

A. Barna, L. Kotis, J. L. Lábár, A. Sulyok, M. Menyhárd, A. L. Tóth, L. Illés, and P. Panjan (JSI)

In the previous year we have shown that Ni_3C layer grows at the interface when C/Ni bilayer is bombarded either by Ga^+ or Ni^+ projectiles, and if their projected range is in the range of the layer thickness. The C/ Ni_3C interface is flat and sharp (rms roughness is less than 1 nm). It was an important point in understanding the sharp interface to recognize that the distributions of the Ga^+ and Ni^+ projectiles are strongly different, which is not expected based on the ballistic model. This is shown in Fig. 1; the Ni maximum at the interface, which is expected is missing. The mixing maximum can be explained by the relaxation processes resulting in desegregation of the Ni took

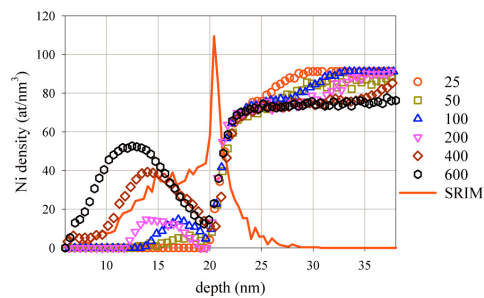


Figure 1 The comparison of the measured and simulated Ni profiles. Bombardment conditions: 20 keV, 0° .

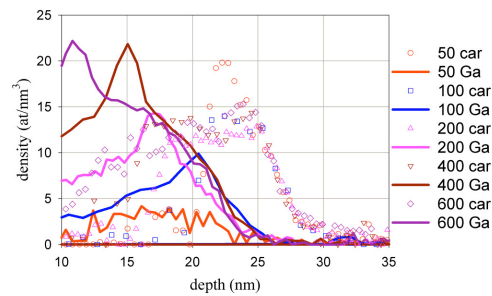


Figure 2 The Ga (line) and carbide (symbol) distributions as a function of depth for fluences shown in figure.

place after the ballistic process is terminated. Ni_3C is a metastable compound with positive heat of formation, which cannot form at equilibrium conditions. In the present case we suppose that its formation is possible by a vacancy assisted process. If this is really the mechanism involved then there should be a correlation between the vacancy distribution and the carbide formation. The vacancy distribution is determined by the projectile penetration, while the vacancy concentration also depends on the type of projectile. Fig. 2 shows the distributions of the projectile and carbide for various fluences; there is good correlation. Summarizing the compound formation observed is a vacancy assisted solid state reaction, and the kinetics of the growth of the compound layer is described by Stefan equation.

MD-based simulation of ion-erosion and nanotopography on Si

(OTKA, MÖB-DAAD, HPC-Europa)

P. Süle

The low-energy ion-bombardment induced surface nanotopography and the nanopatterning of Si has been investigated by atomistic simulations using a new approach based on *molecular dynamics* (MD). A new approach has been utilized for speeding up the simulations using a reasonable cutoff in time and increased cooling rates for keeping in hand the system temperature.

To account for thermally activated diffusion, the temperature has been increased to 900 K (annealing) and scaled back to room temperature. The combination of such reasonable steps during the simulation of ion-erosion allows us the generation of ion-eroded nanotopographies of Si. We get an unexpectedly rich variety of nanopatterns formed by the self-organization of the crater rims and adatoms islands generated by the individual ion impacts. Our results reveal that the low-energy (0.5 keV) ion-sputtered Si surface is not smooth, deep nanoholes of sub-20 nm length scale rule the landscape.

We report on an ion-sputtering induced high surface area density of $\sim 3100 \text{ m}^2/\text{g}$ (nearly 8 times larger than that of the flat surface) as estimated by MD-based computer simulation and on nanotopography consisting of voids beneath the surface reminiscent of nanoporous Si obtained by chemical etching..

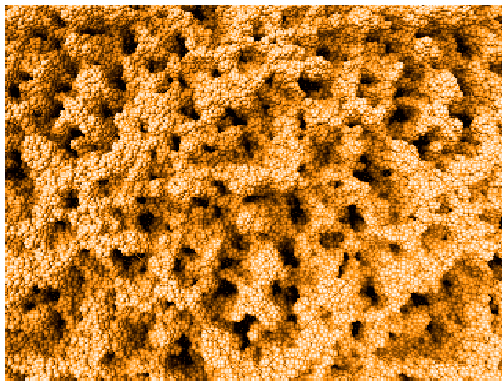


Figure 1 Nanotopography of Si after 0.5 keV ion-sputtering.

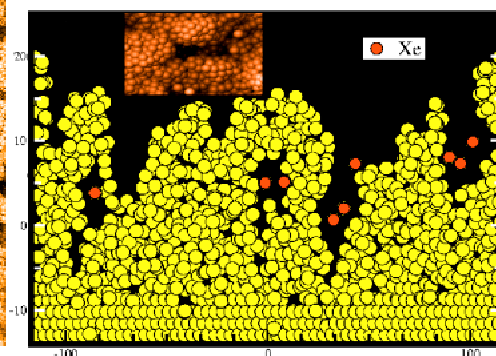


Figure 2 The cross-sectional slice of the ion-sputtered Si slab.

Trial and error method for determination of ion beam induced damage at GaAs surfaces

(Hungarian-South-African TET Project)

A. Sulyok, M. Menyhárd, and J. B. Malherbe

XPS depth profiling was used to study the low energy ion bombardment induced changes of GaAs surface. 2p and 3d XPS peaks of As and Ga, respectively, were measured in stationary states produced by 2000 eV and 500 eV Ar⁺ bombardment, and in the transition between these stationary states.

Ga in-depth distribution was estimated by using a simple layered model in which the XPS intensities were evaluated by taking into account the different kinetic energies of peaks. The concentrations of the first two atomic layers were free parameter, followed by an exponential attenuation (also free parameter) to the bulk value of 50 % (see Fig. 2). These values were chosen in a fitting procedure to reproduce the experimental peak ratios. The evaluation showed a Ga deficiency (As enrichment) at the first atomic layer and Ga enrichment below.

Many solutions have been received but based only on the data provided the stationary states no unique solution could be chosen. The transition region yielded further information for the damage caused by 2000 eV ion bombardment. Since the 500 eV ions has much less influence on the target atoms than 2000 eV ions, it can be regarded as a depth profile measurement to determine the alteration caused by previous 2000 eV ion bombardment. The atomic mixing of 500 eV Ar ions were also considered in the model calculation.

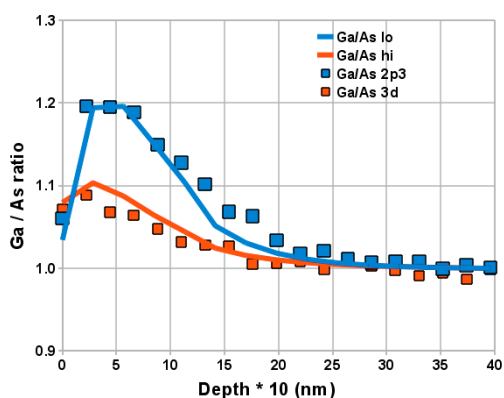


Figure 1 Depth profiles of Ga/As ratios for low and high energy peaks. Dots – measurement, line – calculation.

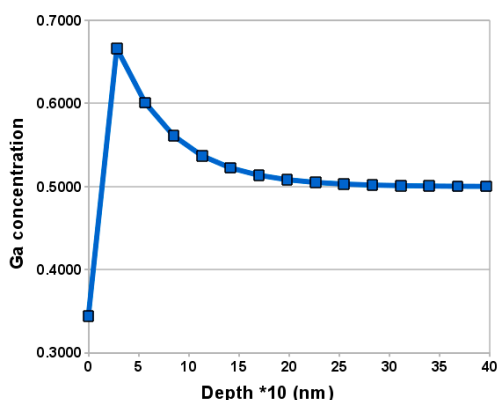


Figure 2 Reconstructed internal Ga distribution at GaAs surface after 2keV Ar ion bombardment.

We simulated the whole transition (Fig. 1) and it resulted in the internal Ga distribution in the 2000 eV stationary state as well (Fig. 2). This concentration reconstruction is the first quantitative data for low energy ion bombardment.

NTPCRASH

(NKTH TECH-08-A2/2-2008-0104)

M. Menyhárd, L. Kotis, S. Gurbán, A. Sulyok, A. Tóth, L. Illés, C. Balácsi, A. Petrik, V. Varga, and F. Wéber

Car industry is continuously looking for new materials for weight reduction. The introduction of the new material cannot affect the passenger safety, however in this quest the NTPCRASH consortium decided to find some new material for rear underrun protection application. We have studied carbon fiber reinforced composite systems made in Hungary. Two different samples were prepared. The actual structures and compositions are confidential and not given here. From the point of view of underrun the sliding should also be considered. To reveal the tribological behavior of the chosen material we have measured the coefficient of friction as a function of sliding length. It increased considerable for both material but the rates were strongly different. The surface morphology and chemistry also changed during the test. Figure 1 show the SEM image of the surface where the coefficient of friction increased much faster. The change of the surface chemistry was characterized by XPS studies. The XPS analysis could identify two carbon components, shown in figure 2. The relative amount of these two components changes during the test, showing that the chemical state of the two carbon components is affected by the wear.

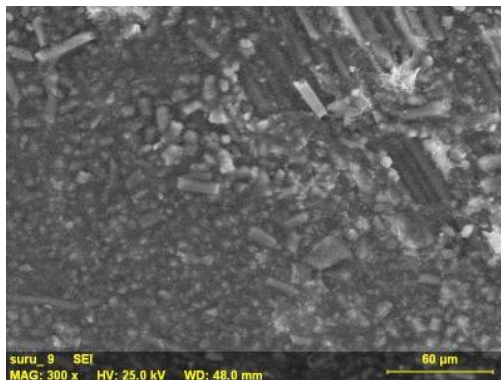


Figure 1 The SEM image of the surface after the tribological test.

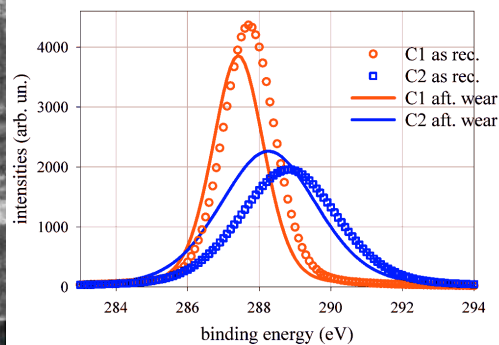


Figure 2 XPS spectra of the two carbon components. Symbols and lines show the two components before and after the test, respectively.

Nanostructured thin layers for dissolvent vapour sensors

(NKTH-METANANO)

G. Sáfrán, G. Pető, P. Soós, O. Geszti, Z. Fogarassy, and J. L. Lábár

Nowadays environmental challenges require both self-restraint of human beings and deployment of leading-edge technologies. Gases and dissolvent vapours released by industry represent an extreme load to nature. Detection of output molecules and control of environmentally friendly production necessitates various dissolvent vapour sensors based on nanomaterials. We pointed out, within the METANANO project, that nanostructured Au layers (Fig.1.) can be utilized for detection of dissolvent vapour in air. The electrical measurements were carried out by the van der Pauw four-point method with a hardware and software developed in MFA.

The layers were structured, contacted, and exposed to saturated vapours of acetone, petroleum-ether, trichlor-ethylen and ethanol. We measured electrical resistance changes attributed to work function, tunneling and/or hopping through discontinuous nanocrystals affected by the adsorbed dissolvent molecules.

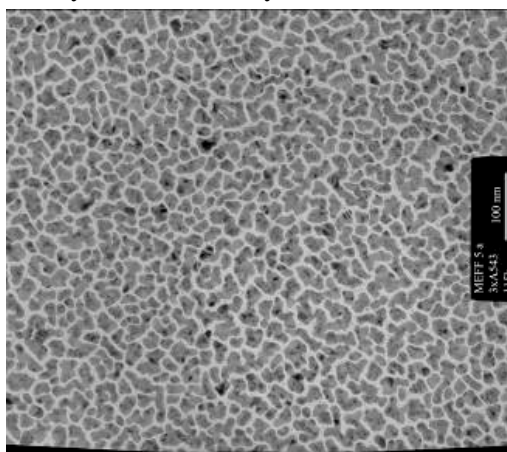


Figure 1 TEM micrograph of a 5nm thick discontinuous Au layer on carbon foil.

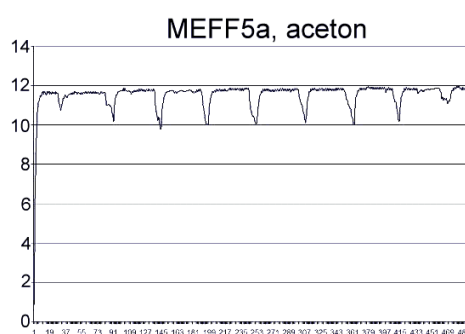


Figure 2 Response of the sensor to multiple exposures of acetone vapour (9 times 5 seconds with 30 seconds pauses).

The vapour expositions of the sensors were implemented 9 times for 5 sec with 30 seconds pauses. The recovery time of the sensors was 1~1.5 seconds (fig. 2.)

The nanolayers prepared by laser ablation and ion bombardment (PG1) showed higher noise and potential offset. They worked reasonably for ethanol exposure, and hardly for other solvents, and showed a strong temperature coefficient of resistance (TCR). The samples prepared by thermal vacuum deposition (MEFF5) proved to be stable, with no potential offset and no remarkable TCR. They were sensitive to polar dissolvents e.g. acetone and ethanol and showed a weak response to petroleum-ether.



Ceramics and Nanocomposites Department

Head: Csaba BALÁZSI, Ph.D., senior scientist

Research Staff

- János VOLK, Ph.D., Deputy Head of Department
- Péter ARATÓ, D.Sc.
- László BARTHA, D.Sc. Professor Emeritus *
- Csaba Sándor DARÓCZI, dr. Univ.
- András DEÁK, Ph.D. **
- István GAÁL, C.Sc. *
- Gréta GERGELY, Ph.D. **
- Nguyen Quoc KHANH, Ph.D.
- István Endre LUKÁCS, Ph.D.
- Judit PFEIFER, C.Sc *
- Attila Lajos TÓTH, Ph.D.

Ph.D. students / Diploma workers

- Róbert ERDÉLYI, Ph.D. student
- Eszter FÜLÖP, Ph.D. student
- Viktória HALÁSZ, diploma worker
- Péter KONCZ, diploma worker
- Viktória KONRÁD, diploma worker
- Imre KULCSÁR, diploma worker
- Péter KUN, diploma worker
- Áron NAGY, diploma worker
- Valentin SÓTI, diploma worker
- Zoltán SZABÓ, Ph.D. student
- Orsolya TAPASZTÓ, Ph.D. student
- Mihály TÓTH, diploma worker

Technical Staff

- Levente ILLÉS, engineer
- Attila PETRIK, engineer
- Viktor VARGA, technician
- Ferenc Viktor WÉBER, engineer

* **part time**

** **on leave**

The main task of the laboratory is to study the relationships between processing parameters, micro- and nanostructures and properties of ceramics and their nanocomposites. Some recent activities:

- investigation of structural, mechanical, electrical, biological properties,
- development of carbon nanotube/nano-graphite silicon nitride composites,
- 1D, 2D and 3D semiconductor (ZnO, WO₃) oxides for sensor devices,
- nano-hydroxyapatite biocomposites for medical and environmental uses, outcome of advanced preparing methods.
- development of nanostructured stainless steels by powder metallurgy,
- pilot scale production of silicon nitride tools and parts exist as well.

Our department has co-operations with universities and the industry as well. Joint laboratories with BTU (Chemical Nanostructures and Electron-Beam Lithography) have been set up. Our proven research staff actively participates in training and supervising of undergraduate and graduate students (Summer School, TDK, M.Sc, Ph.D.); and gives chairs, scientific committee members to international conferences.

Silicon nitride-based nanocomposites

(OTKA K63609)

O. Tapasztó, F. Wéber, G. Gergely, A. Petrik, J. Pfeifer, P. Arató, and C. Balácsi

In the earlier years our department reached significant successes in the research of ceramic matrix composites (CMCs), we worked out first processing technology for nanocomposite with carbon nanotube reinforcing phase.

In this year our work focused on the morphology of carbon additives. The effect of the following factors was examined in detail:

- Application of a new sintering method Spark Plasma Sintering (SPS) instead of hot isostatic pressing (HIP)
- Replacement of carbon nanotubes by graphene or exfoliated graphite that is modification of the shape of particles of carbon additive
- Finding the optimal milling procedure that is modification of the size of the particles of carbon additive

The effect of different sintering methods has been studied in co-operation with Materials and Surface Science Institute of Limerick University by SPS and our Department by HIP. Electron microscopy reflected the difference between the chosen procedures. Majority of carbon nanotubes after HIP treatment formed bundles, while a quasi-periodical arrangement developed in samples obtained by SPS with a characteristic distance about 200 nm (Fig. 1 and Fig. 2). Some publications suggest that, while the average temperature during SPS is significantly lower than during HIP, additional energy is given by the electrical current to the contacts resulting in high local temperatures. This mechanism may be responsible for the unusual features of SPS.

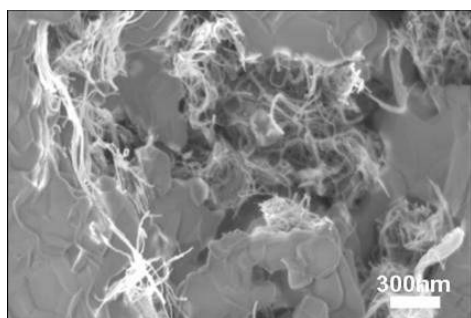


Figure 1 Nanocomposite after HIP.

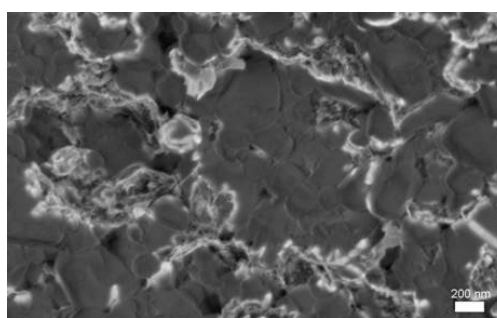


Figure 2 Nanocomposite after SPS.

Silicon nitride ceramics reinforced with either exfoliated few-layer graphene or multi-walled carbon nanotubes have been investigated by mechanical measurements in co-operation with Institute for Manufacturing Technologies of Ceramic Components and Composites, Universität Stuttgart, Germany. The graphene-reinforced composites

showed better mechanical properties, than the carbon nanotube contained ones under the same experimental conditions (Fig. 3).

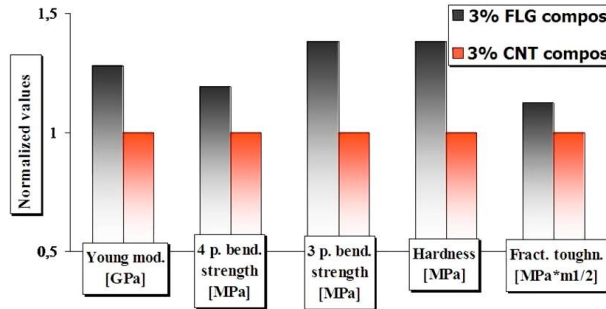


Figure 3 Comparative diagram of different mechanical properties of few layer graphene (gray) and carbon nanotube (red) reinforced Si-N composites prepared under the same experimental conditions.

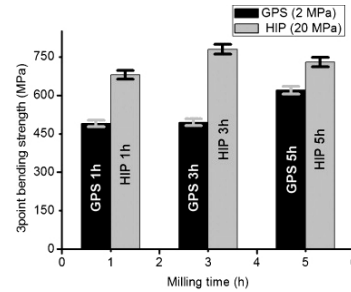


Figure 4 3-point bending strength of nanocomposites as a function of the milling time for GPS and HIP.

The effect of milling time on the three point bending strength is shown in Figure 4. The composition of ceramic component was: 90wt% Si₃N₄, 4wt% Al₂O₃ and 6wt% Y₂O₃; 3wt% carbon nanotube was added. The powder mixtures were milled in distilled water in high efficiency attritor mill with high rotation speed, 4000rpm. Best results were achieved by intermediate milling times (3h) which assured a high enough final density and good nanotube dispersions, but preserved the mechanical properties of nanotubes.

Multilayer graphene nanosheets by exfoliation of graphite in high efficient attritor mill

P. Kun, F. Wéber, A. Petrik, V. Varga, ZE Horváth, L. Illés, and C. Balázi

Graphene multilayers have been prepared by mechanical method based on milling graphite in highly efficient attritor mill. The results showed that the best dispersion

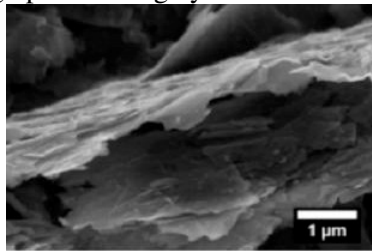


Figure 1 SEM micrograph of nanographite milled by attritor after 10h milling.

media is ethanol, and 10 hours of intensive milling proved to be the most efficient way to separate the graphite layers as it was shown by scanning electron microscopy (Fig. 1). The results showed that intensive milling in ethanol is the enhanced way to separate the graphite layers, rather than in water or in air. The average thickness of graphene multilayers was LC = 13.76 nm according to XRD measurement. These results implicate that the graphene multilayers were composed of approx. 40 graphene layers on average.

Nanostructured oxide dispersed strengthened steels

P. Koncz, F. Wéber, A. Petrik, V. Varga, and C. Balázsi
(in co-operation with KFKI-AEKI and Istanbul Technical University)

The development of oxide dispersed strengthened (ODS) steels has been conducted in the field of fast reactor fuel cladding application and fusion reactor materials application. ODS steels show high strength at high-temperatures. ODS steels have attracted attention for advanced nuclear power plants applications such as fast and fusion reactors. We developed ODS steels produced by intensive milling together with spark plasma sintering. The structure of powders is considerably changed after intensive combined (wet and dry) milling.

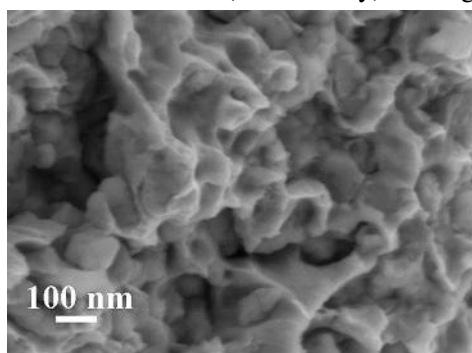


Figure 1 SEM images of the fracture surface of sintered austenitic ODS with 1 wt% Y_2O_3 addition.

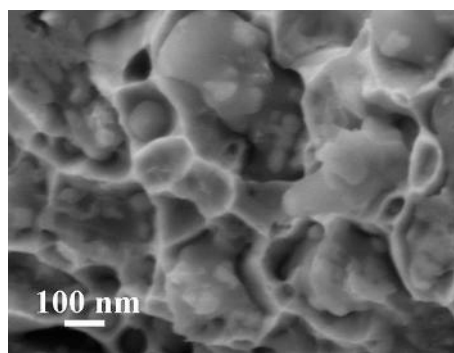


Figure 2 SEM images of the fracture surface of sintered martensitic ODS with 1 wt% Y_2O_3 addition.

Grains of steel with 100 nm mean size have been observed by SEM in austenitic ODS steels (Figs. 1 and 2). In comparison the martensitic ODS steels microstructure consisted of grain size with 100-300 nm in average. Combined milling resulted high hardness and strength.

Tungsten Oxide Functional Ceramics

(MTA-OTKA-NSF)

C. Balázsi, J. Pfeifer, I. Lukács, A. K. Nagy, and A. L. Tóth

The excellent gas sensing properties of the tungsten oxides have been manifested first of all in nanostructure open structured forms. We produced nanofibrous tissues containing reasonable amount of tungsten oxide by electrospinning method. A solution of polymer cellulose-acetate (CA) and inorganic addition is put in a syringe, which is controlled by a step motor. The solution leaves the needle, and flies to the target (a metal plate) driven by the high voltage switched between the target and the needle. The solvent evaporates in the air and the dry matter forms a fibrous tissue.

Tungstic acid hydrate ($\text{H}_2\text{WO}_4 \cdot \text{H}_2\text{O}$) and tungsten oxide hydrate ($\text{WO}_3 \cdot 1/3\text{H}_2\text{O}$) were added to the polymeric precursor. We analyzed the samples' structure with scanning electron microscope (Fig. 1). The tungsten content of certain fibers was monitored by energy dispersive spectroscopy (Fig. 2).

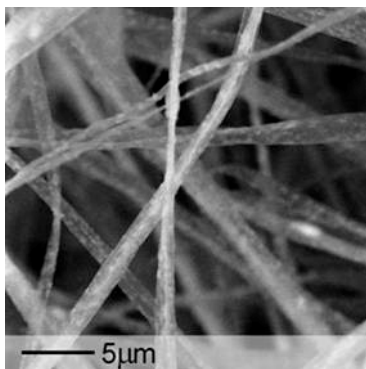


Figure 1 SEM image of cellulose acetate tissue doped by $\text{WO}_3 \cdot 1/3\text{H}_2\text{O}$.

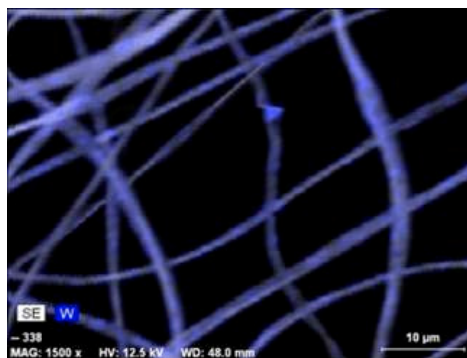


Figure 2 EDS map of cellulose acetate tissue doped by $\text{WO}_3 \cdot 1/3\text{H}_2\text{O}$.

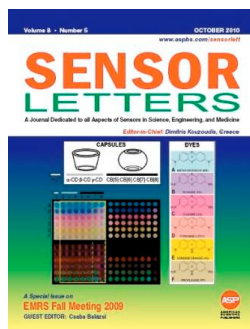


Figure 3 A special issue of *Sensor Letters* has been edited by Csaba Balázsi in this emerging field of Novel Bio and Chemosensing Materials for Health, Safety and Security Applications.

Nanoparticulate Langmuir-Blodgett films

E. Fülöp, and A. Deák

Langmuir-Blodgett technique is used to create monomolecular or monoparticulate thin films (Fig. 4). In our laboratory we focus on creating nanoparticle thin films of amorphous silica (Stöber) and core-shell nanoparticles with metal, especially gold cores and silica shells. Our goal is to create films with special optical, structural and electro-optical properties. Organized Stöber silica films can be made in a wide size range of the silica particles. They can be used for the investigation of interactions between nanoparticulate masks and ion-irradiation, and nanosphere lithography. For the core-shell LB-films we use silica coated gold nanorods (Fig. 5). The optical properties of the film can be tuned with the size and aspect ratio of the gold nanorod and with the thickness of the silica shell. The layers are disordered, so the optical properties of the films correspond to the optical properties of the particles in solution.

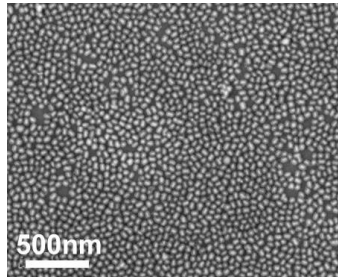


Figure 4 AuSiO films.

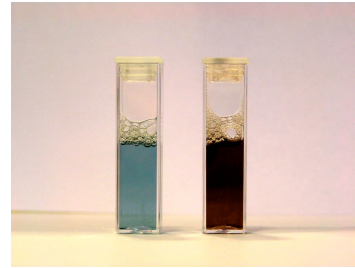


Figure 5 Gold solutions with tuned optical properties.

Improvements in FIB TEM Lamella Preparation

A. L. Tóth, L. Illés, G. Sáfrán, and G. Z. Radnóczy

The transmission electron microscopy (TEM) is one of the most versatile methods of the visualization and investigation of micro- and nanosized structures. The ideal TEM sample has to be free of artefacts. The amorphization is one of the most detrimental artefact of ion beam preparation, and unfortunately the Si samples are sensitive to amorphization. We optimized the milling sequence, the angle of incident beam, the intensity and energy of the Ga^+ ion beam current, in order to decrease the amorphization (Fig. 1). Combining the capabilities of the updated SmartSEM software, instead of a fixed 30 keV, a wider (10-30 keV) energy range became accessible. Fig. 2 shows a very broad ($\sim 1\mu\text{m}$) amorphized region (I) in the Si in a non optimized sample. This is marked by the arrow between the edge of the sample and the start of crystalline region (O). Amorphized thickness is $\sim 120\text{nm}$.

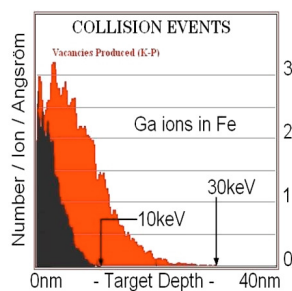


Figure 1 Ga^+ penetration for 10 and 30 keV in Fe target (SRIM calculation).

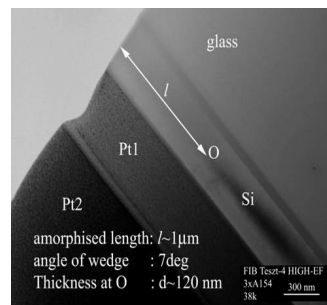


Figure 2 Very broad $\sim 1\mu\text{m}$ amorphized region (I) in Si in a non optimized sample.

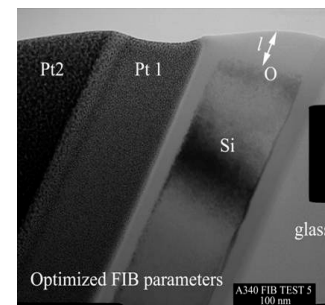


Figure 3 The sample with optimized FIB parameters.

Fig. 3, however, represents a sample with optimized FIB parameters that exhibit $\sim 90\text{nm}$ broad amorphized region, corresponding to 11nm amorphized thickness, if we estimate identical wedge shape of the thinned edge of the sample. This means a much higher quality TEM sample with less artefact.

Bending modulus measurement of vertical ZnO nanowires

(OTKA PD77578)

R. Erdélyi, L. Illés, and J. Volk

In the last five years a considerable effort has been done to investigate the mechanical properties of low dimensional zinc-oxide nanostructures such as nanorods (NRs) and nanowires (NWs). This interest is mainly fueled by the appearance of novel ZnO NW based energy harvesting and mechanical sensor devices. The basic mechanical quantities strongly influence the attainable device performance such as output voltage of a nanogenerator or sensitivity of a piezoelectric force sensor.

Our work aims to make a systematic mechanical, electrical, and coupled electromechanical investigation on ZnO NR/NW. The main goal of 2010 was to determine the bending modulus of as-prepared vertical ZnO NRs. We performed a well controlled in situ bending test in a scanning electron microscope on individual ZnO nanorods. The crystallographically aligned vertical nanocrystals were grown by wet epitaxial growth method through an electron beam generated pattern. They show good homogeneity, their length and top facet diameter vary in the range of 1.3-1.5 μm and 97-113 nm, respectively (Fig. 1). The nanorods, which are fixed at their roots by the substrate, were bent at their free end along the $\langle 110 \rangle$ crystallographic direction by a calibrated atomic force microscopy cantilever mounted on a nanomanipulator arm (Fig. 2). The typical deflections, caused by $\sim 40\text{-}60$ nN lateral loads, fallen in the range of $\sim 50\text{-}100$ nm. In order to take into the account the non-uniform cross section along the vertical axis, we proposed a two-part mechanical model, which is built up from a lower truncated circular, and an upper truncated hexagonal cone. The obtained bending modulus is 36.0 ± 8.3 GPa, which is significantly lower than that of the bulk ZnO (140 GPa).

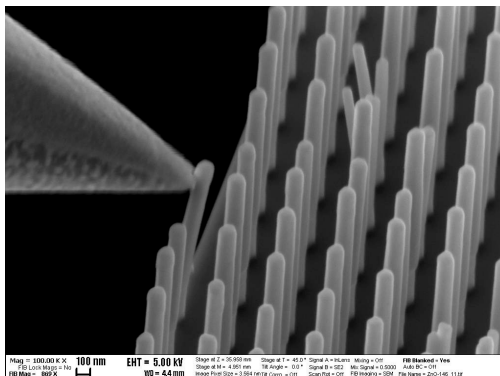


Figure 1 Scanning electron micrograph on highly ordered ZnO nanowire array.

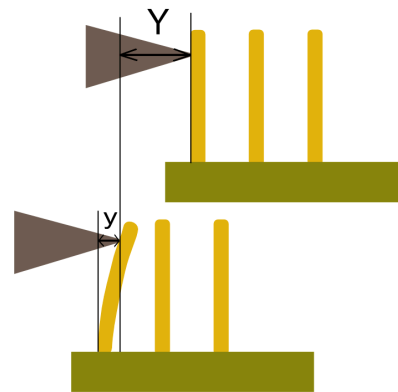


Figure 2 Schematic illustration of the in-situ bending experiment in the scanning electron microscope.

Patterned grown ZnO nanorod arrays for 3D photonic devices

Z. Szabó, R. Erdélyi, J. Makai, J. Balázs, and J. Volk

On-purpose positioned epitaxial ZnO nanorods were grown on transparent substrate by wet chemical method. Optical diffraction and transmittance measurement showed the two-dimensional ordering of the nanorods as well as the high and wavelength-dependent transparency. The realized model structure promises novel applications such as three-dimensional solar cells and photodetectors.

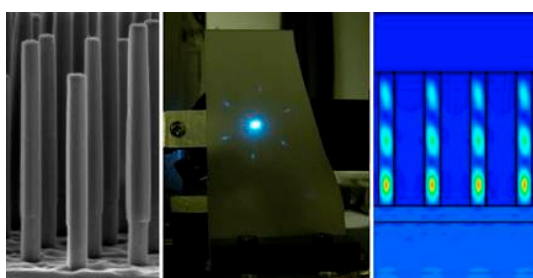


Figure 1 SEM image of the nanorods (left), the resulted hexagonal diffraction pattern (middle), and the FDTD simulated light distribution (right).

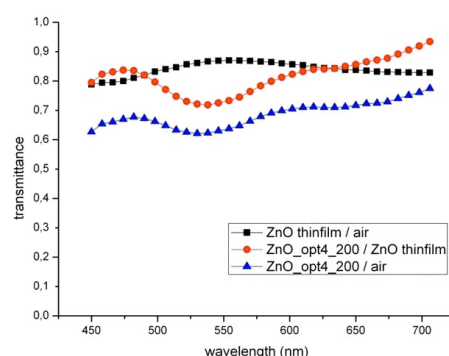


Figure 2 The spectral transmittance of the bare, thin film, and nanorod array.

The high degree of vertical alignment can be ascribed to the epitaxial ZnO seed film deposited on a c-plane sapphire substrate by pulsed laser deposition method (Fig. 1). The seed pattern for the growth was created by electron beam lithography system. The $200 \times 200 \mu\text{m}^2$ pattern is defined as spots which are arranged in a triangular lattice where the lattice parameter was set to 740 nm. The highly ordered ZnO nanorods were grown hydrothermally through the electron beam patterned PMMA layer in an aqueous solution contained the same molar amount (4 mM) of zinc nitrate hexahydrate $[\text{Zn}(\text{NO}_3)_2 \cdot 6\text{H}_2\text{O}]$ and hexamethylenetetramine $[(\text{CH}_2)_6\text{N}_4]$ (HMTA) in a multipurpose oven (85 °C, 3.5 hours). The length and the diameter of the nanorods were 2–3 μm and 200–350 nm. In the laser diffraction measurement the nanorod pattern was illuminated from the back-side of the sample by an attenuated and collimated laser beam. We screened the diffraction patterns on a piece of roughed glass by using subsequently Ar ($\lambda=488\text{nm}$) and He-Ne ($\lambda=633\text{nm}$) laser. Transmittance measurement (Fig. 2) was taken by a similar arrangement by using halogen lamp source instead of the laser, an additional monochromator and a photodetector. The positioning of the ca. 100 μm diameter spot was adjusted via an eye-piece. Both optical measurements were compared with finite-difference time-domain simulations in a computational domain of $10 \times 10 \times 5 \mu\text{m}^3$ which involves the top region of the substrate, the nanorods having tapered geometry as well as a topmost layer for air.

Substrate effect on the growth of vertical nanowires

(MTA-JSPS mobility grant, 117)

R. Erdélyi, I. E. Lukács, Z. E. Horváth, and J. Volk

Vertically aligned ZnO nanowire (NW) arrays attract a great interest due to a variety of astonishing potential applications in photonics, piezotronics as well as in chemical and biological sensing. These applications require different kinds of nanostructures concerning the geometry of the NWs and the degree of their alignment.

In our previous works we demonstrated highly uniform on purpose positioned epitaxial ZnO NRs which were hydrothermally grown on ZnO single crystal. However, in most of the applications an alternative substrate material is preferred i) to reduce the cost, ii) to integrate the nanostructure with the Si technology or iii) to attain light confinement in the NR/NW by refractive index contrast at the bottom of the cavity. In case of wet chemical methods a ZnO seed layer is needed, which strongly affects the geometry and orientation of the NRs/NWs to be grown on the top of it. Our work aims to investigate the effect of the seed layer on the geometry and alignment of the patterned grown ZnO NRs by using five different types of ZnO seed surfaces: single crystal (Figs. 1a, 1f), pulse laser deposited (PLD) layers on three different substrates (on Al_2O_3 (Figs. 1b, 1g), on Pt/ Al_2O_3 (Figs. 1c, 1h), on Si (Figs. 1d, 1i)), and sputtered polycrystalline layer (Figs. 1e, 1j). The high adatom mobility in PLD growth technique allows the ZnO to crystallize readily even on amorphous substrates, such as the native SiO_2 passivation layer on the surface of the Si substrate.

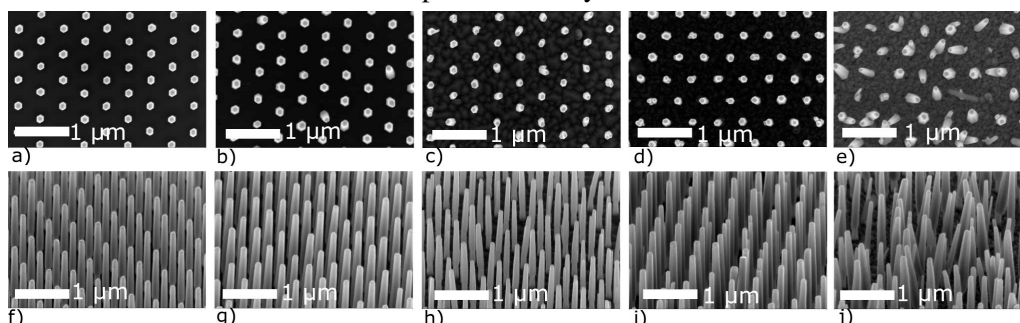


Figure 1 Scanning electron micrograph of vertical ZnO nanowires grown on different substrates.

The effect of the crystallinity of the seed layer on the grown nanowire arrays was investigated by an x-ray diffractometer (XRD) system having 2-dimensional detector. The mis-orientation angles of all the unit cells in the seed layer (mosaicity) and in the nanorod array were evaluated by the “full width at half maximum” value (FWHM) of the XRD χ -rocking curve. It turned out that the FWHM of χ -peak of ZnO rods show almost the same value as that of the corresponding substrates, indicating that the alignment of the grown ZnO nanorods is mainly affected by the mosaicity of seed layer rather than by the surface roughness.

Highly ordered vertical ZnO nanorods by nanosphere lithography

Z. Szabó, E. Fülöp, I. E. Lukács, and J. Volk

Nowadays, there is a high demand for large-scale highly ordered nanorods for new type of devices such as 3D solar cells, photodetectors, photonic crystals etc. However, the common nanopatterning methods are either too slow for large areas (e-beam, focused ion beam), or they need extremely expensive and high-resolution masks (photolithography, nanoimprint lithography, self-powered electron lithography).

In this work we use nanosphere lithography (NSL) as a cheap and straightforward method for large area patterning. NSL uses self-assembled monolayer of micro/nanospheres (NS) (Stöber silica, polystyrene) as a photolithography mask to generate hexagonally ordered holes in the underlying photoresist. Nanospheres function as lenses hence bring the UV light into focus beneath themselves. According to our 3D finite-difference time-domain (FDTD) simulation, when illuminating the photoresist/NS structure with UV light (i-line, 365nm) the peak intensity in the 200nm thick photoresist layer can be 6 times higher than that of the incident beam which allows selective development for the hexagonally arranged focal spots (Fig. 1).

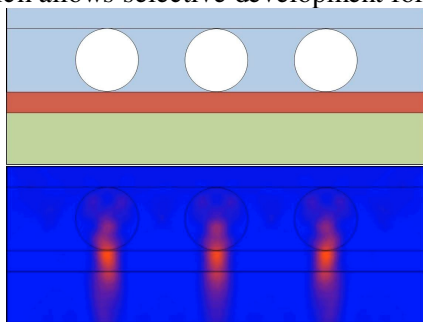


Figure 1 FDTD simulation: Cross section of the device geometry and of the intensity distribution.

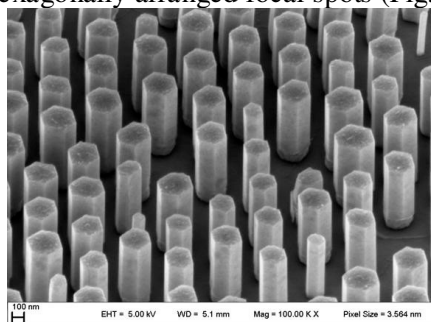


Figure 2 SEM image of the nanosphere lithography patterned and hydrothermal grown ZnO nanorods.

In order to demonstrate the NSL method experimentally, at first a thinned (~180nm) photoresist was spin coated to a 5×5mm² ZnO single crystal substrate. After pre bake, silica sphere (500nm diameter) monolayer was deposited by Langmuir-Blodgett (LB) technique, which ensures a closed packed NS arrangement. The optimized exposure energy was 12mJ/cm², which is lower than the standard dose in conventional lithography because of the focusing effect. After the removal of silica nanospheres by a quick HF rinse, the photoresist was developed in 1:2 developer-water solution for 30s. The hydrothermal growth of the ZnO was carried out in an equimolar (10mM) solution of zinc nitrate hexahydrate [Zn(NO₃)₂·6H₂O] and hexamethylenetetramine [(CH₂)₆N₄] at 95 °C for 2 hours. According to the SEM observation the vertically aligned 700-750nm long and 260-280nm diameter nanorods are indeed arranged in a hexagonal lattice (Fig. 2).

Organic-inorganic heterostructures for third generation photovoltaic cells

(AUT-HUN S&T mobility grant, AT-1/2008)

R. Erdélyi, Z. Szabó, Z. Baji, Z. Lábadi, I. Bársony, and J. Volk

Hybrid photovoltaic cells combine advantages of both organic and inorganic semiconductors. They have organic materials that consist of conjugated polymers that absorb light as the donor and transport holes. Inorganic materials in hybrid cell are used as the acceptor and electron transporter in the structure.

Our work aims to build novel ZnO nanowire (NW) and p-type polymer based hybrid photovoltaic cells by the infiltration into NWs. The main goal of 2010 was to optimize the infiltration of semiconducting polymer into NWs. At first standard bulk heterojunction solar cell was fabricated in a multilayer structure of glass/ITO/PEDOT:PSS/P3HT:PCBM/Ca/Al as a reference device. The solar cell showed relatively high power efficiency ($\eta=3.28\%$) at $V_{OC}=550$ mV, $I_{SC}=9.91\text{mA}/\text{cm}^2$, and $FF=0.603$ values (Fig. 1). In accordance with the requirements of organic solar cells, ZnO nanowires with low diameter ($<30\text{nm}$) and with relatively limited length ($<300\text{nm}$) were fabricated. We compared two ZnO thin film deposited by atomic layer deposition (ALD) and reactive plasma sputtering method. It was found, that on the ALD seed layer the NWs grow in lower density ($\sim 70/\mu\text{m}^2$) than on the sputtered layer ($\sim 400/\mu\text{m}^2$). Further difference that the NWs grown on the sputtered layer are aligned more to the surface normal. Both types of glass/ITO/ZnO/NW stacks showed relatively high optical transmittance in the visible region ($T>73\%$) and relatively low sheet resistivity ($<40\ \Omega/\text{cm}$), which are indispensable for high performance hybrid solar cells. The affinity of ZnO nanowire arrays for the infiltration of poly(3-hexyl-thiophene) (P3HT) was investigated by using three different solvents: chloroform, chlorobenzene, and dichlorobenzene. Although the chloroform solution showed the most homogenous layer in optical microscope, SEM observations revealed that both chlorobenzene and dichlorobenzene solvents show better infiltration (Fig. 2).

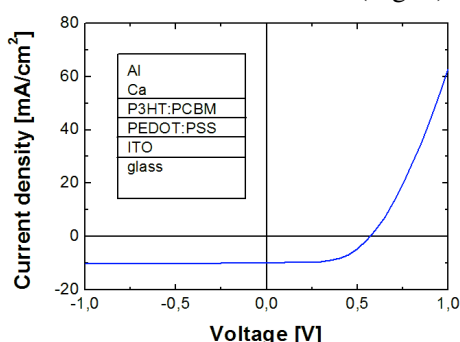


Figure 1 I-V characteristic of a standard bulk-heterojunction solar cell.

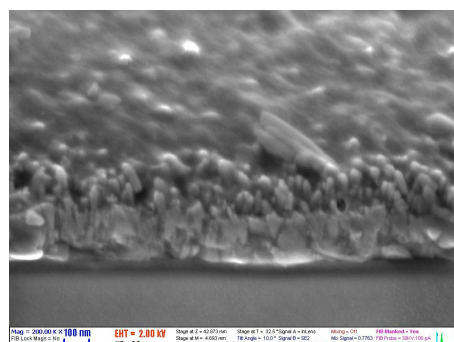


Figure 2 ZnO nanowire array infiltrated by chlorobenzene solution of P3HT.

Synthesis of horizontal ZnO nanowires for integrated sensor fabrication

(OTKA K76287)

N.Q.Khánh, J. Volk, I. Lukács, M. Tóth, Z. E. Horváth, and R. Erdélyi

ZnO as a biocompatible, wide band gap semiconductor is a very promising candidate material for chemical and biosensor application. One of its advantages is the ability to grow ZnO nanowires (NW) with high aspect ratio, which increases the sensitivity of the NW based sensor via the high surface to volume ratio. So far, most of work concerning the synthesis of ZnO NWs reported on the formation of vertical NWs. However, the synthesis of horizontal ZnO NWs, which is more compatible with the planar IC technology is a key issue in the fabrication of the smart sensors. In our present work we have applied the wet chemical technique and electrospinning as a simple, easy-to-scale-up method for synthesis of horizontal NWs.

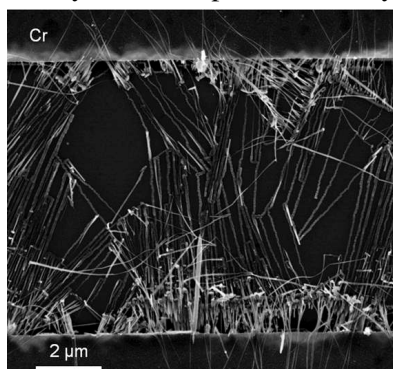


Figure 24 Plan-view FESEM image of ZnO nanowires laterally grown in 1 mM aqueous zinc nitrate/(HMT) solution at 95 °C for 13.5 h.).

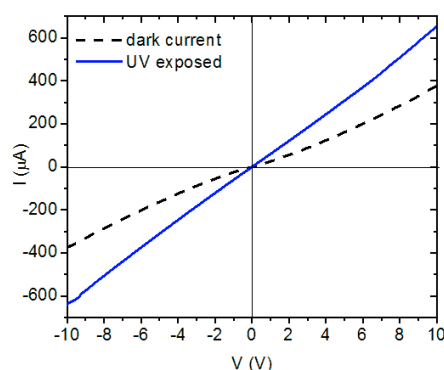


Figure 25 I–V characteristics between the two neighboring electrodes bridged by the laterally grown ZnO nanowires measured in air.

In this approach, chrome layer has been deposited on the top of the RF sputtered ZnO seed layer to prevent the growth of NWs in vertical direction. After patterning of the Cr electrodes and the ZnO seed underneath by lift-off the nanowires have been synthesized in 1 mM zinc nitrate and hexamethylenetetramine equimolar aqueous solution at 95°C for 13 hours. As shown by Figure 24 many wires have grown laterally on the oxide surface of the substrate from both electrodes. Their thickness is in the range of 40-60 nm. Though most of them did not reach the opposite electrode in this sample because the wide gap (8.5 μm), several wires cross with the other ones grown from the opposite side, thus ensuring the connection between the two electrodes. The I-V curves of the device drawn in Figure 25 shows the ohmic conduction. When the device is exposed to UV light (360 nm) the current increases due to extra-charge carriers generated in crystalline ZnO by high energy photons.



Complex Systems Department

Head: György SZABÓ, D.Sc., scientific advisor

Research Staff

- István BORSOS
- Imre EÖRDÖGH, dr. Univ.
- Zoltán JUHÁSZ, Ph.D.
- Géza ÓDOR, D.Sc., scientific advisor
- Károly SZÁSZ, engineer
- Attila SZOLNOKI, Ph.D.

Ph.D. students / Diploma workers

- Lilla CZAKÓ, B.Sc. student
- Livia HANUSOVSKY, B.Sc. student
- Márton HEGEDŰS, B.Sc. student
- Gábor MÁNDI, M.Sc. student
- J. K. PÁLFALVI, B.Sc. student
- Melinda VARGA, M.Sc. student
- Ádám WAGNER, M.Sc. student

The main scientific activity is focused on the statistical physics of different non-equilibrium systems. In collaboration with Heinig and Liedke (FZD, Dresden-Rossendorf) Géza Ódor and István Borsos developed a computer facility (of 4 TFlop capacity) based on the application of graphical processors. It is demonstrated that this hardware with suitable software can enhance significantly both the speed of simulations and the size systems investigated. Within the framework of a DAAD-MÖB mobility project the interfacial pattern formations are studied by Monte Carlo simulations. The appearance of Griffiths phase is also investigated numerically for the traditional contact process on a set of small world networks by Ódor together with Juhász (SzFKI, Budapest), Munoz (University of Granada) and Castellano (University of Roma "La Sapienza").

Utilising the concepts and tools of non-equilibrium statistical physics the main scientific efforts of this group are concentrated on the investigation of evolutionary games. Many aspects of social dilemmas are studied by Szabó, Szolnoki, and Borsos in collaboration with Perc (Maribor, Slovenia), and Helbing (ETH, Zürich). In these mathematical models players are distributed on the sites of a lattice (or graph) and following one of the possible strategies (e.g., co-operation or defection) they collect income from games with the neighbors. For the evolutionary games the players are allowed to modify their strategy according to a dynamical rule (e.g., by imitating one of their better neighbors). In the last year we studied what happens if the players are allowed to punish their defective co-players. Systematic simulations and analytical treatments were performed to clarify the effect of punishments (quantified by its cost and fine on defecting individuals) for spatial public goods games. It turned out that the institutional (pool) and personal (peer) punishments have different efficiency in the maintenance of cooperative behaviors.

Very recently we have begun to study a new version of evolutionary games where small groups of players choose new strategies in a coordinated way to maximize the group's income. In order to simplify the latter evolutionary rule we have also

investigated the cases of pair interactions when the players' utility functions are composed from their own payoff and the co-player's payoffs with weigh factors Q and $(1-Q)$. This model indicated clearly that, disregarding the noisy effects, the optimal total payoff can be achieved by myopic fraternal players who share their common income equally ($Q=1/2$). Deviation from the fraternal behavior can drive the system into the "tragedy of the commons" for both the selfish ($Q=0$) and altruistic ($Q=1$) players. In the next years we wish to study the spatial competition between the fraternal, the selfish, and the altruistic behavior within the framework of co-evolutionary games.

In collaboration with Tomé (University of Sao Paulo) Borsos and Szabó studied the concept of dynamical graphs and the structure of probability currents along its edges connecting configurations that can transform into each other through the elementary processes for non-equilibrium two-state lattice systems. Considering a simple model, namely a contact process with a weak mutation on a square lattice, the specific entropy production is determined. It is hoped that the latter quantity can be used to quantify the deviation from the detailed balance in many evolutionary games, too.

Juhász and Sipos (Institute for Musicology, Budapest) developed a computer algorithm for the motive identification in large folk song corpora. This method is based on a dynamic time warping algorithm by determining inherent repeated elements of the melodies and on a self-organizing map that learns (and recognizes) the most typical motive contours. Using this system the typical motive collections of 22 national music cultures in Eurasia were determined. The analysis of the overlaps for the national melodies on the common map allowed us to draw a graph of connections exhibiting two distinct groups in agreement with the expectations based on geographical distribution (and history). This method is also applied to quantify the relatedness between languages and genes. The parallel investigation of the folk song, the languages and the genetic data for a large set of nations opens new directions for these interdisciplinary fields of science.

Two engineers, Eördögh and Szász, developed new image processing algorithms including the application of a high resolution line scan camera, software implementation, and test of accuracy and reproducibility. Continuing the previous developments the parameters of their 3D motion control software module was improved and applied for designing flexible calibration cables within an R&D project in the factory Axon.

The international echo to the previous results of this group is characterized by the 1350 citations received during the last two years.

Efficiency of punishments in spatial public goods games

(Hungarian Scientific Research Fund under Grant No K-73449)

G. Szabó and A. Szolnoki

The analogy between the many-particle systems of solid state physics and the multi-agent models of a human system encouraged physicist to adopt the sophisticated methods of statistical physics to the fields of social sciences. Now we demonstrate the efficiency of this approach when considering the importance of punishment in the maintenance of cooperative behavior in human societies. For this goal we consider spatial public goods games (PGG) with players forming five-person overlapping groups on a square lattice. For the simple two-strategy case the players (within all the groups) decide simultaneously whether they contribute a unit sum into a common pool or not. The total investment is multiplied by a factor r and divided equally among the group members irrespectively of their cooperative or defective behavior. In this situation the rational (selfish) players should decline investment if the cost of investment exceeds the part of profit related to their own investment. As a result the selfish players cannot exploit the advantage of mutual cooperation, instead of it, their society evolves into the "tragedy of the commons" where all the players choose defection.

The introduction of punishment, however, supports the maintenance of cooperative behavior. As a result of punishment the defector's income is reduced by a fine while the punisher pays the cost of punishment. Now we study the effects a pool-punishment as an additional strategy in spatial evolutionary PGGs and the results were contrasted with the case of peer-punishment when the punishers pay the cost of punishment only if it is necessary, that is, when the defection is sanctioned. In the case of pool-punishers the punisher's contributions cover the cost of institutions (police, judge, etc.) independently of their efficiency. As a result, in the absence of defection the pure income of peer-punishers is equivalent to those of co-operators considered as "second order free-riders" while a pool-punisher's income is always exceeded by the co-operators. A preceding study on pool-punishment in well-mixed populations concluded that pool-punishers can prevail over peer-punishers only if the second-order free-riders are punished as well. For the present spatial systems the self-organizing spatiotemporal structures help the maintenance pool-punishment and the resultant phase diagrams exhibit a surprisingly rich set of behaviors when tuning the cost and fine parameters for two typical values of multiplicative factor at a fixed noise level.

During the evolutionary imitation process a randomly chosen player x can adopt the strategy from one of the neighbors (y) with a probability $W=1/(1+\exp(P_x-P_y)/K)$ dependent on the payoff difference (P_x-P_y) and a noise parameter K characterizing the stochasticity in the imitation process. The players' payoffs are collected from five five-person PGGs and reduced by the cost of punishment for the co-operators and by the fine for the defectors if the punishment is executed. Initially the players use either C (cooperation) or D (defection) or O (cooperative pool-punisher) strategies and after

a suitable thermalization time the system evolves into a stationary state characterized by the portion of strategies and the resulting spatiotemporal patterns. The results are summarized in fine-cost phase diagrams.

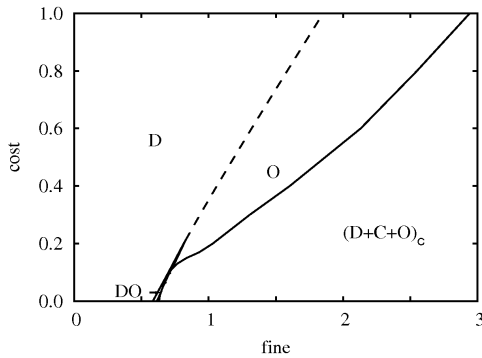


Figure 1 Fine-cost phase diagram for $r=2$ in the low noise limit.

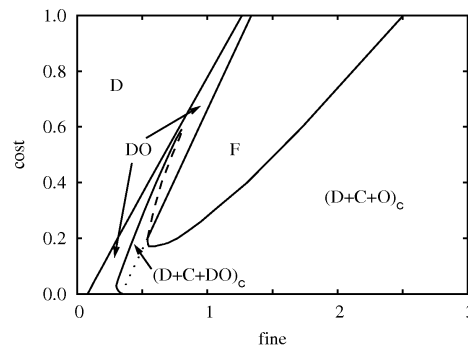


Figure 2 Fine-cost phase diagram for $r=3.5$ in the low noise limit.

Both phase diagrams illustrate that only defectors remain alive (see the D phase in Figs. 1 and 2) for low fine if the cost of punishment does not exceed a threshold value dependent on fine. When increasing the fine for an adequate value of cost if $r=2$ then first the pool-punishers beat defectors (see the phase O in Fig. 1). For higher fine, however, all the three strategies coexist due to the emerging cyclic (rock-paper-scissors type) dominance among them [the latter phase is indicated as $(D+C+O)_c$]. It turned out that defectors and pool-punishers can also coexist within the phase DO. The latter two-strategy phase occurs for higher cost values if $r=3.5$, and it becomes unstable against the appearance of a self-organizing pattern where D, C and DO phases invade cyclically each other. Notice, furthermore, the F phase in Fig. 2 where the cyclic dominance yields growing oscillations in the portion of strategies and finally the system evolves into one of the homogeneous (absorbing) states. For higher values of r the relevance of punishment is reduced because of the higher portion of pure cooperation in the stationary states.

The exploration of the above phase diagrams required the extension of the systematic stability analysis between all possible pairs of subsystem solutions. Similar phenomena are expected when the numbers of strategies are increased in the spatial evolutionary games.



ACTIVITIES

MFA Seminar Talks

13 January 2010

Botond BAKÓ

(Department of Metal Physics Research, CEA-Saclay, France):
“Simulation of dislocations interacting with nanophases in a model FCC crystal”

20 January 2010

Géza ÓDOR

(MTA MFA, Budapest, Hungary): *“Surface pattern formation and scaling described by conserved lattice gases”*

27 January 2010

Attila SZOLNOKI

(MTA MFA, Budapest, Hungary): *“Is it good to have the public bad? – About mutations acting as catalysts”*

17 February 2010

Amadou MIÉVILLE

(Óbuda University, Kálmán Kandó Faculty of Electrical Engineering, Budapest, Hungary): *“Thin film solar cells on plastic substrate”*

22 February 2010

Dr. Didier PRIBAT

(Sungkyunkwan University, Seoul, Korea): *“Synthesis of graphene by ion-implantation”*

24 March 2010

Zsolt CZIGÁNY

(MTA MFA, Budapest, Hungary): *“Modeling of electron diffraction patterns for amorphous and nanocrystalline systems and its application for amorphous and fullerene-like carbon allotropes”*

31 March 2010

Péter BASA

(MTA MFA, Budapest, Hungary): *“Metamaterial-based terahertz optics”*

7 April 2010

Károly TÓKÉSI

(MTA Institute of Nuclear Research, Debrecen, Hungary):
“Interaction of charged particles with capillary inner walls - applications”

14 April 2010

Attila PÉTER

(National Instruments, Budapest, Hungary): *“Measurement techniques and control systems from National Instruments (NI)”*



28 April 2010

Janez KOVAC

(Jozef Stefan Institute, Ljubljana, Slovenia): “*Application of X-ray photoelectron spectroscopy (XPS) to characterize thin organic films and plasma functionalized surfaces*”

13 May 2010

Takahiro NAGATA

(National Institute for Materials Science, Tsukuba, Japan): “*Study of metal/oxide interface by combinatorial method*”

15 September 2010

Péter VARGA

(MTA MFA, Budapest, Hungary): “*Photonics?*”

22 September 2010

Zsolt SZABÓ

(Agency for Science, Technology and Research (A-STAR), Singapore): “*Optical metamaterials*”

29 September 2010

Péter KOZMA

(MTA MFA, Budapest, Hungary): “*Interferometric biosensor based on planar optical waveguides for label-free detection*”

25 October 2010

Peter LIEBERZEIT

(University of Vienna, Vienna, Austria): “*Man-made recognition materials for highly selective chemo- and biosensing*”

8 December 2010

Péter GALAJDA

(MTA Biological Research Center, Szeged, Hungary): “*Bacterial populations in microfluidic chips*”

15 December 2010

János SZÉPVÖLGYI

(MTA Chemical Research Center, Budapest, Hungary): “*About the red mud flood catastrophe at Ajkas*”

Research and Development Partners

- AN, J.S.** (*Hallym University, Korea*)
- BIGOS, Agneska** (*Institute of Metallurgy, Krakow, Polish*)
- CHAE, Chang-Hoon** (*Gangneung-Wonju University, Korea*)
- CHENTSOV, Alexander** (*Institute of Problems in Mechanics, Russia*)
- CHULUP, Zdenek** (*Institute of Physics of Materials, ASCR, Brno, Czech Republic*)
- CRESTOU, Catherine** (*CEMES-CNRS/Université Paul Sabatier*)
- CRESTOU, Jacques** (*CEMES-CNRS/Université Paul Sabatier*)
- FREY, Lothar** (*Erlangen, Germany*)
- HULTMAN, Lars** (*Linköpping, Sweden*)
- INDYKA, Paulina** (*Institute of Metallurgy, Krakow, Polish*)
- IEVTUSHENKO, Arsenii** (*Institute of Semiconductor Physics, Kiev, Ukraina*)
- YAKOVLEV, Yuri** (*Ioffe Institute, Sankt-Peterburg, Russia*)
- KELLING, Jeffrey** (*FZD, Dresden, Germany*)
- KIM, Seong-Gon** (*Gangneung-Wonju University, Korea*)
- KOVAC, Janez** (*Jozefr Stefan, Institute, Ljubljana, Slovenia*)
- KRIZANOVA, Zuzana** (*Institute of Electrical Engineering, Slovak Academy of Sciences*)
- LÁNYI, Stephan** ()
- LAZORENKO, Vasili** (*Institute of Semiconductor Physics, Kiev, Ukraina*)
- LOBOTKA, Peter** (*Institute of Electrical Engineering Slovak Academy of Sciences*)
- MALHERBE, Johan** (*U. Pretoria, Pretoria, South Africa*)
- MIEVILL, Amado** (*FLEXSOLAR Ltd., Switzerland*)
- NUTSCH, Andreas** (*FHG IISB, Erlangen, Germany*)
- PARK, Young-Wook** (*Gangneung-Wonju University, Korea*)
- PERC, Matjaz** (*Maribor University, Slovenia*)
- RADEV, Dimitar** (*Institute of General and Inorganic Chemistry, Bulgaria*)
- RADEVA, Ekaterina** (*Institute of Solid State Physics, Bulgaria*)



ROTARU, Horatiu (*Iuliu Hateganu University, Romania*)

TORRES, Ricardo (*CEMES-CNRS/Université Paul Sabatier*)

SERIN, Virginie (*CEMES-CNRS/Université Paul Sabatier*)

SCHULTZ, Henrik (*Forschungszentrum Dresden Rossendorf*)

THOMAS, Ivan (*Physical Institute, Prague, Czech Republic*)

TSUNEO, Morita (*Tateyama Ltd, Japan*)

UEDA, Yoshi (*Tateyama Ltd, Japan*)

USTINOV, Konstantin (*Institute of Problems in Mechanics, Russia*)

Visitors

ALVES, Eduardo (*ITN, Ion Beam Laboratory, Sacavém, Portugal*)

ARIAKE, Jun (*Akita Institute of Advanced Technology, Akita, Japan*)

ANOOZ, Saud (*Institut für Kristalzüchtung, Berlin, Germany*)

AYALA, Israel (*Beneq Ltd, Finland*)

BOCH, Wolfgang (*Head of Unit, INFISO/FET*)

CHAE, Chang-Hoon (*Hallym University, Korea*)

COTTIER, Kaspar (*U. Wadenswill, Switzerland*)

FLEISCHER, Roland (*Oxford Instruments, Germany*)

CSERNOZATONSZKIJ, Leonid (*Biochemican Institute, SaintPeterburg, Russia*)

JONES, Walis (*Farfield UK*)

LEE, Young Hee (*U. Sungkyunkwan, Korea*)

LIBERZEIT, Peter (*University of Vienna, Wien, Austria*)

PRIBAT, Didier (*U. Sungkyunkwan, Korea*)

VEPREK, Stan (*Department of Chemistry Technical University Munich*)

YONG, Tou Teck U. (*Multimedia University, Cyberjaya, Japan*)



MAGYAR TUDOMÁNYOS AKADÉMIA
MŰSZAKI FIZIKAI és ANYAGTUDOMÁNYI KUTATÓINTÉZET
 HUNGARIAN ACADEMY OF SCIENCES
RESEARCH INSTITUTE FOR TECHNICAL PHYSICS AND MATERIALS SCIENCE



FOTOVILLAMOS MÉRÉSI SZOLGÁLTATÁS

Az MTA Műszaki Fizikai és Anyagtudományi Kutatóintézet több évtizedes tapasztalattal rendelkezik szerves, funkcionális anyagok mérése és minősítése terén. Egyik kiemelt kutatási területe a fotovoltaikus szerkezetek és anyagok előállítása és vizsgálata ipari együttműködésben.

Az MTA MFA 2008-tól üzemelteti a fotovoltaikus napelemek bemérésére és minősítésére alkalmas korszerű vizsgáló-laboratóriumát.

A mérőberendezés műszaki adatai:



Energy Equipment Testing Service Limited (E.E.T.S) PVMT 11250 Module Tester

- A mérhető maximális napelem modul felület:
1.5m x 0.75m.
- A megvilágításhoz Philips 14621 Halo Nr. 55060 típusú halogénizzó mátrixot használ 2% laterális homogenitás mellett.
- A megvilágítás egyenletességének pontossági osztálya: IEC 904-9 szabvány szerint "A".
- A megvilágítás folyamatos üzemmódú, intenzitása 750-1250 W/m² között állítható.
- A megvilágítás erősségét kalibrált referencia cella méri.
- Mérés határok:
 - Feszültség: 0-120 V DC (1% FSO)
 - Áramerősség: 0 - 20 A DC (1% FSO)

A műnaphoz kapcsolt számítógépes mérő-adatgyűjtő rendszer rögzíti:

- a napelem ill. modul áram-feszültség jelleggörbáját;
- a teljesítmény-feszültség jelleggörbáját;
- a minta pillanatnyi hőmérsékletét.

A berendezés külön igény és egyeztetés alapján lehetővé tesz:

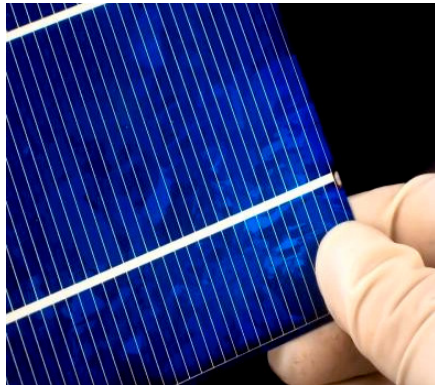
- hőmérsékletfüggő paraméter-vizsgálatot;
- megvilágításfüggő paraméter-vizsgálatot;
- vékonyréteg modulok bemérését.

Visitors: Konkoly-Thege M. út 29-33, BUDAPEST, 1121 HUNGARY, Mail: P.O. Box 49., H-1525, Web: <http://www.mfa.kfki.hu>
 Phone, Director: +36-1-392 2224, Phone, Administration: +36-1-392 2227, Fax: +36-1-392 2226



MAGYAR TUDOMÁNYOS AKADÉMIA
MŰSZAKI FIZIKAI és ANYAGTUDOMÁNYI KUTATÓINTÉZET
 HUNGARIAN ACADEMY OF SCIENCES
 RESEARCH INSTITUTE FOR TECHNICAL PHYSICS AND MATERIALS SCIENCE

Az intézet mérési szolgáltatást ajánl mono- illetve polikristályos napelemeken és napelempaneleken az alábbi feltételekkel:



Mérési beállítások:

- 800 W/ m² , 1000 W/ m² és 12000 W/m² besugárzás, műnappal;
- 25 °C normált hőmérséklet értéken történő mérés.

Mért paraméterek:

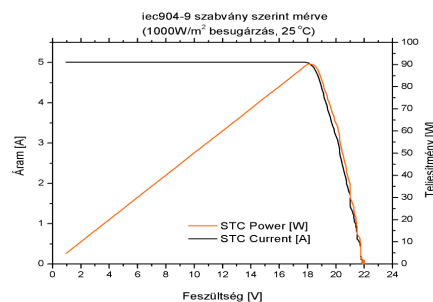
- üresjárású feszültség /open circuit voltage (U_{OC});
- rövidzárási áram / short circuit current (I_{SC});
- maximális teljesítmény, feszültség és áram (U_{MPP} , I_{MPP} , P_{MPP});
- modulhatásfok /solar module efficiency (η);
- kitöltési tényező /fill factor (FF).

A mérési értékeket az IEC 60891 szabvány szerint standard hőmérsékletre korrigálva adjuk meg.

Jegyzőkönyv

A mérésről az MTA MFA jegyzőkönyvet állít ki, amely tartalmazza:

- a modul azonosítóját;
 - gyártó,
 - típus,
 - serial number,
- táblázatot a névleges paraméterekkel;
- táblázatot a mért értékekkel;
- mért karakterisztikákat;
- a mérést végző nevét;
- a mérések idejét.



A szolgáltatás ára

A szolgáltatás ára magában foglalja a vizsgálat elvégzésének költségeit (kalibrálás, mérések) és a jegyzőkönyv készítését. Az ár nem tartalmazza:

- a mintadarab laboratóriumba történő oda- és visszazállítását;
- az egyedi igények alapján kért mérések költségeit.

A standard program szerinti szolgáltatás ára mintadarabonként: 60.000 Ft+ ÁFA.

Nagyobb mennyiség bemérésének megrendelése esetén kedvezményt adunk, speciális igények esetében az ár egyedi megállapodás alapján kerül meghatározásra.

További információ, előzetes műszaki egyeztetés:

Dr. Lábadi Zoltán, laborvezető
labadi@mfa.kfki.hu
 +36-1-392 2222/3528

Visitors: Konkoly-Thege M. út 29-33, BUDAPEST, 1121 HUNGARY, Mail: P.O. Box 49., H-1525, Web: <http://www.mfa.kfki.hu>
 Phone, Director: +36-1-392 2224, Phone, Administration: +36-1-392 2227, Fax: +36-1-392 2226



MAGYAR TUDOMÁNYOS AKADÉMIA
MŰSZAKI FIZIKAI és ANYAGTUDOMÁNYI KUTATÓINTÉZET

HUNGARIAN ACADEMY OF SCIENCES

RESEARCH INSTITUTE FOR TECHNICAL PHYSICS AND MATERIALS SCIENCE

AKKREDITÁLT VIZSGÁLÓLABORATÓRIUM MÉRÉSI SZOLGÁLTATÁSA

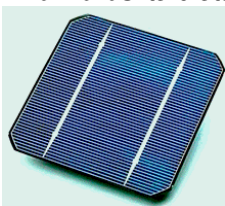
<http://www.ellipszometria.hu/>

Az MTA Műszaki Fizikai és Anyagtudományi Kutatóintézet több évtizedes tapasztalattal rendelkezik anyagok vizsgálata és minősítése terén. Az ellipszometria olyan polarizációs optikai módszer, amely alkalmas mikrométernél vékonyabb rétegek vastagságának nanométeres pontosságú roncsolásmentes mérésére, valamint a réteg törésmutatójának, és számos, a törésmutatótól függő tulajdonságának (pl. kristályosság, homogenitás) meghatározására.

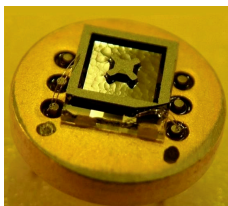
Az MFA Ellipszometria Laboratórium a Nemzeti Akkreditáló Testület által akkreditált, az ISO 17025 szabvány szerint működő mérőlabor. A laboratórium tagja az ANNA konzorciumnak (<http://www.i3-anna.org/>) amely széles körben kínál nanotechnológiához hozzáférhető vizsgálati módszereket.



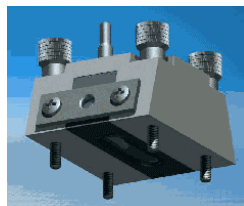
Alkalmazási területek:



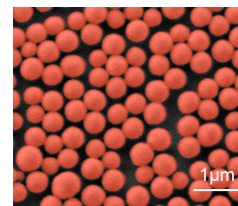
Napelemtechnológia



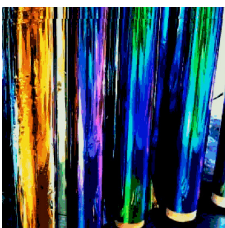
Szenzorikai rétegek



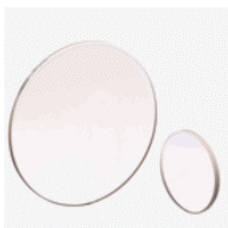
Bioszenzorika



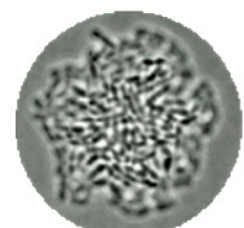
Felületi nanostruktúrák



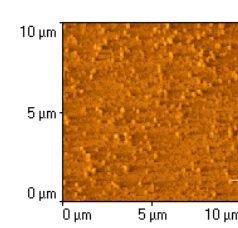
Bevonatok



Felületminőség



Biológiai vékonyrétegek



Nanoérdesség

A legfontosabb minősíthető mintatulajdonságok:

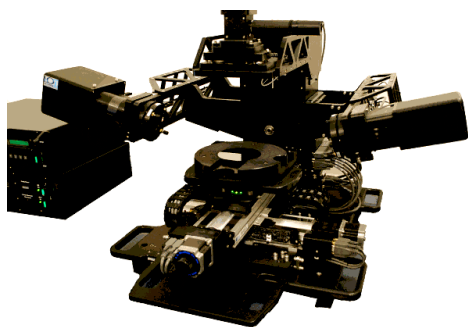
- rétegvastagság (0.5-1000 nm);
- optikai törésmutató (pontosság: ~0.001);
- homogenitás,
- határfelületek minősége;
- porozitás (pl. pórusos rétegben az üregtartalom);
- felületi nanoérdesség;
- réteg-összetétel bizonyos esetekben (pl. Si nanoszemcse tartalom szilíciumdioxidban);
- kristályosság (egykristályos anyagok rácsrendezetlensége, roncsoltsága).

Visitors: Konkoly-Thege M. út 29-33, BUDAPEST, 1121 HUNGARY, **Mail:** P.O. Box 49., H-1525, **Web:** <http://www.mfa.kfki.hu>
Phone, Director: +36-1-392 2224, **Phone, Administration:** +36-1-392 2227, **Fax:** +36-1-392 2226



MAGYAR TUDOMÁNYOS AKADÉMIA
MŰSZAKI FIZIKAI és ANYAGTUDOMÁNYI KUTATÓINTÉZET
 HUNGARIAN ACADEMY OF SCIENCES
RESEARCH INSTITUTE FOR TECHNICAL PHYSICS AND MATERIALS SCIENCE

A mérőberendezés (számítógépvezérelt spektroszkópiai ellipszométer) műszaki adatai:



- Gyártó és típus: Woollam M-2000DI
- Hullámhossztartomány: 192-1690 nm
- Érzékenység: 0.1-5.0 nm (nagyon függ a mintától)
- Maximális mintaméret: 200 mm x 200 mm
- Minimális mintaméret: 5 mm x 3 mm
- Térképezhető felület: 150 mm x 150 mm
- Mérhető minta: **1 mikronnál vékonyabb optikai minőségű vékonyrétegek** (a határfelületek érdessége/hullámossága néhányszor 10 nm-nél kisebb legyen; általában a ránézésre nem fényes, matt felület nem mérhető)

Jegyzőkönyv

A mintaminősítésről a Labor ISO 17025 szabvány szerinti jegyzőkönyvet állít ki.

A jegyzőkönyv tartalmazza:

- (1) a minta leírását;
- (2) a mérési körülmények részletes leírását;
- (3) a mért spektrumokat;
- (4) a kiértékelés során alkalmazott optikai modellek kidolgozásának lépéseit;
- (5) a paraméterillesztések részleteit;
- (6) a meghatározott rétegtulajdonságokat.

A mérési szolgáltatás ára

Az ellipszometriában a kiértékelés munkaigénye nagyságrendekkel nagyobb, mint a mérés. A kiértékelés komplexitása nagyban függ a mintától. A mérés tartalmazza a berendezés kalibrációjának ellenőrzését, referenciamérést etalonmintán, a spektrumok felvételét, az optikai modell kidolgozását, a mérések kiértékelését és dokumentálását, a hivatalos jegyzőkönyv elkészítését. Az ár nem tartalmazza a minta szállítási költségeit. A minimálisan elszámolandó egység egy munkanap.

A mérés+kiértékelés díja munkanaponként: 73000 Ft+ÁFA.

Az alábbi speciális (mikroelektronikai minőségű) minták esetében az egy munkanap alatt megmérhető minták száma:

- termikusan oxidált Si: 10 minta
- leválasztott dielektrikum rétegek (a törésmutató meghatározásával): 5 minta

Nagyobb mennyiség és speciális igények esetén az munkadíj egyedi megállapodás tárgya. A laboratórium egy *díjmentes próbamérés* alapján fenntartja magának a jogot annak eldöntésére, hogy a minta vizsgálható-e.

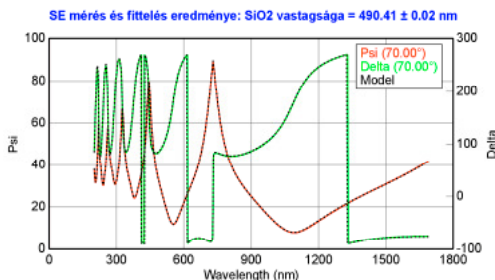
További információ, előzetes műszaki egyeztetés:

Dr. Petrik Péter, laborvezető

petrik@mfa.kfki.hu

+36-1-392-2222/1693

Visitors: Konkoly-Thege M. út 29-33, BUDAPEST, 1121 HUNGARY, Mail: P.O. Box 49., H-1525, Web: <http://www.mfa.kfki.hu>
 Phone, Director: +36-1-392 2224, Phone, Administration: +36-1-392 2227, Fax: +36-1-392 2226



MFA Publications in 2010

1. **Abo S**, Kumano S, Murakami K, Wakaya F, Lohner T, Takai M: "Study on time resolution of single event TOF-RBS measurement", *Nuclear Instruments & Methods in Physics Research Section B-Beam Interactions with Materials and Atoms* 268: pp. 2019-2022. (2010)
2. **Alomari M**, Chuvilin A, Toth L, Pécz B, Carlin JF, Grandjean N, Gaquire C, Forte-Poisson MA di, Delage S, Kohn E: "Thermal oxidation of lattice matched InAlN/GaN heterostructures", *Physica Status Solidi C-Conferences and Critical Reviews* 7:(1) pp. 13-16. (2010)
3. **Alvarez-Quintana J**, Peralba-Garcia L, Labar JL, Rodriguez-Viejo J: "Ultra-Low Thermal Conductivity in Nanoscale Layered Oxides", *Journal of Heat Transfer-Transactions of the ASME* 132:(3) Paper 032402. (2010)
4. **Ansari Farahnaz**, Kavosh Masoud, Horváth R, Ramsden Jeremy: "Particle speciation during PEG-Fe₃O₄ hybrid nanoparticle self-assembly on Si(Ti)O₂", *Journal of Nanoparticle Research* pp. 1-6. (2010)
5. **Attolini G**, Bosi M, Rossi F, Watts B E, Salviati G, Battistig G, Dobos L, Pécz B: "SiC epitaxial growth on Si(100) substrates using Carbon tetrabromide", *Materials Science Forum* 645-648: pp. 139-142. (2010)
6. **Bajáki Á**, Lábár J, Csanády Á, Geszti O, Hargitai H, Kármán FH: "Investigation of noble metal nanoparticles (Ag, Au, Pd, Pt) produced by chemical reduction", *Materials Science Forum* 659: pp. 115-120. (2010)
7. **Balázi C**, Timár I, Verdes S, Bálint A, Horváth P, Borbély T, Lisztes I: "Preparation and examination of nanostructured steel powders", In: *Fascicle of Management and Technological Engineering: Annals of Faculty Engineering Hunedoara. Nagyvárad, Románia, 2010-2010., Nagyvárad: pp. 3.16-3.23.*
8. **Balázi C**: "Development of Multifunctional Silicon Nitride Based Nanocomposites", *Materials Science Forum* 659: pp. 121-126. (2010)
9. **Balázi C**: "Nanosized Hexagonal Tungsten Oxide Based Sensors Prepared by Sol-Gel Method", *Sensor Letters* 8: pp. 694-697. (2010)
10. **Bálint Zs**, Kertész K, Wojtusiak J: "Notes on the high Andean cloud forest butterfly genus Jagiello and its relatives with description of a new species from Peru (Lepidoptera: Lycaenidae)", *Annales Historico-Naturales Musei Nationalis Hungarici - A Magyar Természettudományi Múzeum Évkönyve* 102: pp. 119-142. (2010)
11. **Bálint Zs**, Wojtusiak J, Kertész K, Piszter G, Biró LP: "Spectroboard: an instrument for measuring spectral characteristics of butterfly wings – a new tool for taxonomists", *Genus-International Journal of Invertebrate Taxonomy* 21: pp. 163-168. (2010)
12. **Bányász I**, Berneschi S, Khanh NQ, Lohner T, Fried M, Petrik P, Zolnai Z, Lengyel K, Péter Á, Watterich A, Nunzi-Conti G, Pelli S, Righini GC: "Structural and functional characterisation of slab waveguides written in Er³⁺ - doped tellurite glass, CaF₂, Bi₄(GeO₄)₃ and Bi₁₂GeO₂₀ crystals via implantation of MeV N⁺ ion", *Materials Science and Engineering* 15: Paper 012027. (2010)

13. **Bányász I**, Berneschi S, Lohner T, Fried M, Petrik P, Khanh NQ, Zolnai Z, Watterich A, Bettinelli M, Brenci M, Nunzi-Conti G, Pelli S, Righini GC, Speghini A: "Characterisation of slab waveguides, fabricated in CaF_2 and Er-doped tungsten-tellurite glass by MeV energy N^+ ion implantation, using spectroscopic ellipsometry and m-line spectroscopy", In: *Righini GC, Honkanen S, Jalali B, Pavesi L, Vivien L (Eds.), Silicon Photonics and Photonic Integrated Circuits: SPIE 7719., Bellingham: p. 77190G.*
14. **Beke D**, Pongrácz A, Battistig A, Josepovits K, Pécz B: "Selective Growth of Nanocrystalline 3C-SiC Thin Films on Si", In: *E-MRS 2010 Conference, Symposium F: Wide bandgap cubic Semiconductors: from growth to devices. Strasbourg, France, 2010.11.01, pp. 23-26.*
15. **Benedek Á**: "Nyári iskola az MTA MFA-ban: Bevonatok és rácsok – szilika az aranyon", *Élet és Tudomány, LXV. évf. 39. szám, 2010.09.24. pp.1226-1227*
16. **Benkó T**, Beck A, Geszti O, Katona R, Tugler A, Frey K, Gucci L, Schay Z: "Selective oxidation of glucose versus CO oxidation over supported gold catalysis", *Applied Catalysis A-General 388:(1-2) pp. 31-36. (2010)*
17. **Biró LP**, Kertész K, Horváth E, Márk GI, Molnár G, Vértesy Z, Tsai JF, Kun A, Bálint Zs, Vigneron JP: "Bioinspired artificial photonic nanoarchitecture using the elytron of the beetle *Trigonophorus rothschildi* varians as a "blueprint"", *Journal of the Royal Society Interface 7:(47) pp. 887-894. Paper doi:10.1098/rsif.2009.0438. (2010)*
18. **Biró LP**, Lambin P: "Nanopatterning of graphene with crystallographic orientation control", *Carbon 48:(10) pp. 2677-2689. (2010)*
19. **Biró LP**: "A karámba zárt atomoktól a DNS-ből „ácsolt” 3D szerkezetekig", *Természet Világa 141: pp. 434-436. (2010)*
20. **Biró LP**: "Photonic nanoarchitectures of biologic origin in butterflies and beetles", *Materials Science and Engineering B 169:(1-3) pp. 3-11. (2010)*
21. **Blum I**, Portavoce A, Mangelinck D, Bernardini J, Hoummada K, Daineche R, Lábár JL, Carron V: "Simultaneous Measurements of Lattice and Grain Boundary Diffusion Coefficients via 2-Dimensional Simulations", *Defect and Diffusion Forum 297-301: pp. 978-983. (2010)*
22. **Blum I**, Portavoce A, Mangelinck D, Daineche R, Hoummada K, Lábár JL, Carron V, Bernardini J: "Measurement of As diffusivity in Ni_2Si thin films", *Microelectronic Engineering 87:(3) pp. 263-266. (2010)*
23. **Broitman E**, Czigány Z, Greczynski G, Bohlmark J, Cremer R, Hultman L: "Industrial-scale deposition of highly adherent CNx films on steel substrates", *Surface & Coatings Technology 204:(21-22) pp. 3349-3357. (2010)*
24. **Czakó G**, Juhász Z: "Beljebb a magyar észjárásba", *Budapest: 2010. 320 p.*
25. **Czigány Z**, Hultman L: "Interpretation of electron diffraction patterns from amorphous and fullerene-like Carbon allotropes", *Ultramicroscopy 110:(7) pp. 815-819. (2010)*
26. **Csaba K**, Kiss G, Torocsik B, Labar JL, Gerencser AA, Mandi M, Adam-Vizi V, Chinopoulos C: "Mitochondria from *Artemia franciscana* embryos exhibit a truncated form of ant, associated with atypical effects of its ligands on Ca^{2+} uptake capacity and unique morphology of matrix Ca^{2+} precipitates", *Biochimica et Biophysica Acta-Bioenergetics 1797: pp. 142-143. (2010)*

27. **Detrich A**, Deák A, Hild E, Kovács A, Hórvölgyi Z: "Langmuir and Langmuir-Blodgett Films of Bidisperse Silica Nanoparticles", *Langmuir* 26:(4) pp. 2694-2699. (2010)
28. **Dimopoulos T**, Radnóczy GZ, Pécz B, Brückl H: "Characterization of ZnO:Al/Au/ZnO:Al trilayers for high performance transparent conducting electrodes", *Thin Solid Films* 519:(4) pp. 1470-1474. (2010)
29. **Dobos L**, Pécz B, Tóth L, Horváth ZsJ, Horváth ZE, Horváth E, Tóth AL, Beaumont B, Bougrioua Z: "Al and Ti/Al contacts on n-GaN", *Vacuum* 84:(1) pp. 228-230. (2010)
30. **Dobrik G**, Tapasztó L, Nemes-Incze P, Lambin P, Biró LP: "Crystallographically oriented high resolution lithography of graphene nanoribbons by STM lithography", *Physica Status Solidi B-Basic Solid State Physics* 247:(4) pp. 896-902. (2010)
31. **Fekete Z**, B Sinkovics, I Rajta, G A B Gál, Fűrjes P: "Characterization of the end-of-range geometric effects in complex 3D silicon micro-components formed by proton beam writing", *Journal of Micromechanics and Microengineering* 20: p. 064015. Paper 064015. (2010)
32. **Fekete Z**, Fűrjes P, Kárpáti T, Gál G A B, Rajta I: "MEMS-compatible hard coating technique of moveable 3D silicon microstructures", *Materials Science Forum* 659: pp. 147-152. (2010)
33. **Ferenc K**: "Nyári iskola az MTA MFA-ban: Hogyan lesz a tojásból műcsont?", *Élet és Tudomány*, LXV. évf. 37. szám, 2010.09.10. pp.1174-1176
34. **Frigeri C**, Nasi L, Serényi M, Csik A, Erdélyi Z, Beke DL: "Influence of Hydrogen on the Structural Stability of Annealed Ultrathin Si/Ge Amorphous Layers", *Solid State Phenomena* 156-158: pp. 325-330. (2010)
35. **Gago R**, Vinnichenko M, Redondo-Cubero A, Czigány Z, Vazquez L: "Surface Morphology of Heterogeneous Nanocrystalline Rutile/Amorphous Anatase TiO₂ Films Grown by Reactive Pulsed Magnetron Sputtering", *Plasma Processes and Polymers* 7:(9-10) pp. 813-823. (2010)
36. **Galkin NG**, Dózsa L, Chusovitin EA, Pécz B, Dobos L: "Migration of CrSi₂ nanocrystals through nanopipes in the silicon cap", *Applied Surface Science* 256:(23) pp. 7331-7334. (2010)
37. **Gergely G**, Gurban S, Menyhard M, Jablonski A, Zommer L, Goto K: "The inelastic mean free path of electrons. Past and present research", *Vacuum* 84:(1) pp. 134-136. (2010)
38. **Gergely G**, Lukács IE, Tóth M, Illés L, Wéber F, Balázs C: "Hydroxyapatite – biopolymer mats by electrospinning", In: *Janos Vörös, Marcus Textor (Eds.), European Cells and Materials: 3rd International NanoBio Conference 2010. Zürich, Svájc, 2010.08.24-2010.08.27., Davos: p. 9.*
39. **Gergely G**, Lukács IE, Tóth M, Illés L, Wéber F, Tóth AL, Balázs C: "Production of hydroxyapatite- biopolymer mats by electrospinning", In: *Kollár LP, Czigány T, Karger-Kocsis J (Eds.), Proc. of the 14th European Conference on Composite Materials. Budapest, Hungary, 2010.06.07-2010.06.10., pp. 1-6.*
40. **Gergely G**, Weber F, Lukacs I, Illés L, Tóth AL, Horváth ZE, Mihály J, Balázs C: "Nano-hydroxyapatite preparation from biogenic raw materials", *Central European Journal of Chemistry* 8:(2) pp. 375-381. (2010)

41. **Gergely G**, Wéber F, Lukács I, Tóth A L, Horváth ZE, Mihály J, Balázs C: "Preparation and characterization of hydroxyapatite from eggshell", *Ceramics International* 36:(2) pp. 803-806. (2010)
42. **Gergely G**, Wéber F, Tóth M, Tóth AL, Horváth ZE, Balázs C: "Processing of nano hydroxyapatite from eggshell and seashell", *Materials Science Forum* 659: pp. 159-164. (2010)
43. **Gouma PI**, Ramachandran K, Firat M, Connolly M, Zuckermann R, Balazsi Cs, Perrotta PL, Xue R: "Novel bioceramics for bone implants", 30:(6) pp. 35-44. (2010)
44. **Grand L**, Pongrácz A, Vázsonyi É, Márton G, Gubán D, Battistig G, Karmos Gy, Ulbert I: "A novel multisite silicon probe fabricated by using an economical wet etching process for high quality laminar neural recordings", In: *IBRO Workshop. Pécs, Hungary, 2010.01.21-2010.01.23.*, pp. P7-11.
45. **Gubicza J**, Chinh N Q, Lábár JL, Hegedűs Z, Langdon TG: "Principles of self-annealing in silver processed by equal-channel angular pressing: The significance of a very low stacking fault energy", *Materials Science and Engineering A-Structural Materials Properties Microstructure and Processing* 527 : pp. 752-760. (2010)
46. **Gubicza J**, Chinh N Q, Lábár JL, Hegedűs Z, Langdon TG: "Unique features of ultrafine-grained microstructures in materials having low stacking fault energy", *Materials Science Forum* 659: pp. 171-176. (2010)
47. **Gubicza J**, Máthis K, Hegedűs Z, Ribárik G, Tóth AL: "Inhomogeneous evolution of microstructure in AZ91 Mg-alloy during high temperature Equal-Channel Angular Pressing", *Journal of Alloys and Compounds* 492: pp. 166-172. (2010)
48. **Gucz L**, Stefler G, Geszti O, Sajo I, Paszti Z, Tompos A, Schay Z: "Methane dry reforming with CO₂: A study on surface Carbon species", *Applied Catalysis A-General* 375:(2) pp. 236-246. (2010)
49. **Gyurcsányi RE**, Höfler L, Jággerszki Gy, Makra IT, Tóth AL, Fekete Z, Gubán D, I Bársony, Fűrjes P: "Chemically modified solid-state single gold nanopores for biochemical sensing.", In: *Proceedings of E-MRS 2010 Conference, Symposium B 10. Strasbourg, France, 2010*, p. 27.
50. **Gyurcsányi RE**, Höfler L, Varga T, Gojame S, Takács Á, Lautner G, Jággerszki Gy, Makra IT, Tóth AL, Fekete Z, Gubán D, Fűrjes P: "Chemically modified solid-state gold nanopores for biochemical sensing", In: *Proceedings of BIOSENSORS 2010 Conference. Glasgow, UK, 2010*, p. P2.1.025.
51. **Helbing D**, Szolnoki A, Perc M, Szabó G: "Defector-accelerated cooperativeness and punishment in public goods games with mutations", *Physical Review E-Statistical, Nonlinear and Soft Matter Physics* 81:(5) p. 057104. (2010)
52. **Helbing D**, Szolnoki A, Perc M, Szabó G: "Evolutionary Establishment of Moral and Double Moral Standards through Spatial Interactions", *Plos Computational Biology* 6:(4) p. e1000758. (2010)
53. **Helbing D**, Szolnoki A, Perc M, Szabó G: "Punish, but not too hard: how costly punishment spreads in the spatial public goods game", *New Journal of Physics* 12:(8) p. 083005. (2010)

54. **Henits P**, Kovács Zs, Schafler E, Varga LK, Lábár JL, Révész Á: "Nanocrystallization in $\text{Al}_{85}\text{Ce}_8\text{Ni}_5\text{Co}_2$ amorphous alloy obtained by different strain rate during high pressure torsion", *Journal of Alloys and Compounds 504S*: pp. S91-S94. (2010)
55. **Henits P**, Revesz A, Schafler E, Szabo PJ, Labar JL, Varga LK, Kovacs Z: "Correlation between microstructural evolution during high-pressure torsion and isothermal heat treatment of amorphous $\text{Al}_{85}\text{Gd}_8\text{Ni}_5\text{Co}_2$ alloy", *Journal of Materials Research 25*:(7) pp. 1388-1397. (2010)
56. **Hoglund C**, Alling B, Birch J, Beckers M, Persson POA, Baehtz C, Czigány Z, Jensen J, Hultman L: "Effects of volume mismatch and electronic structure on the decomposition of ScAlN and TiAlN solid solutions", *Physical Review B-Condensed Matter and Materials Physics 81*:(22) Paper 224101. (2010)
57. **Hoglund C**, Birch J, Alling B, Bareno J, Czigány Z, Persson POA, Wingqvist G, Zukauskaitė A, Hultman L: "Wurtzite structure $\text{Sc}_{1-x}\text{Al}_x\text{N}$ solid solution films grown by reactive magnetron sputter epitaxy: Structural characterization and first-principles calculations", *Journal of Applied Physics 107*:(12) Paper 123515. (2010)
58. **Holec D**, Rovere F, Mayrhofer PH, Barna PB: "Pressure dependent stability of cubic and wurtzite phases within the TiN-AlN and CrN-AlN systems", *Scripta Materialia 62*:(6) pp. 349-352. (2010)
59. **Horváth ZsJ**, Basa P, Pap AE, Molnar Gy, Kovalev AI, Wainstein DL, Gerlai T, Turmezei P: "Silicon nitride based non-volatile memory structures with embedded Si or Ge nanocrystals", In: *Communications – Scientific Letters of the University of Zilina. Zilina, Slovakia, 2010*, pp. 19-21.
60. **Horváth ZsJ**, Basa P: "Chapter 7. Nanocrystal memory structures", In: *T V Torchinskaya, Yu V Vorobiev (Eds.), Nanocrystals and Quantum Dots of Group IV Semiconductors, Stevenson Ranch: American Scientific Publishers, 2010*. pp. 225-251., Stevenson Ranch, California, USA, ISBN: 1-58883-154-X
61. **Horváth ZsJ**, L Dobos, B Beaumont, Z Bougrioua, Pécz B: "Electrical behaviour of lateral Al/n-GaN/Al structures", *Applied Surface Science 256*: pp. 5614-5617. (2010)
62. **Iablokov V**, Frey K, Geszti O, Kruse N: "High Catalytic Activity in CO Oxidation over MnOx Nanocrystals", *Catalysis Letters 134*:(3-4) pp. 210-216. (2010)
63. **Ievtushenko AI**, Lashkarev GV, Lazorenko VI, Karpyna VA, Dusheyko MG, Tkach VM, Kosyachenko LA, Sklyarchuk VM, Sklyarchuk OF, Avramenko KA, Strelchuk VV, Horváth ZsJ: "Effect of nitrogen doping on photoresponsivity of ZnO films", *Physica Status Solidi A-Applications and Materials Science 207*: pp. 1746-1750. (2010)
64. **Juhász Z**, Sipos J: "A Comparative Analysis of Eurasian Folksong Corpora, Using Self Organising Maps", *Journal of Interdisciplinary Music Studies 4*:(1) pp. 1-16. (2010)
65. **Juhász Z**: "Classification and Comparison of Different Folk Music Traditions Using Self Learning Algorithms", In: *Hart G W, Saranghi R (Eds.), Proc. of the 13. Annual Bridges Conference, Pécs, Hungary, 2010.07.22-2010.07.28.*, pp. 487-490.
66. **Juhász Z**: "Identification of musical language groups using artificial intelligences", In: *(Eds. G. Lugosi and D. Nagy), Special Issues for the 8th Interdisciplinary Symmetry Festival-Congress of ISIS-symmetry, Austria, 2010.08.23-2010.08.28.*, pp. 116-119.
67. **Juhász Z**: "Motive Identification in 22 Folksong Corpora Using Dynamic Time Warping and Self Organising Maps", *Hirata, Kazantzakis (Eds.), Proceedings of the 10th*



- International Society for Music Information Retrieval Conference. Kobe, Japan, 2009.10.26-2010.10.30., Kobe: pp. 171-176.*
68. **Klein Á**, Jankovics H, Tóth B, Muskotál A, Vonderviszt F: "Flagellin-GFP fúziós fehérje előállítás és jellemzése", In: *Műszaki Kémiai Napok 2010. Veszprém, Hungary, 2010.04.27-2010.04.29., pp. 106-109.*
 69. **Koncz P**, Horváth A, Wéber F, Petrik A, Balázi C: "Diszpergált oxidkerámia szemcsékkel erősített nanoszerkezetű acélok: előállítás és szerkezeti tulajdonságok", *Anyagvizsgálók Lapja 20:(4) pp. 121-128. (2010)*
 70. **Kozma P**, Fodor B, Deak A, Petrik P: "Optical models for the characterization of silica nanosphere monolayers prepared by the Langmuir-Blodgett method using ellipsometry in the quasistatic regime", *Langmuir 26:(20) pp. 16122-16128. (2010)*
 71. **Krauss B**, Nemes-Incze P, Skakalova V, Biró LP, von Klitzing K, Smet JH: "Raman Scattering at Pure Graphene Zigzag Edges", *Nano Letters 10:(11) pp. 4544-4548. (2010)*
 72. **Kucsera P**, Tényi VG, Nemcsics Á, Réti I: "Control of the MBE equipment for growth of nano structures", *8th IEEE International Symposium on Intelligent Systems and Informatics, SIISY 2010., In: SIISY 2010 - 8th IEEE International Symposium on Intelligent Systems and Informatics. Subotica, Szerbia, 2010.09.10-2010.09.11., pp. 659-661., (8th IEEE International Symposium on Intelligent Systems and Informatics, SIISY 2010)(ISBN:9781424473946)*
 73. **Kun P**, Wéber F, Illés L, Horváth ZE, Arató P, Balázi C: "Grafít nanorétegek előállítása és vizsgálata - úton az új típusú szén erősítésű nanokompozitok felé", *Anyagvizsgálók Lapja 20:(3) pp. 70-76. (2010)*
 74. **Kurunczi S**, Németh A, Hülber T, Kozma P, Petrik P, Jankovics H, Sebestyén A, Vonderviszt F, Fried M, Bársony I: "In situ ellipsometric study of surface immobilization of flagellar filaments", *Applied Surface Science 257: pp. 319-324. (2010)*
 75. **Kúsz Á**: "Nyári iskola az MTA MFA-ban: Bevonatok és rácsok – Optikai rács holográfiával", *Élet és Tudomány, LXV. évf. 39. szám, 2010.09.24. pp.1226-1227*
 76. **Lamperti A**, Radnóczy G, Caricato AP, Trautmann C, Ossi PM: "Structural Modifications Induced by Swift Heavy Ions in Thin Films of Yttria Fully Stabilised Zirconia", *Nuclear Instruments & Methods B B268: pp. 3132-3136. (2010)*
 77. **Márton G**, Grand L, Pongrácz A, Vazsonyi E, Ulbert I, Guban D, Karmos Gy, Battistig G: "Neural signal recording by Carbon nanotube covered multisite silicon probe", In: *E-MRS 2010 Conference, Symposium B: Functional biointerfaces. Strasbourg, France, 2010, Paper B91.*
 78. **Márton G**, Pongrácz A, Grand L, Vazsonyi E, Ulbert I, Karmos G, Battistig G: "A novel multisite silicon probe for laminar neural recordings with improved electrode impedance", In: *Proceedings of the 21st Micromechanics and Micro systems Europe Workshop. Enschede, Netherlands, 2010.09.26-2010.09.29., pp. 201-203.*
 79. **Mayer I**, Pető G, Karacs A, Molnár G, Popov I: "Divalent Mn in calcium hydroxyapatite by pulse laser deposition", *Journal of Inorganic Biochemistry 104:(10) pp. 1107-1111. (2010)*
 80. **Mészáros I**, Vértessy G: "Modeling of normal magnetization curves of soft magnetic alloys", *Materials Science Forum 322: pp. 429-434. (2010)*
 81. **Misják F**, Barna PB, Radnóczy G: "Growth of nanocomposite in eutectic Cu-Ag films", *Thin Solid Films 516: pp. 3931-3934. (2010)*

82. **Misják F**, Barna PB, Radnóczy G: "Growth of nanocomposite in eutectic Cu–Ag films", *Thin Solid Films* 518:(15) pp. 4247-4251. (2010)
83. **Mizsei J**, Pap AE, Gillemot K, Battistig G: "Effect of deuterium on passivation of Si surfaces", *Applied Surface Science* 256: pp. 5765-5770. (2010)
84. **Munoz MA**, Juhasz R, Castellano C, Ódor G: "Griffiths Phases on Complex Networks", *Physical Review Letters* 105:(12) pp. 128701-1-128701-4. Paper 128701. (2010)
85. **Muskotál A**, Seregélyes Cs, Sebestyén A, Vonderviszt F: "Structural basis for stabilization of the hypervariable D3 domain of Salmonella flagellin upon filament formation", *Journal of Molecular Biology* 403: pp. 607-615. (2010)
86. **Nagata T**, Volk J, Haemori M, Yamashita Y, Yoshikawa H, Hayakawa R, Yoshitake M, Ueda S, Kobayashi K, Chikyow T: "Schottky barrier height behavior of Pt–Ru alloy contacts on single-crystal n-ZnO", *Journal of Applied Physics* 107: pp. 103714-1-103714-6. (2010)
87. **Nagy AK**, Pfeifer J, Lukács IE, Tóth AL, Balázsi C: "A Candidate for Fabrication of Semiconducting Tungsten Oxide Nanofibers", *Materials Science Forum* 659: pp. 215-219. (2010)
88. **Neidhardt J**, Czigány Z, Sartory B, Tessadri R, Mitterer C: "Wear-resistant Ti-B-N nanocomposite coatings synthesized by reactive cathodic arc evaporation", *International Journal of Refractory Metals & Hard Materials* 28:(1) pp. 23-31. (2010)
89. **Nemcsics Á**, Csutorás M, Tényi VG, Sándor T: "Real time RHEED evaluation with the help of image processing", *8th IEEE International Symposium on Intelligent Systems and Informatics, SIISY 2010.*, In: *SIISY 2010 - 8th IEEE International Symposium on Intelligent Systems and Informatics. Subotica, Slovakia, 2010.09.10-2010.09.11.*, pp. 631-633., (ISBN:9781424473946)
90. **Nemcsics Á**, Réti I, Tényi VG, Kucsera P, Tóth L, Harmat P, Mieville Amadou, Csutorás M, Kupás-Deák B, Sándor T, Bozsik J: "Molekulasugár-epitaxiás nanostruktúrák előállításának műszaki feltételei", *GÉP* 61:(8) pp. 29-32. (2010)
91. **Nemcsics Á**, Takács J, Bozsik J: "Modelling hysteretic phenomena in surface science", *8th IEEE International Symposium on Intelligent Systems and Informatics, SIISY 2010.*, In: *SIISY 2010 - 8th IEEE International Symposium on Intelligent Systems and Informatics. Subotica, Slovakia, 2010.09.10-2010.09.11.*, pp. 389-392. (ISBN:9781424473946)
92. **Nemcsics Á**, Takács J: "Modelling of the hysteretic phenomena in RHEED intensity variation versus temperature for GaAs and InAs surfaces", *Semiconductors* 45: pp. 93-96. (2010)
93. **Nemcsics Á**, Toth L, Dobos L, Heyn C, Stemmann A, Schramm A, Welsch H, Hansen W: "Composition of the "GaAs" quantum dot, grown by droplet epitaxy", *Superlattices and Microstructures* 48:(4) pp. 351-357. (2010)
94. **Nemcsics Á**: "A földből való építkezés néhány aspektusa", *Magyar Építőipar* 60:(3) pp. 103-108. (2010)
95. **Nemcsics Á**: "Adalékok a középkori építéstechnológiához egy Árpád-kori körtemplom rekonstrukciója kapcsán", *Magyar Építőipar* 60:(2) pp. 61-69. (2010)
96. **Nemcsics Á**: "Adalékok a középkori kerektemplomaink eredetéhez", *Magyar Építőipar* 60:(4) pp. 139-144. (2010)



97. **Nemes-Incze P**, Magda G, Kamarás K, Biró LP: "Crystallographic orientation dependent etching of graphene layers", *Physica Status Solidi C-Conferences and Critical Reviews* 7: pp. 1241-1245. (2010)
98. **Nemes-Incze P**, Magda G, Kamaras K, Biró LP: "Crystallographically selective nanopatterning of graphene on SiO₂", *Nano Research* 3:(2) pp. 110-116. (2010)
99. **Nemeth A**, Kozma P, Hulber T, Kurunczi S, Horváth R, Petrik P, Muskotal A, Vonderviszt F, Hos C, Fried M, Gyulai J, Barsony I: "In Situ Spectroscopic Ellipsometry Study of Protein Immobilization on Different Substrates Using Liquid Cells", *Sensor Letters* 8:(5) pp. 730-735. (2010)
100. **Neumann PL**, Horváth ZE, Nemes-Incze P, Molnár G, Vértesy G, Biró LP: "Electrical behavior of indium contacted graphene flakes", *Nanopages* 5: (2010)
101. **Ódor G**, Liedke B, Heinig KH: "Directed d-mer diffusion describing the Kardar-Parisi-Zhang-type surface growth", *Physical Review E-Statistical, Nonlinear and Soft Matter Physics* 81:(4) Paper 049903. (2010)
102. **Ódor G**, Liedke B, Heinig KH: "Surface pattern formation and scaling described by conserved lattice gases", *Physical Review E-Statistical, Nonlinear and Soft Matter Physics* 81:(5) Paper 051114. (2010)
103. **Osherov A**, Makai JP, Balazs J, Horváth ZsJ, Gutman N, Sa'ar A, Golan Y: "Tunability of the optical band edge in thin PbS films chemically deposited on GaAs(100)", *Journal of Physics-Condensed Matter* 22: Paper 262002. (2010)
104. **Ostermaier C**, Pozzovivo G, Basnar B, Schrenk W, Carlin J-F, Gonschorek M, Grandjean N, Vincze A, Tóth L, Pécz B, Strasser G, Pogany D, Kuzmik J: "Characterization of Plasma-induced Damage of Selectively Recessed GaN/InAlN/AlN/GaN Heterostructures Using SiCl₄ and SF₆", *Japanese Journal of Applied Physics* 49:(11) Paper 116506. (2010)
105. **Ostermaier C**, Pozzovivo G, Basnar B, Schrenk W, Schmid M, Toth L, Pécz B, Carlin JF, Gonschorek M, Grandjean N, Strasser G, Pogany D, Kuzmik J: "Metal-related gate sinking due to interfacial oxygen layer in Ir/InAlN high electron mobility transistors", *Applied Physics Letters* 96:(26) Paper 263515. (2010)
106. **Otieno G**, Koos AA, Dillon F, Wallwork A, Grobert N, Todd RI: "Processing and properties of aligned multi-walled Carbon nanotube/aluminoborosilicate glass composites made by sol-gel processing", *Carbon* 48:(8) pp. 2212-2217. (2010)
107. **Pálfalvi JK**, Szabó J, Eördögh I: "Detection of high energy neutrons, protons and He particles by solid state nuclear track detector", *Radiation Measurements* 45: pp. 1568-1573. (2010)
108. **Pécz B**, Stoemenos J, Voelskow M, Skorupa W, Dobos L, Pongrcz A, Battistig G: "Ion implantation enhanced formation of 3C-SiC grains at the SiO₂/Si interface after annealing in CO gas", *Journal of Physics-Conference Series* 209:(1) Paper DOI: 10.1088/1742-6596/209/1/012045. (2010)
109. **Pécz B**, Tóth L, Barna Á, Tsiakatouras G, Ajagunna AO, Georgakilas A: "Microscopy of GaN grown on diamond", In: *Proc. HETECH. Crete, Greece, 2010.10.18-2010.10.20.*, pp. 19-20.
110. **Perc M**, Szolnoki A: "Coevolutionary games—A mini review", *Biosystems* 99:(2) pp. 109-125. (2010)

111. **Peter L**, Csik A, Vad K, Toth-Kadar E, Pekker A, Molnar G: "On the composition depth profile of electrodeposited Fe-Co-Ni alloys", *Electrochimica Acta* 55:(16) pp. 4734-4741. (2010)
112. **Pető G**, Daróczy CsS: "Photoelectric Properties of Ge-Mn Layer Induced by Mn ion Implantation onto Ge(100)", *MAX-lab Activity Report 2009, National Laboratory, Lund, Sweden*, (Eds: U. Johansson, A. Nyberg, R. Nyholm), *Synchrotron Radiation – BeamLine 41*, pp.88-89 (2010. June 24.)
113. **Pfeifer J**, Sáfrán G, Wéber F, Zsigmond V, Koszor O, Arató P, Balázsi C: "Tribology Study of Silicon Nitride-Based Nanocomposites with Carbon Additions", *Materials Science Forum* 659: pp. 235-238. (2010)
114. **Poupin C**, Pirault-Roy L, La Fontaine C, Tóth L, Chamam M, Wootsch A, Paál Z: "Promising PtIr, catalysts for hydroCarbon transformation: Comparison of different preparation methods", *272:(2) pp. 315-319. (2010)*
115. **Rakovics V**: "Optical investigation of InGaAsP/InP double heterostructure wafers", In: *Sukhoivanov I, Shulika O V (Eds.), Advanced Optoelectronics and Lasers (CAOL), 2010 International Conference on. Ukraine, 2010.09.10-2010.09.14., pp. 216-218.(ISBN:978-1-4244-7043-3)*
116. **Rossi S**, Alomari M, Dipalo M, Kohn E, Tóth L, Pécz B, di Forte-Poisson M-A, Delage S, Carlin J-F, Grandjean N: "Nanocrystalline Diamond overgrowth on GaN HEMTs", In: *Proc. HETECH. Crete, Greece, 2010.10.18-2010.10.20., pp. 4-5.*
117. **Schneider J**, Dore J, Christiansen S, Falk F, Lichtenstein N, Valk B, Lewandowska R, Slaoui A, Maeder X, Lábár J, Sáfrán G, Werner M, Naumann V, Hagendorf C: "Solar Cells from Crystalline Silicon on Glass Made by laser Crystallised Seed Layers and Subsequent Solid Phase Epitaxy", In: *25th European Photovoltaic Solar Energy Conference and Exhibition / 5th World Conference on Photovoltaic Energy Conversion. Valencia, Spain, 2010.09.06-2010.09.10., pp. 3573-3576.*
118. **Schulz H**, Ódor G, Ódor Gergely, Nagy FM: "Simulation of 1+1 dimensional surface growth and lattices gases using GPUs", *Comp. Phys. Comm., pp. 1-20., arXiv:1012.0385, (2010)*
119. **Simon A**: "Nyári iskola az MTA MFA-ban: Színes és acélkemény porok – Hegylakó az MFA-ban", *Élet és Tudomány, LXV. évf. 40. szám, 2010.10.01. pp.1262-1263*
120. **Sivakov VA**, Bronstrup G, Pécz B, Berger A, Radnoczi GZ, Krause M, Christiansen SH: "Realization of Vertical and Zigzag Single Crystalline Silicon Nanowire Architectures", *Journal of Physical Chemistry C-Nanomaterials and Interfaces* 114:(9) pp. 3798-3803. (2010)
121. **Süle P**: "Anomalous atomic transport in driven systems: ion-sputtering induced enhanced intermixing and cratering in Pt/Ti", *Nuclear Instruments & Methods in Physics Research Section B-Beam Interactions with Materials and Atoms* 268:(9) pp. 1404-1411. (2010)
122. **Szabó G**, Szolnoki A, Varga M, Hanusovszky L: "Ordering in spatial evolutionary games for pairwise collective strategy updates", *Physical Review E-Statistical, Nonlinear and Soft Matter Physics* 82:(2) p. 026110. (2010)
123. **Szabó G**, Szolnoki A, Vukov J: "Mechanisms Supporting Cooperation for the Evolutionary Prisoner's Dilemma Games", In: *Bandasu B, Chakravarty S R, Chakrabarti B K, Gangopadhyay K (Eds.), Econophysics and Economics of Games, Social Choices and*



- Quantitative Techniques.*, Milano: Springer Verlag, 2010. pp. 24-31., (New Economic Windows), (ISBN:978-88-470-1500-5)
124. **Szabó G**, Tomé T, Borsos I: "Probability currents and entropy production in nonequilibrium lattice systems", *Physical Review E-Statistical Physics, Plasmas, Fluids and Related Interdisciplinary Topics* 82: Paper 011105/1-8. (2010)
 125. **Szabó V**, Muskotál A, Jankovics H, Tóth B, Vonderviszt F: "Baeyer-Villiger monooxygenázok flagellinnel való fúziós konstrukcióinak előállítására", In: *Műszaki Kémiai Napok 2010. Veszprém, Hungary, 2010.04.27-2010.04.29.*, pp. 271-275.
 126. **Szekerés A**, Vlaikova E, Lohner T, Tóth AL, Lisovskyy IP, Lobin SO, Shepeliavyy PE: "Characterization of oblique deposited nanostructured SiO_x Films by ellipsometric and IR spectroscopies", *Solid State Phenomena* 159: pp. 149-152. (2010)
 127. **Szenes G**, Kovacs VK, Pécz B, Skuratov V: "The Effect of Heavy Cosmic-Ray Ions on Silicate Grains in the Interstellar Dust", *Astrophysical Journal* 708:(1) pp. 288-292. (2010)
 128. **Szentpáli B**, Basa P, Fürjes P, Battistig G, Bársony I, Károlyi G, Berceli T: "Millimeter wave detection by thermopile antenna", 5: pp. 564-567. (2010)
 129. **Szentpáli B**, Basa P, Fürjes P, Battistig G, Bársony I, Károlyi G, Berceli T, Rymanov V, Stöhr A: "Thermopile antennas for detection of millimeter waves", *Applied Physics Letters* 96: pp. 1-3. Paper 133507. (2010)
 130. **Szentpáli B**, Basa P, Fürjes P, Battistig G, Bársony I, Károlyi G, Berceli T: "Millimeter wave detection by thermopile antenna", In: *Euroensors XXIV. Linz, Austria, 2010.09.05-2010.09.08.*, pp. 1-4. Paper B3L-B-4.
 131. **Szentpáli B**, Basa P, Fürjes P, Battistig G, Bársony I: "Thermopile as THz Detector", In: *2nd IEEE International Workshop on THz Radiation: Basic Research & Applications, TERA'2010. Ukraine, 2010.09.12-2010.09.14.*, Lviv: pp. 275-277.
 132. **Szerencsi M**, Radnóczy G: "The mechanism of growth and decay of Carbon nano-onions formed by ordering of amorphous particles", *Vacuum* 84:(1) pp. 197-201. (2010)
 133. **Szilágyi IM**, Saukko S, Mizsei J, Tóth AL, Madarasz J, Pokol G: "Gas sensing selectivity of hexagonal and monoclinic WO₃ to H₂S", *Solid State Sciences* 12:(11) pp. 1857-1860. (2010)
 134. **Szocs DE**, Szilágyi E, Bogdán C, Kótai E, Horváth ZE: "Lithium concentration dependence of implanted helium retention in lithium silicates", *Nuclear Instruments & Methods in Physics Research Section B-Beam Interactions with Materials and Atoms* 268:(11-12) pp. 1857-1861. (2010)
 135. **Szolnoki A**, Perc M: "Impact of critical mass on the evolution of cooperation in spatial public goods games", *Physical Review E-Statistical, Nonlinear and Soft Matter Physics* 81:(5) p. 057101. (2010)
 136. **Szolnoki A**, Perc M: "Reward and cooperation in the spatial public goods game", *Europhysics Letters* 92:(3) p. 38003. (2010)
 137. **Szolnoki A**, Wang Z, Wang J, Zhu X: "Dynamically generated cyclic dominance in spatial prisoner's dilemma games", *Physical Review E-Statistical, Nonlinear and Soft Matter Physics* 82:(3) p. 036110. (2010)
 138. **Szűcs E**, Szokolczai K, Simonyi G, Bauernfeind T, Pinter A, Preda I, Medvegy M: "Diagnostic value of body surface potential mapping in assessment of the coronary artery

- lesion after angina pectoris and without repolarization changes on the electrocardiogram", *Journal of Electrocardiology* 43:(4) pp. 326-335. (2010)
139. **Tapasztó O**, Balázs C: "The effect of milling time on the sintering kinetics of Si₃N₄ based nanocomposites", *Ceramics International* 36:(7) pp. 2247-2251. (2010)
140. **Timár I**, Koncz P, Wéber F, Balázs C: "Structural properties of nano-steel powders prepared by powder metallurgy", In: *International symposium on Advanced Engineering and Applied Management – 40th Anniversary in Higher Education (1970-2010): Annals of Faculty Engineering Hunedoara, Romania, 2010.11.04-2010.11.05.*, pp. 73-76.
141. **Tóth AL**: "Elektronsugaras Mikroanalízis Restaurátoroknak (II) EMA", *ISIS-Erdélyi Magyar Restaurátor Füzetek* 10: pp. 9-15. (2010)
142. **Tóth L**, Barna Á, Pécz B, Alomari M, Dipalo M, Rossi S, Kohn E, di Forte-Poisson M-A, Delage S, Carlin J-F, Grandjean N: "Structure of diamond film grown over InAlN/GaN HEMT", In: *Proc. HETECH. Crete, Greece, 2010.10.18-2010.10.20.*, pp. 6-7.
143. **Tóth M**, Gergely G, Lukács IE, Wéber F, Tóth AL, Illés L, Balázs C: "Production of polymer nanofibers containing hydroxyapatite by electrospinning", *Materials Science Forum* 659: pp. 257-262. (2010)
144. **Tóth M**, Gergely G, Wéber F, Lukács IE, Tóth AL, Horváth ZE, Balázs C: "Nanoszerkezetű hidroxipatit-biopolimer kompozitok előállítás és vizsgálata", *Anyagvizsgálók Lapja* 20:(1) pp. 8-15. (2010)
145. **Tunyogi A**, Tancziko F, Bogdán C, Horváth ZE, Szilágyi E: "Characterisation of annealed Fe/Ag bilayers by RBS and XRD", *Nuclear Instruments & Methods in Physics Research Section B-Beam Interactions with Materials and Atoms* 268:(11-12) pp. 1972-1975. (2010)
146. **Tuza R**: "Nyári iskola az MTA MFA-ban: Színes és acélkemény porok – Szerkezeti színek a természetben", *Élet és Tudomány*, LXV. évf. 40. szám, 2010.10.01. pp.1262-1263
147. **Vértesy G**, Tomáš I, Kobayashi S: "Nondestructive evaluation of low Carbon steel by magnetic adaptive testing", *Nondestructive Testing and Evaluation* 25: pp. 125-132. (2010)
148. **Vértesy G**, Uchimoto T, Tomáš I, Takagi T: "Nondestructive characterization of ductile cast iron by Magnetic Adaptive Testing", *Journal of Magnetism and Magnetic Materials* 322: pp. 3117-3121. (2010)
149. **Vértesy G**, Uchimoto T, Tomáš I, Takagi T: "Nondestructive inspection of ductile cast iron by measurement of minor magnetic hysteresis loops", *Materials Science Forum* 659: pp. 355-360. (2010)
150. **Vértesy G**, Uchimoto T, Tomáš I, Takagi T: "Temperature dependence of magnetic descriptors of Magnetic Adaptive Testing", *IEEE Transactions on Magnetics* 46: pp. 509-512. (2010)
151. **Watts BE**, Bosi M, Attolini G, Battistig G, Dobos L, Pécz B: "CBr₄ as precursor for VPE growth of cubic silicon carbide", *Crystal Research and Technology* 45:(6) pp. 583-588. (2010)
152. **Weltsch Z**, Lovas A, Cziráki Á, Tichy G, Tóth AL: "Wetting Ability of Ag(Cu, Zn, Ga) alloys on graphite substrate", *International Journal of Applied Mechanics and Engineering* 15:(2) pp. 389-396. (2010)



153. **Yastrubchak O**, Domagala JZ, Sadowski J, Kulik M, Zuk J, Toth A, Szymczak R, Wosinski T: "Ion-Implantation Control of Ferromagnetism in (Ga,Mn)As Epitaxial Layers", *Journal of Electronic Materials* 39:(6) pp. 794-798. (2010)
154. **Yong TK**, Nee CH, Yap SS, Siew WO, Sáfrán G, Yap YK, Tou TY: "Pulsed laser deposition of nanostructured indium-tin-oxide films", In: *Proc. of SPIE-The International Society for Optical Engineering 7766: Paper 776615*. (2010)
155. **Zajzon N**, Márton E, Pethe M, Sipos P, Németh T, Kovács-Kis V, Uram J Zaharia L, Kis A, Topa B, Papp G, Wieszburg TG: "Mineralogical, magnetic and geochemical investigation of the seasonal PM10 dust fraction from Miskolc, Hungary", In: *20th General Meeting of the International Mineralogical Association (21-27 August 2010, Budapest, Hungary)*, *Acta Minerologica-Petrographica Abstract Series 6* (2010) p. 334.
156. **Zolnai Z**, Deák A, Nagy N, Tóth AL, Kótai E, Battistig G: "A 3D-RBS study of irradiation-induced deformation and masking properties of ordered colloidal nanoparticulate masks", *Nuclear Instruments & Methods in Physics Research Section B-Beam Interactions with Materials and Atoms* 268: pp. 79-86. (2010)
157. **Zommer L**, Jablonski A, Kotis L, Safran G, Menyhard M: "Simulation and measurement of AES depth profiles; a case study of the C/Ta/C/Si system", *Surface Science* 604:(7-8) pp. 633-640. (2010)